Control of Surface Interactions with Ultra-Violet/Ozone Modification at Polystyrene Surface

He Liang

MPhil BSc (Hons)

A thesis submitted in partial fulfilment of the

requirements of the

Robert Gordon University

for the degree of Doctor of Philosophy

January 2014

Certificate of Originality

I declare that I am responsible for the work carried out in this thesis, the original work is my own expect as specified in acknowledgements and none of this work or original work contained therein has been submitted in any previous application for a higher degree.

Dedication

The thesis is dedicated to the memory of my beloved grandparents, Tianlang He and Rongzhen Xu.

Acknowledgements

Firstly, to my grandparents, both passed away in my first year PhD. I cannot describe what you meant to me in words. I wish you are well in another world and I will make you proud.

I would like to thank to my supervisory team, Dr Rachel Knott and Dr Giovanna Bermano, for their continuous supports, advices and guidance throughout the PhD, I have thoroughly enjoyed every moments, I would not finish this work without your encouragement. I would also like to thank Prof Bob Bradley and Dr Chaozong Liu, who both left university in my first two years, for giving me the opportunity to do research in School of Engineering at the Robert Gordon University. I am also extremely grateful to NRP and IDEAS, for the funding for this study.

A sincere note of thanks to George Kidd, Alan McPherson, Dr Douglas Robertson, Dr Hong Parker, and Dr Xiaolei Fan for their continued supports and encouragements when I was depressed and upset. I would like to express my thanks to Dr Stephen Mitchell, Dr Aurik Andrew, Dr Pramod Gadad and Dr Susan Osbeck, for their advices, supports and encouragement throughout my PhD. Huge thanks to Margaret Brown and Dorothy Moir, for their helps in carrying out experiments at School of Pharmacy. Your inputs have been valued and most appreciated.

I would also like to thank Terry Knight and Trishul Baxi, for giving me the opportunity to lead the resident assistant team at St Peters hall, and team fellows Sarah, Warren, Aoife, George, David, Lisa, many thanks for making the these years so enjoyable and memorable.

Many thanks for the friends tried or made me sane, Paul Morgan, David Magee, Louise Magee, Lisa Song, Youwei Huang, Helen Wang, Harry Zhang, Carlos Pestana, Shuai Li, Yan Wang, Rui Yu, Leslie Kuo, Colin Hammond, Bin Liu, Bochen Ren, Ting Hou, Jian Jiao, Weixuan Huang, Akash and everyone in the weekly Sunday basketball game.

Many many thanks to my mum and dad, for their inspirations, encouragements, never ending loves and financial support, cannot thank you enough. And finally Wanfang Yu, thanks for the understanding of my research, I hope after the PhD we can move on with our life together.

Abstract

Surface interactions and reactivity are of critical importance in current biomedical technologies, for example, satisfactory cell attachment and long term viability are essential for optimal *in vitro* tissue culture and for successful implantation and stability of cardiovascular medical implants such as stents and grafts. To achieve this, the control of fundamental forces and the resulting molecular interactions between the relevant surface and absorbing or adhering species in the physiological system is compulsory. This work utilised the surface modification technique of Ultra-Violet/ Ozone to improve the polystyrene biocompatibility by oxidising the surface with additional polar oxygen functional groups without damaging the surface bulk property.

UV/Ozone treatment utilised throughout this study produced controllable oxygen functional groups and led to an increase in surface atomic oxygen level to 41% on unwashed and 35% on washed polystyrene surfaces, washing resulted in the removal of low molecular weight oxidised materials. Surface energy was increased by the addition of oxygen functional groups with the combination of alcohol (C-OR), carbonyl (C=O) and carboxyl (O-C=O); Saturation state was reached after 300s of UV/Ozone treatment where no more oxygen functionalities were incorporated to the surface. Moreover, UV/ozone treatment did not show an effect on the surface roughness studied by atomic force microscopy.

The biological responses of human endothelial umbilical vein cells (HUVECs) were studied at the different level of UV/Ozone treated surfaces. HUVEC adhesion, proliferation and migration were significantly improved by the treatment compared to untreated and tissue cultures plastics (TCPs). Among the levels of UV/ozone treatment studied, 120s and 180s were found to be the most effective and HUVEC proliferation did not seem to be affected by the high level of oxygen. Similarly, the surface oxygen level did not affect the migration over UV/Ozone treated over 60s.

Hypoxic condition significantly increased HUVECs migration on UV/Ozone treated, TCPs and untreated surfaces compared to normoxia, the oxygen rich surface did not favour to HUVECs that underwent regulatory process to enable the cells to increase migration.

Under laminar flow conditions, HUVECs did not only grow, proliferate and migrate but also showed standard responses on UV/Ozone treated polystyrene surface. A decrease in cell size was observed at all shear stress intensities studied (1 dyn/cm^2, 9 dyn/cm^2 and 25 dyn/cm^2) and the decrease was more obvious

at higher shear stress. High shear stress intensity also induced high cell turnovers, which may be related to air bubbles induced at high flow rate.

The overall findings of this study clearly illustrate that UV/Ozone surface treatment can be applied on polystyrene to improve human endothelial cells functionalities in term of adhesion, proliferation and migration in both static and laminar flow environment.

Table of Contents

List of Figures

List of Tables

Abbreviations

Al	Aluminium
AFM	Atomic Force Microscopy
ANOVA	Analysis of Variance
BE	Binding Energy
BMS	Bare Metal Stent
BrdU	5-bromo-2'-deoxyuridine
CA	Contact Angle
CAM	Cell Adhesion Molecules
CDKs	Cyclin Dependent Protein Kinases
CHA	Concentric Hemispherical Analyser
CHO	Chinese Hamster Ovarian Cells
cm^2	Centi Meters Squared
CO_2	Carbon Dioxide
Cr	Chromium
CVD	Cardiovascular Disease
DES	Drug Eluting Stent
DI	Digital Instruments
DMEM	Dulbecco's Modified Eagle's Medium

DMSO	Dimethysulfoxide
DNA	Deoxyribonucleic acid
E	Energy
ECACC	European Collection of Cell Cultures
EC	Endothelial Cells
ECM	Extra Cellular Matrix
EDTA	Ethylene Diamine Tertra-acetic Acid
EDRF	Endothelial Derived Relaxing Factor
EDX	Energy Dispersive X-ray Analysis
eV	Electron Volt
FCS	Foetal Calf Serum
FCS2	The Focht Chamber System 2
Fn	Fibronectin
FTIR	Fourier Transform Infrared
FWHM	Full Width Half Maxima
g	Gram
HOB	Human Primary Osteoblast Like Cells
H	Enthalpy
h	Height of the Flow Chamber

HIF	Hypoxia Inducible Factor
hr	Hour
hν	Photo Energy
HBSS	Hanks Balanced Salt Solution
hECFCs	Human Endothelial Colony Forming Cells
HPLC	High Performance Liquid Chromatography
HUEVC	Human Umbilical Endothelial Vein Cell
HUMEC	Human Uterine Microvascular Endothelial cells
I	Electron Density
I_o	Intensity
KE	Kinetic Energy
kV	Kilovolt
kW	Kilowatt
ULWOM	Ultra Low Weight Oxidised Materials
MAPK	Mitogen Activated Protein Kinases
Min	Minute
Mg	Magnesium
mL	Milli Litre
MSC	Mesenchymal Stem Cell

n	Number of Atoms per Unit Volume
Ni	Nickel
NiTi	Nickel Titanium/Nitinol
nM	Nano Metre
NHS	National Health Service
NO	Nitric Oxide
O•	Oxygen radicals
P	Pressure
Pa	Pascal
P/S	Penicillin and Streptomycin
PBS	Phosphate Buffer Solution
PE	Poly Ethylene
PEEK	Poly Ether Ether Ketone
pH	Power of Hydrogen
PLLA	Poly (L-Lactic Acid)
PMME	Poly Methacrylic Acid co Ethylene Glycol Dimethacrylate
PS	Polystyrene
Q	Desired Flow Rate
r	Target Shear Stress

RF	Radio Frequency
RMS	Root Mean Square
Rq	Surface roughness
S	Atomic Sensitivity Factor
SD	Standard Deviation
SEM	Stand Error of Mean
SFM	Scanning Force Microscope
Si	Silicon
T	Absolute Temperature
Ti	Titanium
TCPs	Tissue Culture Plastics
u	Viscosity of Fluid
UHV	Ultra High Vacuum
UV	Ultra Violet
UV/Ozone	Ultra Violet/Ozone
UK	United Kingdom
Vn	Vitronectin
W	Watts
XPS	X-Ray Photoelectron Spectroscopy

μm	Micro Metre
μL	Micro Litre
$VEGF$	Vascular Endothelial Cell Growth Factors
ΔG_{SL}	Change in Surface Energy
Δ_{ads}	Change in Thermodynamic Function
γ_{SL}	Solid-Liquid Interfacial Tension
γ_{L}	Liquid Interfacial Tension
γ_{LV}	Liquid-Vapour Interfacial Tension
γ_{S}	Solid Interfacial Tension
γ_{SV}	Solid-Vapour Interfacial Tension
$2D$	Two Dimensional
$3D$	Three Dimensional
Φ	Work Function
Θ	Contact Angle At the Edge of The Liquid Drop

Publications

- Enhanced Cell Colonization of Collagen Scaffold by Ultraviolet/Ozone Surface Processing. Chaozong Liu, Fiona-Mairead McKenna, He Liang, Alan Johnstone, Eric W. Abel,Tissue Engineering Part C: Methods. December 2010, 16(6): 1305-1314.

Conferences

- Poster presentation: UVO Processing of Polystyrene Surface and Its Effect on Albumin Adsorption: A XPS Study. He Liang, Rachel Knott, Eric W Abel, Chaozong Liu. UK Society for biomaterials annual conference, Glasgow, 2010.
- Oral speaker: UVO Processing of Polystyrene Surface and Its Effect on Endothelial Cells, He Liang, Giovanna Bernamo, Eric W Abel, Chaozong Liu, Rachel Knott. K. UK Society for biomaterials annual conference, Greenwich, 2011. ISBN 978-0-9559548-2-6.
- Oral Speaker: UVO Processing of Polystyrene Surface and Its Effect on endothelial cell proliferation and migration. UK Society for biomaterials annual conference, Nottingham, 2012.

Chapter 1 Scope and Rationale of the Project

In recent years there has been a great increase in the demand for surgery, where the effective performance of implantable materials especially for cardiovascular disease is essential for success. Implantable cardiovascular devices such as pacemakers, coronary stents, implantable cardiac defibrillators and grafts remain limited in their durability and clinical efficacy due to the absence of appropriate biological interactions at the implant surface and the lack of integration into adjacent surfaces (Meyers et al., 2009). Surface engineering techniques, using either a direct modification or a deposition method, provide routes to control the interactions on the surface of the biomedical device. Surface interactions and reactivity are of critical importance; for example, satisfactory cell attachment and long term cell viability are essential for successful implantation and stability of cardiovascular medical devices whilst control of interactions of blood products with the device is necessary to reduce the risk of thrombosis at the surfaces of the stents. In practice this requires the control of the surface composition, chemistry, energy and topography of the device surface such that interactions with water, electrolyte ions, proteins and cell adhesion molecules can be manipulated to control the formation of the bio-interface. In order to identify some of the issues related to these types of the devices, it may be worth designing a new type of material with the requisite bulk and surface properties, and to modify the outermost surface layers to improve the biocompatibility and influence bio-interaction of existing biomaterials without affecting the bulk properties of the original material. It is compulsory that the surface modification should be specific, thereby leaving the mechanical properties and functionality unchanged while enhancing biocompatibility by improving host tissue response to the surface.

There are several classes of materials used for cardiovascular implants: metals, ceramics and polymers. Polymers such as polystyrene and polyethylene have been widely used for a range of medical applications due to the ease of production, low cost and versatility of manipulation by altering the chemical, physical and mechanical properties. Polystyrene was used in this project as it has been used as an ideal material for many surface modification types due to low specific weight, high chemical resistance and mechanical flexibility. It is also recognised worldwide as a commercially available tissue culture plastic. In addition, untreated polystyrene does not support cellular adhesion of many cell lines due to native surface energy or wettability, therefore it was considered to be a good model material to investigate the effect with a variety of surface modification techniques (Amstein and Hartman, 1975b, Yasuda et al., 1994).

Polystyrene is a thermoplastic polymer with a long chain polymer with carbon backbones as seen in Figure 1.1, and a phenyl ring on carbon atoms in each repeating unit. The form of polystyrene is atactic due to the phenyl rings being randomly distributed on either side of the hydrocarbon backbone. This structure can prevent polystyrene from crystallising but makes it relatively brittle with a glass transition

temperature of 90 °C (Aras and Richardson, 1989). It is well documented that polystyrene can be modified for engineering, industry and biomedical applications by the use of various techniques such as wet, dry and radiation treatments (Curtis et al., 1983, Curtis et al., 1986, Yap and Zhang, 2007, Nitschke et al., 2012, Detrait, 1998, Sun et al., 1999). Moreover, a very common application of polystyrene is its commercial use as a disposable biomedical tissue culture plastic (Amstein and Hartman, 1975a, Curtis et al., 1983, Curtis et al., 1986, Imbert-Laurenceau et al., 2005, Guimard et al., 2007, Browne et al., 2004, Callen et al., 1995, Detrait, 1998, Hin, 2004, Teare et al., 2000, Mitchell et al., 2005a, Mitchell et al., 2005b, Mitchell et al., 2004).

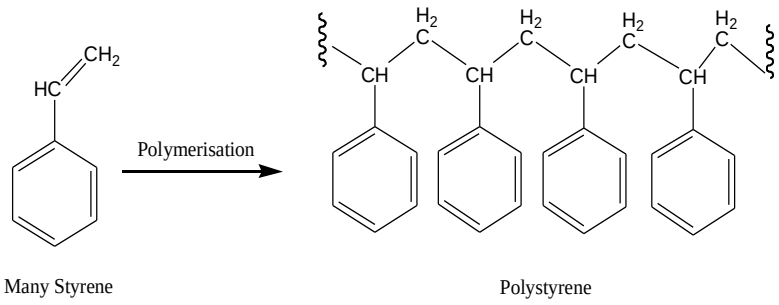

Figure 1.1 Polymerisation of styrene to polystyrene.

It is well documented that biomaterial surface properties such as wettability, bulk chemistry, the ratio of hydrophilicity and hydrophobicity, surface charge and surface roughness, could affect cell adhesion and proliferation (Van Kooten et al., 1992, Onyiriuka, 1993, Lee et al., 1994, García and Keselowsky, 2002, Davidson et al., 2004, Mitchell et al., 2004, McArthur and Shard, 2006, Seal and Panitch, 2006). Surface modification techniques can provide routes to manipulate these surface properties for clinical use. Ultra-Violet/Ozone (UV/Ozone) treatment has been used as a highly controllable surface modification technique for improving polymers wettability; this approach has been previously described to increase the polymer surface oxygen, surface polarity and surface energy for the enhancement of cellular adhesion and proliferation. Furthermore, UV/Ozone treatment does not require sophisticated vacuum apparatus or any wet chemistry handling including residual solvents or other contaminants (Yusilawati et al., 2010). Ozone is naturally produced in the upper atmosphere at altitudes of 20-50 km or formed by the reaction of high energy particles and radiation (Cataldo, 2001a). Reactions between equation 1.1 to equation 1.6 illustrate

the formation of ozone and oxygen's radicals (O•) by UV radiation (Cataldo, 2001a). At a wavelength of 184.9nm, oxygen is excited into two oxygen radicals. M indicates a third molecule which could be excited such as N_2 (Cataldo, 2001b). In equation 1.4, one atomic oxygen radical and one molecular oxygen radical is formed by radiation of ozone at a wavelength of 253.7 nm. Equation 1.5 and 1.6 indicate another two types of oxygen formation may also occur in the system.

$$O_2 + h\nu(\lambda = 184.9nm) \rightarrow 2O\bullet \qquad \text{Equation 1.1}$$

$$O\bullet + O_2 + M \rightarrow O_3 + M^* \qquad \text{Equation 1.2}$$

$$M^* + O_3 \rightarrow O\bullet + O_2 + M \qquad \text{Equation 1.3}$$

$$O_3 + h\nu(\lambda = 253.7nm) \rightarrow O_2\bullet + O\bullet \qquad \text{Equation 1.4}$$

$$O\bullet + O\bullet \rightarrow O_2 \qquad \text{Equation 1.5}$$

$$O_3 + O\bullet \rightarrow O_2 + O_2 \qquad \text{Equation 1.6}$$

The surface changes resulted by UV/Ozone treatment were characterised by X-ray photoelectron spectroscopy (XPS) for surface chemistry change, atomic force microscopy (AFM) for surface roughness change, contact angle and surface energy for wettability analysis. The ultimate goal of this research is to use surface modification techniques to investigate how changes in surface chemistry could affect endothelial cells responses and thereby control the cell-surface interactions. Endothelial cells which are located between at the interface between blood and tissue plays a pivotal role in determining optimal function in order to maintain normal physiological condition. Abnormal functionalities of endothelial cells result in cell injury and dysfunction and it is believed to contribute to a number of heart diseases such as atherosclerosis, hypertension, congestive heart failure, hypercholesterolemia and diabetes mellitus (Ait-Oufella et al., 2010, Gimbrone et al., 2000, Santilli et al., 1992, Haddad et al., 2011, Drexler et al., 1992). To better understand

the interactions between endothelial cells and UV/Ozone treated surface, Human umbilical vein endothelial cells (HUVECs) were used due to their ease of isolation, strong proliferative potential at high passage levels and well-established in cardiovascular research. Cell proliferation and migration were studied as both were recognised as two key indicators of endothelial cell growth.

The behaviour of endothelial cells on UV/Ozone treated polystyrene at low oxygen tension conditions was also investigated. Decrease of blood flow in thrombosis causes the failure of oxygen delivery to target sites. Meanwhile, endothelial cells undergo changes to adapt this low oxygen condition such as various metabolites produced, e.g. nitric oxide, the hypoxia inducible factor and lactate. These changes further promote endothelium proliferation and migration (Michiels et al., 2000, Li et al., 2010, Gadad et al., 2013). Therefore, it is interesting to find out whether endothelial cells may benefit from the oxygen-rich surfaces to undergo normal metabolisms.

In the human body, the vascular endothelium not only responds to humoral factors in circulation but also to the mechanical forces caused by blood flow and cardiac cycle (Traub and Berk, 1998). The mechanical forces include gravitational, mechanical stretch or strain and shear stress. In particular, shear stress is extensively associated with blood flow and it is a very important factor, which determines the long-term maintenance of the structure and function of blood vessel (Fisher et al., 2001). It is known that steady laminar shear stress can be atheroprotective to inhibit both endothelium proliferation and apoptosis (Arslan et al., 2010). Non-laminar flow and turbulent flow shear stress may cause cell turnovers, localisation of atherosclerotic plaque and neointimal hyperplasia (Dardik et al., 2005). The response of endothelial cells on UV/Ozone treated polystyrene surface was investigated in a closed chamber system that provides stable laminar flow.

1.1 Aims and objectives

Overall, the aim of this study is to use surface engineering techniques mainly UV/Ozone techniques, to improve a medical device performance. There are 3 objectives to this study:

- Characterise the UV/Ozone treated polystyrene surface in terms of surface elemental composition, chemistry, energy and roughness.
- Investigate the UV/Ozone modified polystyrene surfaces with respect to endothelial cell proliferation

and migration.

- Investigate the endothelial cell morphological change under flow induced shear stress conditions.

Chapter 2 General Introduction

In recent years there has been a great increase in the demand for surgery, where the effective performance of implantable materials is essential for successes. Implantable biomedical devices remain limited in their durability and clinical efficacy due to the absence of appropriate biological interactions at the implant surface and the lack of integration into adjacent surface (Meyers et al., 2009). Surface engineering techniques, using either a direct modification or a deposition method, provide routes to controlling the interactions on the surface of the biomedical device. Surface interactions and reactivity are of critical importance in biomedical technologies; for example, satisfactory cell attachment and long term cell viability are essential for optimal *in vitro* tissue culture and for successful implantation whilst control of interactions of blood products with the device is necessary to reduce the risk of thrombosis at the surfaces of stents and other vascular implants. Treatments which offer this control are in great demand. It is well known that most cell types have near optimal attachment characteristics on functionalised (polar, oxidised) surfaces (Mitchell et al., 2005a, Mitchell et al., 2004a, Mathieson and Bradley, 1994), whilst the specific adsorption characteristics of water, electrolyte ions and protein molecules (Browne et al., 2004) are strongly dependent upon additional factors, for example, surface charge, species concentration, *p*H of the environment and mass-transport all of which influence the precise character of the boundary (Stern) layer which forms at the bio-interface.

2.1 Biomaterial

The definition of biomaterials is to indicate materials that constitute parts of medical implants, extracorporeal devices, and disposables that have been utilised in medicine, surgery, dentistry, and veterinary medicine as well as in every aspect of patient health care (Dee et al., 2003). Biomaterials used in medical devices are intended to interact with the biological system in which they are placed based on their mechanical properties, chemical stability and biocompatibility (Mitchell et al., 2005a). The successful application of biomaterials is determined by factors such as biocompatibility, sterilisability, functionality and manufacturability. In addition other factors, which are out with the control of devices include the techniques employed by the surgeon and the health condition of the patients. Biocompatibility includes the acceptance of an artificial implant by the surrounding tissues and by the body as a whole. The successful design of biocompatible biomaterials should not irritate the surrounding structures, provoke abnormal inflammatory responses or incite an immunologic reaction (Park and Bronzino, 2002).

For cardiovascular diseases CVDs, the development of biomaterial has been limited due to the deficiency of satisfactory materials of strength and durability. A unique closure for cardiovascular biomaterials is thrombosis, the blood clots result in heart attacks, paralysis, strokes, hemolysis and other organ failures (Gimbrone et al., 2000, Ait-Oufella et al., 2010). Another closure of these materials is the excessive growth of tissues surrounding the device; it may be related to the reaction of the material, stresses on the surrounding tissues or the degraded products of the material.

Cardiovascular biomaterials can be divided into two categories: biological or synthetic materials as shown in Table 2.1. Materials of biological substances include pericardia, arteries and veins and heart valves, heparin and collagen are mostly related to coating on the cardiovascular devices. Polymers, such as polystyrene (PS) and polyethylene (PE) are particularly attractive as biomaterials; the former is extensively used when growing cells in the laboratory, whilst the latter is of great importance in recent manufacture of components of various implantable cardiovascular devices, including stent and vascular graft, and also for the larger artificial joints such as hips, and for the one-piece fabrication of smaller components, for example, finger joints. Biodegradable polymers such as poly (L-lactic acid) have considered to be another options for manufacturing stents, it has the advantage of not only being presented as a foreign material once deployed in the vessel but also with a controllable drug release rate (Qi et al., 2013a). Metal alloys such as titanium (Ti), nickel (Ni), nitinol (NiTi), 316L stainless steel (316 LL) etc. used in manufacturing of stents due to well suited mechanical properties (Sun et al., 2008).

I Biological	II Synthetic Biomedical Materials
Pericardia	***Polymeric***
Arteries	*Ultra High Molecular Weight Polyethylene, Polymethylmethacarylate, Polyethyletherketone,Silicone, Polyurethane, Polyetrafluoroethylene*
Veins	*Poly(L-lactic acid)*
Heart valves	***Metallic***
Collagen	*Stainless Steel, Cobalt- based Alloy, Titanium Alloy, Nitonol, Platinum*
Heparin	***Composite***
	Carbon Fibre/Polyethyletherketone

Table 2.1 The classification of biomaterials for CVDs (Hin, 2004).

2.2 Interface of cell and biomaterial

Cell-biomaterial interaction and reactivity play an important role in biomedical technologies and the interaction between the biological environment and biomaterials takes place at the material-fluid interface (Mitchell et al., 2005a). Biomaterials and medical devices are increasingly being used for advanced prostheses in cardiovascular, orthopaedic, dental, ophthalmological and reconstructive surgery, in interventions such as angioplasty and hemodialysis, in surgical sutures or bioadhesives, and as controlled drug release devices. For example, optimal cell attachment and long term viability are compulsory characterisations for *in vitro* tissue culture, for successful implantation and for the stability of medical devices whist the surface of the control of blood interactions is essential to reduce the risks of thrombosis at the device, such as stents and other vascular implants (Davidson et al., 2004). All of these require precise control of the fundamental molecular forces relating to surface chemistry (Mitchell et al., 2004a), wettability (Park et

al., 2004), surface energy (Ko and Ma, 2009) and surface charge (Sun et al., 2008) and the resulting molecular interactions which occur between a surface in contact with the body issues and the adsorbing or adhering species in the physiological environment. In practice this requires control of the surface composition and chemistry of the device such that interactions with water, electrolyte ions, proteins and cell adhesion molecules can be manipulated to control the formation of the bio-interface (Ton-That et al., 2000). Figure 2.1 shows a schematic diagram of interactions between cell and surface. In the physiological system, the biological substances such as blood, tears, serum, etc. are rapidly grafted with a protein layer when they reach the surface of implants. The cells do not adhere directly to a substrate; instead they adhere to a preabsorbed protein layer, which contains certain amino acid sequences acting as cell binding domains.

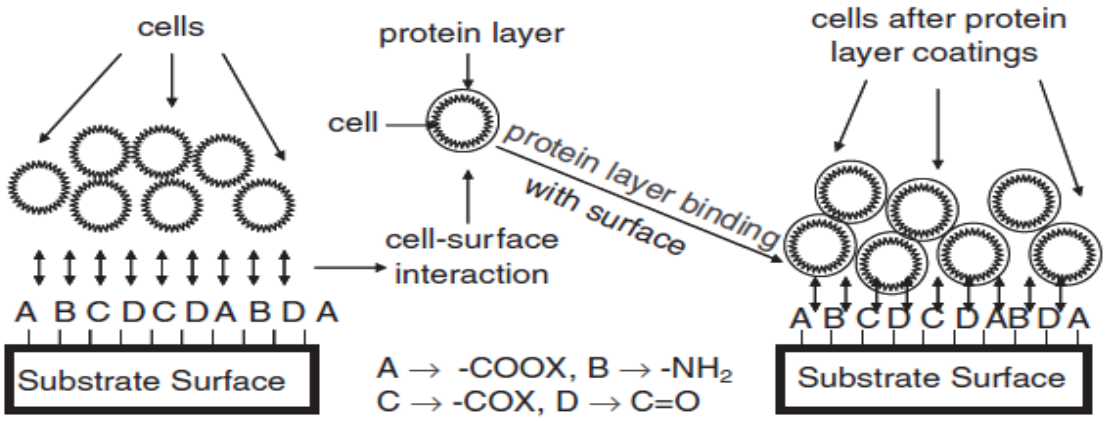

Figure 2. 1 A schematic diagram of cell surface interaction (Bouafsoun et al., 2006).

2.3 Surface wettability

Surface wettability can be referred to the ability of a liquid to maintain the contact to any solid surfaces. It is believed that surface wettability plays a key role in the interaction of cells and the biomaterial. The wettability can be affected by the orientation of surface functional groups, the wetting solution, ionic concentration and pH. A hydrophobic surface is determined by Vogler to have a water contact angle higher than 65° and a hydrophilic surface to have a water contact angle of less than 65° (Vogler, 1998). The measurement of water contact angle can be used as an indicator to evaluate protein adsorption. Brash and Horbett first demonstrated that protein adsorption increased with decreasing wettability of the surface also known as the hydrophobic rule (Thomas and John, 1987). On a hydrophobic surface, water molecules act as an ice-like

structure and have much lower entropy than the water molecules in bulk, in contrast to hydrophilic surfaces, water molecules exhibit relatively more-dense water structure, in which it is less reactive and hard to remove. Protein adsorption on a hydrophilic surface is weak with a conformation near to its native state. As a result, protein adsorption to a hydrophilic surface is generally reversible, whereas to hydrophobic surface it is not. When the protein solution comes in contact with the hydrophilic surface, the water will first be absorbed to the surface and form a thin layer. The protein molecules have to diffuse through this water layer to interact with polystyrene surface, and form a less dense layer of protein on UV/Ozone processed polystyrene surface. In contrast, water has a low affinity with the pristine hydrophobic polystyrene surface and the initially formed water film could easily be dispelled by protein, and form a denser protein layer. Literature suggests cell types such as human osteosarcoma cells (MG63) are dependent on surface contact angles; a reduction of 80% was observed when increasing the contact angle from 57˚ to 122˚ on plasma modified polystyrene surfaces with siloxane coating (Denis 2010). Interestingly, Shen et al. reported the inverse behaviour of vascular endothelial cells on adhesion and migration on silicon oxide coating on silicon wafers, cells were observed to exhibit a tendency for migration on hydrophobic surfaces (98˚) and maximally adhered to very hydrophilic surfaces (26˚) (Shen et al. 2012).

2.4 Surface topography

The majority of material surfaces have undulations and probably steep gradients and pores landscape, these parameters can have a strong determination of material performance (Assender et al., 2002). Surface topography also plays a vital role in determining the biocompatibility of biomaterials. The surface topography of implants is known to affect the way in which cells and tissues interact with the surface. A variety of phenomena have been found, but four cell behaviours may be of particular relevance to the implant interface: 1. Contact guidance, i.e. oriented surface features, such as grooves; 2. Cell selection, i.e. the process whereby surface topographic features, such as roughness; 3. Cell differentiation, i.e. the differentiation of cells is influenced by the topography of the surfaces with which they are in contact; 4. Cell-mediated matrix organization, i.e. cell traction acts on the extracellular matrix to produce tracts of cells and fibres between two or more centres of attachment (Ellingsen and Lyngstadaas, 2003).

Many researchers have found that a grooved surface topography with features in the range of 1 to 10 μm can affect the orientation of cell attachment to surfaces (Dunn and Brown, 1986, Den Braber et al., 1998, Walboomers et al., 1998). As cells are oriented by the grooves, they in turn orient the extracellular matrix by

their fractional forces and migration. The extracellular matrix would also be altered relative to what occurs on smooth surfaces by changes in gene expression and secretion of fibronectin and matrix metalloproteinase. Walbommers et al. conclude that microgrooves create the mechanical stress which influences cell spreading and forces the cells to become aligned with surface microgrooves, this was noted from the results of seeding rat dermal fibroblasts on plasma treated polystyrene grooved surfaces with ridge and groove widths of 1, 2, 5 and 10 μm (Walboomers et al., 1998). Van Kotten et al. found that there was increased orientation of human skin fibroblasts on 2 μm grooved surfaces compared to 5 μm and 10 μm surfaces, their results also indicated that cells proliferated at a slower rate on smooth surfaces (Van Kooten et al., 1998).

2.5 Surface functional group

A large amount of work has been undertaken to understand the effects of specific surface functional groups on cell adhesion and growth. Different functional groups have been found to support cell adhesion, spreading and growth such as amine, carboxyl and carbonyl groups (Mitchell et al., 2004a, Mitchell et al., 2005a, Teare et al., 2000a, Mangipudi et al., 1995).

Ertel and his colleagues found that the oxygen content of plasma modified polystyrene surfaces was correlated with cell growth of bovine aortic endothelial cells (Ertel et al., 1990). He also concluded that cell growth might correlate better with specific oxygen containing functional groups rather than with total oxygen. Further works from this group found that bovine aortic endothelial cells growth was increased with increasing carbonyl concentration but no correlation with hydroxyl or carboxyl concentration was found (Ertel et al., 1992).

Teare et al. stated that the increased amounts of surface hydroxyl and carboxyl groups have a positive effect on cell affinity to the substrate surfaces, whereas topographical changes can be discounted, and there is a direct correlation between the surface free energy, the surface chemistry of the UV/Ozone treated polystyrene and the rate of cell attachment (Teare et al., 2000a). Moreover, Cooper studied the effects of various terminal functional groups on self-assembled monolayers (Elaine Cooper, 2000). Murine 3T3 fibroblasts and primary human osteoblasts were cultured on self-assembled monolayers formed by the adsorption of alkanethiols of varying terminal groups and alkyl chain length on gold. For both types, the highest levels of attachment and growth were found on carboxylic acid terminated self-assembled monolayers and the lowest levels of the long chain methyl terminated ones. On hydroxyl

terminated surfaces, the fibroblasts attached poorly while osteoblasts attached and proliferated nearly as well as on carboxylic acid terminated surfaces. Furthermore, Brandley et al concluded that both hydroxyl and carboxyl groups supported cell attachment and growth using mouse fibroblasts (Brandley et al., 1987). Lee et al. treated PE sheets with different chargeable functional groups such as acrylic, carboxylic and amide groups by corona discharge treatment and evaluated the cellular response of Chinese hamster ovary cells. Their results showed the surface coated with amine groups was the best for cell adhesion, spreading and growth due to the positively chargeable character in aqueous cell culture (Lee et al., 1994). Different to other researchers work discussed, there was a negative effect on cell adhesion, spreading and growth on the surface grafted by carboxylic groups and they believed that it was due to the increased wettability not the character induced by negative charges (Endemann and Schiffrin, 2004).

2.6 Surface interactions with protein

Proteins can be described as long chain copolymers which consist of valued combinations of about 20 different amino acids. Each amino acid has the same fundamental structure but differing only in the side chain. Each amino acid chain consists of an amino group and a carboxyl group on either side. A peptide bond is formed when an amino group from one molecule covalent bond to the carboxyl group of another as seen in Figure 2.2. Two of the three peptide bonds in a peptide unit are free to rotate. Side groups can be polar or non-polar (hydrophilic or hydrophobic), acid and basic. It is known that 5 amino acids have charged polar side groups; 8 amino acids have non-polar side groups and 7 have neutral polar side groups (Teare et al., 2001). The combination of different amino acid residues sequences determine the wide variety of 3-dimmensional protein structures that interact by hydrogen bonding, hydrophobic bonding, ionic bonding, salt bridges and disulphide bridges. The role of the sequence of amino acids in generating diversity can be appreciated by a brief review of the properties of the amino acid side chains. Some of the amino acids have side chains that carry no charge at any pH yet exhibit considerable polar character such as serine and threonine (Barrias et al., 2009). The ionisable side chains vary from fairly acidic ones to more basic amino acids such as the imidazole group in histidine and the still more basic amino groups in lysine and arginine that carry full charges at *pH* 7.4 (Kwok and Neumann, 1999).

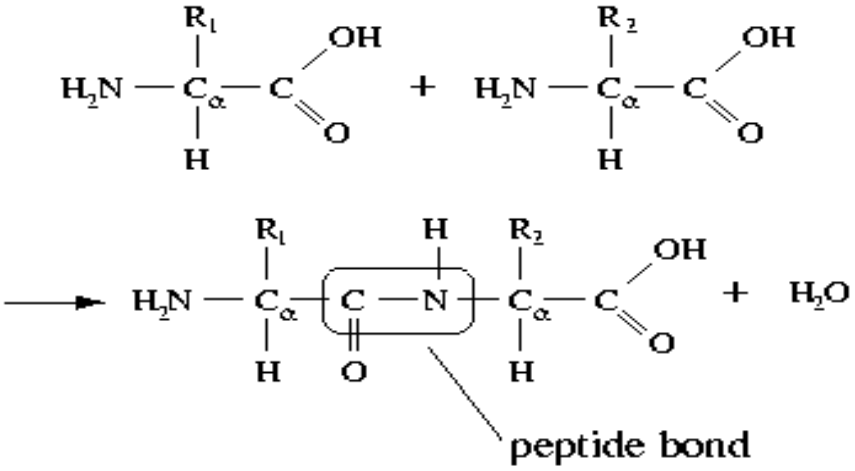

Figure 2. 2 Peptide bond linking two amino acids.

The natural environment of protein is aqueous; however, protein will tend to accumulate at the interface when it comes in contact with another immiscible phase. Protein adsorption is the result of interactions present between the resulting molecules and the relevant surfaces. For the process of adsorption to occur it must result in a decrease in the Gibbs energy, G of the system.

$$\Delta_{ads} G = \Delta_{ads} H - T\ \Delta_{ads} S < O$$

Where H is enthalpy, S is entropy and T is the absolute temperature, Δ_{ads} indicates the change in the thermodynamic function that results from the adsorption process. Therefore, adsorption will occur if it results in a decrease in enthalpy or an increase in entropy (Teare et al., 2000b).

Extracellular matrix (ECM) is a complicated protein network that includes adhesive glycoproteins such as vitronectin, fibronectin and laminin etc. and they are involved in the interaction between the protein layer and the surface of the material. Figure 2.3 shows the mechanism of protein adhere onto different surfaces, the molecules from the protein layer could have polar, ionic and hydrophobic properties and they can react with the substrate in numerous ways depending on the distinct domain. It is necessary that the cells function normally and proliferate by migrating to a critical size by forming further local contacts with ligand binding sites which depend on the availability of the materials surface properties including topography, wettability and surface functional groups (Bouafsoun et al., 2006, Poulsson et al., 2009).

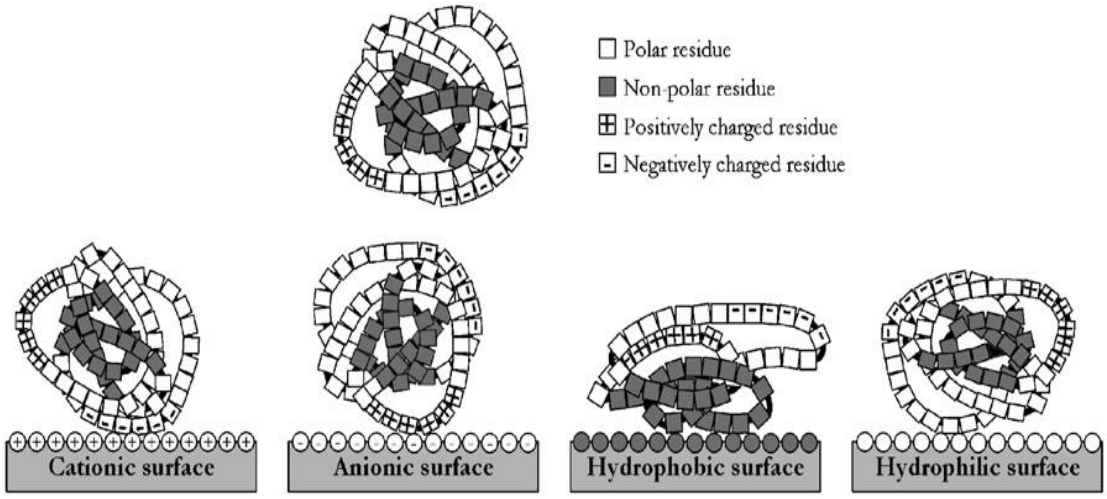

Figure 2. 3 Mechanisms of protein adhere onto different surfaces (adapted from Poulsson et al., 2009).

2.7 Surface modification techniques

There are many surface modification techniques developed for all varieties of biomaterials to modulate a biological response and improve medical device efficiency. Approaches include reduction of protein adsorption and thrombogenicity, control of cell adhesion, growth and differentiation, modulation of fibrous encapsulation and osseointegration, improved wear and/or corrosion resistance, and potentiation of electrical conductivity (Ratner et al., 2004).

Generally there are two categories of surface modification: (1) Physical and chemical modification above the original surfaces involving alterations to the atoms, compounds, or molecules on the surface by chemical reactions, etching and mechanical roughening/polishing and patterning. (2) Biological surface modifications such as protein adsorption, immobilisation of biological molecules and cell seeding techniques as shown in Table 2.2. A schematic representation of the variety of methods commonly used for the surface modification is shown in Figure 2.4.

Physical surface modification can fall into two areas: the first involves the chemical alteration of surface structure and the second involves the deposition of an additional external layer to the substrate surfaces. Chemical surface modification changes the surface chemical composition by either wet treatments or grafting. Wet treatments are carried out by directly employing a solution onto the surfaces to change the surface chemistry; grafting is to modify the surface by creating well defined surface functionalities i.e.

covalently bonding suitable macromolecular chains to the surface. In this study, ultraviolet Ozone (UV/Ozone) is described in detail as used as the key treatment.

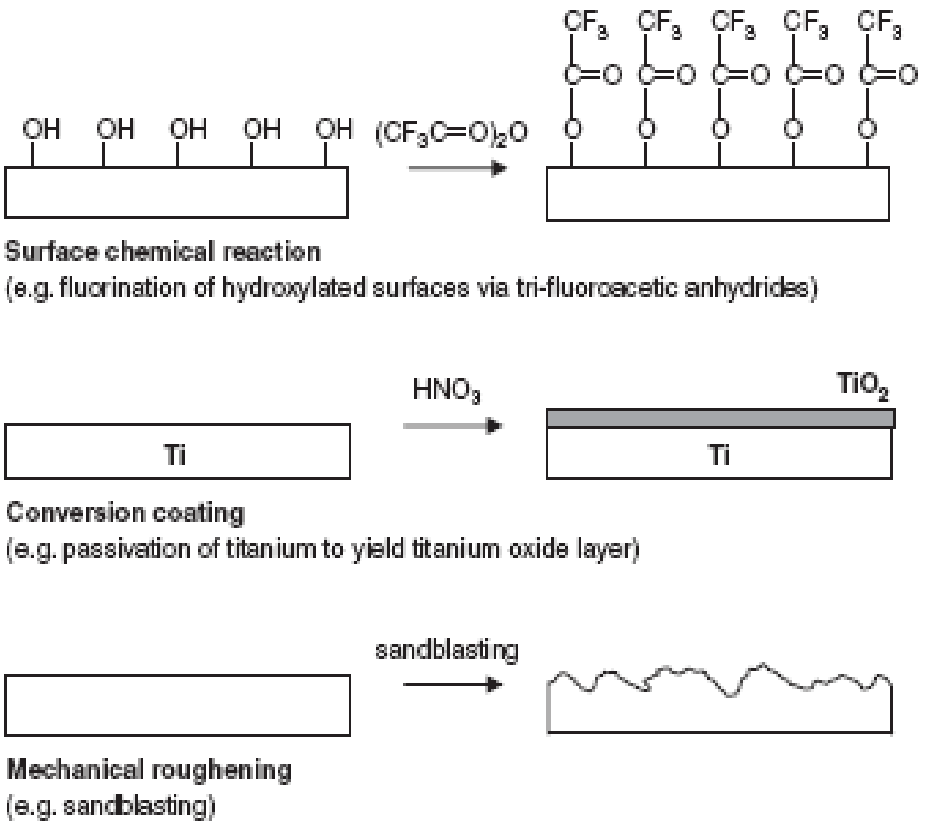

Figure 2. 4 Schematic representations of common physical/chemical surface modification.

Physical & Chemical	Biological
Physical deposition • Ion assisted • Langmuir-Blodgett • Solvent coating **Modification of original surface** • UV/Ozone • Acid etching • Gamma irradiation • Plasma treatment • Corona discharge **Covalently bound coating** • Plasma deposition • Radiation grafting • Photografting **Surface texturing** **Laser ablation** **Plasma etching**	**Protein adsorption** • Fibronectin • Albumin • Collagen **Immobilisation of biological molecules** • Heparin • Albumin • Collagen • Fibronectin • Binding domain molecules • Drugs • Many others **Cell seeding** • Endothelial cell lining

Table 2.1 Surface modification techniques on polymers.

2.7.1 Flame, laser, corona surface modification

High energy species are required to modify the surfaces of polymers as they are characteristically non-reactive material. In nature, these high energy species can be found as fire and lightning. Flame treatments are commonly used for surface modification, while laser, corona and plasma treatments to some extent mimic the effects of lightning. These physical treatments cause matter such as atoms and atomic clusters to be generated and deposited on the surface of substrate.

Flame treatment was first developed to improve the wetting and adhesion properties of polyolefin films in 1950s. The species formed by high temperature flame using propane or methane includes ions, radicals and molecules in excited states. The effects of the treatment can be fixed by the flame composition, flame temperature, sample movement and distance between the sample and flame. Flame treatments are often used to modify paperboard or relatively thick polyolefin materials rather than polymers as the long treatment times can alter the bulk properties. Along with flame processes, corona treatment is by far the most widely used. The discharge effect happens when high energy electromagnetic fields are formed close to charged thin wires or electrodes causing ions to be formed.

2.7.2 UV/Ozone surface treatment

Photo-chemical reactions occur as a result of absorption of light by chromophores within a molecule and the subsequent activation of its singlet and triplet states. Photo-degradation is the process by which chain scission and crosslinking occurs upon irradiation within an inert atmosphere such as a vacuum or nitrogen atmosphere. Photo-oxidation happens when a polymer is subjected to UV irradiation in the presence of oxygen, though chemical reactions being active by photons with short wavelengths (Rabek, 1996a). UV/Ozone surface modification utilises UV lamps operated between wavelength of 180 to 400nm which takes the advantages of this reaction causing the crosslinking or fragmentation of activated photons of the polymer surfaces (Garbassi et al., 1997).

There are four main processes which are involved in photo-oxidation: the first is initiation where the free radicals are produced; the second is propagation in which the free radicals formed from initiation process react with oxygen species; the third is chain branching where peroxy and oxy radicals are formed along with secondary polymer radicals; the final step is termination where different free radicals react with one another and may cause crosslinking (Rabek, 1996a).

The initiation process of photo-oxidation of polymers (PH) is shown from Equation 2.1 to 2.3. UV radiation can produce oxygen radicals, Ozone and other molecules in the presence of oxygen that can be excited. The interaction of the above radicals can remove the hydrogen atoms from the polymer and produce alkyl radicals and hydroperoxy radicals (Equation 2.1). When light is absorbed by a chromophoric impurity (RH), polymer can also be excited to radicals and hydroperoxy radicals (Equation 2.2). These can also react with the polymer to produce polymer alkyl radicals and hydroperoxy radicals (Equation 2.3) (Rabek, 1996a, Rabek, 1995). Propagation occurs once these have been created.

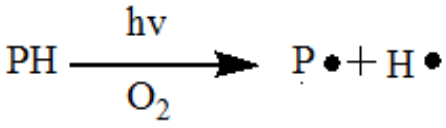

Equation 2.1

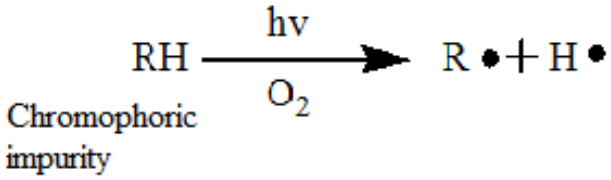

Equation 2.2

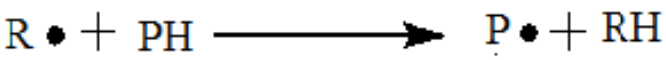

Equation 2.3

In Propagation as shown in Equation 2.4-2.7, the first step is the reaction of the free radicals with oxygen resulting in the formation of peroxy radicals. The rate of this reaction diffusion controlled due to the requirement of oxygen. Propagation then continues by abstraction of hydrogen by peroxy radicals from another unreacted polymer molecule (Equation 2.5). Hydroperoxide radicals may also be produced by reaction of the hydrogen radicals with oxygen. The photolysis efficiency of hydroperoxides can determine the rate of propagation, where new free radicals of hydroxyl and oxy radicals are formed (Equation 2.6). These radicals may then contribute to further propagation by the abstraction of hydrogen by the polymer oxy and hydroxyl radicals (Equation 2.7) (Browne, 2001, Rabek, 1996a). At this stage, chain branching is ready to occur.

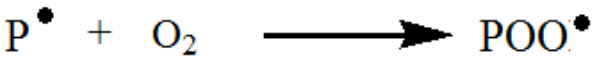

Equation 2.4

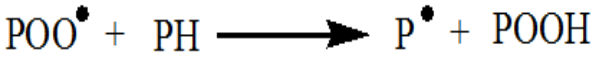

Equation 2.5

Equation 2.6

Equation 2.7

Equation 2.8 to 2.11 shows the types of reaction of chain branching occurring during propagation. β-scission reaction resulting in chain scission and end carbonyl or aldehyde formation (Equation 2.8 and 2.9) (Rabek, 1996b, Rabek, 1995). Ketones can also be formed in the reactions (Equation 2.10). Disproportionation reactions can result in the formation of a carbonyl and a hydroxyl group between two alkoxy radicals (Equation 2.11) (Rabek, 1996a, Browne, 2001, Poulsson, 2007b).

1. β-scission chain reactions

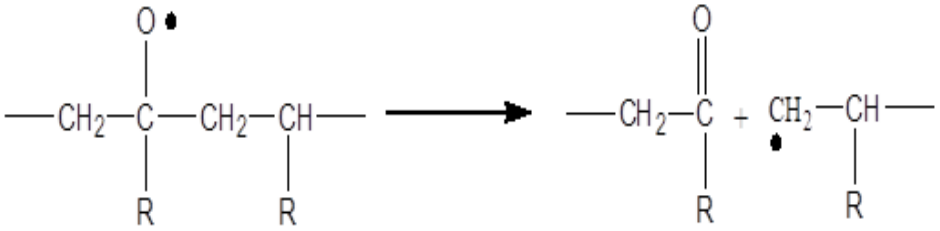

Equation 2.8

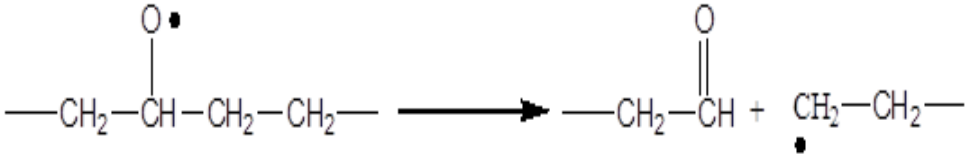

Equation 2.9

2. Ketone formation within the polymer chain

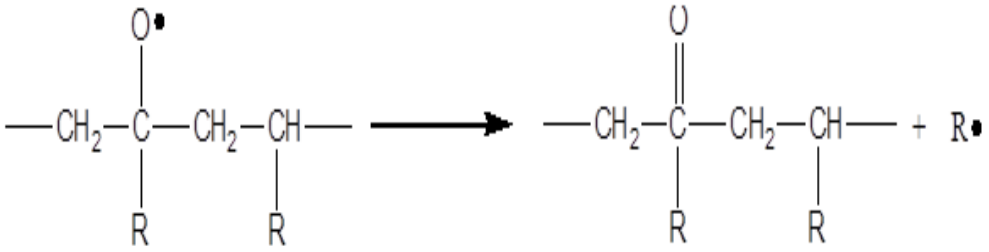

Equation 2.10

3. Disproportionation reactions between two alkoxy radicals

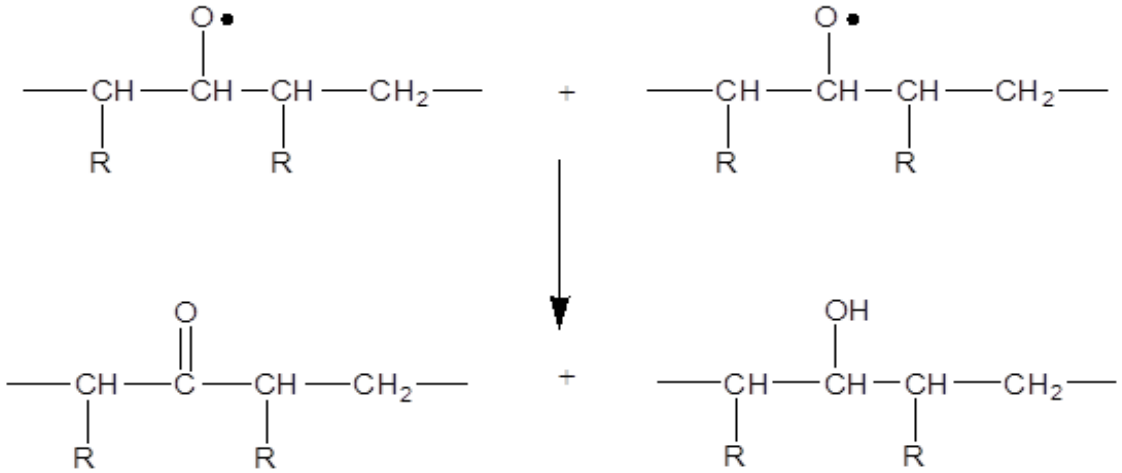

Equation 2.11

The photo-oxidation can be terminated when free radicals produced combine with each other resulting in crosslinking for example as shown from Equation 2.12 to 2.15.

1. Termination: examples of bimolecular combination

$$P\bullet + P\bullet \longrightarrow P\text{-}P \qquad \text{Equation 2.12}$$

$$P\bullet + PO\bullet \longrightarrow POP \qquad \text{Equation 2.13}$$

$$P\bullet + POO\bullet \longrightarrow POOP \qquad \text{Equation 2.14}$$

$$P\bullet + PO\bullet \longrightarrow POOP \qquad \text{Equation 2.15}$$

Low molecular weight molecules can also react with polymer radicals to form hydroperoxides, alcohols, carbonyls and as end groups ketones, aldehydes and carboxylic acids, thereby causing chain scission and resulting in termination (Equation 2.16 to 2.24).

2. Reaction with low molecular weight radicals in termination.

$$P\bullet + HO\bullet \longrightarrow POH \qquad \text{Equation 2.16}$$

$$P\bullet + HO_2\bullet \longrightarrow POOH \qquad \text{Equation 2.17}$$

$$P\bullet + R\bullet \text{ (or } H\bullet) \longrightarrow PR \text{ (or } PH) \qquad \text{Equation 2.18}$$

$$PO\bullet + HO\bullet \longrightarrow POOH \qquad \text{Equation 2.19}$$

$$PO\bullet + HO_2\bullet \longrightarrow POH + O_2 \qquad \text{Equation 2.20}$$

$$P\bullet + R\bullet \text{ (or } H\bullet) \longrightarrow PR \text{ (or } PH) \qquad \text{Equation 2.21}$$

$$PO_2\bullet + HO\bullet \longrightarrow POH + O_2 \qquad \text{Equation 2.22}$$

$$PO_2\bullet + HO_2\bullet \longrightarrow POO\text{-}OOH \longrightarrow POOH + O_2 \qquad \text{Equation 2.23}$$

$$PO_2\bullet + R\bullet \text{ (or } H\bullet) \longrightarrow POR \text{ (or } POH) \qquad \text{Equation 2.24}$$

A summary of the reactions occurred during the photo-oxidation of polystyrene is shown in Figure 2.5. The reaction starts with the initiation where alkyl and peroxy radicals are produced. At the propagation step, the reactions can continue amongst the ethyl groups to form oxy radicals or within the phenyl ring to form alkyl radicals. Unsaturated end groups such as allyl and acetophenone can lead to the formation of conjugated polyene structures which can absorb light in the 260nm to 400nm wavelength region and therefore may be the key factor for the yellowing of polystyrene (Gillen et al., 1993).

X-ray photoelectron spectroscopy (XPS) findings reveal that a decrease in the aromaticity of polystyrene is believed to be related to phenyl ring opening (Clark and Munro, 1984, Peeling and Clark, 1981, France and Short, 1997). Ring opening mechanisms may result in the formation of conjugated long chain dialdehyde groups that may also be related to the yellowing of polystyrene (Peeling and Clark, 1981, Weir, 1977). Subsequent oxidation may lead to the formation of short chain carbon dioxide, carboxylic acids, carbon monoxide, hydroperoxide, benzaldehyde, acetophenone (Shiono et al., 1978) and carbonates with further oxidation (Onyiriuka, 1993a). It has also been suggested that quinone type structures may also occur and play an important in the yellowing of polystyrene (Rabek and Ranby, 1974, Rabek, 1996a, Poulsson, 2007b, Mitchell, 2006b, Browne, 2001).

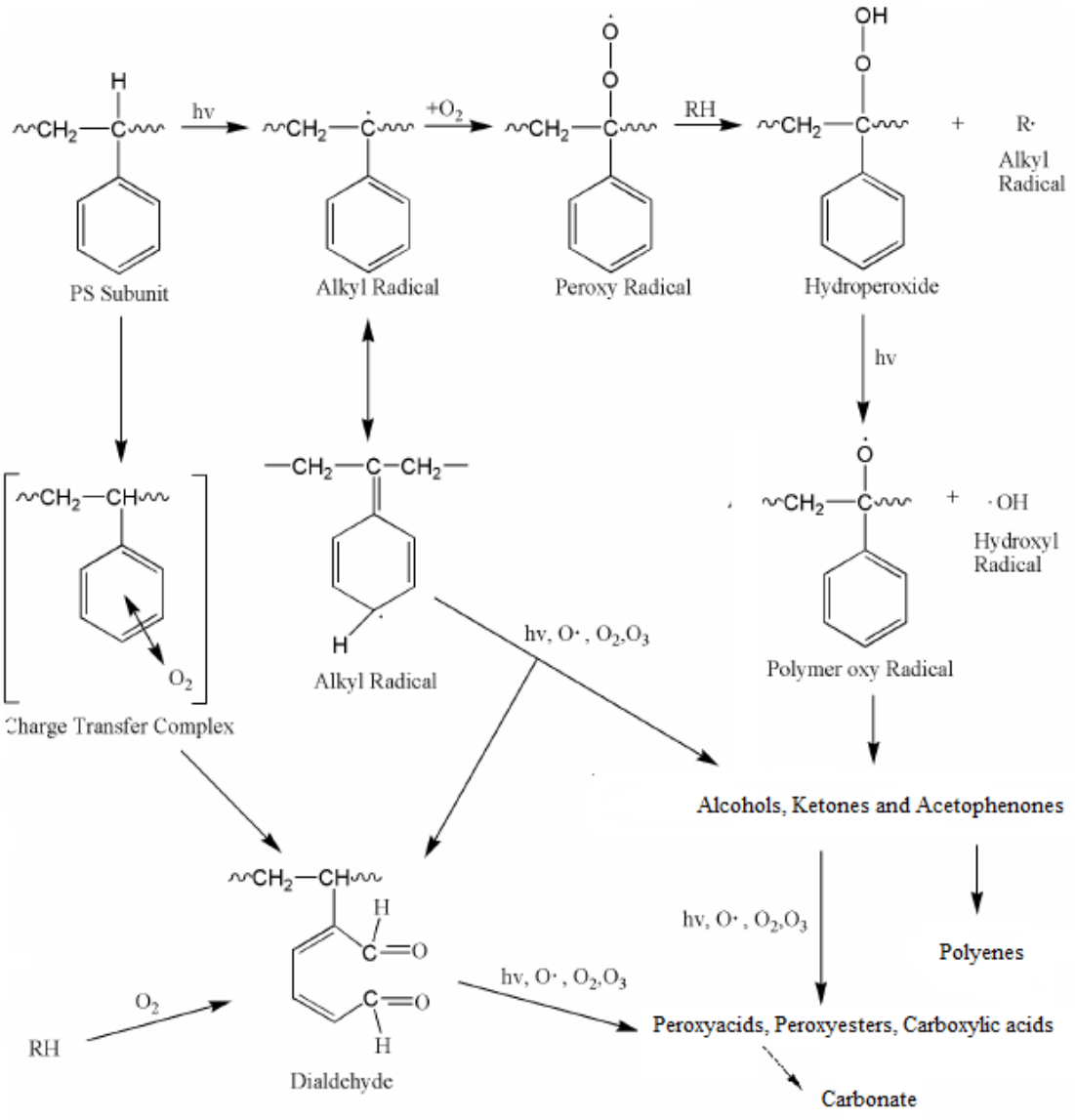

Figure 2. 5 A summary of some of the possible reactions happening in the surface of polystyrene during the process of photo-oxidation (Mitchell, 2006b, Clark and Munro, 1984, Rabek, 1995, Cataldo, 2001, Shard and Badyal, 1991a, Browne, 2001).

Ozone is naturally produced in the upper atmosphere at altitudes of 20-50 km or formed by the reaction of high energy particles and radiation (Cataldo, 2001). UV/Ozone have been used to modify the surface chemistry and improve the surface wettability of a number of polymers such as polystyrene, polyethylene, polypropylene, poly ethylene terephthalate (PET), poly ether ether ketone (PEEK) and poly vinyl fluoride. UV/Ozone treatment is a promising method to modify the surface properties to be more biocompatible which can promote cell proliferation without damaging the bulk properties (Bullett et al., 2004, Davidson et al., 2004, Teare et al., 2000b, Poulsson, 2007a).

UV/Ozone has been successfully used to promote cell attachment and proliferation on polymer surfaces with different cell types and has also been used as the first step in grafting biomolecules. Teare et al. had used the UV/Ozone method to modify standard untreated polystyrene cell culture dishes to promote cell proliferation, their results showed that cell adhesion occurred much faster for oxidized surfaces rather than the untreated ones (Teare et al., 2000a), they also investigated a range of cell lines on UV/Ozone treated polystyrene dishes with and without serum, they found that cells adhered to the surface in the absence of serum which is a direct correlation between the surface free energy and surface chemistry of the UV/Ozone treated polystyrene substrate and the rate of cell attachment. Similar result was measured by Poulsson and her colleagues, the overall human primary osteoblast-like (HOB) cell attachment, functionality and mineralization were found to be enhanced on the UV/Ozone treated ultra-high molecular weight polyethylene surfaces compared to untreated (Ammar et al., 2009).

UV/Ozone treatment can also be used to sterilise in various industrial products such as foods and cosmetics, UV/Ozone sterilization technology is widely used to overcome the old heat sterilization. By exposing food to high temperature, only the surface of foods is sterilised and also deteriorates the quality of foods. UV light could destroy DNA of microorganisms leading to disinfection of microorganisms on surfaces. (Yasuda et al., 1994, Kwok et al., 1997, Dhathathreyan and Maheshwari, 2002). As the treatment itself does not require vacuum apparatus or sophisticated gas handling equipment, it is a very cheap and easy way to control the surface oxygen levels of polymer substrates. Overall, many previous studies had shown that surface energy will be increased by the time of UV/Ozone treatment leading to improve the surface printability, physical adhesion and biocompatibility.

2.7.3 Plasma surface modification

Plasma surface modification is known as a unique method to modify the materials surface property of the materials, such as hardness, corrosion resistance, tribiological, chemical and physical properties without affecting the bulk attributes (Sawin, 1985, Chan and Ko, 1996, Chu et al., 2002). Nowadays, many new innovations of medical products, materials and surgical procedures involve polymeric or metallic devices must meet certain clinical and cost limitations. Chief among these pressures is to improve the biocompatibility between the physiological environment and the biomaterial surfaces. For coronary implants, the surface comes in contact with blood or protein requiring special modification to meet the requirement of biocompatibility. Monomers such as amine, carbonyl and carboxyl functional groups can be attached to the biomaterial surfaces by plasma modification; amine groups can act as hooks for anticoagulants and reduce the thrombogenicity.

Plasma is partially or fully ionized gas containing electrons, ions, and neural atoms or molecules, also known as the fourth state of matter (Egitto and Matienzo, 1994). This technology is widely employed in different fields of research including microelectronics, metallurgy, polymer engineering, biomedical engineering (Mendon et al., 2008) etc. Several of the largest manufacturing electronics industries use a plasma-based process such as plasma etching and plasma-enhanced chemical vapour deposition. There are various ways of producing plasma sources. Electron separation form atoms or molecules in the gas state or ionization to produce plasma (Chu et al., 2002). Ionization will only happen when an atom/molecule gains enough energy from an outside excitation source or via interaction (Pethrick, 1996). The most common ones are gaseous (radio frequency glow discharge plasma, electron cyclotron resonance, corona discharge plasma and atmospheric arc plasma), metallic and laser-based plasma sources (Sawin, 1985, Morita and Hattori, 1985).

There are various methods of plasma surface modification techniques such as plasma etching, crosslinking, deposition and functionalisation as shown in Figure 2.6 (Shrauner and Jagannathan, 2002, Sharma and Barthwal, 2008, Mousinho et al., 2004) (Xu et al., 2009).

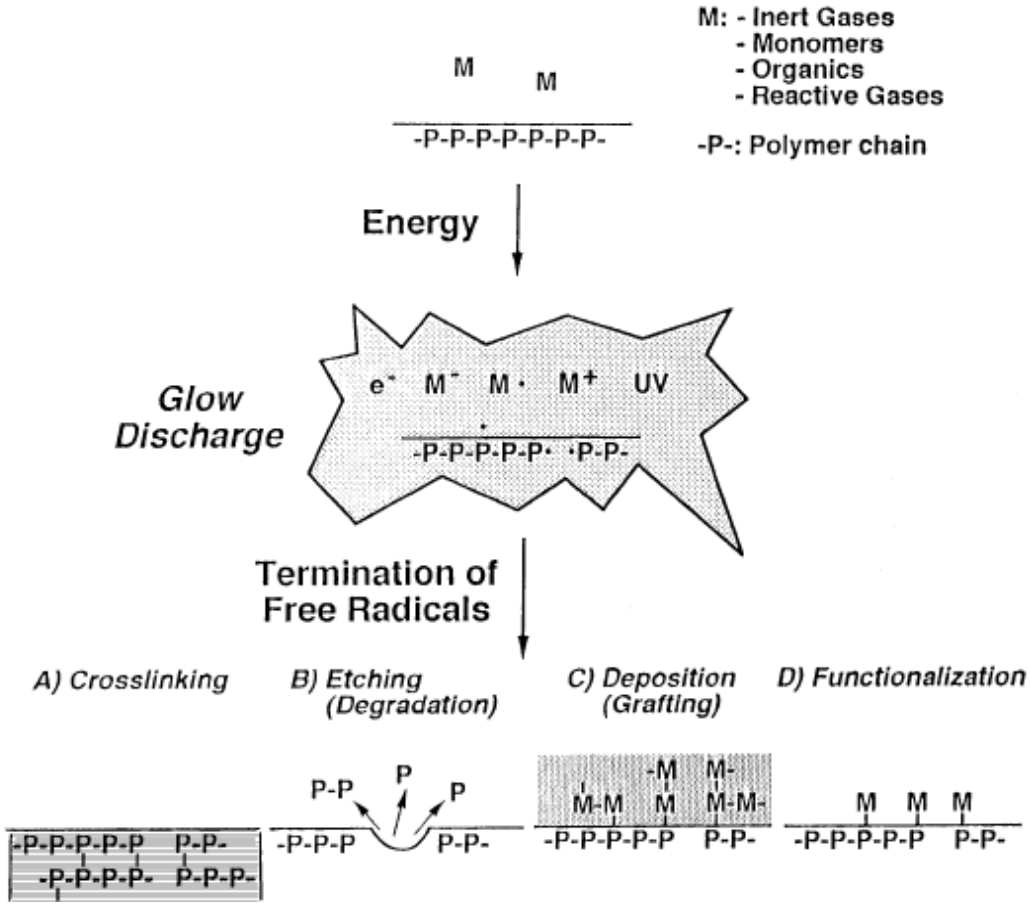

Figure 2. 6 Schematic of the reaction mechanisms of plasma surface modifications, adapted from (Tirrell, 1996).

Sputting or etching is the ability of the plasma process to break covalent bonds in a polymer through bombardment with high-energy particles (Cardinaud et al., 2000). During the process, the substrate is under a negative voltage and an argon plasma is generated, then the electric field forces the ions accelerating towards the substrate. The argon ions are not able to go very deeply into the substrate because the energy is very low and a big part is transferred to the surface atoms via elastic and inelastic collisions (Chu et al., 2002). This technique can be used as the pre-treatment for plasma implantation and deposition (Dupont Gillain et al., 2000).

Plasma immersion ion implantation also known as PIII is developed as an alternative to conventional line-of-sight ion beam implantation (Sharma and Barthwal, 2008). The plasma formed at the treatment

chamber is utilized directly to conduct ion implantation rather than using an ion extracted beam. During the process, the substrate is placed in the chamber and immersed in the plasma with high negative pulsed voltage to the sample stage. Positive ions in the plasma are accelerated towards the substrate surface resulting in ion implantation (Brandley et al., 1987). It is used widely to modify the surface of metals to improve mechanical properties such as hardness, friction coefficients, wear resistance and corrosion resistance (Chen et al., 2008, Fernández et al., 1996).

Plasma deposition is widely used in coating thin films; the advantages are low cost and uniformity. Moreover, it can be used to coat different types of surfaces such as polymers, metals and attach specific proteins. For biomedical applications, plasma polymer deposition is of great scientific strategy to control the surface chemistry for tissue engineering and also the corrosion protection of automotive components (Wu and Thiagarajan, 1996). The plasma vapour deposited coating protects the substrate which could be damaged in the biological environment and could also stop the substrates leaching. It is reported that plasma deposited acrylic acid coating on poly ethylene terephalte (PET) substrates enhanced the 3T3 murine fibroblast cells adhesion and growth compared to uncoated surface (Lüscher and Barton, 1997, Detomaso et al., 2005). Similar results were demonstrated by Gignate et al. who grow mesenchymal stem cells (MSCs) on acrylic acid coated surfaces (Gigante et al., 2008). The *in vitro* biological cell response was also compared to MG-63, a line derived from human osteoblasts which are commonly used to test the biocompatibility of materials for the application of bone tissue engineering, both results showed satisfactory compatibility and modulatory effects which may have a potential in 2D or 3D scaffolds for bone tissue reconstruction (Griffioen and Molema, 2000). The treatment can also allow surfaces to be patterned with spatial resolutions of less than 5 μm (Mitchell et al., 2004b).

2.7.4 Biological surface modification

Cell adhesion is very important in tissue engineering research. Cell surface receptors and cell adhesion proteins bound to the material surface determine the interaction between the cells and material, biological surface modification can maintain the mechanical properties of the material and also improve the surface biocompatibility instead of developing new materials. A common strategy to modify polymer surface is to coat substances that has the desired biological properties via physical adsorption, for example, fibronectin (Fn) is a cell adhesive protein found in extracellular matrix (ECM) which improves biocompatibility and cell adhesion (Zhang et al., 2009).

As a well-known efficient anticoagulant, heparin is a heterogeneous compound with an average molecular weight of 15,000 Da and a range of 3000-30,000 (Friedrich et al., 1998). Heparin is a kind of sulfated polysaccharide that consists of sulfonic, sulfoamino and carboxyl groups. The combination of coagulation factor and anticoagulation factor could be catalysed by the heparin molecules that play a vital role in the process of blood (Ton-That et al., 1999). Heparin is widely used to prevent thrombus formation if the concentration of heparin is sufficiently high (Geuskens et al., 1978b). However, after incubation in plasma or blood, the release rate of heparin from the surface decreases rapidly, usually after 1-24 hour, no heparin release can be detected while in clinic use often require a couples of day to a week. As a result the activity of immobilized heparin can be significantly reduced compared to unbound heparin (Hinrichs et al., 1997). Hinrichs and his colleagues designed a heparin release system where the release rate remains constant for a prolonged period of time and the release rate can also be adjusted by immobilized heparin onto a porous substrate that provides more surface areas via hydrolysable bonds (Hinrichs et al., 1997). Despite over 70 years of effective clinical use of heparin, lepirudin (Refludan, Berlex Laboratories, Wayne, NJ) and argatroban (Glaxo SmithKline Pharmaceuticals, Research Triangle Park, NC) are considered as alternatives with better biological variability and immunogenicity (Mureebe, 2008).

Albumin is water soluble protein that is found in numerous forms in nature. In the human body, albumin is the most abundant protein present in the blood which plays vital role in transporting all kinds of substances such as hormones and drugs through the blood also delivering essential fatty acids to the muscle tissue and regulates the process of osmosis. It is known that the adsorption of albumin on the surface of biomaterial can prevent other proteins causing thrombus from adsorbing at these sites in clinical situations. Chang et al. suggested to coat albumin as a way to prevent surface induced thrombosis (Chang, 1974). Several ways could be used to coat albumin on the polymer surface. Physical adsorption can be used to form an albumin layer, enhancing the albumin affinity of the surface by grafting long chain carbon molecules, cross-linking of the adsorbed albumin with glutaraldehyde and photografting of albumin onto the surfaces (Strobel et al., 1995). In the long term, thrombogenic proteins in blood can displace albumin from the surface to create a favorable environment for platelet activation (Amiji and Park, 1993), therefore, albumin has to be covalently bonded to the surfaces to maintain the biocompatibility effects.

Fibronectin (Fn) is a high molecular weight around 440k Da glycoprotein of the ECM binds to integrin which is a membrane spanning receptor protein (Deng et al., 2009). It is believed that Fn is a key factor involved in cell adhesion, migration, growth and differentiation and also plays a vital role in wound

healing and embryonic development (Liu et al., 2011). There are varieties of pathologies such as cancer and fibrosis related to the altered Fn expression, degradation and organization (Shao et al., 2001). Poot and his colleagues used polyethylene as a substrate bound Fn to evaluate the cell adhesion and proliferation. They founds that a good spreading and proliferation of human endothelial cells were only found on PE precoated with Fn or PE in which Fn was indirectly bound by a monoclonal antibody. The result showed that Fn bound to a solid substrate could provide a biochemical signal necessary for the process of cell proliferation (Ferreira et al., 2005).

2.8 Surface characterisation analysis

Several surface analytical techniques can be used to characterise the effects caused by UV/Ozone treatment on polystyrene surfaces. The following techniques were used in this study: X-ray photoelectron spectroscopy (XPS), contact angle and atomic force microscopy (AFM). An overview of the techniques used in this study is shown in Table 2.3.

Technique	Principle	Use and depth
X-Ray Photoelectron Spectroscopy (XPS)	Incidents X-rays liberate core-level electrons, where binding/kinetic energy depends on the atomic orbital within parent atom and chemical milieu of atom.	High resolution technique, identifies surface composition of all elements at the surface exceeding 0.1 atomic % expect H and He, depth of 1-10nm.
Contact Angle	The angle of a three phase line between solid surface, liquid and vapour in equilibrium.	Measure of surface wettability, easy method to characterise aqueous-biomaterials interfaces, depth 0.2-1 nm.
Atomic Force Microscopy (AFM)	Surface topography imaged by induced deflection of a cantilever, this is measured by reflected laser light and a photodiode.	Quantitative 3-D images, showing surface properties like roughness, friction, elasticity and hardness, depth resolution 0.1nm, shows the outermost atomic planes of a surfaces.

Table 2.2 An overview of the surface characterisation techniques used in this study.

2.8.1 X-ray photoelectron spectroscopy (XPS)

XPS is widely used for surface chemistry analysis on polymer materials (Clark et al., 1974b) (Clark and Dilks, 1979, Clark and Harrison, 1981b) and is one of the most powerful characterisation techniques for the quantitative analysis of chemical surface composition (Briggs, 1990). XPS mainly consists of three components: the X-ray generator, the energy analyser and an electron detector which are all maintained at ultra-high vacuum (UHV) chamber. Figure 2.7 shows a schematic of the Kratos Axis His photoelectron spectrometer used throughout this work.

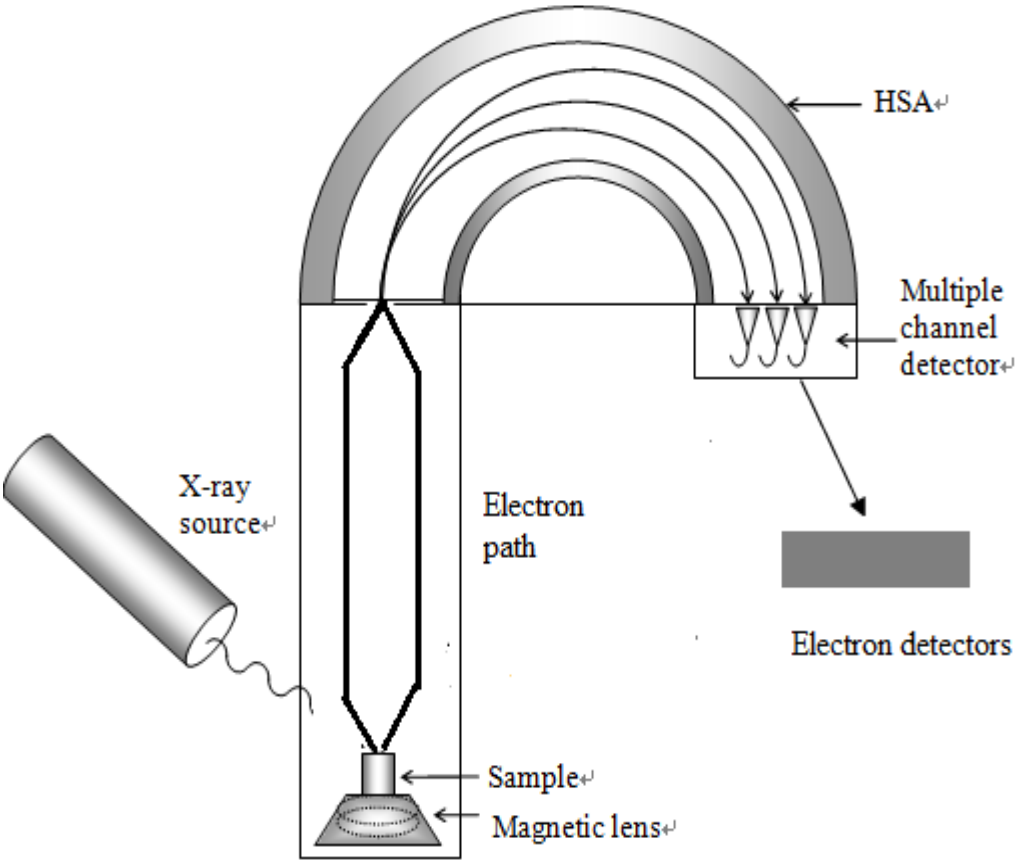

Figure 2. 7 Schematic view of the Kratos HSi photoelectron spectrometer fitted with X-ray source, a hemispherical analyser and a multiple channel detector (Osbeck, 2011).

A sample is irradiated in UHV with X-ray and the interactions between an X-ray photon and an inner-shell electron causes a complete transfer of the photo energy to the electron, which then has enough energy to leave an atom and escape from the surface. This process happens in a UHV chamber in the

range of between 10^{-8} to 10^{-10} millibar. The reason to operate under UHV is due to low energy electrons which are easily scattered by residual gas molecules, it would result in a decrease in intensity and increase the noise within the spectrum (Briggs, 1990).

Two criteria must be satisfied for XPS anode material to generate X-ray. Firstly, the material is able to emit X-rays with enough energy to induce photo-ejection of core level electrons from all elements in the periodic table. Secondly, the anode material must produce a natural X-ray line width to avoid excessively broadening the resultant spectrum. Aluminium and Magnesium with AlKα and MgKα photons of energy 1486.6 eV and 1253.6 eV respectively, are the most common anode material used (Barr, 1994).

Monochromation was used to reduce the amount of photoelectron spectra other than from Kα 1 and 2 X-ray lines. The X-rays emitted from a material not only consist of Kα 1 and 2 but also other low intensity satellite lines, such as Kα 3, Kα 4 and Brehmsstrahlung radiation, which is produced when a charged particle like an electron decelerates. The only selection of Kα 1 and Kα 2 X-ray lines can be achieved by dispersion of X-ray flux by diffraction by a crystal (Van Grieken and Markowicz, 2001).

Charge compensation is applied to sample charging though a low energy electron flood gun when a monochromated source does not generate low energy electrons. The monochromated X-rays bombard the sample and the photoelectron spectrum emitted from the sample is entered into the concentric hemispherical analyser (CHA) which increases the resolution of the electron spectra.

XPS is concerned with the photoemission form a core level by an X-ray photon of energy in the range of 100-2000 eV. The binding energy of the electron can be calculated by the Equation 2.25.

$$E_{binding} = E_{photon} - E_{kinetic} - \Phi \qquad \text{Equation 2.25}$$

Where $E_{binding}$ is the energy of the electron emitted from one electrom configuration within the atom, E_{photon} is the energy of the X-ray photons, $E_{kinetic}$ is the kinetic energy of the emitted electrons, Φ is work function which depends on the sample and the spectrometer. This equation assumes that the photoemission process is elastic because of no loss of the energy, thus each X-ray will give rise to a series of photoelectron peaks that reflect the discrete binding energy of the electrons present in the sample surface under consideration.

Multiple channel detectors are used to detect the electron spectroscopy. These are cone like openings and a tube of high resistivity, semi-conducting glass with a high secondary electron emission coefficient. The input end of the tube is at ground or some low positive potential while the output end is at a high positive voltage. The incident electrons hit the wall of the cone and create a cascade of secondary electrons. These electrons are accelerated down the channel by the positive bias and in turn hit the wall of the tube and create more electrons. A charge collector is fitted at the end of the tube which can achieve a gain of 10^8.

The spectrometer in XPS can be manipulated by using a different range of pass energies. Two types of scans can be performed: survey scans and narrow scans. A survey scan can be performed using high pass energy across all the kinetic energies in short time. In the survey scan, a large transmission is allowed in the analyser but with relatively low resolution. To perform a narrow scan, small pass energy is used and the resolution is improved with the increase of the dwell time. Narrow scans are normally operated to apply the detailed chemical shift information.

The kinetic energy of photo-emitted electrons can be influenced by the chemical environment of an atom. A non-equivalent atom of the same element is a solid arise core level peaks with different binding energy (Siegbahn et al., 1967). The binding energy varies related to whether an electron is withdrawing or donating a chemical group is bonded to an atom. These changes are known as chemical shifts and have been well documented on many polymers and compounds since 1970s (Clark et al., 1974a, Clark, 1977, Clark and Harrison, 1981a, Beamson and Briggs, 1992). Examination of the C1s peak position to the saturated hydrocarbon can be used to determine the nature of the examined surface. Table 2.4 shows the review of chemical shifts as a result of the oxygen functional groups.

Functional Groups	Chemical Shift of Primary C1s (eV)	Chemical Shift of Secondary C1s (eV)	Average Shift
Hydrocarbon **C-C/C-H**	**No Shift**	**285.0**	**No Shift**
Alcohol/Ether **C-OH/C-O-C**	**1.1 – 1.7**	**0.2**	**1.5**
Carbonyl **C=O**	**2.8 – 3.8**	**0.4**	**3**
Carboxyl/Ester **O-C=O**	**3.5-4.3**	**0.4**	**4.2**
Shake-up satellite **π-π***	**5.7-6.2**	**7**	**6**

Table 2.3 Binding energy shifts as a result of various oxygen functional groups (Beamson and Briggs, 1992, Li et al., 2005a, Davies et al., 1989, Vandencasteele and Reniers, 2010).

Shake-up satellites are a result of the outgoing photoelectron which simultaneously interacts with a valence electron and excites it to a higher energy level. The electron energy is slightly reduced transition, which leads to the appearance of satellite structures at a higher binding energy than the core level position. Aromatic shake-up peak can indicate the amount of atomicity in polymer surfaces. A certain proportion of electrons that are emitted from aromatic rings and unsaturated conjugated polymer regions have a reduced kinetic energy. This is due to the fact that when they were emitted, part of their photo energy was transferred to other electrons within the aromatic ring or conjugated component of the polymer (Rivière and Myhra, 1998).

2.8.2 Contact angle and surface energy

The measurements of contact angle and surface energy are very useful for generating information about the outer atomic layers of a materials surface. As shown in Figure 2.8, contact angle is referred as the angle of a three phase line between a solid surface, a liquid and a vapour in equilibrium. It has been used extensively as a simple and fast technique to determine the wettability of the surface (generally referred as hydrophobicity/hydrophilicity), due to the convention of probing a solid surface in air using water drops. This behaviour of surface wettability is known to affect many of the biological responses to the biomedical implants surfaces, such as protein adsorption, platelet activation, platelet adhesion, blood coagulation and cell adhesion properties (Xu and Siedlecki, 2007, Vogler, 1999, Lee and Lee, 1998, Faucheux et al., 2004).

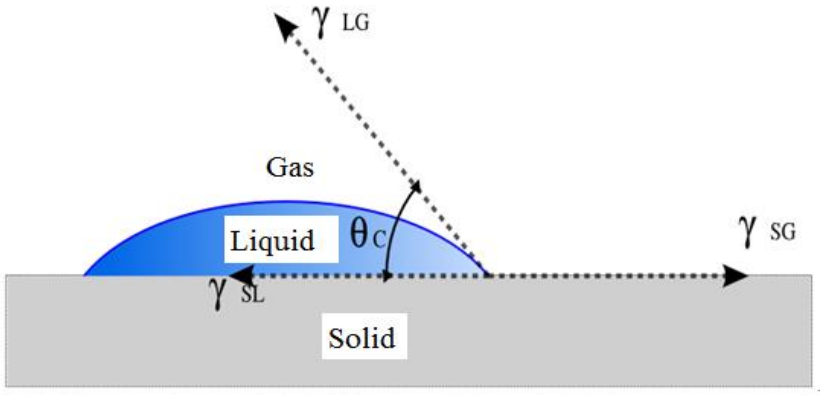

Figure 2. 8 Schematic of the contact angle measured on solid surfaces and the interfacial energy balance of the three phase line.

The measurements of contact angle can be used as a means of surface energy calculation. The surface energy is referred as the excess energy from the surface atoms, because the out layer does not have the sufficient amount of bonds to the closest neighbouring atoms. The bonds of the atoms not satisfied will lead a much higher energy state of these atoms than the internal atoms and this higher energy state is also known as surface energy. There is strong link between surface energy and surface hydrophobicity/hydrophilicity. Surface energy can be described as the interactions with many types of materials; surface hydrophobicity/hydrophilicity is only the interaction with water. A material with high surface energy can interact more with water because of the huge capacity of water for bonding. It has been reported that hydrophilic surfaces (high surface energy) are more favourable for cell adhesion and proliferation on many cell types, such as fibroblasts, endothelium and osteoblasts (Lim et al., 2008, Van Kooten et al., 1992, Dekker et al., 1991).

Thomas Young firstly described the contact angle measurement in 1805 for determining the interaction energy between a liquid and solid in presence of vapour. When a liquid drop is in contact with the surface of a solid, it interacts with the surface and stays on the surface in a shape of varying degrees as shown in Figure 2.4, and the contact angle can be measured by Young's method (Equation 2.26).

$$\gamma_{SG} = \gamma_{SL} + \gamma_{LG} \cos\theta \qquad \text{Equation 2.26}$$

The interfacial forces in the following equation: γ_{SG} (solid-vaopur), γ_{SL} (solid-liquid), γ_{LG} (liquid-vapour), θ (contact angle at the edge of the liquid drop). The angle which a drop assumes on a solid surface is the result of a balance of the adhesive force between the liquid and the solid and the cohesive forces within the liquid (Johnson and Dettre, 1969). At the equilibrium, the sum of the surface tensions in the solid plane should be zero because the liquid is free to move until the equilibrium forces are achieved. Equation 2.27 shows the change in free energy associated with the drop-particle adhesion (ΔG_{SL})

$$\Delta G_{SL} = \gamma_{SL} - \gamma_{SG} - \gamma_{LG} \qquad \text{Equation 2.27}$$

The Young-Dupre equation (2.28) indicates the free energy of the interface between solid and liquid when combing Equation 2.26 and Equation 2.27 together.

$$-\Delta G_{SL} = \gamma_{LG}\,(1+\ \mathrm{COS}\theta) \qquad \text{Equation 2.28}$$

Several methods such as sessile drop method, vertical rod method, the tilted plate method and the cylinder method are available to measure surface wettability depending on the form of the surface. For flat solid surfaces, sessile drop method is extensively used, a droplet of the liquid is allocated on the interested area of surface and the contact angle is measured through the liquid phase. The drawbacks of the other contact angle techniques are larger and often more complicated sample geometries required.

Owen and Wendt firstly described that the interfacial tension can be separated to the underlying interactions between the molecules. They assumed the division of the total surface energy of a liquid or a solid into two, a dispersive force and a polar component, and they proposed that the polar interactions occurred between the solid and liquid could be calculated by a geometric mean expression of the following equation.

$$\gamma_{SL} = \gamma_S + \gamma_L - 2(\gamma^d_S \gamma^d_{LG})^{1/2} + 2(\gamma^p_S \gamma^p_{LG})^{1/2} \qquad \text{Equation 2.29}$$

In the Equation 1.35, γ_L is the surface tension of liquid; γ_S is the surface tension of solid or free energy. The d and p are the respective dispersive and polar components.

By combining Equation 2.28 and Equation 2.29 together, into a new equation (2.30), it is possible to characterise the surface free energy (dispersive and polar component) from the measurement of contact angles using two different liquids (Owens and Wendt, 1969).

$$\gamma_{LG}\,(1+\ \mathrm{COS}\theta) = 2(\gamma^d_{sL} \gamma^d_{LG})^{1/2} + 2(\gamma^p_{sL} \gamma^p_{LG})^{1/2} \qquad \text{Equation 2.30}$$

2.8.3 Atomic force microscopy (AFM)

The first AFM was invented by Binnig and his colleges in 1986 (Binnig et al., 1986) based on the success of scanning tunnel microscopy (Turner et al., 2007). It can produce three-dimensional images of solid surfaces at very high resolution (atomic level) and can also provide non-conducting samples compared to scanning tunnelling microscopy (Kada et al., 2008). Neither a vacuum environment nor any special sample preparation is required and can work in ambient or liquid environment.

AFM can measure not only the changes in surface topology but also the frictional force on an atomic scale. This is one of the most important requirements for analysing the modified material surfaces. AFM was firstly used to characterise the surface in 1986 and offers the ability to perform high resolution of surface morphology and nanostructure, studies of local material properties, compositional mapping of heterogenous samples and probing of sub-surface sample structure (Binning et al., 1986). Large information on a variety of polymer types has been established via AFM studies of polymer topology, nanostructure and also molecular order (Magonov and Heaton, 1996, Magonov and Reneker, 1997). Quantitative information can be collected using AFM on surface roughness, height, diameter and volume distribution of grains and features of the surfaces, depths of holes, scratches and cracks. Other surface information such as mechanical adhesion, hardness, friction and elasticity can also be given by AFM. Furthermore, AFM can be used to measure the modified surfaces changes like passivation, polishing and sterilisation (Dhadwar et al., 2003, Aime et al., 1994, Raghavan et al., 2000). By increasing the tip sample forces, plastic deformation and non-indentation of polymer materials can be also studied.

The principle of AFM is quite simple. A sample is probed by a sharp tip made of Si_3N_4 or Si mounted (Dupont Gillain et al., 2000) on a cantilever which moves across the surface of a sample in a raster scan as shown in Figure 2.9. The interaction force between the cantilever tip and the surface is determined by measuring the deflection of the cantilever. Deflections of the cantilever are reported by a reflected laser beam to a multi segmented photodiode. The amounts of light reaching each of the segments of the photodiode can be compared and used to generate a deflection voltage signal. Finally, the deflections are converted by photoelectric circuitry into height information and become as a digital image (Kada et al., 2008).

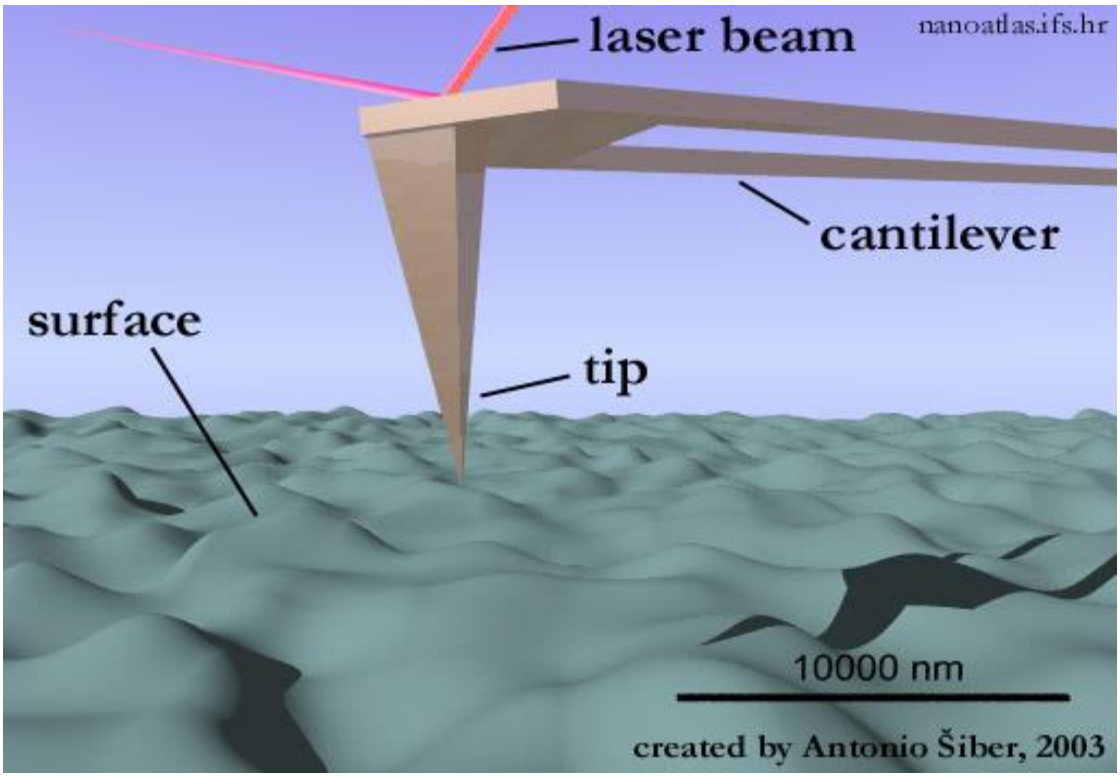

Figure 2. 9 Schematic 3D representation of AFM principles, adapted from (Siber, 2003)

There are two main modes of operation in AFM: contact mode and tapping mode, and both methods can be operated in air or in a liquid condition (Dvir et al., 2006, Sokolov et al., 1997, Samyn et al., 2010). In contact mode, the tip and the sample are in contact during the scan as the name suggested. The tip is raster-scanned across the surface of sample in x-y plane and a feedback system is used to maintain a constant force between the force and surface. One of the disadvantages of this mode is that shear forces may exist on the sample surface during imaging as the tip is dragged over the sample (Boussu et al., 2005). The tapping mode is developed to solve the problems of damaging the sample surface when examining soft materials such as biolayers (Simon and Durrieu, 2006). In the tapping mode, a cantilever oscillates with a high amplitude and the tip is in contact with the sample surface in every vibration period. The tapping mode can produce high resolution images both in air and fluid without inducing destructive frictional forces. The tips only tap the surface so the interactions are reduced greatly (Meyers et al., 2009). The tapping mode was used to investigate the surface topographic changes induced by UV/Ozone treatment in this study.

2.9 Cardiovascular diseases

In the UK, coronary heart disease is the leading cause of death, affecting approximately 2.7 million people with the condition and about 8.2 x 10^5 deaths each year. It is suggested by National Health Service that the disease is more frequent in male than female before the age of 50 and the chance of developing the disease occur similar after (NHS, 2012). The accumulation of plaques composed of collagen, fatty deposits and overgrowth of smooth muscle cells, on the walls causes the arteries to become narrow and blocks the flow of the blood to the heart, this process is known as atherosclerosis and a diagram is shown in Figure 2.10. The use of pharmacological intervention can reduce the symptoms of coronary heart disease such as the administration of low-dose aspirin, statins, beta blockers, nitrates and anti-arrhythmic medication (Leor et al., 1999).

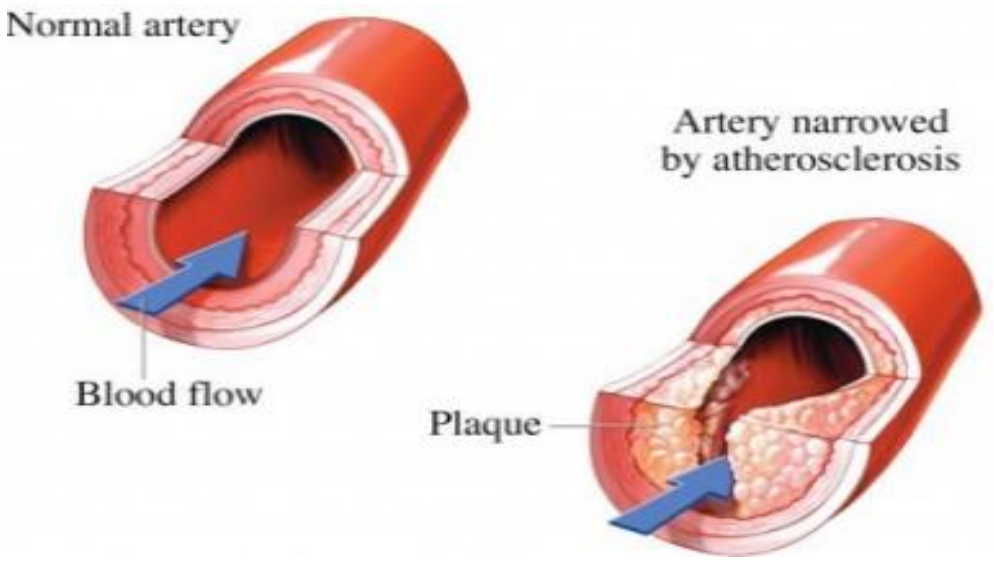

Figure 2. 10 Comparison of normal artery and an dysfunctional artery caused by atherosclerosis (Nucleus-Medical-Media, 2013).

However, if the symptoms cannot be controlled pharmacologically then surgical intervention may be required. This may include the use of coronary bypass surgery, angioplasty, stenting, the implantation of pacemakers and valve replacement as the main procedures. Taking endovascular stent for an example, a coronary angioplasty is one of the surgical operation procedures, which allows the blocked and narrowed arteries to be widened to improve blood flow. It is also known as percutaneous transluminal coronary angioplasty or percutaneous coronary intervention with approximately 70,000 coronary angioplasties

being carried out each year in the UK (Kelly et al., 2008). After the angioplasty, a bare metal stent (BMS) is placed in the blocked blood vessel. A stent is a small wire metal mesh used to re-open the artery. As shown in Figure 2.11, a balloon catheter is guided into the blocked site of the artery; the balloon is inflated to expand the stent to form a scaffold, which can push the plaque up against the wall. Once the stent is deployed, the balloon catheter is removed. However, the failure of these biomedical implants is related to restenosis, a process which may be due in part to the poor hemocompatibility resulting by non-optimised surface or toxic ions such as Cr, Ni, Co released from BMS (Qi et al., 2013b). It is reported that about a maximum of 25% of the patients suffered restenosis within six months (Dangas and Kuepper, 2002). The introduction of drug eluting stent (DES) had significantly reduced restenosis and the repeat revascularisation compared with BMS as much as 70% since 1994 (Mani et al., 2007). Similar to BMS, DES is made of metal as backbone, an antiproliferative drug such as paclitaxel and sirolimus, for inhibition of excessive cell growth, and drug carrier made by polymers for releasing the drug.

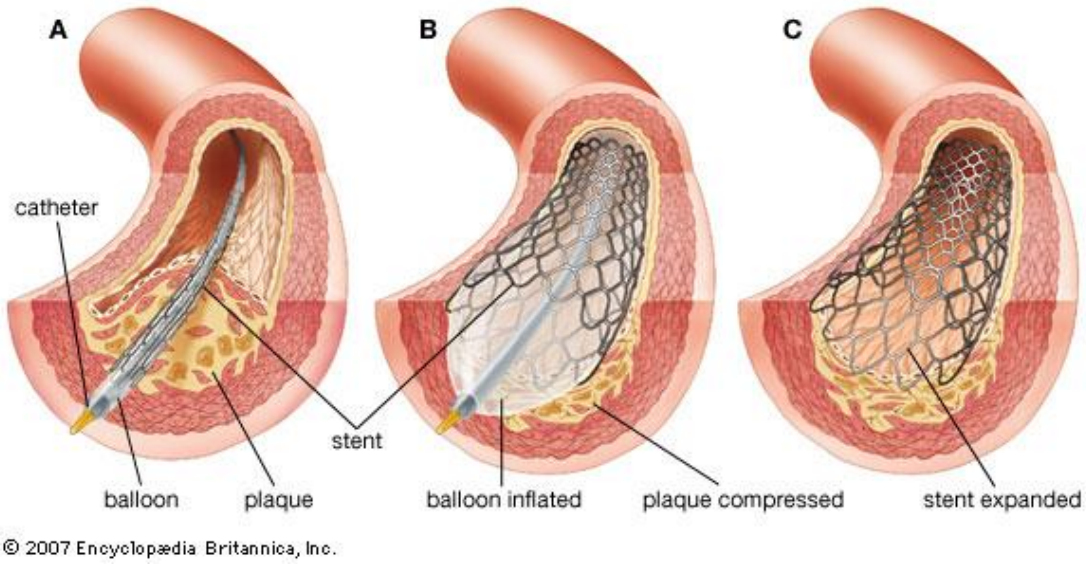

Figure 2. 11 The process of coronary stent procedure. A) A cardiac catheter, encased in an inflatable balloon and a wire mesh stent is placed to the obstruction where blocked by atherosclerotic plaque. B) The wire mesh stent is expanded and compressed by the inflated balloon. C) Balloon on the catheter is deflated and removed from the obstruction and the stent is left to expand against the narrowing site.

Despite the success of DES compared with BMS, a number of clinical trials reported late stent thrombosis and delayed endothelialisation due to long-term safety and efficacy (Mani et al., 2007). The key trigger lies on stent is a foreign object within the vessel and hereby another approach to overcome this issue is

the design of the biodegradable stent. After 3-6 month of the biodegradable stent implanted, the block site will be reopened and reorganised by stabilising function of the stent, and then the stent is degraded or absorbed following the healing process (Snyder and Helmus, 2004, Erbel et al., 2007). These stents are made by either polymers such as poly lactic acid, poly glycolic acid, poly caprolactone, or metals (Mg based or Fe based alloys) (Venkatraman et al., 2008). Stack and his colleagues developed the first biodegradable stents made of poly (L lactic acid) and implanted to canine model; their result was encouraging and showed that occurrence of very limited thrombosis in 18 months (Stack et al., 1988). Biodegradable stents made by metal seem to be more promising, Biotronik presented at the EuroPCR conference 2011 for the clinical result of first biodegradable stent implanted in human, the result showed no cardiac death, no target vessel myocardial infarction and stent thrombosis were observed within the first 6 month, the restoration of vasomotion and the return of natural vessel angulation at both 6 and 12 month suggested a real restoration of the vessel's nature structure (Haude et al., 2013).

Another approach in vascular stent technologies is achieving the appropriate interactions with proteins and cells so as to get rapid coverage with endothelial intima cells whist preventing the over growth of smooth muscle cells and fibroblasts resulting in intimal hyperplasia. A common approach to avoid the issue is to seed the material surface with autologous endothelium and implant back to the human body. There are two commonly used ways to seed the implant surfaces; the first method is to seed the surface with a solution of cells and the second method is to precondition under the flow followed by the first methods. The prior method is not promising as there is poor formation of a confluent endothelium monolayer and low endothelium retention rates when firstly introduced, however, it is improved by surface coating techniques, change of ECM composition and geometry (Schneider and Dichek, 1997). The latter is suggested to form a confluent endothelium monolayer with satisfactory endothelium retention rates by precondition the seeding under flow induced shear stress (Kloner, 2009).

2.10 Cell proliferation

Cell division and cell differentiation are the two fundamental processes for the development of an organism in the body. In order to maintain the normal function within the body, both of these pathways have to be rigorously regulated and coordinated. The understanding of the molecules that orchestrates the cell cycle is important in order to identify the mechanisms to control the formative pathways.

Cell cycle can be described as the stages of a eukaryotic cell for division from the time it is created from a parent cell to mitosis stage as shown in Figure 2.12. During this sequence of stage, the chromosomes are duplicated by a parent cell and then rise to two identical cells with the same DNA content. There are four distinct phases involved in cell cycle: gap phase one (G_1 phase), DNA synthesis phase (S phase), gap phase 2 (G_2 phase), and mitosis phase (M phase). G_1 phase is the first phase within interphase, a drastic increase in RNA and protein occurs during the G_1 phase. In S phase, the DNA replication occurs and it finishes when all the chromosomes have been replicated. During G_2 phase, the formation of microtubules is involved which is necessary for the process of mitosis and the cell increases in size in order to give rise to the two daughter cells. Following G_2 phase, the cell undergoes mitosis also known as M Phase. During the prophase of mitosis, two DNA molecules disentangled and condensed to form chromosomes, the spindle apparatus has moved to opposite of the cell. In metaphase, the spindle fibres were attached to the centromeres of the chromosomes and align the chromosome at the equatorial plate. Sister chromatids are separated after the spindle fibres shorten and centromeres split during the anaphase then the chromosomes arrive at the poles of their respective spindles in the telophase. Followed by the last stage of mitosis, cytokinesis, in which splitting the daughter cells part. Alternatively cells can also enter into G_0 phase and exit from the cell cycle, it shows the fundamental step to differentiate the cell and induct gene expression leading to a specialised phenotype (Pucci et al., 2000, Harper and Brooks, 2005).

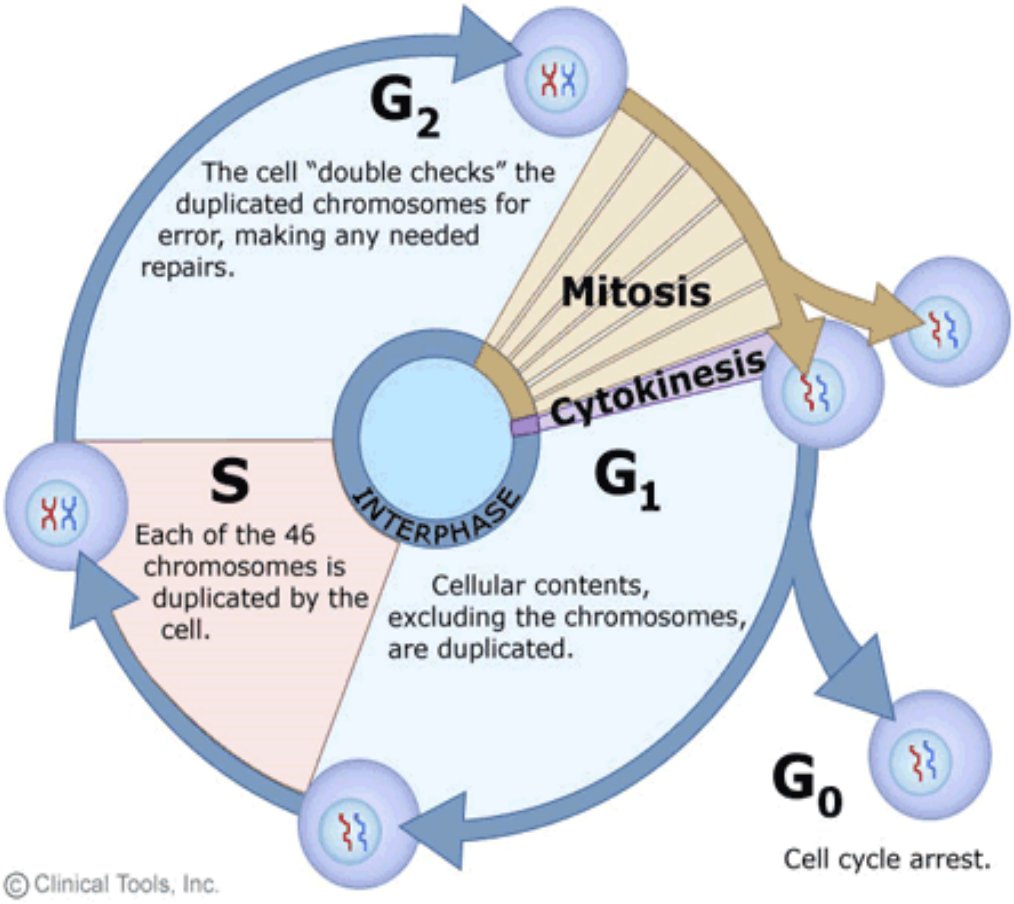

Figure 2. 12 An overview of the sequenced cell cycle event to produce two genetically identical cells from one parent cell. As showed in this diagram the cell cycle has four phases: G_1 phase to allow the cell grows and ready to synthesis DNA; Synthesis phase to allow the cell to synthesis DNA; G_2 phase to continuously growth of the cell during the gap between DNA synthesis and mitosis; Mitosis phase to produce two daughter cells with the same DNA content where the cell stops to grow at this stage. The period between mitotic divisions (G_1, S and G_2 phase) is interphase. There is also a special gap phase known as G_0 where the cells undergo quiescent or senescent to avoid aberrant proliferation from the internal and external cellular environment.

The regulation of the cell cycle progress is extremely important including the detection and repair of any damage and also the potential for uncontrolled cell division. Each molecular event of the cell cycle is ordered and directional and is not reversible. Key molecules controlling the cell cycle progress are cyclins and cyclin dependent protein kinases (CDKs) (Augustin, 2004). In 2001, L Hartwell, R Hunt and P Nurse were awarded Nobel Prize in Physiology or Medicine for the discovery of these key regulators of the cell cycle (Nobelprice.org, 2001). Cyclin molecules are proteins and found to degrade periodically during each cell cycle, this was firstly discovered by T Hunt by using sea urchins as a model system in the early

1980s and approximately 10 forms have been identified in humans. The cyclins are not enzymatic and require binding to the CDKs molecules which are also inactive without a cyclin partner. This regulates the CDKs activity in DNA replication and mitosis, and selects the proteins to be phosphorylated at specific regulatory sites.

There are several biochemical checkpoints in the cell cycle progresses, these checkpoints act as the switches to decide the condition of the cells to continue into the next stage, in another word, a cell will not be allowed to progress if it fails to meet the required condition. Alternatively, it will undergo apoptosis or enter G_0 phase (Pietenpol and Stewart, 2002, Van Vugt et al., 2005). The first switch is the G_1 phase checkpoint in which to decide the cell meets the condition to enter the DNA synthesis phase. They key event of this checkpoint is the regulation of CDKs phosphorylation on tyrosine and residues. The second switch is DNA synthesis phase checkpoint to detect any damaged DNA damage including double strand breaks and stalled replication forks. The detection can slow down the DNA replication process and it stablises stalled replication forks so that the DNA synthesis can undergo through replication after the repair. The third switch is located at the end of the G_2 phase. The cell signals the start of mitosis if pass this checkpoint. The last switch is the spindle checkpoint which plays a pivotal role in controlling duplication of centrosomes; it ensures normal chromosome segregation and avoiding aneuploidia.

2.11 Cell migration

Endothelial cell migration is essential to many pathologic and physiologic events such as angiogenesis (Zhao and Guan, 2011), tissue morphogenesis (Aman and Piotrowski, 2010), would healing (Tremel et al., 2009), embryogenesis (Viveiros et al., 2011), cancer metastasis (Steven B, 2006) and vascular graft healing (Zhang et al., 2011). There are mainly two kinds of migrations. The first is random migration in which occurs when the cell migrate independently of a gradient of a chemostactic stimulus of paracrine or autocrine nature (Mastyugin, 2004). The second is directional migration also known as chemotaxis in which the direction of the cells responds to spatial and temporal gradients and it is pivotal for many eukaryotic cell types (Rappel, 2002). The cell can transmit the signal across the plasma membrane and localize the response by only interacting with the chemoattractant in chemotaxis (Janetopoulos and Firtel, 2008).

Cell migration is a highly organised process primarily led by the actin networks located beneath the cell membrane and this event includes three general steps as shown in Figure 2.13. Firstly, the protrusion of a cell at the leading edge by polymerization of actin filaments towards the cell membrane; secondly, adhesion of the cell at the leading edge and deadhesion of a cell at the body and rear; Finally, the cell is pulled forward by the contractile force generated by the acto-myosin network.

There are various studies on the mechanisms of endothelial cell migration with controllable environment. More recently Ahmed and his colleagues used the direct imaging of fluorescent tagged cells to visualise the migration in the transgenic mice (Ahmed et al., 2002). A large number of intracellular signalling molecules have been associated with cell migration such as lipid kinases, phospholipases, MAPK cascades and scaffold proteins but the Gho GTPases was found to play a key role in regulating the biochemical pathways related to cell migration (Raftopoulou and Hall, 2004).

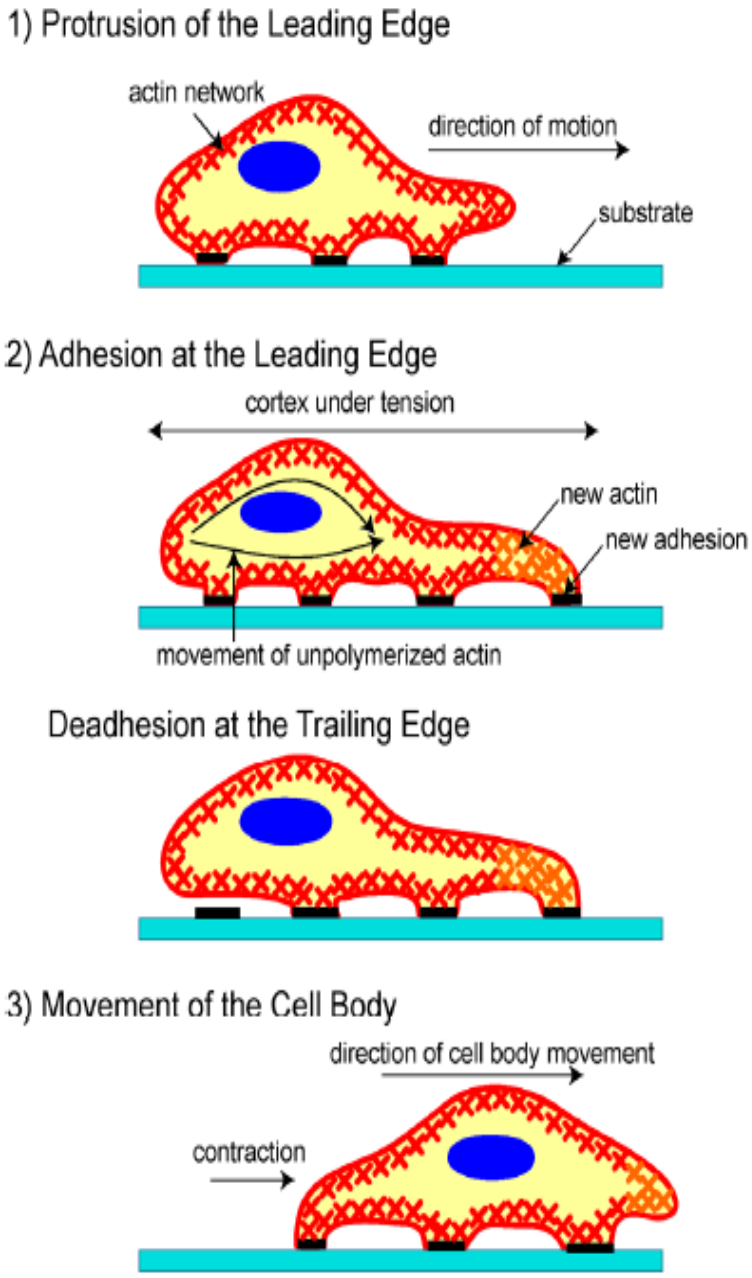

Figure 2. 13 The main events of endothelial cell migration. Protrusion of the cell at the leading edge by actin filaments polymerization once determining direction to move, then the cell adheres to the substrate at the leading edge and deadheres at the body and rear, finally the cell is puller toward by contractile force (Ananthakrishnan and Ehrlicher 2007 The forces behind cell movement).

2.12 Vascular Endothelium

After Furchgott & Zawadzki discovered endothelial-derived relaxing factor (EDRF) in 1980s, endothelial cells had been recognized to play a pivotal role in vascular homeostasis, angiogenesis, thrombosis, inflammation and repair of injured tissues (Sumpio et al., 2002). Vascular endothelium is located at the interface between blood and tissue to modulate the control of vascular function. In an adult person, the endothelium is estimated to cover 3000 m^2 of surface area and is the biggest endocrine organ weighing about 1500 grams in human body (Selwyn et al., 1997). Figure 2.14 shows the overall physiological function of the endothelium. Under basal conditions endothelium acts as a gatekeeper between the blood and tissues, and the functions include the transportation of solutes and essential nutrients across the endothelium, the maintenance of vascular tone and thromboresistant surface and the switch of different kinds of vasoactive hormones (Wu and Thiagarajan, 1996). Thus the functional endothelium is pivotal for blood flow and antithrombotic activity because of the humoral factors released by the endothelium to control relaxation and contraction, thrombogenesis, fibrinolysis, and platelet activation (Lüscher and Barton, 1997). A variety of vasoactive substances are produced and released by endothelial cells, such as prostacylin and nitric oxide which both inhibit platelet aggregation and result in vasodilation. The mediators released above respond to the chemical stimuli such as bradykinin, thrombin and other hemodynamic forces alterations like changes in blood flow or pressure (Sumpio et al., 2002). There are also phenotypic variations in response to different endothelial cell activities in the vascular tree, for example, cells in different locations between arterial and venous vessels can not only express different protein markers but also responded differently to the same stimulus (Sumpio et al., 2002).

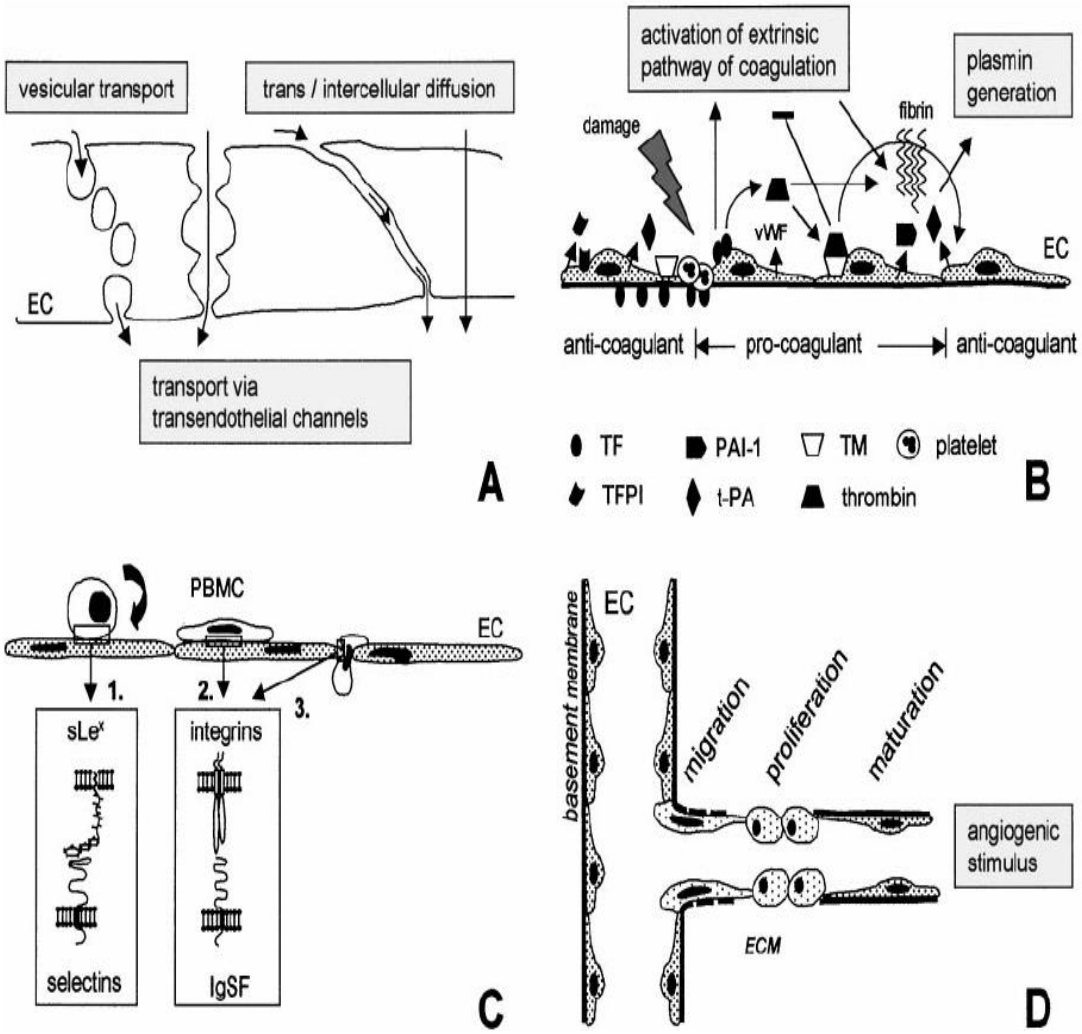

Figure 2. 14 Physiological functional integrity of the endothelium in the body. A, a semi permeable barrier is formed by the endothelium for the transportation of various peptides, proteins and other soluble molecules. B, determination of the role of endothelium in haemostatic balance and its regulation of coagulation. C, endothelium activates leukocyte and also facilitates leukocyte adhesion transmigration. D, the active role of endothelium in the process of angiogenesis. EC, endothelial cells; IgSF, Ig superfamily; PAI-1, plasminogen activator inhibitor; PBMC, peripheral blood mononuclear cells; sLe^x , sialyl Lewis X; TFPI, Tissue Factor pathway inhibitor; TM, thrombomodulin (Griffioen and Molema, 2000).

Endothelial cells have several functions in the human body and their optimal functionality is necessary to maintain normal physiological conditions, such as the control of hemostasis, exerting effects on platelets, the coagulation and fibrinolysis. Abnormal stimulation of endothelial cell activities have been associated with endothelial cell injury, dysfunction and activation to promote a prothrombotic and antifibrinolytic state and thus they are believed to contribute to a variety of human diseases including atherosclerosis (Selwyn et al., 1997), hypertension (Cahill et al., 2001), congestive heart failure (Sumpio et al., 2002), hypercholesterolemia and diabetes mellitus (Sharma et al., 2011). However the mechanisms causing endothelial cell dysfunction are not well established. Davey et al. believed that it is related to oxidative stress by the vascular endothelium which controls the passage of the circulating cells and macromolecules from blood to tissue. Reactive oxygen species can work as an indicator; they can participate in the cell growth and cell adaption responses at low concentration when cells are injured; they can also cause cellular damage or death at high concentration (Davey et al., 2010). In atherosclerosis, it is found that the formation of fatty streak and monocyte adhesion on the vessel wall is at the earliest stage. Cell dysfunction causes excessive stimulation of superoxide anions which degrades Nitric oxide (NO) before reaching the target tissues. NO plays an important role in vasodilatation and inhibits platelet adherence and aggregation, smooth muscle proliferation, and endothelial cell leukocyte interaction, therefore, the diminishing concentration of NO may be in response to the initiation and progression of atherosclerotic lesions (Poredoš, 2001).

2.13 Endothelium under flow induced shear stress

As described above, vascular endothelium plays an important role in the functioning of vascular system in human body. *In situ* vascular endothelium is exposed to a various mechanical forces such as gravitational, mechanical stretch or strain and shear stress, particularly shear stress extensively associated with blood flow (Fisher et al., 2001). The flow is the key in determining vascular pathology as it not only acts as a selective filter between the vessel wall and blood but also maintains body homeostatic functions such as homeostasis modulation, response to inflammation and regulation of smooth muscle cells contraction (Orozco and Silva, 2010, Li et al., 2005b, Barakat et al., 2006). The flow induced fluid shear stress as shown in Figure 2.15 can manipulate vascular endothelium function by the subsequent activation of mechanosensors, intracellular signalling pathways, specific transcription factors and the expression of genes and proteins (Fisher et al., 2001).

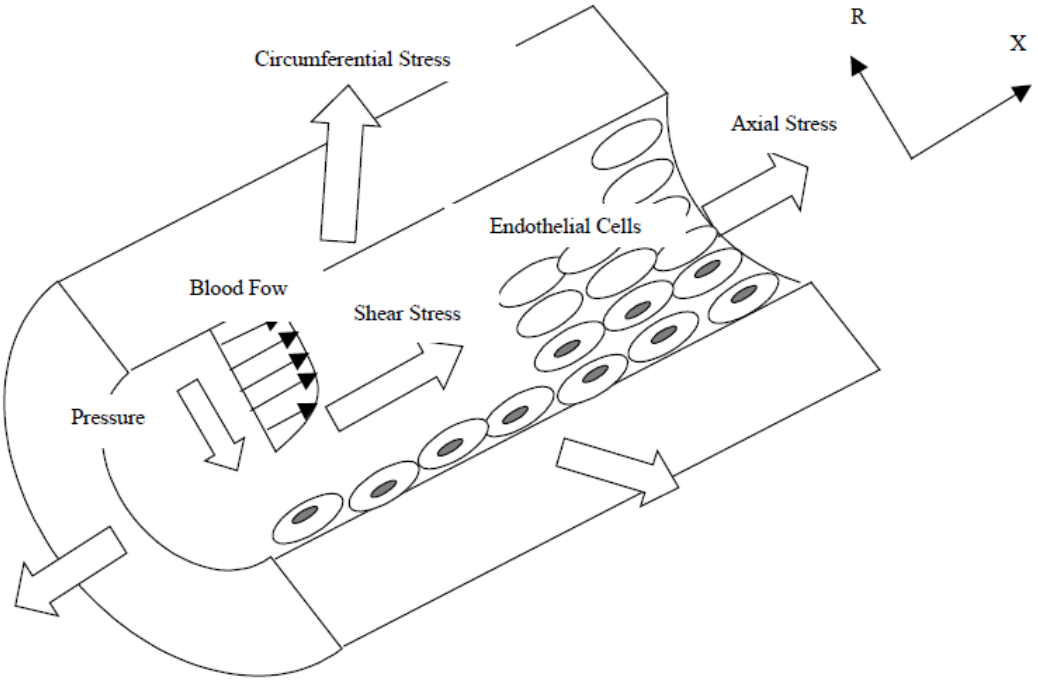

Figure 2. 15 Schematic diagram illustrates endothelium and blood flow induced shear stress in vessel wall (Arslan et al., 2010a).

Shear stress is the tangential force derived from the friction of the blood flow with the endothelium surface (Chen et al., 1999); the unit of shear stress is Pascal (Pa) or dyne/cm^2 in which 1 Pa equals 10 dyne/cm^2. Various responses are produced by static endothelium when exposed to shear stress, Barakat et al. reported that some of the responses occur within seconds of the flow such as activation of K^+ and Cl^+ channels and of guanosine triphosphate binding proteins, release of some agonists including acetylcholine, adenosine triphosphate and NO, increase in cell membrane fluidity and decrease in intracellular pH (Barakat and Lieu, 2003, Barakat et al., 1999, Jacobs et al., 1995, Nakache and Gaub, 1988, Olesen et al., 1988, Burns and DePaola, 2005, Morigi et al., 1995). The endothelium which acts as a selective barrier between the vessel wall and the blood is then active and release a number of molecules. The unidirectional shear stress applied to the endothelium surface can cause reorganization of adhesion surfaces and align with the flow direction (Davies, 2009). Even a small increase of shear stress intensity (0.5 dyne/cm^2 to 1 dyne/cm^2) can significantly affect endothelial hemostasis such as transmigration of leukocytes (Cinnamon et al., 2001). This flow induced structural alterations shows the steady shear stress

can lead to the formation of an endothelium phenotype which is believed to be resistant to atherosclerosis development (Barakat and Lieu, 2003).

The *in vivo* environment is so complicated and difficult to reproduce in an experimental setting; various models have been designed to learn the effect of the flow on endothelium based on one or multiple stimulus such as shear stress and pressure. Also the type of flow influence on endothelium, for example, steady laminar, sinusoidal and oscillatory, disturbed and turbulent flows (Helmlinger, 1991, Thoumine et al., 1995, DePaola et al., 1992, Gimbrone et al., 2000, Davies et al., 1986, Topper et al., 1996). Akimoto et al. reported that vascular endothelial cell proliferation was inhibited by steady shear stress by releasing cyclin dependent kinase inhibitor p21 and they found that the cell cycle was blocked by shear stress before entering into S phase. The exposure to shear stress caused cell population accumulated in the G_0/G_1 phase as well as a decreasing cell numbers in the S phase and G_2/mitosis (Akimoto et al., 2000). In Comparison to laminar flow, turbulent flow induces various shear stress frequencies and flow directions. Davies reported that as low as 1.5 dyn/cm^2, turbulent flow stimulated endothelial cell turnover accompanied by no cell alignment, discernible cell retraction and cell loss (Davies et al., 1986). The results from these studies demonstrate that not only shear stress affects endothelium but also that the response differs to each flow pattern.

Shear stress is the most widely studied mechanotransduction system and flow chamber is designed to evaluate the effect of the hemodynamic forces *in vitro* to mimic the condition. The devices act as a controllable *in vivo* vessel environment and require the control of flow rate to manipulate the shear stress. There are currently two main types of systems to isolate the effects of shear stress on endothelium: cone and plate and the parallel plate flow chamber. The cone and plate flow chamber was developed by Dewey et al, the chamber imposed rotation about a cone axis oriented perpendicular to the surface of a flat plate (Dewey CF, 1981, Dewey, 1984b). The parallel plate flow chamber which was used in this work has two slits on either end of the plate which creates a uniform laminar flow by pressure differential. This type of flow chamber is selected because of the practicability: the ease setup of the system and homogenous flow and stress.

Chapter 3 Materials and Methods

The interaction between the surface material of a medical device and tissue interface is dependent upon surface chemistry. It is therefore important to characterise the surface of the material and to understand its biological responses. Several methods are available for surface characterisations but the selection of the most appropriate method is dependent on the types of material and on the potential application of that material. This chapter discusses the materials, surface modification techniques; surface characterisation analysis and finally the biological responses of endothelial cells to the modified surface are also described. All the reagents and chemicals used in this work are of analytical grade and purchased from Sigma Aldrich unless indicated.

3.1 Materials

In this study, untreated polystyrene was utilised for UV/Ozone treatment, analysis and respective cell culture experiments. The polystyrene surface used throughout this study is flat and untreated with the thickness of 0.2mm produced by Goodfellow, UK.

3.2 Surface modification

Various surface modification techniques exist for different applications, and this work mainly applied UV/Ozone surface modification technique as described in Section 2.7.2. The process of photo oxidation happens when polymeric materials such as polystyrene are exposed to UV irradiation in the presence of oxygen. Polystyrene surfaces in this work were treated with a UVO/Ozone cleaner. The lamp emits UV light at various wavelengths (184.9nm and 253.7nm) which excites molecular oxyen to form atomic oxygen and ozone as well as photosensitising the polymer surface (Weir, 1977, Tang et al., 1982, Ton-That et al., 1999, Shard and Badyal, 1992).

3.2.1 UV/Ozone treatment

Polystyrene surfaces were treated with a UVO/Ozone cleaner (Model 42-220, Jelight Company Inc., California, United States). This treatment unit contains a low pressure mercury vapour grid lamp to produce UV to irradiate the sample surface. The lamp can emit UV light at various wavelengths (184.9nm to 253.7nm) which excite molecular oxygen to form atomic oxygen and ozone as well as

photosensitising the polymer surface. The unit was switched on for at least 45 minutes to warm up before used. Polystyrene surfaces were then irradiated for range of treament times from 10s to 900s. The samples were fitted at a distance of 3 centimetres from the vapour grid lamp where the heat produced in the treatment could reach $90°C$ according to the manufacturer. Immediately after treatment, the sample surfaces were washed by gentle agitation with High Performance Liquid Chromatography (HPLC) grade water (Milipore, resistivity 18 MΩ cm) for a maximum of 60 minutes to remove the low molecular weight oxidised materials produced during the treatment. The samples were then dried at room temperature before further surface characterisation was performed.

3.3 Surface characterisation analysis

To observe the effect of UV/Ozone treatment on polystyrene surface, several analytical techniques were used in this study; the theories are briefly described in Section 2.8.

3.3.1 Experimental of X-ray photoelectron spectroscopy

All the X-ray photoelectron spectroscopy (XPS) measurements were carried out under a Kratos Axis His five channels X-ray photoelectron spectrometer operated at 150W and at a residual vacuum of 10^{-7} Pa with the analyser in fixed analyser transmission mode (monochromatic AlKα source of energy of 1486.6 eV). An ion diffusion pump was operated to maintain the vacuum for the analysis chamber and a turbo molecular pump (Type TPU 060, Pfeiffer, Asslar, Germany) backed up by a 8 vane rotary pump (model number RV8, Edwards, West Sussex, UK,) was used to maintain the vacuum in the introductory chamber. Charge neutralisation was operated to all samples with a low energy electron flood gun (-2.3 V bias voltage, -1.0 electron filament voltage and +1.91 A filament current). Three spectra were obtained for each sample. Survey spectra was measured between the binding energy of 0 and 1000 eV, narrow scan spectra was obtained by measuring carbon 1s between 282 and 295eV and oxygen 1s photoelectrons between 526 and 536 eV. Elemental composition were analysed from the peak spectra from narrow scan after subtraction of a Shirley background and using relevant empirical atomic sensitivity factors. XPS Peak 4.1 software programme (Dr Kwok, Chinese University of Hong Kong) was used to obtain peak fittings. All the results of mean elemental surface compositions and standard deviation from at least three separate samples are reported in this chapter.

3.3.2 Experimental of surface contact angle and energy measurements

The wettability of the UV/Ozone treated surfaces was assessed with a FTÅ125 Dynamic Contact Angle Analyser (First Ten Ångstroms, USA). A sessile drop of deionised H_2O towards the treated surfaces was performed by this system for each measurement. The wettability of the surfaces were assessed by photographing a static 20µl droplet of deionised H_2O on the surface with a digital camera (Sony, Melvica, USA) and measuring the angle direct from a sequences of images taken by the camera automatically. At least three measurement of contact angles were carried out on each sample and triplicate samples were analysed for contact angle measurement.

3.3.3 Experimental of AFM

Surface topology of the untreated polystyrene surfaces and the UV/Ozone treated surfaces were examined by a Digital Instruments (DI) Nanoscope IIIa SPM (Vecco, UK) under ambient conditions. The AFM was calibrated in the x, y and z directions using a DI calibration standard (Vecco. UK). The surfaces were measured in contact mode using silicon nitride tips (Vecco, UK). The analysis was carried out using the software (DI version 4.23r6). Root mean square (RMS) roughness (*Rq*) for each surface was calculated by the software using Equation 3.1.

$$Rq = \sqrt{\frac{(Z_1^{\,2} + Z_2^{\,2} + Z_3^{\,2} + \ldots + Z_N^{\,2})}{N}}$$

Equation 3.1

The Rq is calculated from the average of height deviations taken from the mean data plane, where *Z* is the height above the mean height value and *N* is the number of *Z* values as shown in Equation 3.1. Mean image *Rq* was calculated from at least 3 sample areas of 20 × 20 µm areas, the mean *Rq* and standard deviation reported. The exact same size sample area was applied on all the sample surfaces, as roughness is to increase with increasing area (Browne et al., 2004).

3.4 Cell cultures techniques

All aseptic cell cultures procedures were carried out in a dedicated cell culture laboratory within a laminar flow cabinet (Aura 2000, Bioair Instruments, Pavia, Italy). Glassware was sterilised in an oven at 180 °C for 3 hr prior to use and cell culture media was warmed to 37 °C before use. Cell culture materials were purchased from Sigma-Aldrich (Poole, UK) and all cell culture disposal plastics were from Fisher Scientific (Loughborough, UK) unless otherwise indicated.

3.4.1 Endothelial cells

Human Umbilical Vein endothelial cells (HUVECs) were chosen as a cell model to investigate the interaction between cells and the polystyrene surfaces modified by UV/Ozone treatment. HUVECs were purchased from European Collection of Cell Cultures (ECACC) and propagated from a cryopreserved immortalised cell culture originally isolated from normal human umbilical vein. HUVECs were used in this study between passages number 60-70. Cells were normally cultured in Dulbecco's modified eagle's medium (DMEM, D5796, 4.5µg/mL glucose, L-glutamine and sodium bicarbonate) containing 10% foetal calf serum (FCS) and 1 unit/ml penicillin, 1 µg/mL streptomycin and placed in a constant atmosphere incubator (Galaxy S, Wolf Laboratories, York, UK) at 37°C with 5% CO_2 and 95% air known as normoxia. Similarly, the combination of 5% CO_2, 5% O_2 and 90% air (not including O_2) is for HUVECs cultured under hypoxia condition, nitrogen was inflated into the incubator to reduce the oxygen concentration to create the hypoxic atmosphere.

3.4.2 Cell resuscitation

HUVECs were purchased as a cryopreserved vial which contained 3.75 x 10^5 cells/mL. The vial was thawed by dipping one third into a 37°C water bath and the cell suspension from the vial was transferred to a sterlise flask (75cm^2) containing 10ml of cell culture medium. After incubation for 24 hr at 37°C with 5% CO_2, the cell culture media was replaced to remove any cell debris, unattached cells and any traces of dimethysulfoxide (DMSO). Cell culture media was replaced every two days until cells reached 80% confluency. Cells were then split prior to setting up specific experiments or for long term storage.

3.4.3 Cell passage

Cell passage or cell splitting is the process of sub culture of cells in order to allow cells to increase in number in specific conditions. To sub culture cells, growth medium (DMEM with 1% FCS, 1 unit/mL penicillin, 1 µg/mL streptomycin) was discarded and the flask was washed with phosphate buffered saline (PBS) three times. The flask was then incubated for 10 min in the final wash to remove any medium containing serum. Trypsin was used to remove the adherent HUVECs from the culture surface; 5ml of 0.25% (v/v) trypsin solution was added to the flask and incubated for a further 10 min to detach the cells. The flask was checked using the optical microscope to observe cell detachment. Following detachment of the majority of cells from the surface, an equal volume of growth medium containing FCS was added to the flask to neutralize the enzyme activity of the trypsin which may damage the cells if left in contact for longer times. The cell solution in the flask was then transferred to a sterile centrifuge tube and spun in a centrifuge (Biofuge PrimoR, Heraeus, Germany) under 220g force for 8 min. After centrifugation, the supernatant was carefully discarded into a waste beaker and 1 mL of fresh growth medium was added to the cell pellet. Cell counting was then performed as described in Section 3.4.4 and, for routine subculture, a cell suspension containing 5 x 10^3 cells/cm^2 was transferred to a new flask with 10 mL of fresh growth medium and left in the incubator to allow the cells to attach and proliferate. The flask was checked daily under the optical microscope to monitor progress and potential contamination.

3.4.4 Cell counting

The counting of cells was carried out using an improved Neubauer cell haemocytometer (Weber Scientific International, West Sussex, UK) under an optical microscope. Briefly, trypsinised cells were collected by centrifugation, and washed once in PBS. Cells were re-suspended in 1 ml of medium and a small volume was incubated with an equal volume of 0.4% (v/v) trypan blue solution and transferred to the haemocytometer. Trypan blue is a vital staining method to selectively stain dead cells. Live cells with intact cell membranes were not coloured since the dye is unable to diffuse into the cell via the cell membrane. However when the cell membrane is damaged, typical of dead cells, the trypan blue passes through the cell membrane and dead cells appear blue in colour. Cells that had absorbed the trypan blue dye were considered not viable. Routinely only cell cultures exhibiting a satisfyingly high level of viability (>95%) were considered acceptable for experimental use.

A common device used for cell counting is the counting chamber. The most widely used type of chamber is a haemocytometer, and it was originally designed for performing blood cell counts. To prepare the

counting chamber the mirror-like polished surface was carefully cleaned with lens paper. The cover slip was also cleaned. Cover slips for counting chambers were specially made and are thicker than those for conventional microscopy, since they must be heavy enough to overcome the surface tension of a drop of liquid. The main divisions separate the grid into 9 large squares (like a tic-tac-toe grid) as shown in Figure 3.1. Each square has a surface area of one square mm, and the depth of the chamber is 0.1 mm. Cell suspensions were mixed appropriately so that the cells did not overlap each other on the grid, and were uniformly distributed.

To determine the cells count, an aliquot of 20 µL of cell suspension after the centrifugation as described in Section 3.4.3 was mixed with 0.4% (v/v) trypan blue solution at 50:50 ratio and left for one min to allow the penetration of the dye to any non-viable cells. Then a pipette was used to transfer 10 µL of the cell suspension mixed with trypan blue dye to the edge of the cover slip on the haemocytometer. The cells were counted using a hand tally counter under an optical microscopy at 10 x objective and focus on one set of 16 corner square (Figure 3.1). The haemocytometer was moved to another three sets of 16 corner squares to carry on counting.

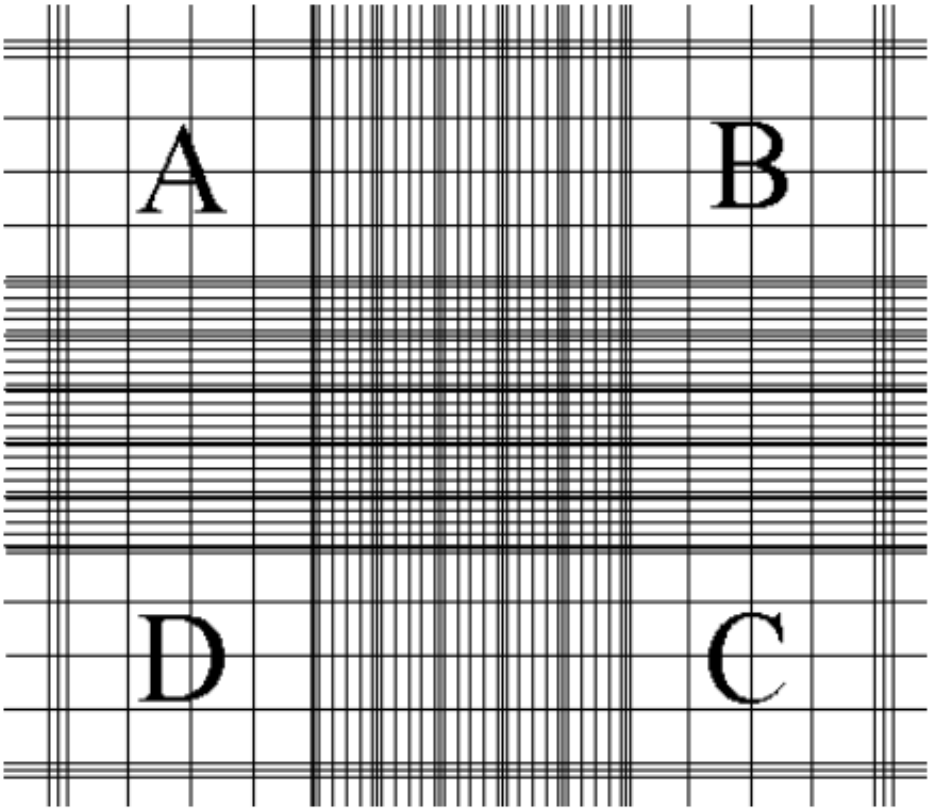

Figure 3. 1 A layout of the Neubeur haemocytometer under the microscopy. There are nine 1.0 mm^2 x 1.0 mm^2 large squares isolated from each other by the triple lines. The total cell count were taken from area A, B, C and D with each of the larger corner 1mm^2 consisting 16 small squares.

The total cell counting numbers from all 4 sets of 16 corner squares = (cells/mL x 10^4) x 4 squares from each haemocytometer grid. The overall cell count is divided by 4 to get a mean of each 16 squares and multiply by 2 to adjust for the dilution factor to get the final cell count. For example, if the total cell count from all four sets of 16 corner squares is 100, then the final cell density is 100/4 x 2 x 10^4/mL.

3.4.5 Long term cell storage

The cell pellet after centrifugation was re-suspended in cryopreservation medium (DMEM with 10% FCS and 10% DMSO). The cell suspension was divided into 1ml cryopreservation vials in the concentration of 3.75 x 10^5 cells/mL. All the vials were labelled with cell line name, passage number, concentration and date, and then transferred to Mr Frosty (C1562, Sigma-Aldrich, Poole, UK) which is a passive freezer with isopropyl alcohol and allows the temperature to steadily reach -80°C. After 24 hr, the vials were placed into a labelled cryo-vial container and immersed in a liquid nitrogen tank (LS3000, Taylor and Wharton, USA).

3.4.6 Alamar blue cell viability assay

Cell proliferation and viability were assessed by the Alamar Blue assay (R6892, Sigma-Aldrich, Poole, UK). The Alamar Blue assay incorporates a fluorometric/colorimetric growth indicator based on the detection of metabolic activity. The system incorporates an oxidation-reduction (REDOX) indicator that both fluoresces and changes colour in response to a chemical reduction of growth medium resulting from cell growth. As cells grow in culture, innate metabolic activity results in a chemical reduction of the immediate surrounding environment. Continued growth maintains a reduced environment while inhibition of growth maintains an oxidized environment. Reduction related to growth causes the REDOX indicator to change from oxidised resazurin (non-fluorescent, blue) to a reduced form resorufin (fluorescent, red) as shown in Figure 3.2. In this study, the Alamar blue assay was mainly used to monitor cell proliferation in the continuous culture systems and to further explore the proliferation trend within specific time period in a range of culture conditions.

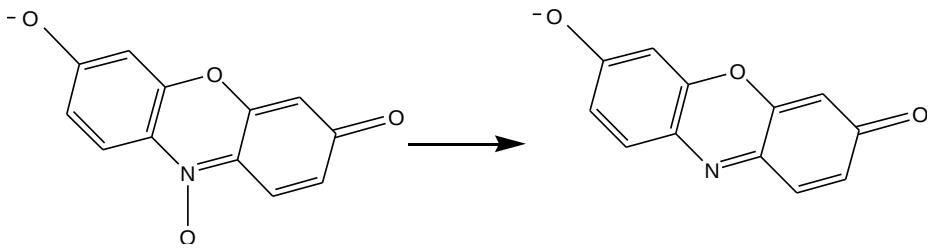

Figure 3. 2 The conversion of resazurin to resorufin. Resazurin is a non-fluorescent compound, which is converted to highly red fluorescent resorufin via reduction reactions of living cells. There is a proportional relationship between the amount of fluorescence produced and the total number of living cells.

In general, Alamar blue stock solution was diluted into fresh cell growth medium to get 10% working solution. This working solution was mixed and sterilised with 0.2 μm filters and then kept in the fridge and wrapped in foil until ready to use. To assess cell standard viability over a period of time, triplicate samples were required for each measurement. HUVECs were allowed to grow on cell culture plastics until 80% confluent, and cells were harvested, counted and diluted to gain a range of cell concentrations of 5.0×10^2, 1×10^3, 1×10^4 and 1×10^5 cells/mL in growth media. A volume of 100 μL of cell suspension was added to each assay well of a 96 well plate and incubated at 37°C with 5% CO_2 to allow cells to attach to the surface. The next morning, the media was aspirated from the wells and cells were washed three times with sterile PBS. 100 μL of Alamar Blue working solution was added into each well and incubated at 37°C with 5% CO_2 for 90 min and the plate was wrapped in foil to protect from the light. Then the plate was read with a spectrometer at 570nm and the reading was considered as t=0 hr. Further reading were taken at 1, 6, 12, 24, 48 and 72 hr. Empty wells with no cells attached were used as blank.

3.5 Fluorescent staining

3.5.1 Phalloidin staining

Phallotoxins such as several biotinylated Phalloidin and phallacidin derivatives are widely used to investigate the distribution of the protein F-actin within cells. Phalloidin is a bicyclic heptapeptide which specifically binds to the interface between the subunits of F-actin and locking adjacent subunits together. The binding between Phalloidin and F-actin can happen at nanomolar concentrations, thereby resulting in an enormously useful technique for labelling, identifying and quantifying F-actin in living or fixed cells as well as visualizing individual actin filaments *in vitro*. Phalloidin staining is different from antibodies as the affinity of binding will not change appreciably with actin from other sources. Phallodin can also stabilize F-actin by inhibiting depolymerisation caused by cytochalasins, potassium iodide, and elevated temperatures (Invitrogen, 2006). Phalloidin (Alexa Fluor® 488, Invitrogen, UK) was used to investigate the F-actin distribution within cells in this study. It was isolated from the deadly *Amanita Phallouides* mushroom and used extensively in imaging applications to selectively visualise F-actin However, it is reported in a few studies that this technique was less effective due to the failure of permeation to cell membranes; cell exhibited several toxic effects and died frequently (Cooper, 1987).

In general, the cells were washed three times with prewarmed sterile PBS and then fixed in ice cold 4% methanol free paraformaldehyde solution for 10mins in 24 well plates. 0.1 % Triton X-100 in PBS was added to lyse the cells. To reduce nonspecific background staining with Phalloidin conjugates, the cells were pre incubated with 1% FCS in PBS prior adding in Phalloidin staining working solution. 400 µL of Phalloidin staining solution was added to the cells and incubated for 20 min at room temperature. The lid was placed on the plate to avoid evaporation of the Phalloidin staining solution. Finally, the cells were washed three times with PBS, air dried and mounted in Citifluor, a permanent fluorescence mounting media. The images were taken using a fluorescence microscopy (IM150, Leica DC, Germany) with excitation in a range of 450-480nm and emission in a range of 500-550 nm.

3.5.2 5-*Bromo*-2-*Deoxyuridine staining (BrdU)*

5-Bromo-*2*-Deoxyuridine staining (BrdU) is the abbreviation of *5*-bromo-*2*-deoxyuridine which is a thymidine analogue commonly used for cell proliferation assays and for the detection of new DNA synthesis. BrdU can be incorporated into new DNA synthesis of replicating cells occurring during S phase of the cell cycle as a substitution of thymidine. BrdU antibodies were then used to detect the incorporated compound indicating cell undergoing proliferation. Cells labelled with BrdU were then detected using fluorescently-labelled (Invitrogen protocol 2010).

BrdU staining Kit was purchased from Roche Applied Science (C11296736001, Penzberg, Germany). In generally, HUVECs were grown in 24 well plates, washed three times with sterile PBS, before being labelled with BrdU. Four hundred µL of a BrdU solution diluted 1to 1000 with fresh cell growth medium (final concentration of 10 µM), was added to each well and incubated at 37^{o}C with 5% CO_2 for 60 min. The cells were then fixed with ethanol fixative solution for 20 min at -15^{o}C before washing three times with PBS to remove any BrdU labelling medium. Further washes with PBS were required to remove the ethanol fixative and then followed by adding 200 µL anti-BrdU working solution to the wells and incubated at 37^{o}C with 5% CO_2 for 30 min. The same procedures were followed before adding anti-mouse-lg-fluorescein working solution to complete the detection. Cells were washed another three times before addition of 400 µL anti-mouse-lg-fluorescein working solution, and then incubated at 37^{o}C with 5% CO_2 for 30 min. Finally, the cells were washed with PBS and air dried and Citifluor was also added for observation under the fluorescence microscopy (IM150, Leica DC, Germany). The excitation wavelength was in the range of 450 to 500 nm and detection in the range of 515 – 565 nm.

Images were captured under the fluorescence and optical lenses on the cell of interests and both of images were stacked together. Both of the images were formatted to the size of 6cm x 7cm (height x width), fluorescence image was dragged on top of the optical one, a cross mark was shown when matched perfectly (Microsoft PowerPoint 2007).

Determination of cell activity was measured by manually counting the number of BrdU stained cells using Image J freeware (Version 1.46r, Wayne Rasband, National Institute of Health, USA). Fluorescent cells (proliferating) and unstained cells (quiescent) were counted per square ($2.7 \times 10^4\ \mu m^2$) blindly placed at three positions of each stacked image. The result is presented in the percentage ± SD of counted proliferating and quiescent cells in the mean of three separate measurements.

3.6 Radial Cell migration assay

To measure the effect caused by the UV/Ozone modified surfaces on cell migration, a radial migration assay was chosen to perform the measurement. The outer diameter of 8mm glass tubes (Corning, UK) were cut into 6mm x 8mm glass corning rings. The ring was placed in the centre of the modified surface and a 50 μL of HUVECs suspension were carefully seeded into the glass ring at a concentration of 2.4×10^5 cells/mL. The plates with cells were incubated at 37°C with 5% CO_2 overnight to allow cells to adhere and form a circular monolayer on the surface. The next morning, formation of the circular monolayer was carefully determined under the microscope. Figure 3.3 shows a typical circular monolayer formed on UV/Ozone treated surfaces by this technique. All the rings were carefully removed from the plates and 1.5 mL of pre-warmed growth media was added after the successful formation of the monolayer.

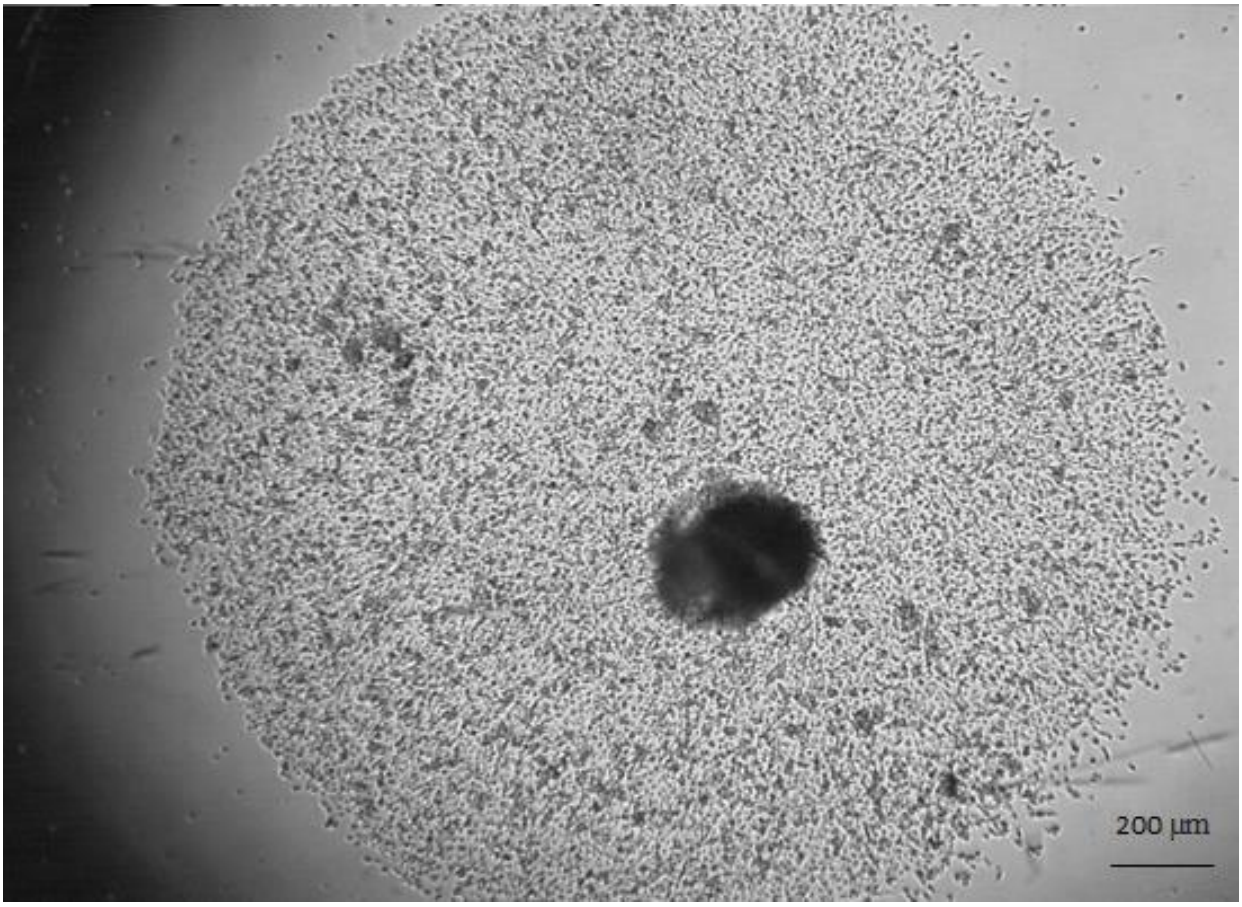

Figure 3. 3 Typical image of a HUVECs circular monolayer on UV/Ozone treated surfaces at day 0. The black label is used as a reference point for measurement.

The monolayers were inspected using an inverted microscope (Leica, Germany) and images were acquired digitally under 25 x magnifications at day 0, 1, 2 and 3. For measurement of radii, a Leica QWin (Image Processing & Analysis software, v2.8) was used to generate circles combined with a radial grid at an angle of 9 degrees between two radii was superimposed on the image of a monolayer. Figure 3.4 shows the image analysis carried out using Leica Qwin software to measure cell migration distances. Permanent marker was used to label a centre point on the underside of the plate and a line was drawn manually to the edge of the monolayer including the labelled centre point by using the annotation function of the software. This manually drawn black line can be transferred to the same cell image captured in different days as shown in Figure 3.5 to allow for correlation from one time point to the next.

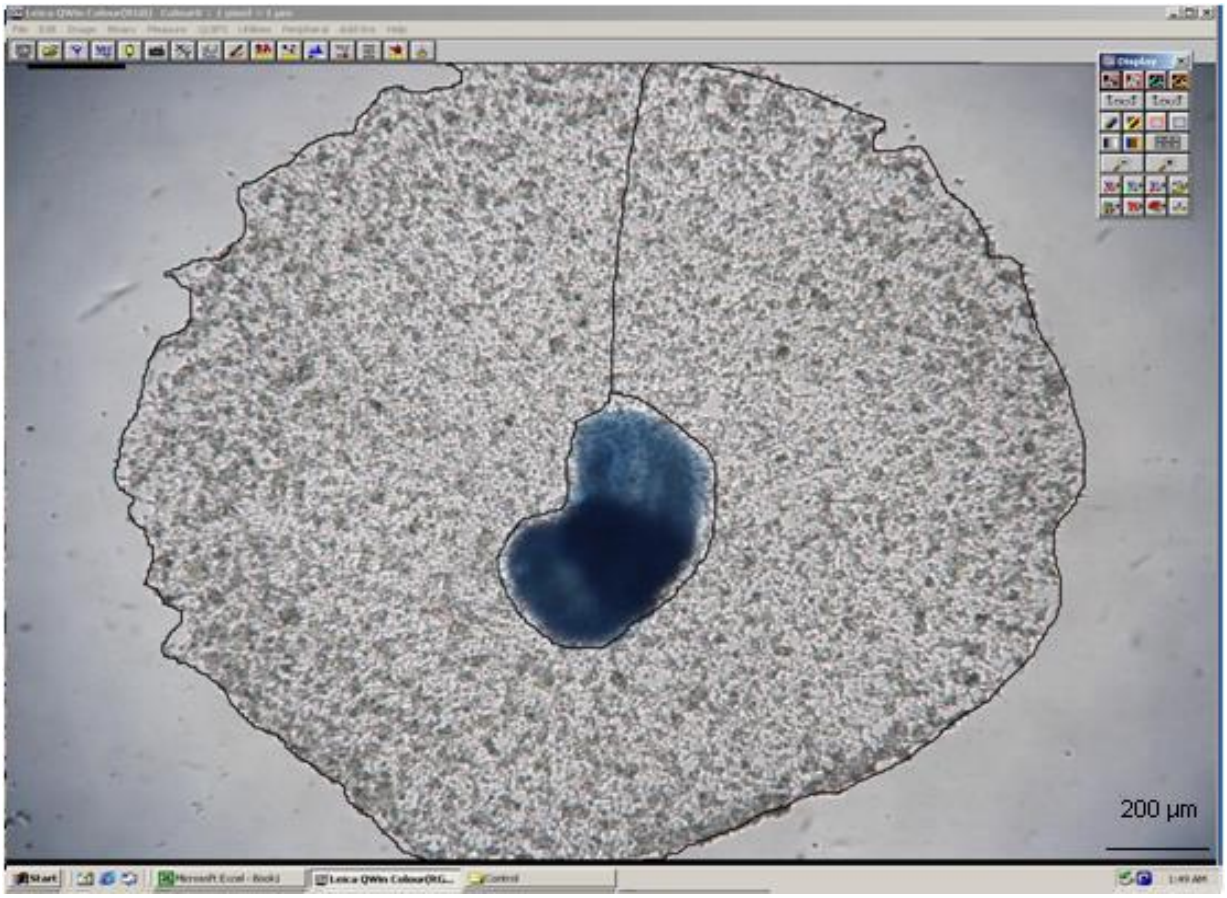

Figure 3. 4 Software image processing of a cell monolayer formed on UV/Ozone 120s treated surfaces at t=0 hr. The blue label is used as a reference point for measurement.

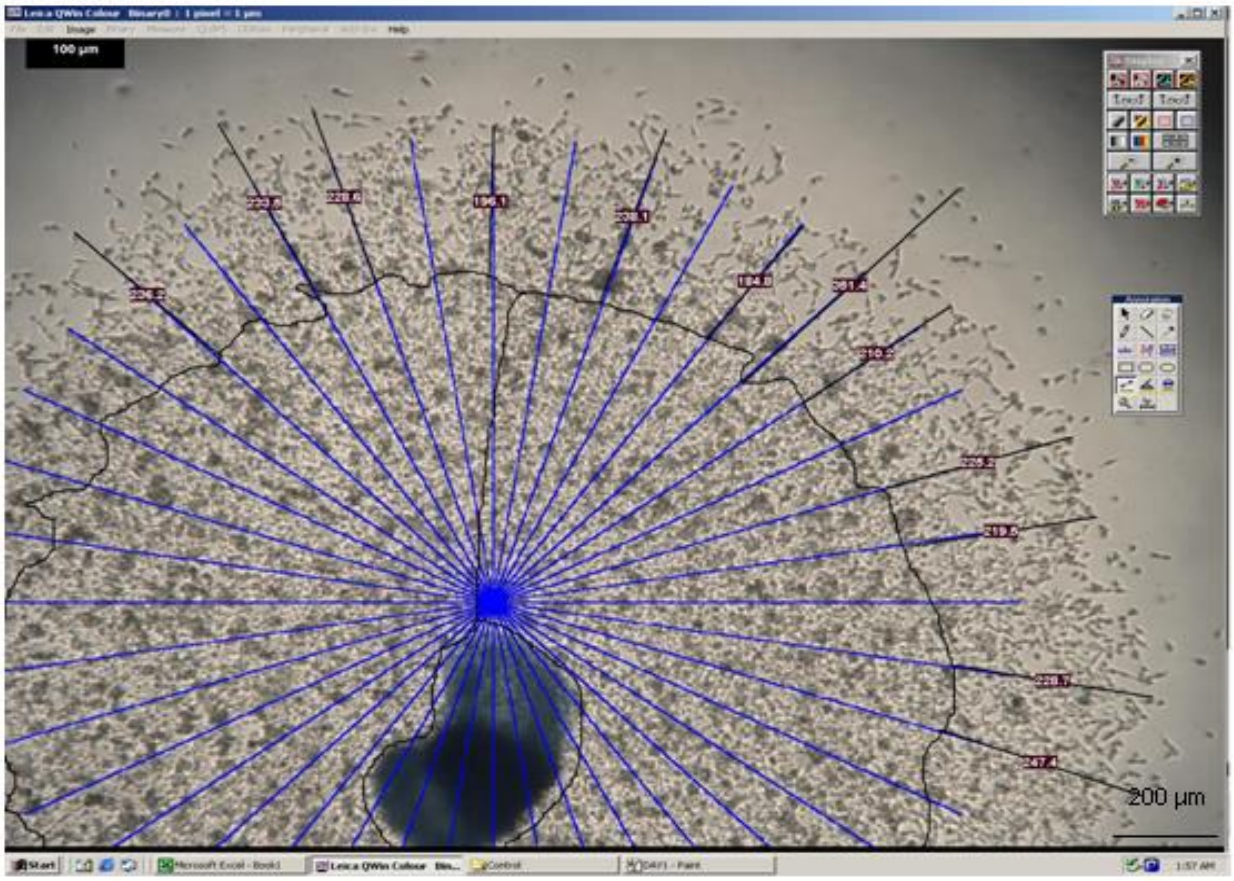

Figure 3. 5 Software image processing of Cell monolayer formed on UV/Ozone 120s treated surfaces at t=24 hr. The blue radial spiked with the angular distances at 9^{o} was placed in the center of the cell monolayer. The lengths of the spikes were adjusted not to excess the boundary of the cells to secure a good visibility.

The radial migration distances were measured by replacing the manually drawn line on images taken on same cells at different incubation time. The migration distances were measured by the differences between the boundary and migrated cells on the same spike. In total, lengths of 20 radial lines per images were recorded and noted on a Microsoft Excel document. The same procedure was carried out on cells grown for 48 hr and 72hr and measurement compared with those taken at T=0. Net migrations were noted as mean ± SEM of 40 results from radii unless otherwise indicated in the result chapter. The experiments were carried out three times on each.

3.7 Endothelium under flow system

3.7.1 Sample preparation

The polystyrene sheet (Goodfellow, UK) was cleaned by sonication in 70% methanol and gentle agitation with High Performance Liquid Chromatography (HPLC) grade water (Milipore, resistivity 18 MΩ cm) after being cut into 30mm diameter circle disks to fit the flow chamber. The surfaces were treated uniformly with a UV/Ozone cleaner (Model 42-220, Jelight Company Inc. USA) for 120 seconds as previously described in Section 3.2.1. Immediately after the treatment, the sample surfaces were again cleaned by HPLC grade water for a maximum of 60 minutes to remove the low molecular weight oxidised materials produced during the treatment and removed to a cell culture hood to dry for subsequent use in cell culture.

HUVECs were seeded on the UV/Ozone treated surface before assembling within the flow chamber. HUVECs at a concentration of 2.4 x 10^5 cells/mL were carefully added into the glass corning rings (6mm x 8mm, Corning, UK) that were located in the centre of the treated polystyrene surface. Cells were incubated at 37^{o}C with 5% CO_2 overnight to allow adhesion and formation of a circular monolayer on the surface. Next morning formation of the circular monolayer was carefully monitored under the microscope, the ring was carefully removed and then the surface with the adherent cells was assembled into the chamber for the flow experiments.

3.7.2 Perfusion chamber set up

The perfusion chamber that was used (FCS2, purchased from Intracel, Bioptechs, Inc. UK) is a closed system and also a live-cell micro-observation chamber, that can provide high volume laminar flow perfusion with Koehler illumination and temperature control (although the temperature control was not used for these flow experiments). A fluid pathway was created by isolating the microaqueduct slide from the UV/Ozone treated surfaces with a singular gasket (1mm thickness, 14mm x 22mm rectangle shape). Two T shaped grooves on the surface of the micro-aqueduct slide (Figure 3.6) ensure that the fluid media seeks the path of least resistance and generates laminar flow before reaching the cells. According to the manufacturer, this design eliminates the additional requirement of a metal perfusion ring and gaskets, which are the common drawbacks of most conventional chambers.

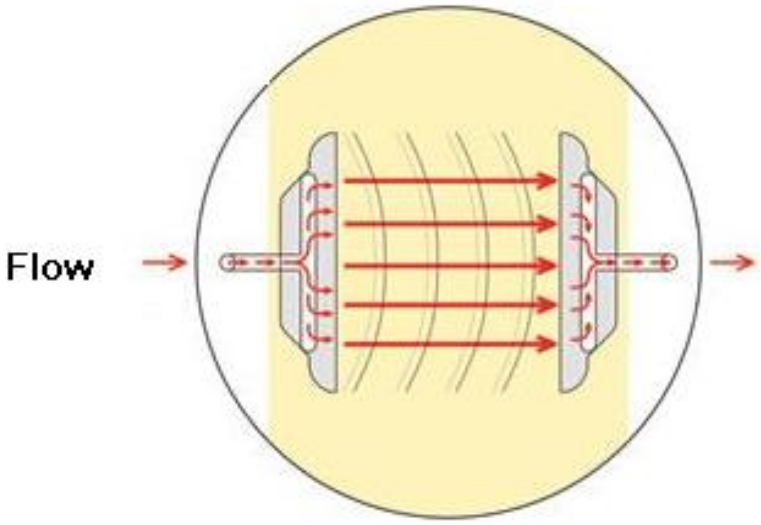

Figure 3. 6 An aerial view of fluid flow patterns in the micro-aqueduct perfusion chamber. The red line indicates the direction of the flow. The laminar flow is generated due to the etched channel, which introduces the fluid gently across the specimen. Image is slightly modified from the equipment manual (Bioptechs manual 2008).

Figure 3.7 illustrates an isometric view of the perfusion system. Using this system the cell culture media was delivered by gravity flow through the chamber. This technique is simple for installation and costless for operating, although the control of the flow rates is more difficult than using a mechanical pump. In this experimental configuration, the cell culture media (DMEM with 10% FCS, 1 unit/mL penicillin and 1 µg/mL streptomycin) was located on a steel stand, 30 cm higher than the microscope to create a gravity feed system with a section of sterile tubes connected to the flow chamber. The flow rate of this system was controlled by a roller clamp connected to the exhaust tube attached to the other side of the chamber, which leads into a catch basin. The flow speed was measured by the volume of the media with respects to the time taken to flow through the system; the roller clamp was carefully adjusted to ensure the flow speed was constant at the flow speed required. For example, to measure the flow speed of 1 mL/min, the catch basin was replaced by a 10 mL measuring cylinder. The total volume from the cylinder was measured a few times after 5 minutes and the roller clamp was carefully adjusted to ensure the next measurement will be close to a total volume of 5 mL, the media was discarded after each measurement. Other methods may be used to control the rate of the perfusion flow including varying the vertical distance between the two reservoirs or by a stopcock that regulates the flow from the upper reservoir, however, it was not used in this study.

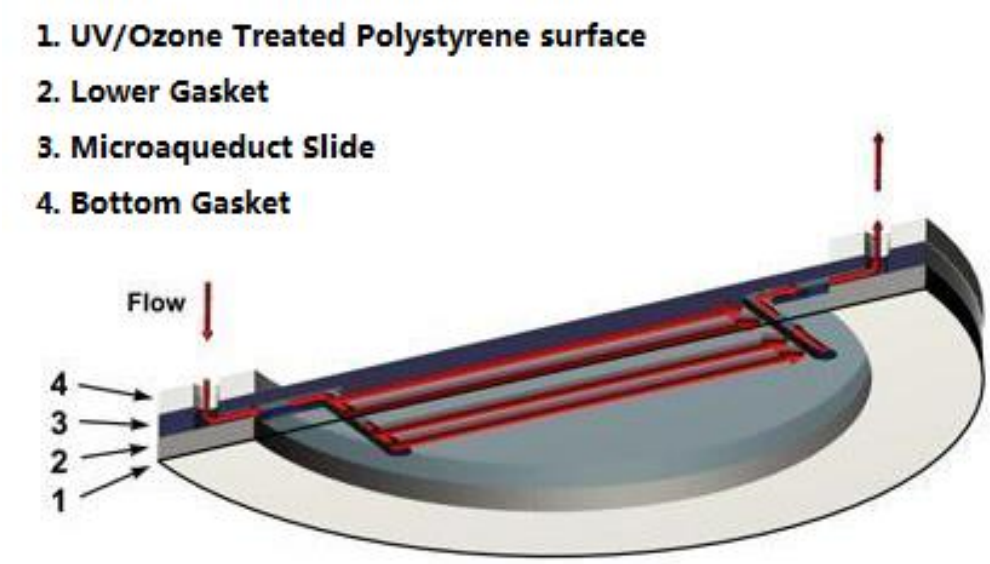

Figure 3. 7 An isometric view of optical cavity of the perfusion chamber. The red line indicates the direction of the laminar flow. The microaqueduct slide contains a transparent glass but rendered as a solid to improve the contrast. Image is adapted from the equipment manual (Bioptechs manual 2008).

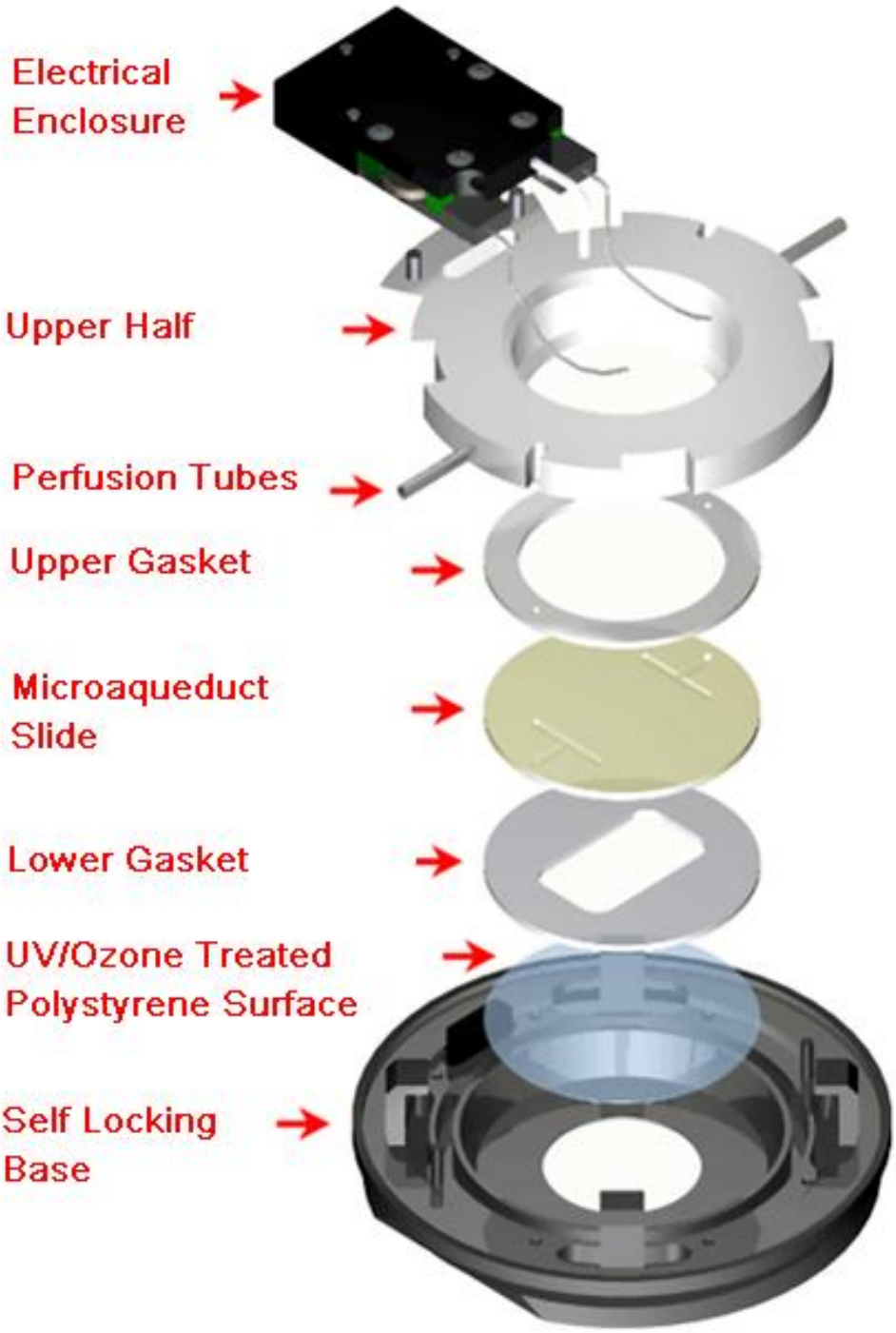

Figure 3. 8 An expanded view of the FCS2 micro environmental flow chamber. Image is adapted from the equipment manual (Bioptechs manual 2008). Electrical enclosure is designed for temperature control and it was not used in the study.

3.7.3 Shear Stress calculation

In order to determine the shear stress of the cells exposed at the different flow rates, following formula was used:

$$Q = r*w*h^2 / 6*u \qquad \text{Equation 3.2}$$

Where Q is the desired flow rate, r (dyn/cm^2) is the target shear stress intensity acting tangentially on the cells, w (1.4 cm) is the width of the flow chamber, h (0.1 cm) is the height of the flow chamber, and u is the viscosity of the fluid cell culture medium (DMEM itself is about 0.0084 poise and 0.012 poise with 10% serum). The shear stress values used in our investigations ranged from 1 dyn/cm^2 to 21 dyn/cm^2 as shown in Table 3.1, which is within the physiological range for arteries and veins (~0.1 dyn/cm^2 – 60 dyn/cm^2) (Paz et al., 2011, Tseng et al., 2010).

Flow rate	Shear stress intensity
1 mL/min	1 dyn/cm^2
10 mL/min	9 dyn/cm^2
25 mL/min	21 dyn/cm^2

Table 3.1 Summary of the fluid shear stress intensities induced by the flow rates used in this study.

3.7.4 Cell viability and morphology changes

The microaqueduct design of the flow chamber enables effective Koehler illumination with high numeric aperture optics for inverted modes of the microscope to observe any changes (Bioptechs manual 2008). Images were taken every 10 minutes with an inverted Microscope at 10x and 25x magnification (DMI

4000B, Leica Microsystems, Germany). Images were taken at the same position at each time point in order to evaluate the change in cell morphology in response to different flow rates. Under the flow period of 120 mins, the UV/Ozone treated surface with cells was carefully removed from the chamber for further cell viability tests. Trypan blue viability staining was used to measure cell viability after two hours of flow. Changes in cell morphology occurring after exposure to the laminar flow were examined by visual inspection and serial time lapse imaging and by determining the distribution of F-actin as discussed in Section 3.5.1.

3.7.5 Quantification of HUVEC area under different flow conditions

Changes in size of HUVECs under different flow conditions were measured by using Image J freeware (Version 1.46r, Wayne Rasband, National Institute of Health, USA). Three Steps were used to carry out measurements: 1). Setting the scale of measurement was changed from pixels to micrometers; 2). Measuring HUVEC area before the flow; 3). Measuring HUVEC area after the flow.

3.7.5.1 Setting the scale

The scale from pixels to micrometers was done by the command (Analyse>Set Scale) as shown in Figure 3.9. As all the images were taken with a definition of 1616 x 1216 pixels and the conversion ratio was 0.75 pixels/µm. This conversion rate was applied to all measurements.

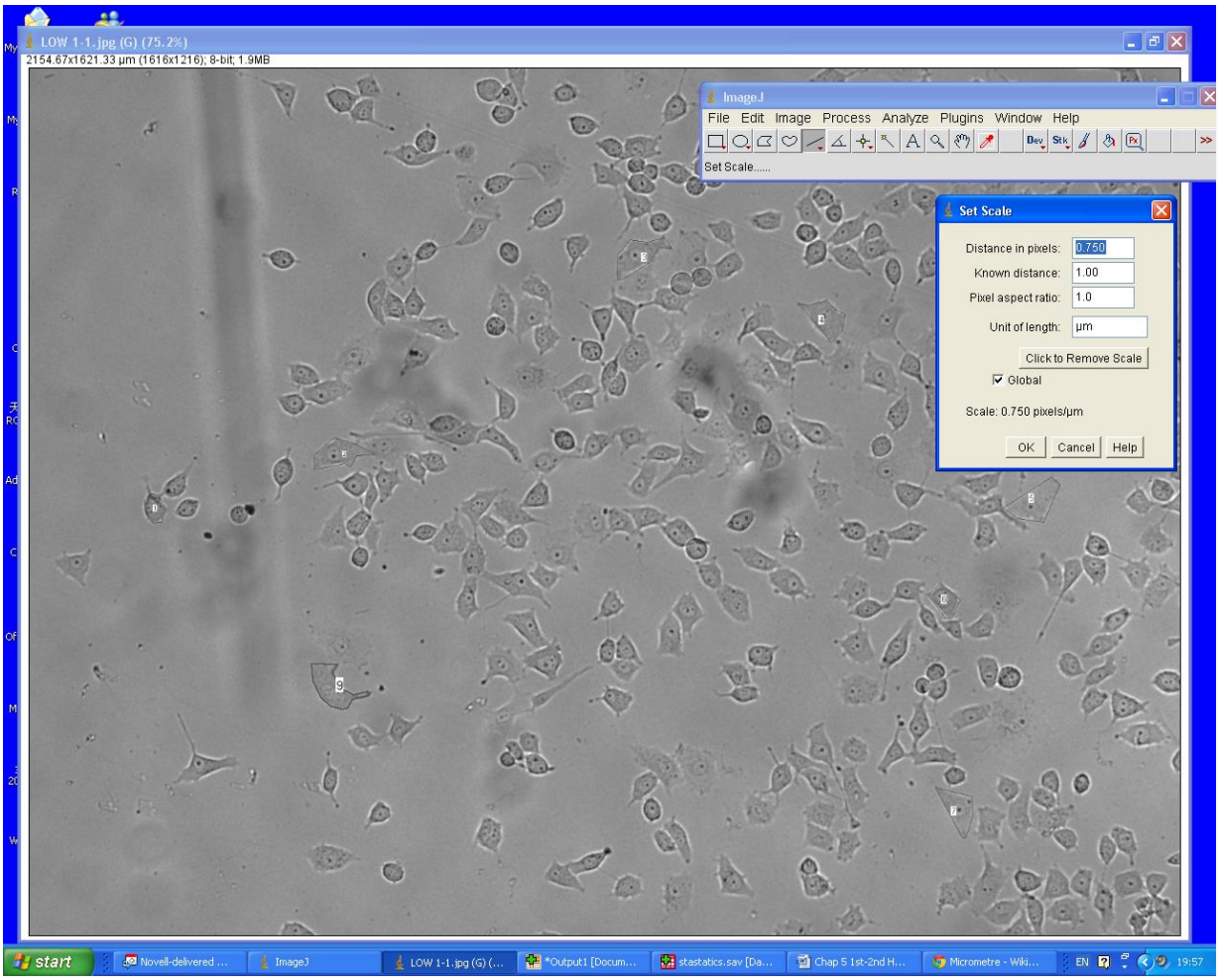

Figure 3. 9 The scale conversation setup for measurement of HUVEC area, a typical image of HUVEC to be measured and the scale converted.

3.7.5.2 Cell area measurement before the flow at t =0 (hr)

HUVEC area before flow shown as t0 was measured by using the command of polygon selection. Area of each HUVEC was defined by mouse highlighting the whole area of each cell. Eight HUVEC were selected for the measurement before the flow and the same eight HUVEC were measured again after the flow. Figure 3.10 shows a typical measurement of 8 random HUVECs before the flow.

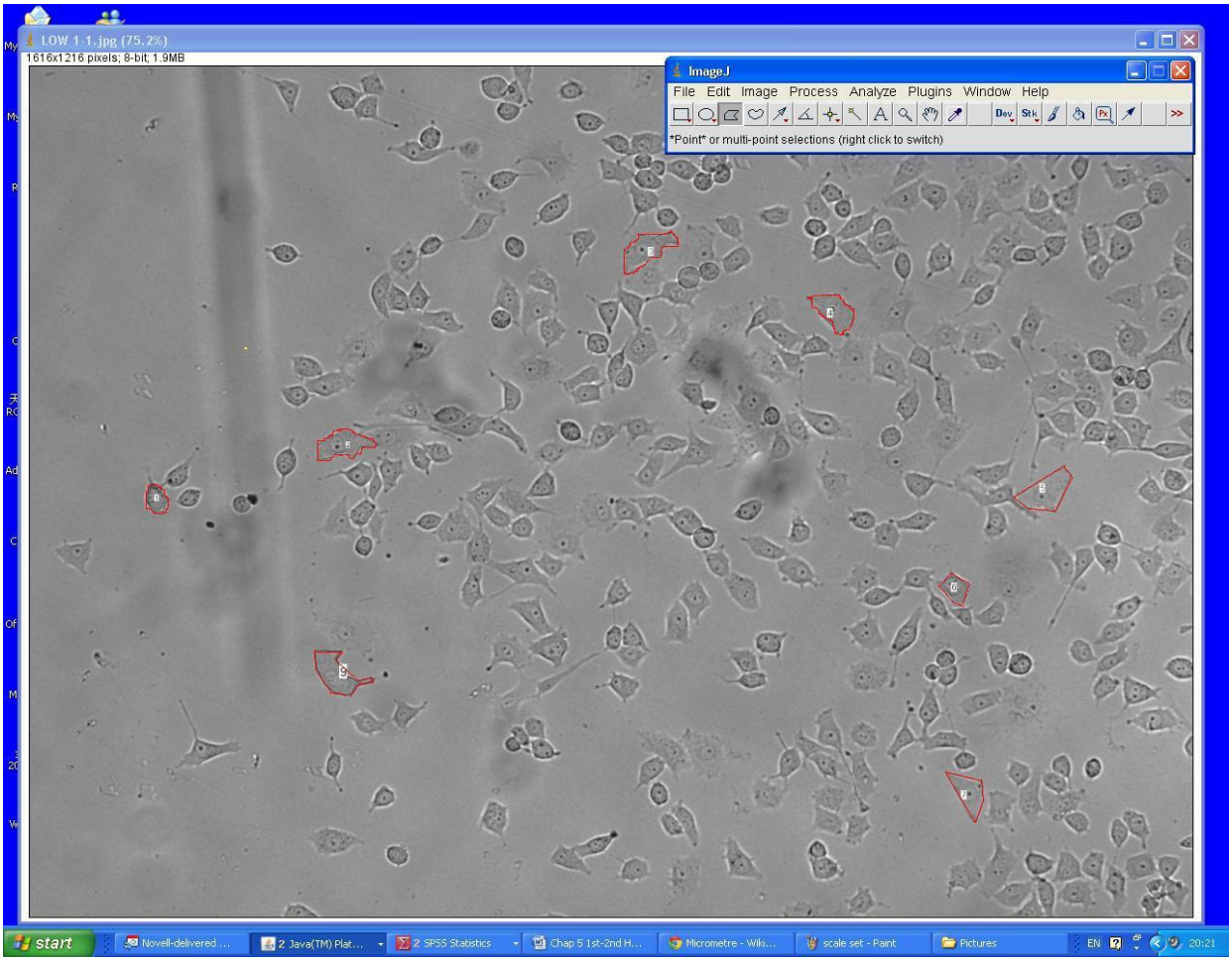

Figure 3. 10 Measurement of HUVEC size before the flow at t=0. Eight random cells were picked and the area was taken by using the command of polygon selection on UV/Ozone treated polystyrene at the flow rate of 10 mL/min.

3.7.5.3 Cell area measurement before the flow at t =2 (hr)

Figure 3.11 shows the measurement of HUVEC area after two hours of flow. Eight random HUVECs selected at t=0 hr were applied to the same cells after the specified period of the flow.

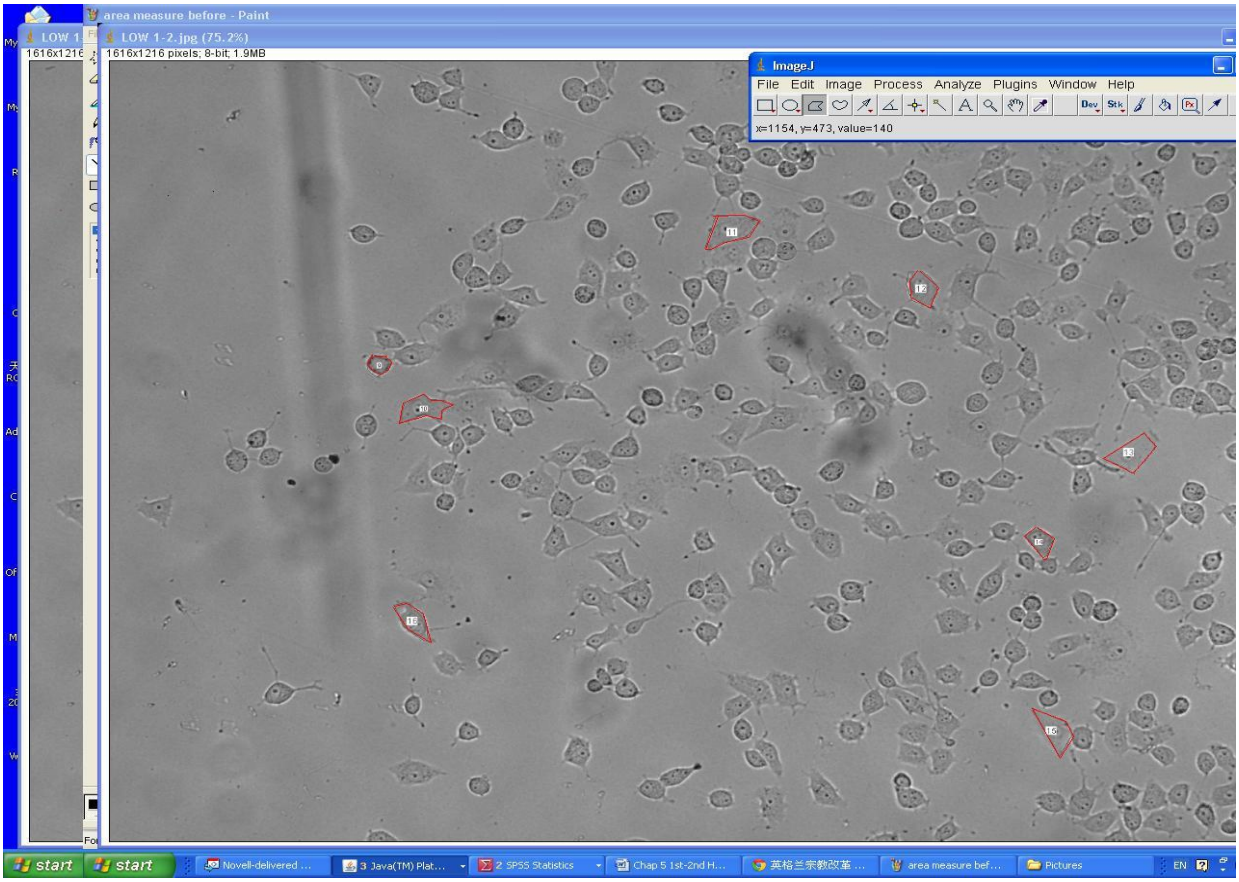

Figure 3. 11 Measurement of HUVEC area after the flow at t=2 (hr). The area measurement was applied to the eight random HUVECs selected before the flow (Figure 2.10).

3.7.5.4 Determination of area change under the flow conditions

A total number of eight random individual HUVECs were measured for each experiment with the lowest and highest findings deducted for accuracy. The net change in cell area in response to the respective flow rate was calculated using the following formula:

$$Net\ reduction = (R_1-R_2)/R_1 \times 100\% \qquad \text{Equation 3.3}$$

where R_1 is the measurement of HUVEC before the flow (t=0 hr), R_2 is the measurement of the same HUVEC after the flow (t=2 hr).

3.7.6 Determination of cell viability under the flow conditions

At the end of flow, the surfaces with cells were carefully removed from the chamber and stained by 0.4% trypan blue; cell counts were achieved from digital images acquired using an optical microscope. To obtain the cell death over the 120 mins flow at different flow rate, three boxes ($2.7 \times 10^4\ \mu m^2$) was blindly placed on the trypan blue digital image using Image J freeware as discussed in the previous section, live and dead cells were counted manually per box, with three replicates of each flow rate.

3.8 Statistical Analysis

Statistical analysis was performed on the data resulting from the cell experiments. Student's t-test was used to perform statistical analysis on the date resulting from HUVEC proliferation and was analysed with Microsoft Excel 2007. The statistical analysis on HUVEC migration is more complex performed by analysis of variance (ANOVA) followed by Boferroni post host test, $*p< 0.05$, $**p<0.01$, $***p<0.001$ when compared as indicated.

Chapter 4 Characterisation of Ultra-Violet/Ozone (UV/Ozone) Treated Polystyrene Surfaces

4.1 Introduction

The major challenge of many current available biomaterials is due to their non-optimised surfaces, for example, satisfactory cell attachment and long term viability are essential for optimal *in vitro* tissue culture and for successful implantation and stability of artificial joints whilst control of blood interactions is necessary to reduce risks of thrombosis at the surfaces of stents and other vascular implants. The pre-treatment of these biomaterials to modify the surface chemistry is therefore of critical importance to improve the biocompatibility.

Such treatment of polymers is necessary because the intrinsic properties of polymer surfaces are hydrophobic in nature and this is not an ideal surface to support satisfactory adhesion of cells for biomedical purposes (Mathieson and Bradley, 1996, Liu et al., 2011). One example of such treatment is that oxidation process which can introduce a range of oxygen-containing functional groups to the polymer surfaces.

UV/Ozone treatment is the of the most efficient way of controllable modification for producing tissue culture grade polystyrene with a greater consistency in surface oxygen compared to the conventional methods such as plasma chemical deposition which requires the use of vacuum apparatus (Davidson et al., 2004, Dupont Gillain et al., 2000). As previously described, UV/Ozone treatment has been used on a number of polymers including: Polystyrene (Teare et al., 2000a, Mitchell et al., 2004b, Browne et al., 2004, Geuskens et al., 1978b), Polyethylene (Poulsson et al., 2009), Poly ethylene terephthalate (PET) (Ton-That et al., 1999, Teare et al., 2000b, Friedrich et al., 1998), Poly ether ether ketone (PEEK) (Mathieson and Bradley, 1994, Mathieson and Bradley, 1996), Polypropylene (Strobel et al., 1995, Nie et al., 1999, Wang et al., 2000), Poly vinyl fluoride (Zhang et al., 2009, Deng et al., 2009), to modify the surface chemistry and increase the surface wettability (Liu et al., 2011, Mathieson and Bradley, 1996), printability (Shao et al., 2001), physical adhesion (Ferreira et al., 2005) and biocompatibility (Davidson et al., 2004, Liu et al., 2011, Teare et al., 2001, Teare et al., 2000a).

The advantage of the UV/Ozone treatment that it only modifies the surface and leaves the bulk property within the material unaltered (Mathieson and Bradley, 1994, Mathieson and Bradley, 1996). The difference between the surface and the bulk of a material is because of fewer neighbouring atoms in the surface molecules which increase the surface free energy. At atomic scale, this energy exists unterminated bonds and the bonds react instantaneously to form new bonds and compounds in a reactive environment such as air or water at a metal face, thus lowering the surface energy (Vepari et al., 2010). Introduction of

this modified material to a biological system leads to the reaction of interfaces between the material and surrounding tissue, therefore it is important to understand the modification process and the resultant interaction within the biological environment.

This chapter reports the surface functional groups, wettability, surface free energy and topology changes induced by the UV/Ozone treatment of polystyrene surfaces. The surface analysis techniques used to assess these changes include X-ray photoelectron spectroscopy (XPS), atomic force microscopy (AFM), and contact angle measurement (CA) and are described in Chapter 3. This surface analysis demonstrated that the UV/Ozone surface treatment is effective on the PS surfaces and produced changes in the level of surface oxygen concentration and surface free energy, which results in the increase of surface polarity and wettability.

4.2 Experimental

4.2.1 Materials

The main material used for surface modification was polystyrene. The polystyrene used (M_w = Ca. 280 000) in this study with the thickness of 0.2 mm was purchased from Goodfellow, UK. All the reagents and chemicals used in this work were of analytical grade and purchased from Sigma Aldrich unless specified.

4.2.2 UV/Ozone surface modification

The sample preparation for UV/Ozone treatment has been fully discussed in Section 3.2.2. Polystyrene surfaces were treated with a UVO/Ozone cleaner (Model 42-220, Jelight Company Inc., California, USA) for an range of treament times from 10s to 900s.

4.2.3 Experimental set up of XPS

All the XPS results were analysed under a Kratos Axis His five channels X-ray photoelectron spectrometer operate at 150W at a residual vacuum of 10^{-7} Pa with the analyser in fixed analyser transmission mode (monochromatic AlKα source of energy of 1486.6 eV) as discussed in Section 3.3.1. XPS Peak 4.1 (Dr Kwok, Chinese University of Hong Kong) was used to obtain peak fittings. All the results of mean elemental surface compositions and standard deviation from three separate samples are reported.

4.2.4 Experimental set up of wettability analysis

The wettability of the UV/Ozone treated surfaces was assessed with a FTÅ125 Dynamic Contact Angle Analyser (First Ten Ångstroms, USA) as described in Section 3.3.2. A sessile drop of deionised H_2O towards the treated surfaces was performed by this system for each measurement. Three times on each sample and triplicate samples were performed for each contact angle measurement, the results of contact angles in this chapter are presented as the mean of these values and standard deviation are provided.

4.2.5 Experimental set up of AFM

UV/Ozone treated polystyrene surfaces were examined by a Digital Instruments (DI) Nanoscope IIIa SPM (Vecco, UK) as discussed in Section 3.3.3. The results are presented as the mean of these values and standard deviation on three separate samples.

4.3 Results

4.3.1 Characterisation of UV/Ozone treated polystyrene surfaces using X-ray photoelectron spectroscopy

Untreated and UV/Ozone treated polystyrene surface were characterised by XPS to determine the surface chemistry before and after treatment. As shown in Figure 4.1, the result of the XPS produced a high resolution C1s spectrum of polystyrene surface which shows that the untreated polystyrene has no oxygen incorporation due to the symmetrical envelope. A large carbon peak was at 285 electron volt (eV), this peak consists of one slightly offset component which has been fitted as closely as possible by the software to given literature values of peak positions (Geuskens et al., 1978b).

The fitted peak shown in blue has been fitted to the expected binding energy emitted from aromatic carbon atoms and the saturated hydrocarbon of the polystyrene backbone. This result explains the characteristic of polystyrene and matches the standard spectra obtained by Briggs (Briggs, 1990). The red peak at 291.7 eV is a much smaller peak compared to the blue one and this envelope contains several components known as aromatic π-π^* shake-up satellite peak in addition to the core electron excitation, valence electrons can simultaneously become excited into a vacant level (Briggs and Seah, 1995). These peaks appear at a higher binding energy than the carbon 1s peak, and are typical of polymeric systems with unsaturated bonds, frequently present in polymers with aromatic pendant groups such as polystyrene (Garbassi and Morra, 1994). The occurrence of this peak has already been discussed in Section 3.8.1.

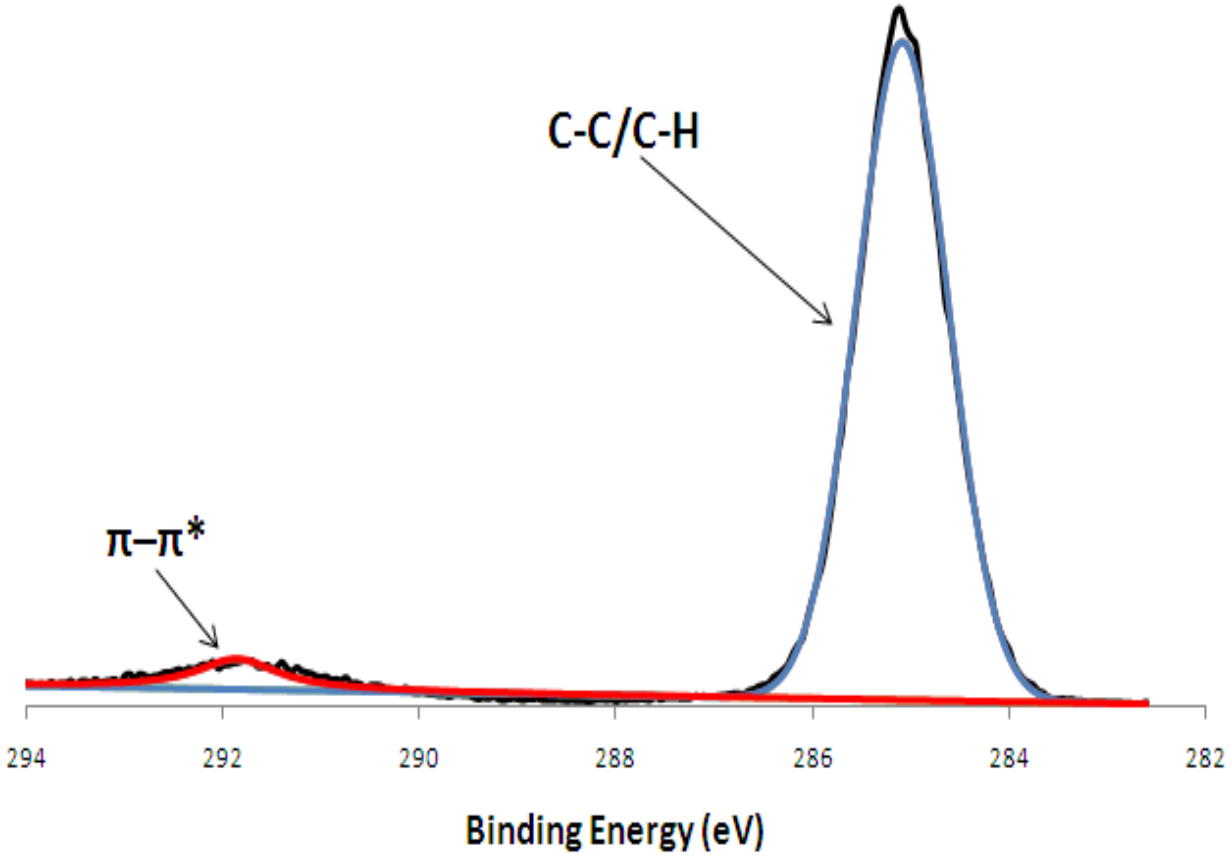

Figure 4. 1 High resolution C 1s fitted XPS spectrum of untreated polystyrene surface showing that the peak only contains hydrocarbon functionalities and π–π* shake up satellite.

As previously discussed in Chapter 3, UV/Ozone treatment photosensitises the surface leading the incorporation of oxygen into the surface of the polymer. A high resolution C1s spectrum of UV/Ozone modified polystyrene after 10s treatment is shown in Figure 4.2. There is an extra component (purple fitted curve) as compared to the spectrum in untreated polystyrene (Figure 4.1). This new peak is at 286.5 eV and meets the finding of other researchers (Teare et al., 2000b, Davidson et al., 2005). This peak contains the binding energy of any functional group where carbon has single bond to oxygen such as hydroperoxides (RO-OH), peroxides (RO-OR), hydroxyls (OH^-) or ethers (C-O-C). Alcohol (C-OR) represented in Figure 4.2 is the short hand notation for these groups. 10s treatment is considered as an early stage of the UV/Ozone irradiation and more amount and species of both carbon and oxygen related functional groups can be seen with the increase of treatment period.

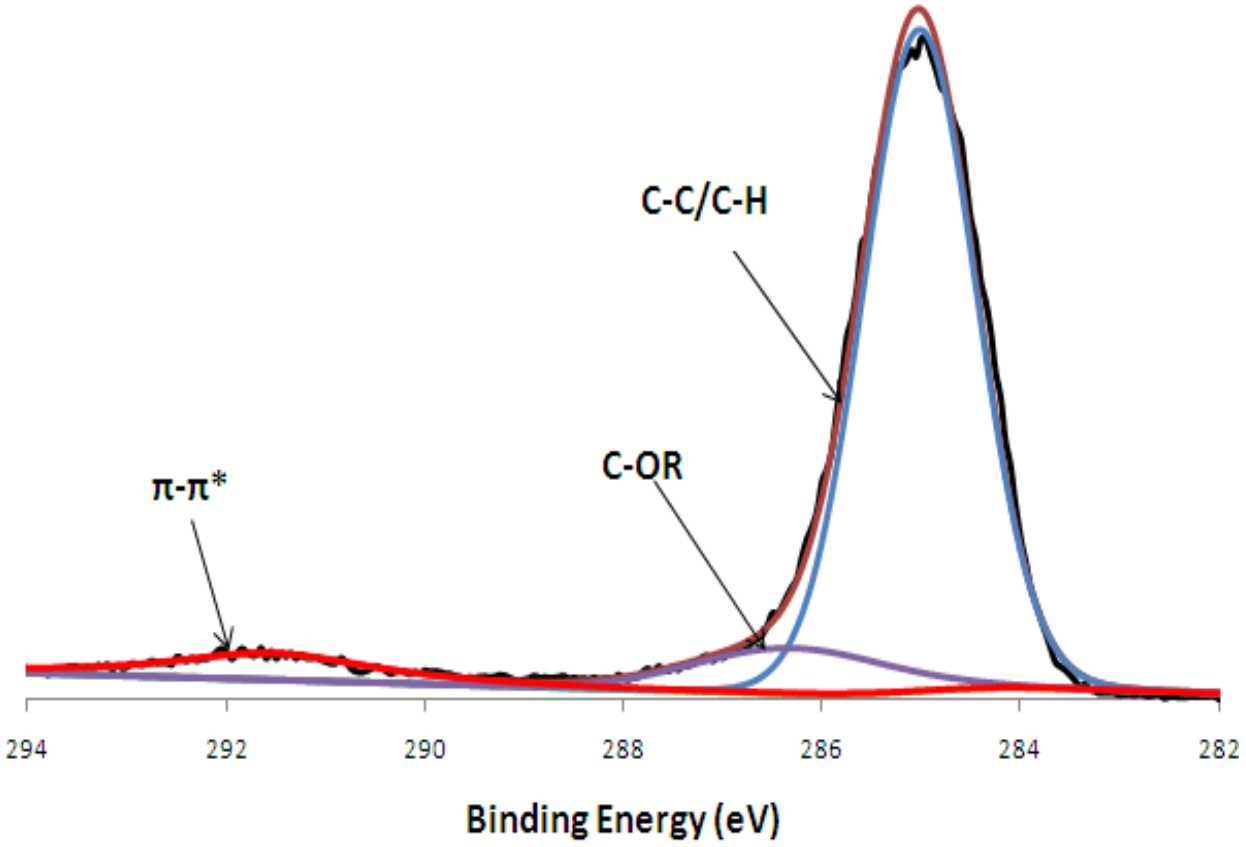

Figure 4. 2 High resolution of C1s peak fitted spectrum of UV/Ozone treated polystyrene after 10s UV/Ozone treatment, showing the functional groups incorporated and π–π* shake up satellite.

The effect of washing leads a change in the surface chemistry of the UV/Ozone treated and untreated polystyrene as seen in Figure 4.3. The incorporation of oxygen to the polystyrene surfaces led to the formation of oxygen containing functional groups such as alcohol/ether (C-OR), carbonyl/di-ether (C=O), carboxyl/ester (O-C=O). Figure 4.3A shows the distribution of oxygen containing functional groups within the C1s envelope, of unwashed substrates after 200s UV/Ozone treatment. The high resolution C1s envelope has been resolved into 4 chemically shifted components. The shifted peaks were typical of hydrocarbon groups (C-C/C-H, the main peak of the spectrum), where the remaining peaks were those of C-OR, C=O, O-C=O and the π-π^* shake-up satellite with the chemical shifts respectively around 1.5 eV, 2.8 eV, 4.2 eV and 6.5 eV. The above chemical shifts are the same when compared to standard chemical shifts for primary and secondary C1s species. The full width half maximum (FWHM) of the hydrocarbon peak for the untreated polystyrene was approximately 0.9 eV, while UV/Ozone has resulted in an increase in FWHM to approximately 1.5eV. The broadening of the peak area was due to the introduction of oxygen containing functionalities to the surface of the substrate. In Figure 4.3B, same chemically shifted peaks are shown after the washing process but with decreased intensity of the incorporated oxygen functional groups.

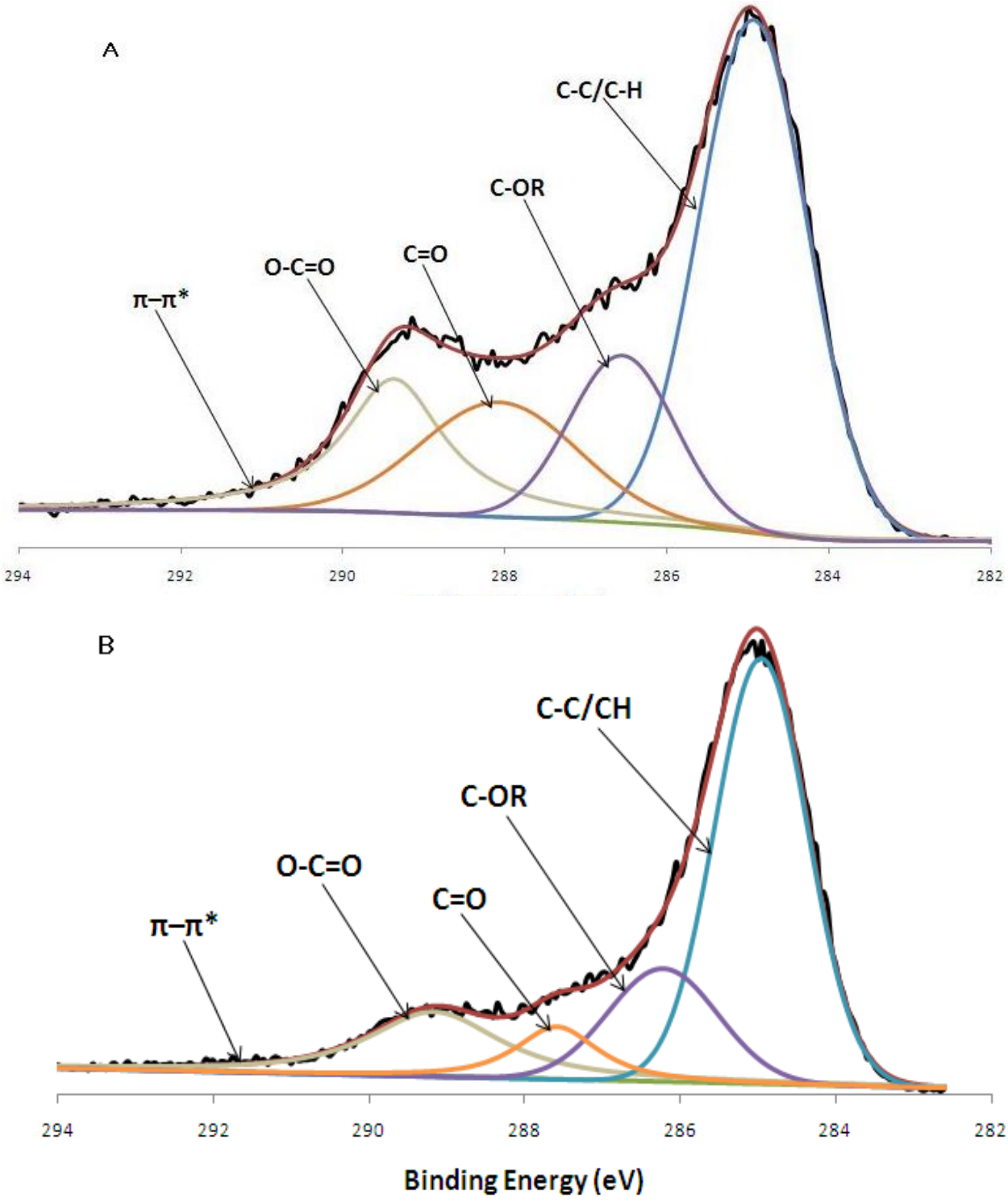

Figure 4. 3 High resolution of C1s peak fitted spectrum of UV/Ozone treated polystyrene after 200s UV/Ozone treatment, showing the functional groups incorporated. Unwashed (upper) and water washed (lower).

XPS analysis of the untreated polystyrene surfaces indicated no oxygen content suggesting that the surfaces were hydrophobic. Analysis of UV/Ozone treated polystyrene surfaces showed that the surface oxygen concentration increased with increasing treatment time up to 41 atomic % on unwashed polystyrene and 35 atomic % on washed surfaces after 900s as seen in Figure 4.4. Between 300 and 900s, very little increase is seen for both washed and unwashed polystyrene surfaces. The treated substrates were washed with distilled Milli Q water and this process led to a decrease in surface oxygen concentration levels due to the removal of low molecular weight oxidised products. As described above these loosely bound low molecular weight fragments did exist as a result of scission products from the photo oxidation process with extended treating times. Analysis of both treated and untreated surfaces indicated that the saturation of the oxygen concentration was reached after approximately 300s, leading to an increase in reactive products formed by the loosely bound low molecular weight oxidised products.

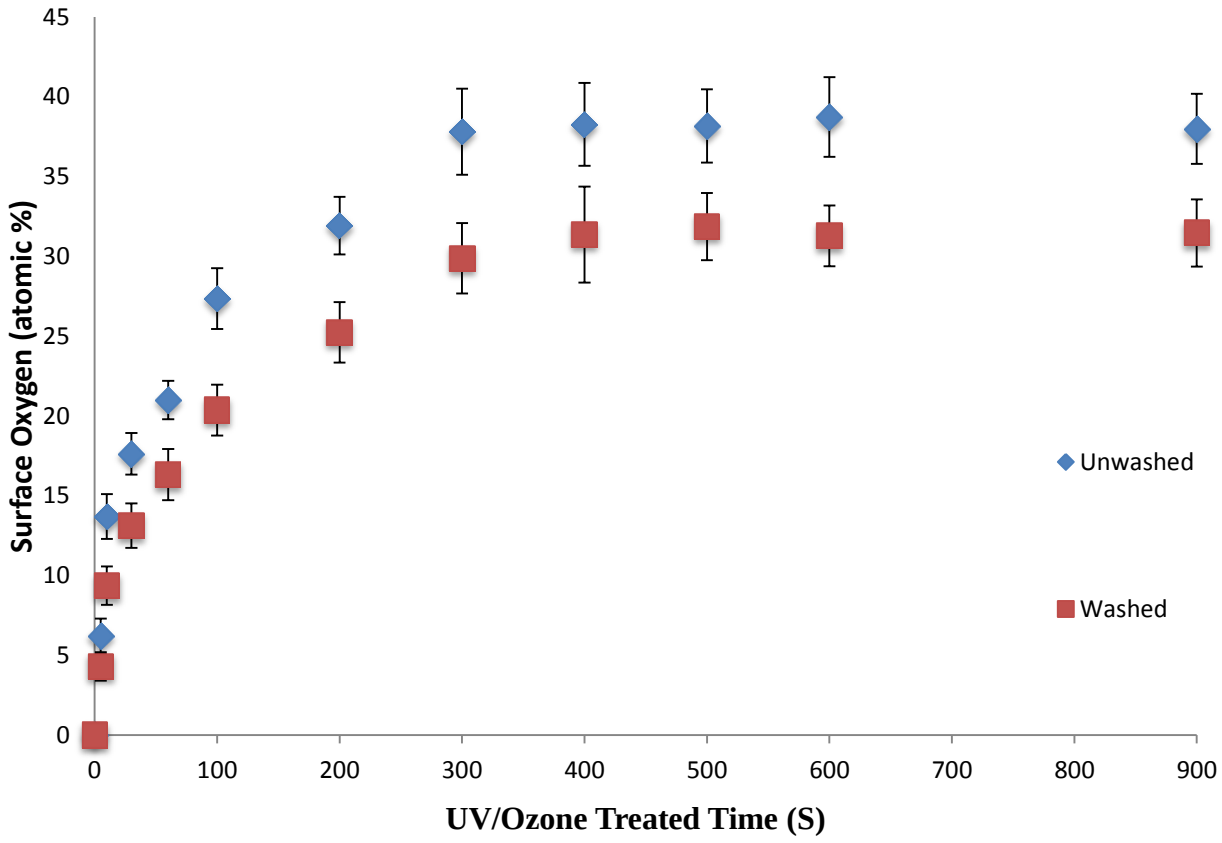

Figure 4. 4 Surface oxygen concentration of the washed and unwashed UV/Ozone treated polystyrene surfaces up to 900s treatment time, determined by XPS. Oxygen concentration increases with treatment to 900s; Sharp increase is seen in the first 300s, after which the increase is marked. Washing reduced the oxygen level as a result of the removal of low molecular weight oxidised products (±5% standard deviation, n=3).

The distribution of incorporated oxygen functional groups by UV/Ozone treatment up to 900s is shown in Figure 4.5. The atomic concentration of each functional group was calculated by the relative areas of the individual peaks from the XPS of washed UV/Ozone treated polystyrene. The levels of oxygen functional groups increased sharply with increasing UV/Ozone treatment up to 200s. Extended process from 200s to 900s, the concentration of each functional group remained constant suggests the surface oxygen has reached the saturated state. In contrast, π-π* peak has the largest peak area (6.2%) and dropped rapidly with the treatment time up to 200s (2.5%) and remained constantly between 200s to 900s treatment. The dominant oxygen functional group is C-OR (18%) measured at the longest treatment time and the formation hydrogen peroxide may suggest the increase of C-OR. Ring opening and pendant aromatic ring ablation within the oxidation process are suggested to be the reason for the decrease of π-π* peak (Teare et al., 2001, Teare et al., 2000a, Mitchell et al., 2004b, Mitchell et al., 2005b).

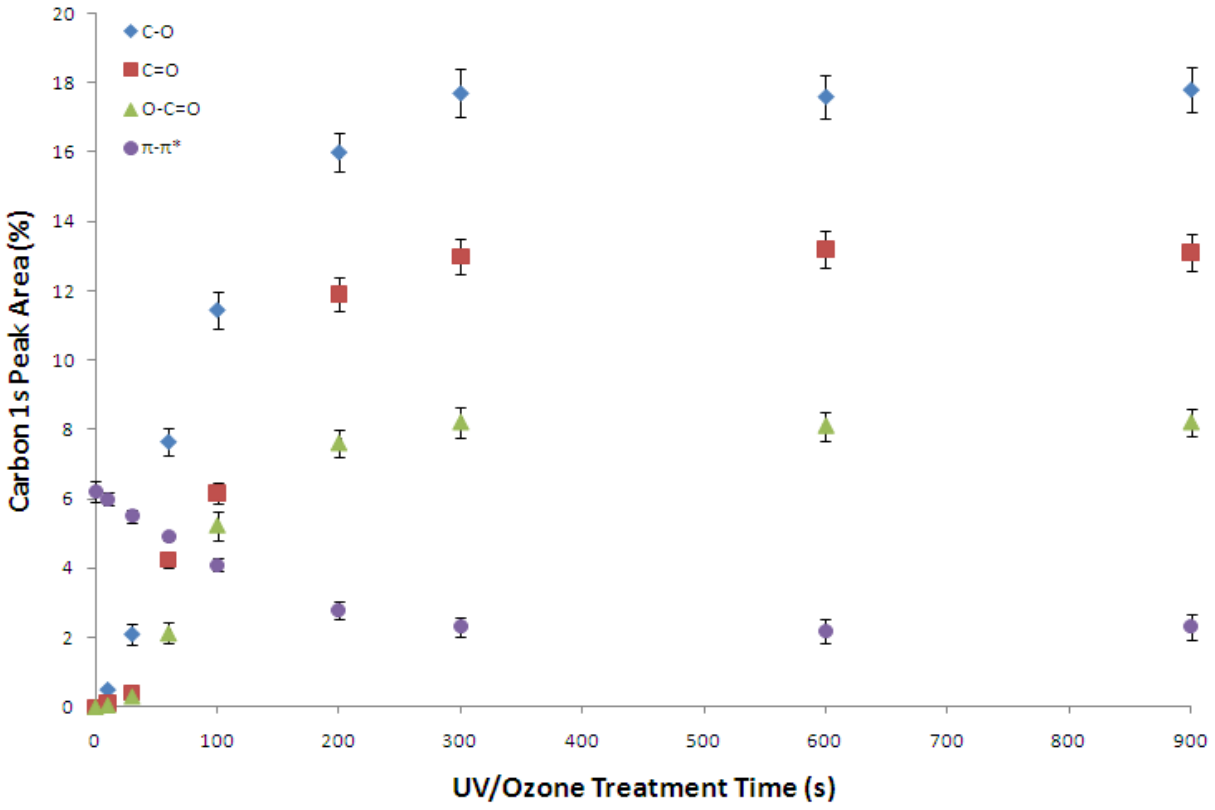

Figure 4. 5 Distribution of oxygen functional groups of UV/Ozone treated polystyrene after washing as a function of exposure time up to 900s (±5% standard deviation, n=3).

4.3.2 The wettability and surface energy analysis of UV/Ozone treated polystyrene surfaces

The measurement of contact angle on the untreated polystyrene surface was 90° and the finding is consistent with the others reported (Teare et al., 2000a, Callen et al., 1995, Teare et al., 2000b). The results showed that the surface become hydrophilic as a result of the introduction of oxygen. The contact angle reduces with the UV/Ozone treatment time up to 47° (after water washing) when exposure to UV for 300 seconds further processing will lead the water contact angle off as shown in Figure 4.6. The result is consistent with the oxygen level concentration as observed by XPS analysis previously discussed in this chapter.

Figure 4.7 shows the change of water wettability (in terms of water contact angle) during the first 120s treatment, it indicates that there is a linear decrease in water contact against the increase of treatment time ($R^2 = 0.97$).

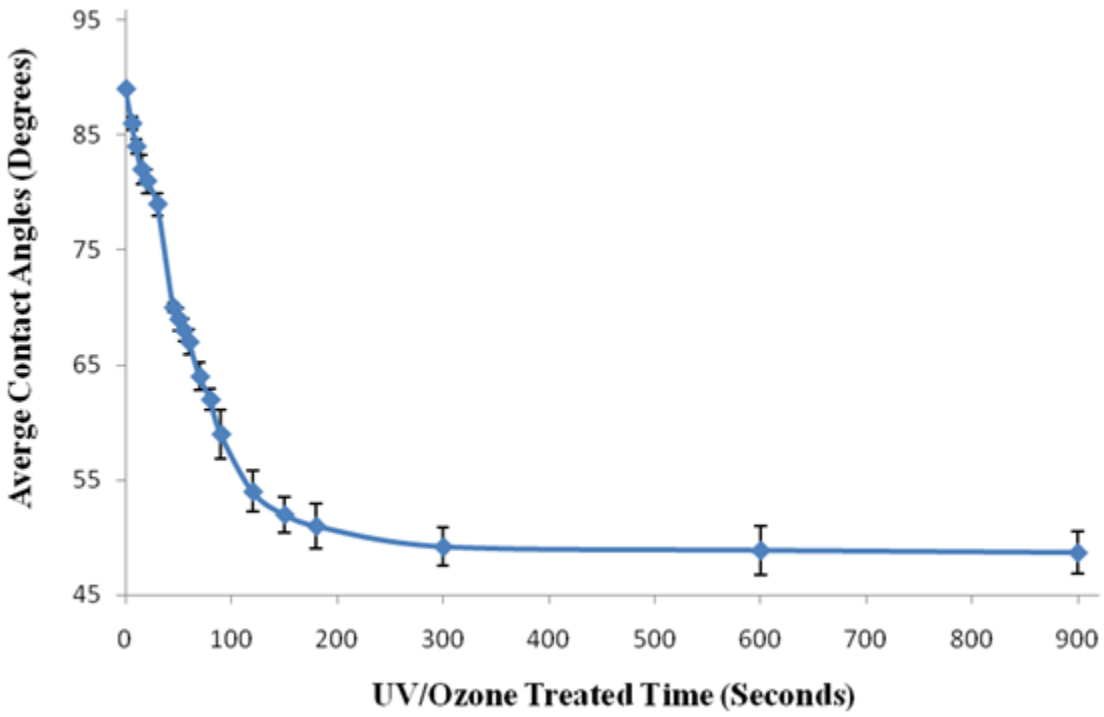

Figure 4. 6 The water contact angle of UV/Ozone treated polystyrene after washing from 0 to 900s treatment time (±5% standard deviation, n=3).

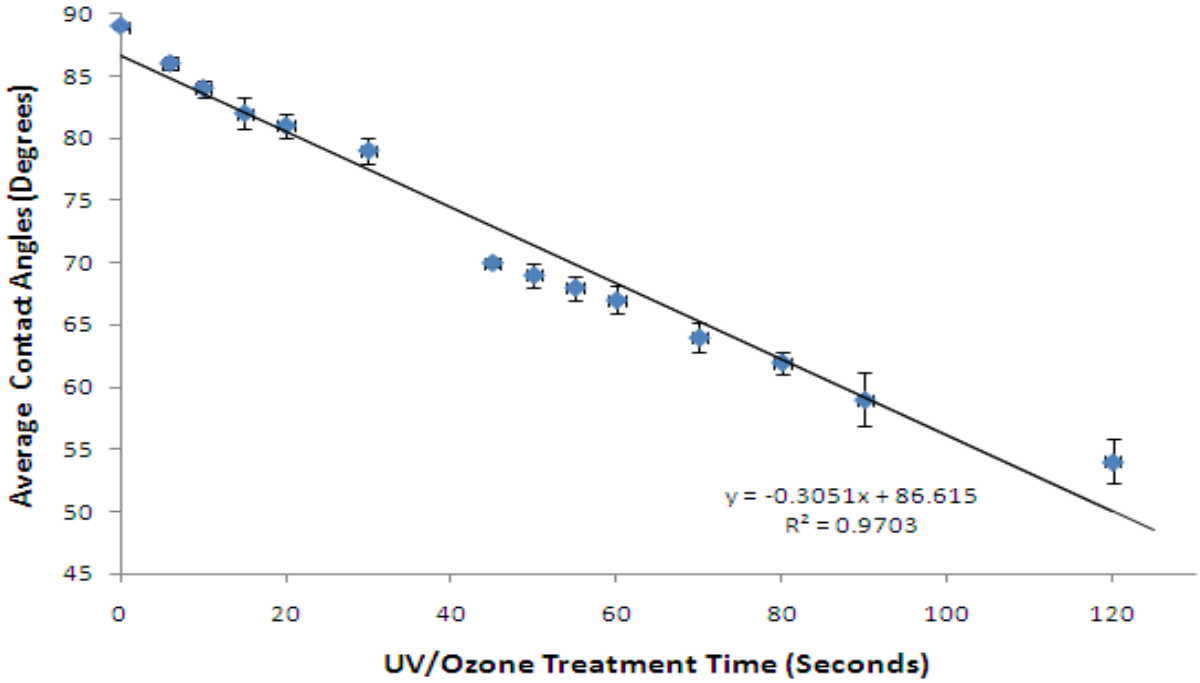

Figure 4. 7 The water contact angle of UV/Ozone treated polystyrene after washing up to 120s treatment (±5% standard deviation, n=3).

The total surface free energy was measured by using the Owens and Wendt method (Rudawska and Jacniacka, 2009). In Owens and Wendt theory, the total surface energy of a solid or liquid is divided into components which are a dispersive force and a polar component (Ton-That et al., 2000). Surface energies were measured with the average water contacts angles from water and di-iodomethane which has a surface tension of 72.8 mJ/m^2 and 50.8 mJ/m^2 respectively. As seen in Figure 4.8, the total surface free energy was found to be 40.9 mJ/m^2 on the untreated polystyrene and the value increased to approximately 54 mJ/m^2 at the surface subject to 900s treatment. Greatest increase was observed in the initial 200s, the surface energy and the polar component increased rapidly whist dispersive component remained fairly constant.

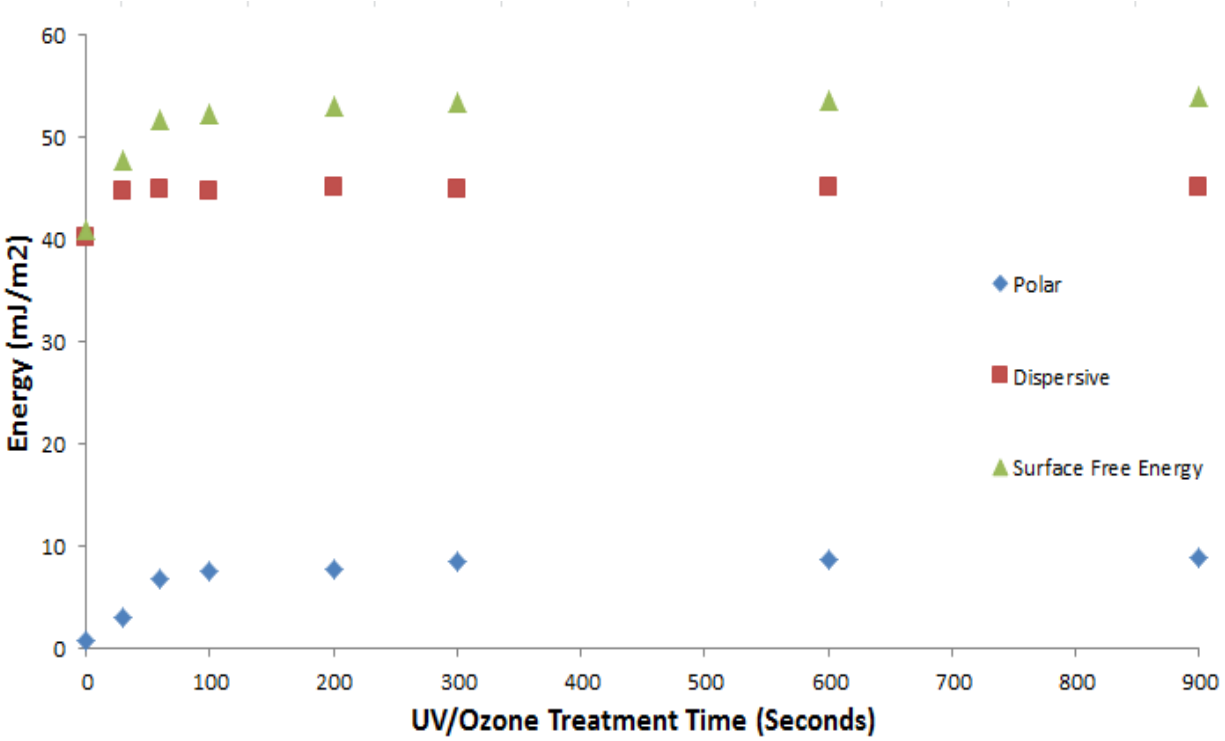

Figure 4. 8 Total surface free energy consists of both dispersive and polar of water washed UV/Ozone polystyrene surfaces up to 900s treatment time.

Another similar effect to washing was also seen upon leaving polystyrene surface in air known as aging. The aging effect on the surface wettability was evaluated on treated polystyrene that had been exposed to various duration of UV/Ozone treatment up to 300s, by measuring the water contact angle up to 21 days as shown in Figure 4.9. In the first five days, a loss of oxygen as a result of the increase of contact angle was observed and then was found to be relatively constant after the storage for up to 21 days.

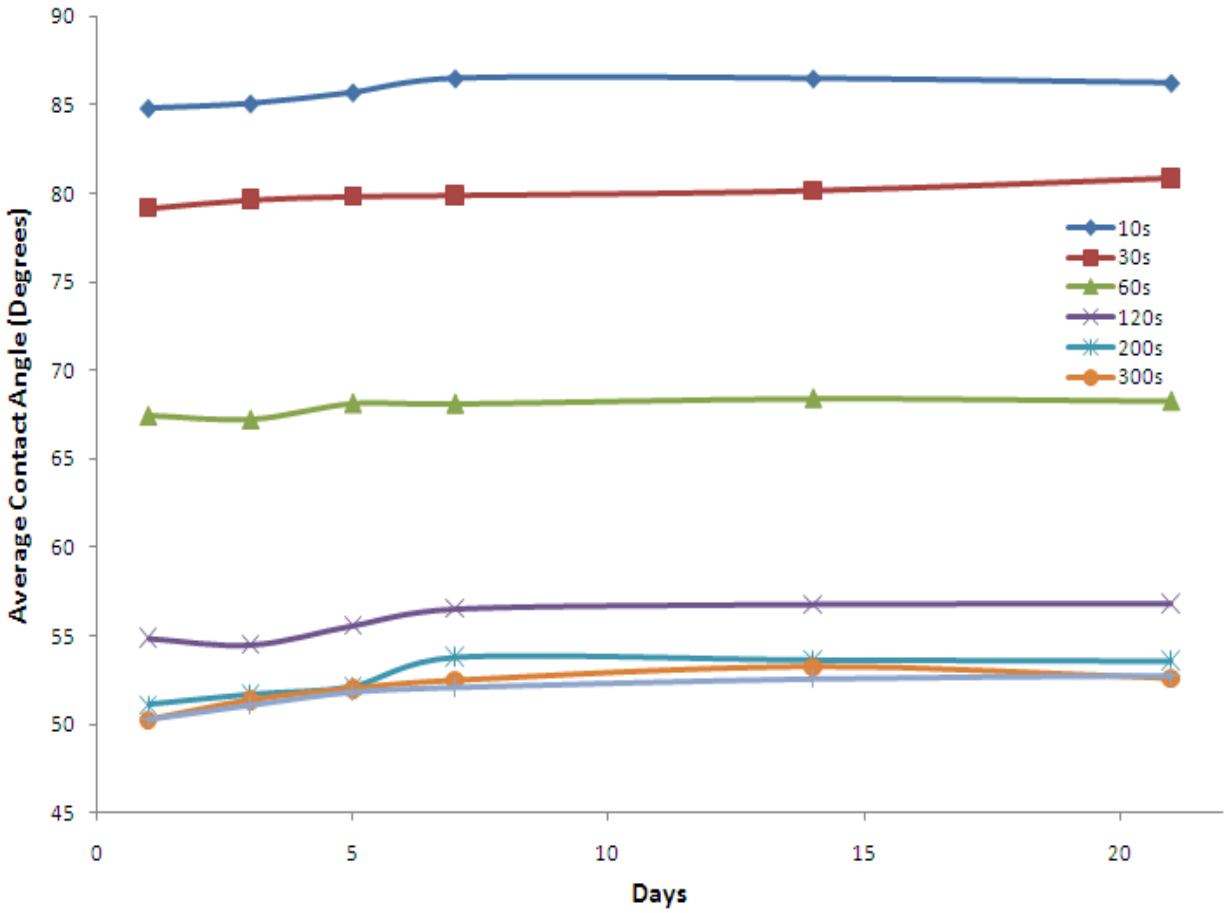

Figure 4. 9 The aging effect of storage time on the wettability for UV/Ozone treated polystyrene surfaces up to 300s treatment time in 21 days analysis.

4.2.3 Surface roughness analysis of UV/Ozone treated polystyrene surfaces

The finding of root mean square (RMS) surface roughness (*Rq*) of water washed UV/Ozone treated polystyrene surfaces relative to treatment time is shown in Figure 4.10. It can be seen that the surface roughness has a maximum value of 4.5±0.43 nm at the treatment time of 900s and a minimum value of 3.3±0.26 nm at the treatment time of 20s, but there are no significant changes among each sample compared to the untreated polystyrene surface and TCPs.

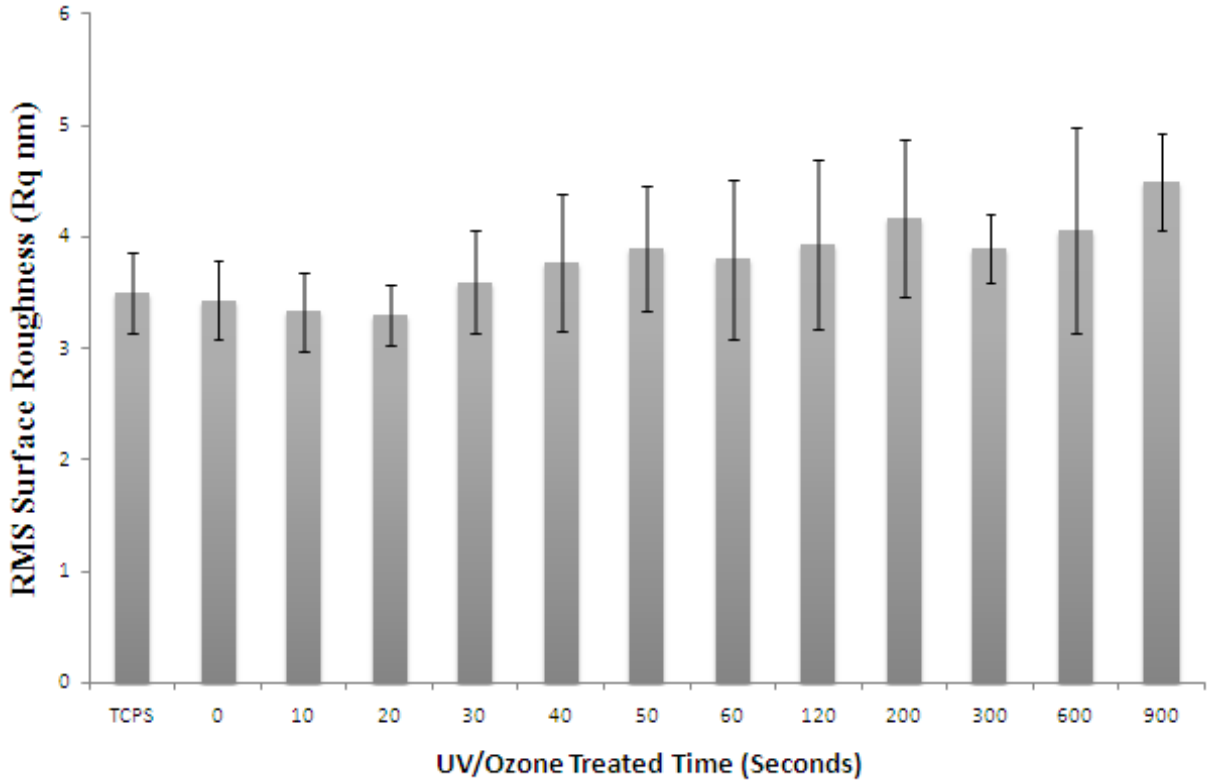

Figure 4. 10 The surface roughness of water washed UV/Ozone treated polystyrene surfaces relative to exposure time in seconds (±5% standard deviation, n=3)

4.4 Discussion

The result shows that UV/Ozone treatment incorporated oxygen functionalities to the untreated polystyrene surface. UV/Ozone led to an increase in surface oxygen level up to 41% for unwashed polystyrene surface and 35% for washed polystyrene surfaces after 900s treatments. Saturation state was reached after 300s treatment resulting from an equilibrium reached between the oxygen oxidised to the surface and the loss of volatile photolysis materials from the surface, the finding is similar from other researchers (Shard and Badyal, 1991b, Callen et al., 1995, Ton-That et al., 1999, Mitchell, 2006a, Poulsson et al., 2009, Poulsson, 2007a).

The difference in surface oxygen levels between the washed and unwashed was the result of the removal of low molecular weight oxidised materials. Washing led to a significant reduction of all the functional groups incorporated and the reduction was due to the removal of low molecular weight polymer scission products occurred via Norrish type 1 and 2 mechanisms during the process of UV/Ozone treatment (Geuskens et al., 1978a). It has previously been reported that the decrease of carbonyl and carboxyl/ester type groups was greater which is thought to be a results of these groups requiring more polymer scission to be incorporated and these low molecular weight fragments being removed by washing (Teare et al., 2000a, Davidson et al., 2005).

The low molecular weight oxidised material can make a significant impact to the biological environment (Davidson et al., 2005, Mathieson and Bradley, 1996, Mitchell et al., 2005b, Teare et al., 2000a). For example, the scission products which are water soluble may influence the biocompatibility of the oxygen modified surface by altering the ionic constitution of cell culture media, contacting the surfaces thereby affecting the cell adherence, attachment and growth in the biological system (Sadana, 1992, France and Short, 1998). It is also possible that those scission materials are cytotoxic due to the components of aldehydes and ketones (Davidson et al., 2005). The removal of the low molecular weight oxidised materials on polymers after the treatment of UV/Ozone is vital for clinical use. For example, the debris remained on the unwashed surfaces of a biomedical implant will inevitably interfere with the physiological system surrounding the tissue due to uncovalently bonded to the material surfaces. The process of washing of the modified surfaces ensures the consistency and also ensures the removal of any possible cytotoxic components existed. Mitchell et al. suggested that the low molecular weight fragments significantly affect the cell attachment and proliferation and further oxygen reduction was observed after washed by ethanol and methanol (Mitchell et al., 2004b).

The XPS spectrums confirmed the UV/Ozone induced oxygen incorporation by broadening of C1s peak. The oxygen functional groups were estimated by the deconvolution of the C1s spectrum, consisting of alcohol/ether (C-OR), carbonyl/di-ether (C=O) groups and carboxyl/ester groups (Briggs and Beamson, 1993). It is believed that alcohol/ether groups were the domination at the low levels of UV/Ozone treatment; carbonyl/di-ether groups and carboxyl/ester groups were formed with longer treatment (Callen et al., 1995, Lubarsky et al., 2004, Teare et al., 2001, Ton-That et al., 2000). As discussed above that washing led to a reduction in surface oxygen, and the reduction was observed equal in all oxygen functionalities. The remaining oxygen functional groups were suggested to be bound into the polystyrene backbone and trapped within the outermost layer of the surface (Callen et al., 1995, Davidson et al., 2005, Poulsson, 2007a).

Wettability and surface energy are two surface factors suggested to influence protein adsorption, conformation and subsequently cell attachment, proliferation and migration. A number of studies have reported that cells such as endothelium, fibroblast prefer hydrophilic rather than hydrophobic surfaces (Vogler, 1998, Callen et al., 1995, Curtis et al., 1983, Mitchell et al., 2004b). As described in Section 3.2.3, the definition of contact angle is the angle of a three phase line which occurred between a solid surface, a liquid and a vapour in equilibrium. It has been reported that the surface oxygen concentration determines the wettability of polymer surfaces (Teare et al., 2000b) and the wettability of these surfaces is directly related to the increase in surface oxygen and this can be attributed to an increase in the polar component of the surface energy via introduction of oxygen containing species (Friedrich et al., 1998). The increase in surface energy is consistent with the XPS findings which a large amount of carbon oxygen functional groups introduced during the treatment period. These observations obtained are similar with the results shown in literature (Yasuda et al., 1994, Kwok et al., 1997, Dhathathreyan and Maheshwari, 2002). The overall surface energy measurement values are dependent on the pair of liquids employed and the equation in the method used for calculation (Mangipudi et al., 1995, Tirrell, 1996).

Aging effect suggested that an overall decrease in carbon oxygen functional groups occurred and the majority loss component is O-C=O functional group (Teare et al., 2000b). It is also reported that the polymer samples kept sealed and out of the direct light were shown to be stable up to 8 months (Friedrich et al., 1998, Callen et al., 1995).

It was demonstrated that surface roughness can influence on cell adhesion (Curtis et al., 1983, Domke et al., 2000, Ellingsen and Lyngstadaas, 2003, Teare et al., 2000a), thus it is important to know the changes

in surface roughness changes with increasing UV/Ozone treatment. Treatment showed that surface roughness was not affected by UV/Ozone treatment, the variation is much less than the results reported by Rahul et al., that the treatment was found to influence the cell proliferation and adhesion (Rahul et al., 1994).

4.5 Conclusion

UV/Ozone treatment can be regarded as a fast, easy and inexpensive surface modification method for introducing oxygen functional groups onto the polystyrene surfaces or the other polymer materials. The treatment may be of interests for clinicians as it does not require complicated process such as vacuum condition or any sophisticated monomer compared to plasma modification methods. Overall, UV/Ozone treatment increased the surface oxygen content with the correlation of treatment period on the untreated polystyrene surfaces. A sharp increase was found in the surface oxygen in the initial 300s and the saturation was reached after 300s treatment as a result of an equilibrium being reached between oxygen incorporation by photo oxidation and loss of volatile photolysis products from the surface. Treatment times longer than 900s did not affect the surface oxygen content any further. The difference in the surface oxygen levels of washed and unwashed surfaces was due to the removal of the lower molecular weight oxidized material, which were produced due to polymer scission as a result of the UV/Ozone treatment. The loosely bound low molecular weight products were removed by washing as these products not only interface with physical adhesive properties, but would also influence on pH and ion concentration leading to changes in protein adsorption, configuration and cell-biomaterial interaction. The oxygen incorporation was confirmed by changes which led to broadening of the C1s peak after the UV/Ozone treatment. The incorporation of oxygen containing functional groups was estimated by deconvolution of the C1s spectrum, showing a combination of ether/alcohol, carbonyl and carboxylic acid/ester, which were shown by the chemical shifts for the C1s spectrum.

The measurement of contact angle on the untreated polystyrene surface was approximately 90° and reduced with the UV/Ozone treatment time up to approximately 50° after water washing and remained constantly after 300s of treatment. The surface energy measured using Owens and Wendt method shows an increase from 40.9 to 54.0 mJ/m^2 with increasing treatment time. Storage of the various UV/Ozone treated surfaces in air shows that a loss of oxygen due to the increase of contact angle in the first five days

and then was found to be constant for up to 21 days. Surface roughness analysis using AFM shows there is no systematic effect by the irradiation.

These results demonstrate the characteristics that are believed to facilitate cell growth. The modified surfaces were then used in a series of experiments to determine the ability of endothelial cells in term of adhesion, proliferation and migration. These characteristics are explored in the following chapter.

Chapter 5 Human Umbilical Vein Endothelial Cell Proliferation and Migration on UV/Ozone Treated Polystyrene Surfaces

5.1 Introduction

Following characterisation of the UV/Ozone treated polystyrene surface reported in chapter 3, the ability of human umbilical vein endothelial cells (HUVECs) to grow on the modified surface was investigated. HUVEC is widely used as an endothelial model *in vitro* vascular research due to the ease of isolation, strong proliferative potential at higher passage numbers and also the well established *in vitro* angiogenesis studies (Bagley et al., 2003, Augustin, 2004). The previous chapter demonstrated that UV irradiation oxidised the polystyrene surface and this resulted in the formation of functional oxygen groups including the combination of ether/alcohol, carbonyl and carboxylic acid/ester. The change in surface chemistry was shown to increase wettability which is believed to influence both protein adsorption and conformation and subsequently cellular responses such as cell adhesion and proliferation (Browne et al., 2004, Cataldo, 2001, Davidson et al., 2004, López Gejo et al., 2005, Mitchell et al., 2004b). Moreover, the results reported in previous chapter showed that the polystyrene surface chemistry produced by UV/Ozone treatment share similarities with the surface chemistry of commercial available tissue culture plastics (TCPs), which are routinely used as a surface for cell growth. The untreated polystyrene surface offers very limited support for cell attachment and proliferation on the other hand (Curtis et al., 1983, Poulsson et al., 2009, Teare et al., 2000a).

The aim of the work described in this chapter was to determine the ability of endothelial cells to grow on the modified surface and to optimise their response by treatment with UV/Ozone in comparison with tissue culture plastics (TCPs) and an untreated surface. In order to investigate the effect of UV/Ozone treatment on HUVECs, both cell proliferation and migration were examined as these are recognized as two key indicators of endothelial cell growth. Cell proliferation and migration are necessary processes in angiogenesis (Carmeliet, 2005). De Donatis et al. hypothesise that either migration or proliferation is induced at a given time for a single cell activity (De Donatis et al., 2010). Furthermore, the effect of a hypoxic environment on HUVEC response was also investigated in this work. Hypoxia occurs when the oxygen level in tissue is below optimal conditions to maintain cell function, the cause can be either the physiologic reasons such as strenuous exercise or pathophysiologic circumstances such as carcinogenesis and subsequent angiogenesis (Li et al., 2010). The insufficiency of oxygen will initiate a series of responses to enable the cell to respond which includes improved glucose homeostasis and increased cell proliferation (Semenza et al., 1991, Semenza, 2000).

To investigate the cell responses on the modified surfaces, the effect of the UV/Ozone treatment on cell proliferation was examined by the alamar blue cell viability assay, cell morphological change was determined by Phalloidin staining; 5-bromo-2'-deoxyuridine (BrdU) staining was used to assess the cell activity, proliferation whereas cell migration was determined by using an radial migration assay (Gadad et al., 2013b, Gadad et al., 2013a).

5.2 Methods

5.2.1 Surface preparation

As previously described in Section 3.2, the polystyrene surface was treated with UV/Ozone for 120s and the surface was cleaned, dried and sterilised for cell culture studies.

5.2.2 Cell culture

HUVEC was used to investigate the biological effects caused by UV/Ozone treatment on polystyrene surfaces due to its versatile research applications. HUVECs are relatively easy to culture and are a valuable cell model for human vascular research, such as angiogenesis, inflammation, atherosclerosis, blood clotting, vasoconstriction and vasodilation. The Growth and propagation of HUVEC were fully discussed from Section 3.4.1 to 3.4.3.

Hypoxic cell culture experiments were carried out as described in Section 3.4, where HUVECs were incubated in a humidified atmosphere of 5% CO_2, 5% O_2 and 90% air (not including O_2) in a Galaxy R CO_2 incubator at 37°C. Nitrogen was inflated into the incubator to reduce the oxygen concentration to create the hypoxic atmosphere. Nomoxic condition is 5% CO_2 and 95% air in contrast to hypoxia.

5.2.3 Cell proliferation assay

The Alamar blue assay was used to monitor cells proliferation in a continuous way over a period of time (0 hr to 48h) and to explore the trend of cell proliferation within a specific time period. Experimental details are presented in Section 3.4.5. The results are presented in this section as net absorbance reading (nm) and presented as mean of 3 experiments or representative of 3 experiments.

5.2.4 Cell migration assay

The measurement of cell migration was achieved by seeding HUVECs with a concentration of 2.4 x 10^5 cells /mL within a sterilised 6 x 8 mm cloning ring (outer diameter x height). The cells formed a circular monolayer of dimensions and pictures were taken of the monolayer in the same position at different time points as specified in the text in order to monitor cell migration. The migration distance was determined using the Qwin software (Leica). Details have been fully described in Section 3.4.7. The results were presented as net migration in micrometers (µm) and analysed with SPSS (version 17.0). The results are presented as mean of 3 seperate experiments.

5.2.5 Cytochemical staining

To visualize specific proteins, cytochemical staining was used. Phalloidin staining was used to examine the distribution of F-actin in this study. Phalloidin is a bicyclic heptapeptide, which specifically binds to the interface between the subunits of F-actin and locking adjacent subunits together as discussed in Section 3.4.7.1. BrdU staining was used to distinguish cells which were proliferating or quiescence as described in Section 3.4.7.2.

5.2.6 Statistical analysis

All the results data were statistical analysed. Student's t-test was used to perform statistical analysis on the date resulting from HUVEC proliferation and was analysed with Microsoft Excel 2007. The effect between cell proliferation on the UV/Ozone treated and TCPs were compared to untreated polystyrene surfaces, $*p<0.05$ was considered to be significant. The statistical analysis on HUVEC migration is more complex performed by analysis of variance (ANOVA) followed by Boferroni post host test, $*p< 0.05$, $**p<0.01$, $***p<0.001$ when compared as indicated.

5.3 Results

The effect of UV/Ozone treatment on HUVECs proliferation was determined by Alamar Blue assay which provides quick and reproducible results to allow the ease comparison with untreated polystyrene. The Alamar Blue cell viability assay was used to measure the influence of UV/Ozone treatment on cell proliferation on the modified surfaces. TCPs were used as positive control as commercially designed for ideal cell attachment and proliferation purposes. Untreated polystyrene surface was used as negative control as literature suggests they provide limited support for cell growth due to its surface chemistry (Curtis et al., 1983, Mathieson and Bradley, 1996, Teare et al., 2000a, Mitchell et al., 2005a).

5.3.1 The effect of UV/Ozone treatment on HUVECs proliferation over 48 hour period

To ascertain the UV/Ozone treatment effect on cell proliferation, a comparison was made with TCPs and untreated polystyrene surfaces as shown in Figure 5.1. The result shows cell growth increased on all surfaces over 48 hr periods, and both 120s UV/Ozone treated and TCPs showed significantly higher cell growth than untreated polystyrene at the incubation time examined proving more effective than untreated surface. As early as 6 hr following initial seeding difference was evident with net absorbance reading of 0.03 ± 0.01, 0.068 ± 0.01, 0.067 ± 0.004 nm for untreated, TCPs and UV/Ozone 120s treated respectively. The net absorbance for 6 hr shows an increase of 55% was observed on 120s UV/Ozone treated than untreated surface and similar on TCPs when comparing to untreated surfaces. Generally, the net absorbance reading for the untreated surface was lower than 120s UV/Ozone treated surface (54% lower at 6 hr, 55% at 24hr and 53% at 48hr) and TCPs (54% lower at 6 hr, 43% at 24hr and 39% at 48h), statistical analysis shows the difference was significant for TCPs and UV/Ozone treated compare to untreated at 24 hr and 48 hr. Furthermore, comparisons of cell proliferation between TCPs and 120s UV/Ozone treated polystyrene over 48 hr showed that the TCPs were 22% lower than 120s UV/Ozone treated and it was statistically significant.

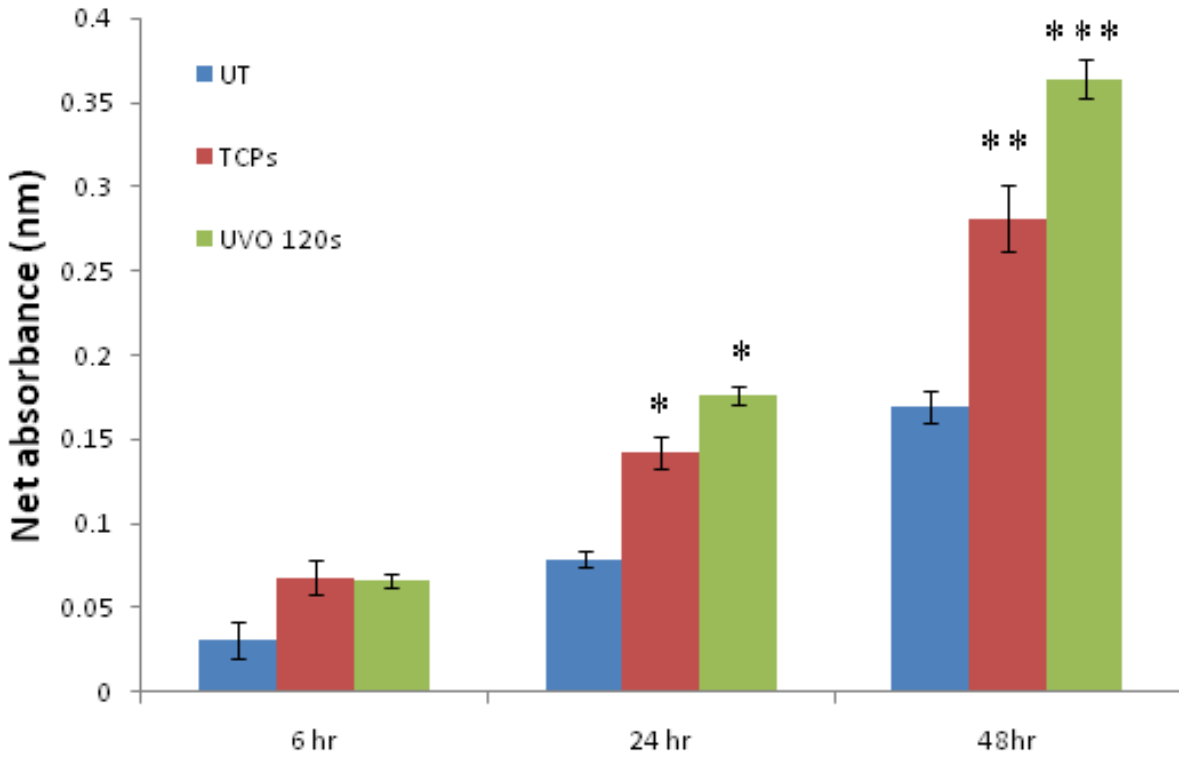

Figure 5. 1 Cell proliferation of HUVECs on UV/Ozone treated polystyrene surfaces. UT refers to untreated polystyrene, TCPs refers to tissue culture plastics and UVO 120s refers to 120 seconds UV/Ozone treatment period. Cell proliferation was compared to untreated surfaces as a control showed in dark blue bar. No significant difference was seem between all groups at 6 hr, significant difference was shown on TCPs and UV/Ozone treated surfaces compared to untreated at 24 and 48 hr. The initial seeding well density was $7,800x10^3$ cells/cm^2 (*$p< 0.05$, **$p<0.01$, ***$p<0.001$by student t-test of unequal variance, n=6).

A comparison of reorganisation of F-actin cytoskeleton over 48 hr was made between UV/Ozone 120s treated and untreated as shown in Figure 5.2. After 48 hr of incubation, the pattern and distribution of F-actin on untreated surfaces illustrated that cell were not adhering to untreated surfaces to enable cells to spread and proliferate as mostly spherical shape shown due to the unfavour surfaces (Figure 5.2a) and very few polygonal shaped were also found (Figure 5.2c). In contrary, F-actin was distributed well spread, more intensive and prominent on UV/Ozone 120s treated surfaces, formation of the stress fibres of polygonal shaped HUVECs were also seen in over 48 hr incubation (Figure 5.2d).

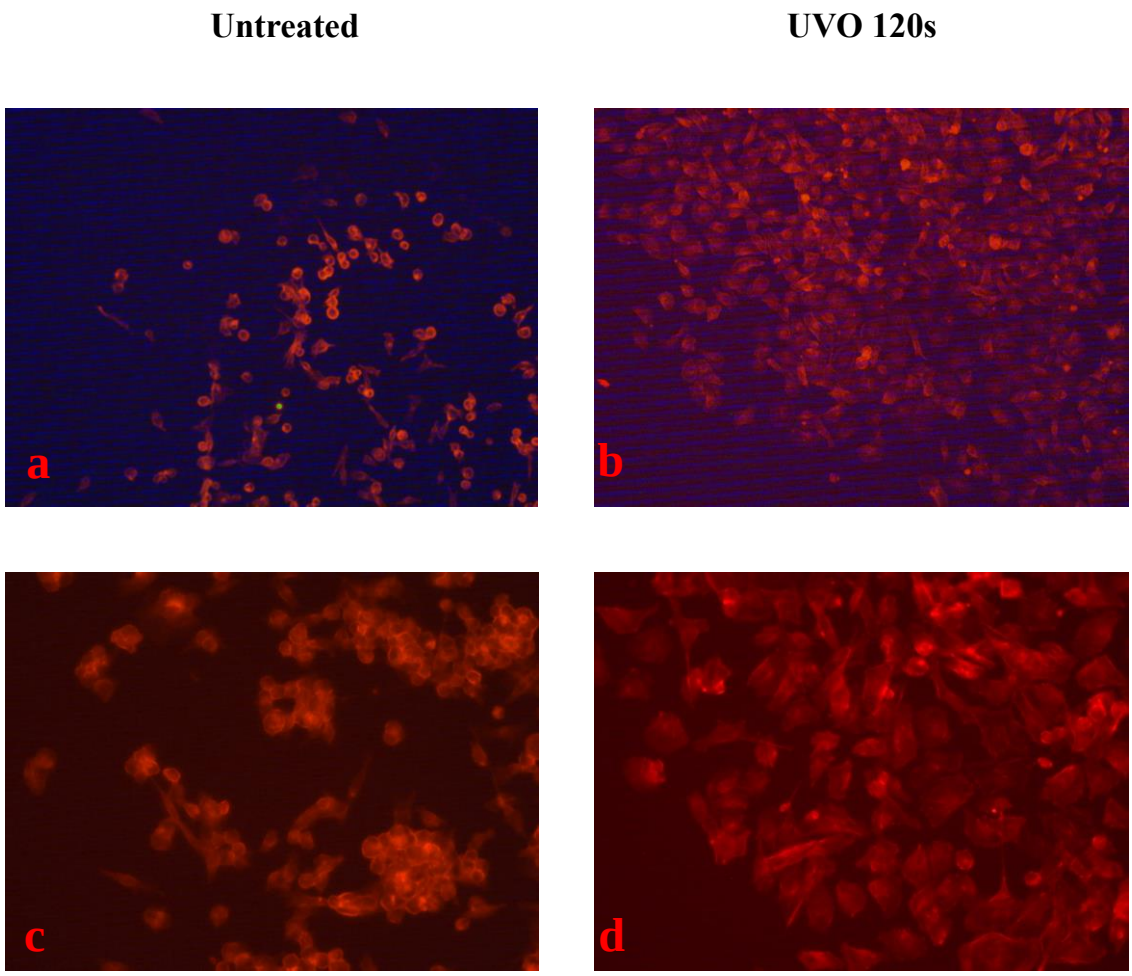

Figure 5. 2 Comparison of F-actin distribution by Phalloidin staining between UV/Ozone 120s treated and untreated over 48 hr. A and C show the distribution of F-actin on untreated polystyrene surface (x10 and x25 magnification respectively). B and D show the F-actin distribution on UV/Ozone 120s treated polystyrene surfaces (x10 and x25 magnification respectively). HUVECs at A and C, B and D are different to each other.

5.3.2 The effect of UV/Ozone treatment length on the proliferation of HUVECs over a 48 hour period

Having established the effect in proliferation between UV/Ozone treated, untreated and TCPs, the influence of duration of UV/Ozone treatment was also studied. After 6 hour of incubation, UV/Ozone treated surface supported the attachment of cells even at a very short treatment period (10s) which was 56% more than untreated surfaces (Figure 5.3). Similar results were found at a high level of UV/Ozone treatment period with an increase of 48% on UV/Ozone 60s treated, 54% on UV/Ozone 120s treated, 56% on UV/Ozone 180s treated, 61% on UV/Ozone 300s treated, 55% on UV/Ozone 600s treated and 49% on UV/Ozone 900s treated. After 24 hours, the result showed that cell proliferation on surfaces treated for 180s and 300s were significantly higher than untreated surface with an increase of 61% and 62% respectively ($p<0.01$) compared to the rest of UV/Ozone treatment periods, the reading were 50% (10s), 52% (60s), 55% (120s), 58% (600s), 50% (900s) higher compared to untreated surfaces which was also statistically significant ($p<0.05$). Over 48 hours, greatest increase was observed with 60s, 120s and 180s of UV/Ozone treatment compared to untreated surface with an increase of 51%, 53% and 53% respectively ($p<0.001$). The increase of reading of UV/Ozone treated periods of 10s, 300s, and 600s compared to untreated surfaces were 48% , 51% and 47% respectively ($p<0.01$), the lowest increase was 39% compared to untreated surface which was also statistically significant ($p<0.05$).

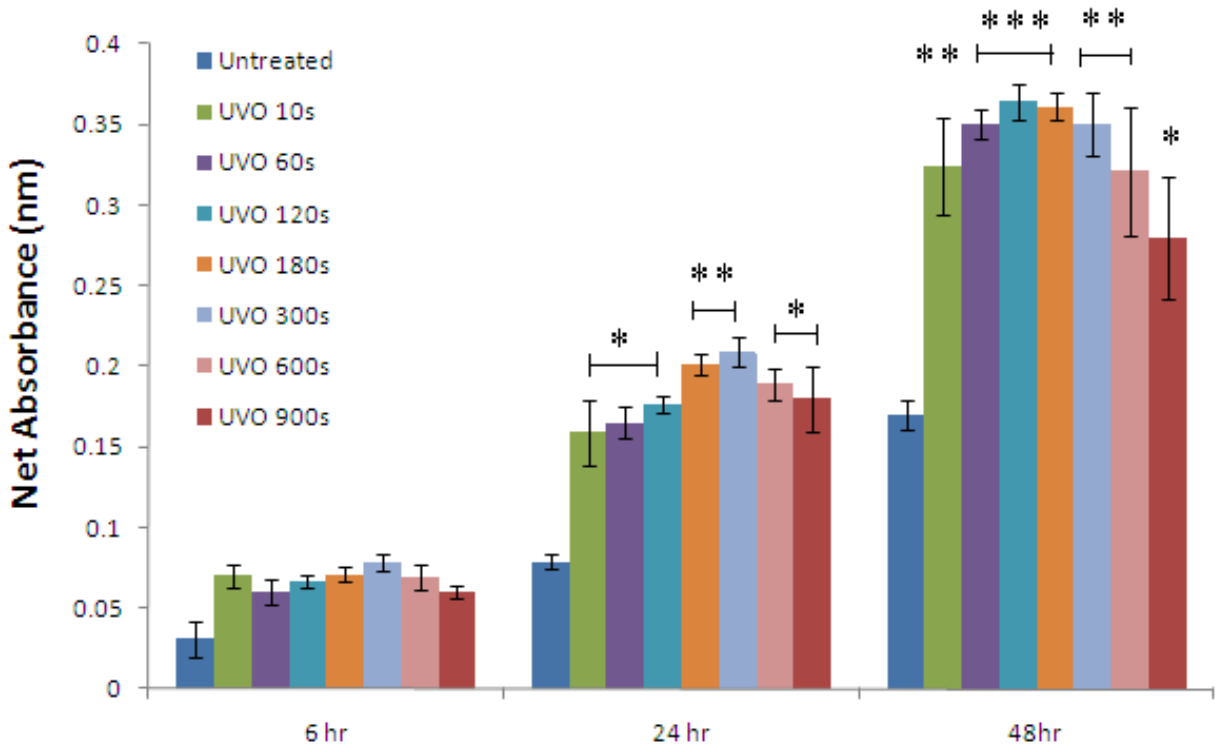

Figure 5. 3 The effect of the level of UV/Ozone treatment on HUVECs proliferation over the period of 48 hours. UVO 10s/60s/120s/180s/300s/600s/900s refers to the period of 10 seconds/60 seconds/120 seconds/180 seconds/300 seconds/600 seconds and 900 seconds of UV/Ozone treatment. Statistical analysis was compared all levels of UV/Ozone treated surfaces to untreated surfaces (dark blue bar). The initial seeding well density was 7.800 x 103 cells/cm2. (*p< 0.05, **p<0.01, ***p<0.001by the student test of unequal variance, n=6)

5.3.3 The effect of UV/Ozone treatment on HUVECs migration over 48 hour period

The above finding had shown that UV/Ozone treatment significantly enhanced the ability of HUVEC to adhere to and proliferate compared to untreated polystyrene surfaces, and then the effect of UV/Ozone on HUVECs migration was investigated

Increased net migration distances in both TCPs and UV/Ozone 120s treated surfaces were observed when compared to untreated polystyrene surfaces at 6hr onwards as shown in Figure 5.4. At 6 hr, there is no significant difference between TCPs and UV/Ozone treated (TCPS: 36.71±2.34 µm, UVO 120s: 37.55±2.09 µm) but the migrated distance on both of them are found to be significantly higher than untreated polystyrene (26.68±1.89 µm) with an increase of 27% and 29% respectively. Over 24 hr of incubation, the migration of HUVECs on TCPs and UV/Ozone treated for 120s was significantly increased (39% and 36%) compared to untreated. (TCPS: 104.82±7.76 µm, UV/Ozone 120s: 99.38±4.02 µm, untreated: 64.41±4.32 µm). Similar results were found over 48 hr with an increase of 39% on TCPs and 38% on UV/Ozone 120s treated (TCPS: 203.64±10.32 µm, UVO 120s: 205.79±12.02 µm, untreated: 124.17±9.32 µm). Overall HUVECs rate of migration was greater on both UV/Ozone 120s treated and on TCPs than on the untreated surface. There were no significant differences between UVO 120s treated and TCPs at all periods examined. The migration of HUVECs at 48 hr was significantly higher than at 24 hr and 6 hr for all the test conditions.

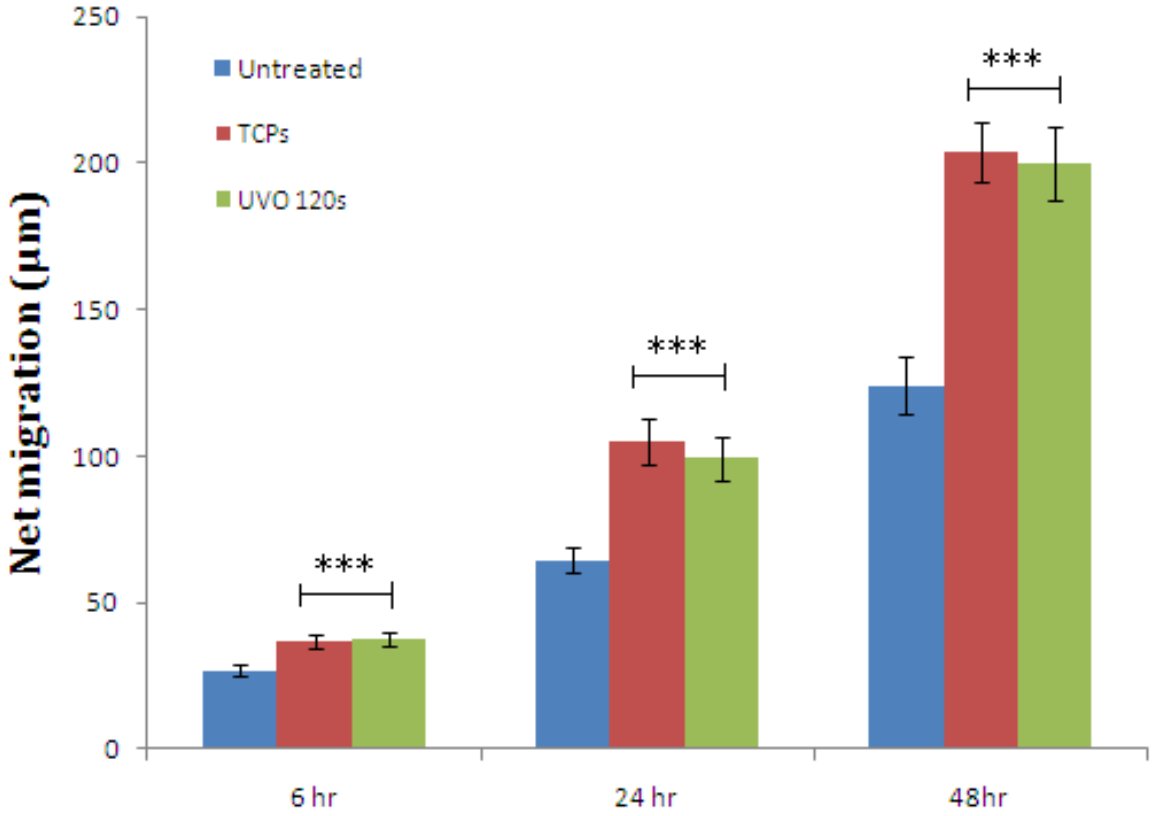

Figure 5. 4 The effect of UV/Ozone treatment on distance of cell migration compared to untreated, TCPs and UV/Ozone 120s treated polystyrene surfaces. HUVECs were seeded at a density of $1.2x10^4$ cells/cm^2 and incubated overnight to form the monolayer. The ring was taken out in the next morning and this time point was stated as 0 hr. The result is shown in the mean of net migration of HUVECs ± SD at 6hr, 24 hr and 48 hr from three individual experiments. Statistical analysis was made between TCPs/UV/Ozone 120s treated to untreated surfaces (***$p < 0.001$, analysis of variance (ANOVA) followed by Boferroni post host test when compared to untreated surfaces, n=40).

Actin cytoskeleton reorginasation such as F-actin is strongly linked to the mechanisms of cell motility of most cells migration. Figure 5.5 shows the distribution of F-actin on untreated and UV/Ozone 120s treated polystyrene surfaces. The distribution of F-actin is more intense on UV/Ozone treated compared to untreated as discussed in the previous section. Grouped spherical shaped distribution is mostly seen on untreated surfaces at 6 hr due to the unfavour contact surfaces; at 24 hr, some HUVECs adopt the condition followed by changing shape to polygonal. In contrary, the distribution of F-actin is well spread, more dominant and polygonal shaped; higher magnification also indicates the formation of stress fibres and the staining is prominent towards the direction of migration.

Figure 5. 5 The effect of UV/Ozone treatment on cell morphology compared to untreated surfaces at 6 and 24 hr incubation. The comparison is made by the distribution of F-actin with Phalloidin staining at left, centre and right of the HUVECs monolayer with the magnification of x10 and x25.

	Untreated	UV/Ozone 120s treated
6 hr	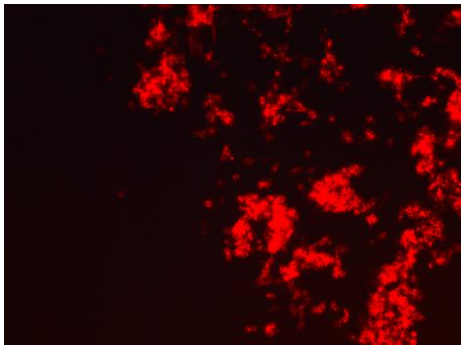	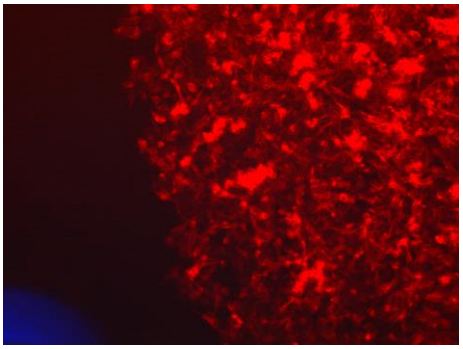
	x10	x10
	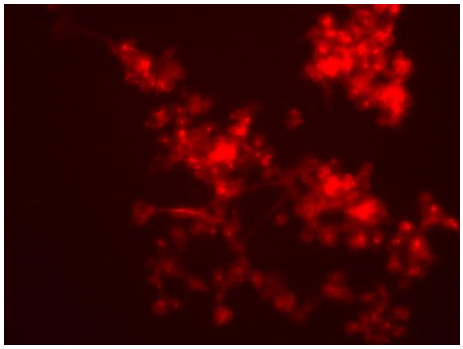	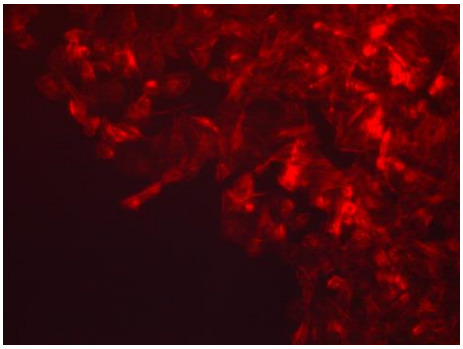
	x25	x25
24 hr	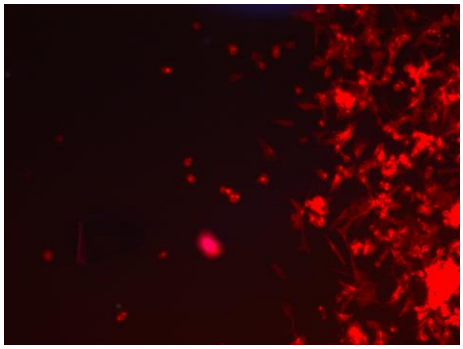	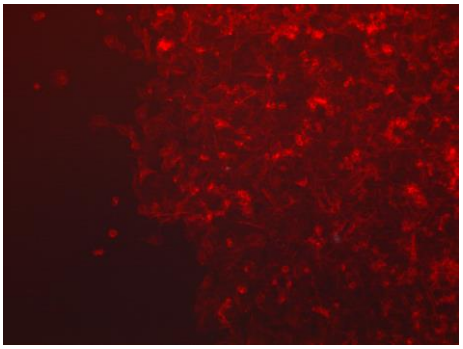
	x10	x10
	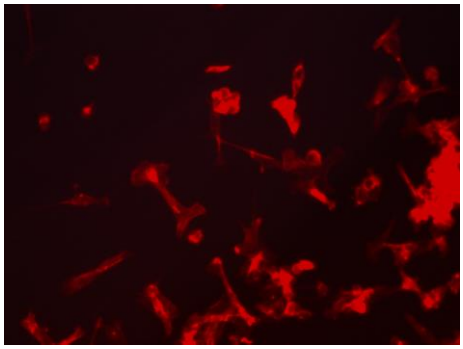	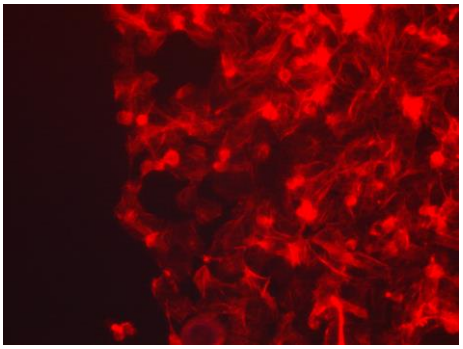
	x25	x25

Comparison of HUVEC proliferation of left, centre and right of the monolayer was made at 6 hr and 24 hr as shown in Figure 5.6. The result is presented in the percentage of total cell counts of BrdU stained (proliferating) and unstained HUVECs (quiescence) as described in Section 3.5.2. As shown in Figure 5.7, the percentage of counted HUVECs underwent proliferation on the left, centre and right are respectively 21±8.52 %, 31.75±4.99 % and 21.25±1.26 % at 6 hr; quiescent HUVECs were about 3 times more in the left and right (79±8.52 % and 78.75± 1.26 %), and about 2 times more in the centre (68.25±4.99 %), statistical analysis shows there is no significant difference of proliferating cells located between the different positions in the monolayer, and the same is also found in migrating cells. Over 24 hr, slight increase in proliferating cells was seen at left, centre and right measured, with respectively 31.75± 6.29 %, 39.25±4.78 % and 34.5±2.38 %; an decreased number of quiescent cells were found at all positions with respectively 68.25±6.29 %, 60.75±4.78 % and 65.5±2.38%. No significant difference was seen in proliferating and quiescent cells between the locations. Moreover, statistical analysis further indicates that there is also no significant difference in left and centre positions tested compared to respective position at 6 hr and 24 hr, however, significant difference in cells proliferating and migrating is seen on the right (***$p<0.05$).

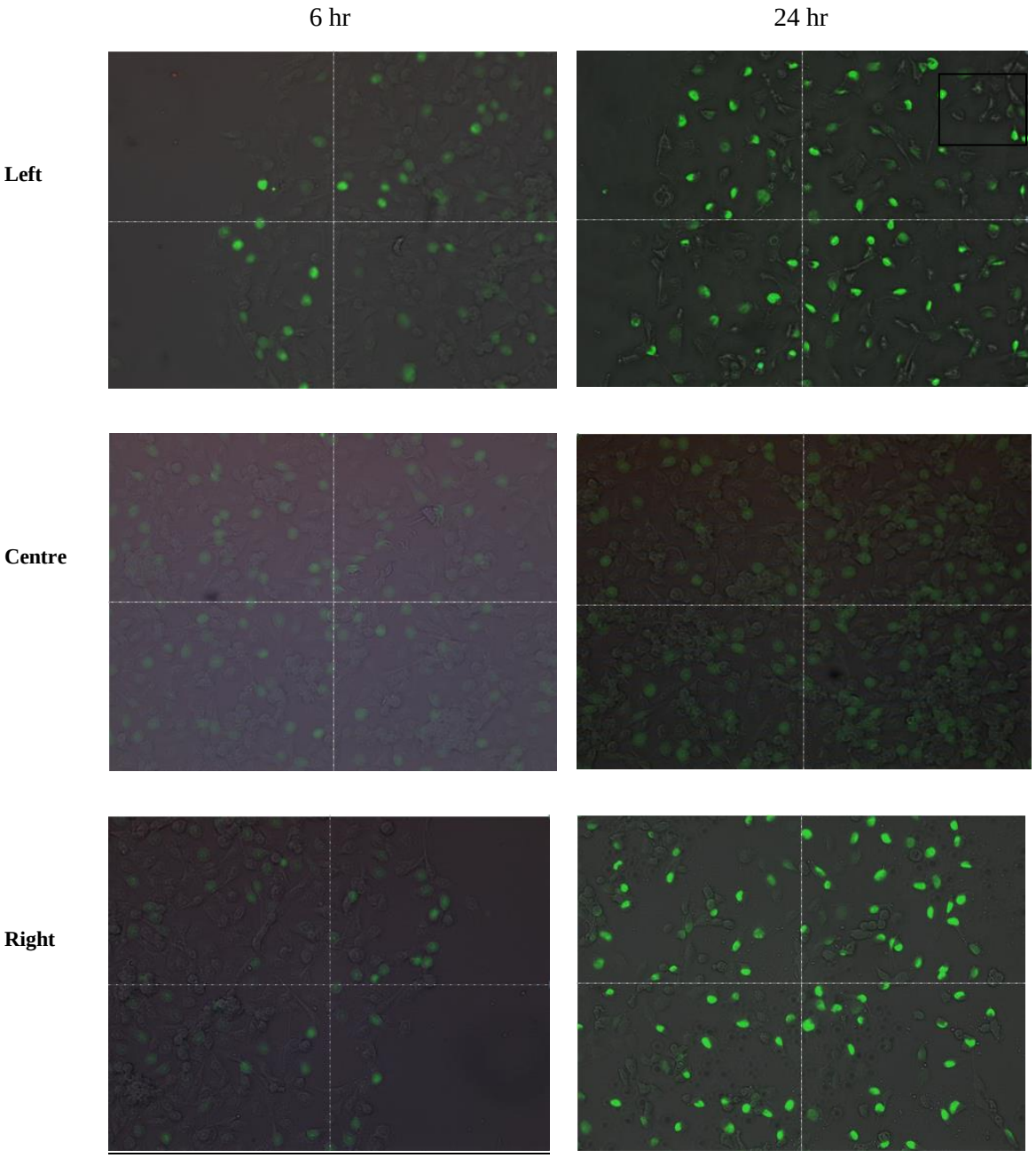

Figure 5. 6 BrdU staining of HUVECs on UVO 120s treated polystyrene at 6 and 24 hr. All the images shown were stacked with the same picture captured at bright field and fluorescence, the cross line was to ensure that both images are perfectly matched. Three different areas of UVO 120s treated surfaces were investigated from the left edge, centre and right edge on the monolayer.

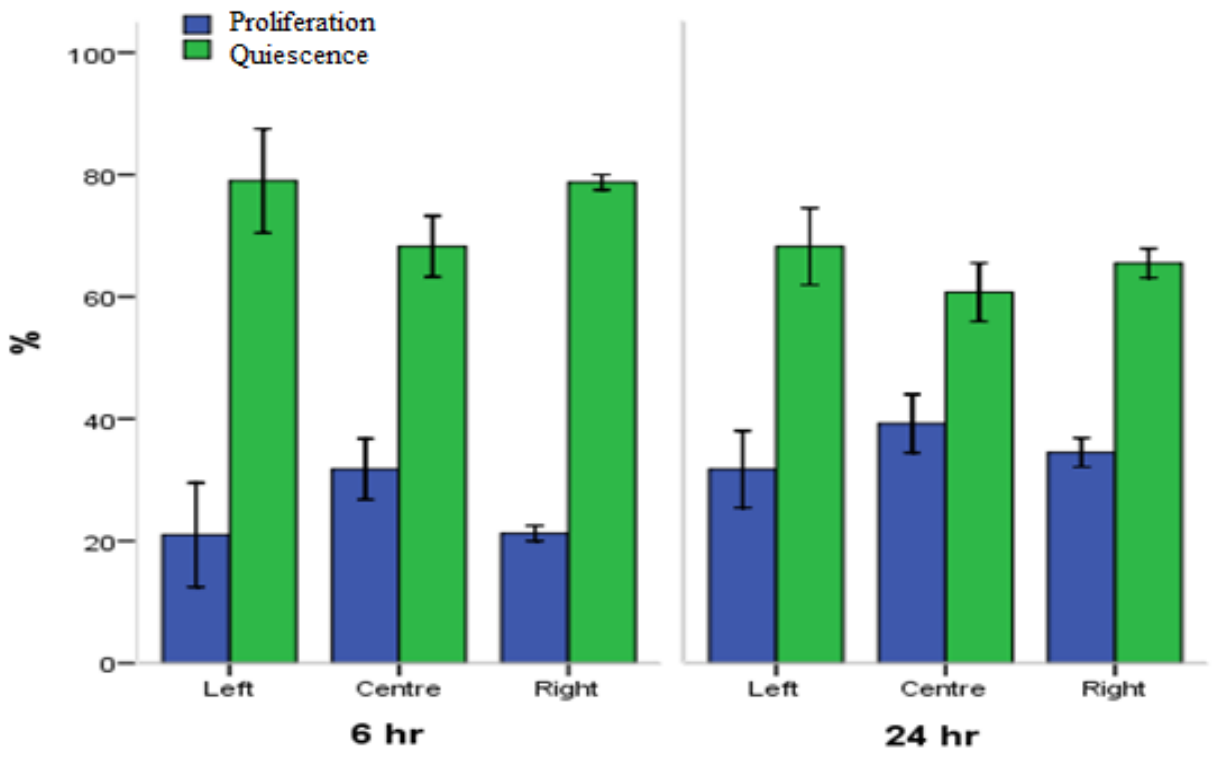

Figure 5. 7 Comparison of HUVEC activity on UV/Ozone 120s treated polystyrene surface at 6 hr and 24 hr. Proliferating and quiescent HUVECs were manually counted from a box ($2.7x10^4$ μm^2) blindly located at three positions using image J freeware and the result was shown in mean of percentage±SD of total counted proliferating and quiescent HUVECs in three separate experiments.

5.3.4 The effect of duration of UV/Ozone treatment on the migration of HUVECs over a 48 hour period

To ascertain if the duration of UV/Ozone treatment influences HUVECs migration, polystyrene surfaces were treated for 10s, 60s, 120s and 300s UV/Ozone. The treatment induced an overall surface oxygen of 9.36%, 16.32%, 21.36% and 29.87% respectively. No direct correlation between increased surface oxygen concentration and cell proliferation was evident and previously discussed in Section 4.3.2.

HUVECs migration on all the UV/Ozone treated surfaces were significant higher compared to untreated surfaces at all times examined as shown in Figure 5.8. At 6 hr, the net HUVECs migration distance (μm) on untreated surfaces was 26.68 ±1.89 μm and for UV/Ozone 10s, 60s, 120s and 300s were 32.29±3.23 μm, 36.23±2.36 μm, 37.55±2.09 μm, 33.55±2.58 μm respectively, and statistical analysis showed that there was significant difference of all UV/Ozone treated surfaces compared to untreated surfaces with an increase of 17% on UV/Ozone 10s treated, 27% on UV/Ozone 60s treated, 29% on UV/Ozone 120s treated and 20% on UV/Ozone 300s treated ($p<0.05$). HUVECs migration on UV/Ozone 60s and 120s were significant more than UV/Ozone 10s (11% and 14% respectively) which was statistical different ($p<0.05$).

Over 24 hr of incubation, the net migration of HUVECs on UV/Ozone 10s (85.280±5.02 μm) was slower with 11% (UVO 60s: 95.36±6.36 μm), 14% (UVO 120s: 99.38±4.02 μm) and 17% (UVO 300s: 102.26±8.36 μm) less compaed, there are no significant differences of migration distances between UVO 60s, 120s and 200s, however, they are all significantly different to 10s treated which has the lowest overall surface oxygen concentration. All UV/Ozone treated were significantly higher compared to untreated surfaces (25%, 32%, 36% and 27% respectively). The results obtained over 48 hr were similar to those observed at 24 hr. The lowest migration distance was measured on 10s UVO treated surface (183.61±4.36 μm), the migration distances of HUVECs on UVO 60s, 120s and 300s are significant higher with an increase of 7%, 9% and 15% respectively ($p<0.05$) and the distances are respectively 196.36±10.69, 199.89±12.32 and 203.36±11.01 μm with no significant difference between them. The migration distances were all significantly higher compared to untreated with an increase of 33% on UV/Ozone 10s treated, 37% on UV/Ozone 60s treated, 38% UV/Ozone 120s treated and 39% UV/Ozone 300s treated.

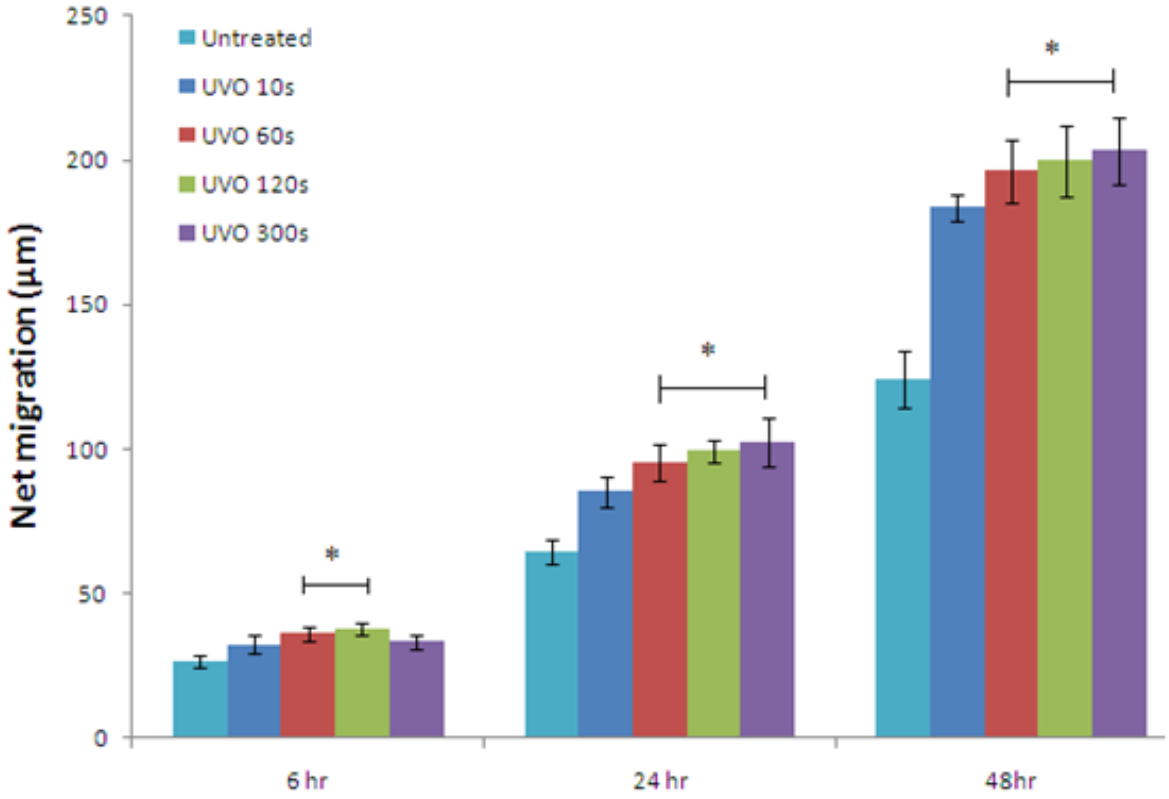

Figure 5. 8 Effect of the duration level of UV/Ozone treatment on HUVEC migration distance compared to untreated and UV/Ozone treated surfaces. HUVECs were seeded at a density of $1.2x10^4$ cells/cm^2 and incubated overnight to form the monolayer recorded at 6hr, 24 hr and 48 hr. The result is shown in the mean of net migrated distances from three separate experiments. (***$p < 0.05$, analysis of variance (ANOVA) followed by Boferroni post host test when compared to UV/Ozone 10s treated polystyrene surfaces, n=40).

5.3.5 The effect of oxygen tension on HUVECs migration

To assess the effect of oxygen tension on HUVECs migration, the net migration distances on UV/Ozone 120s treated and untreated along with TCPs under hypoxic condition (5% CO_2, 5% O_2 and 90% air) were compared to normoxic condition (5% CO_2 and 95% air) over 24 hr incubation period as shown in Figure 5.9. After 6 hour incubation, the net migration on untreated, TCPs and UV/Ozone 120s treated in both normoxia and hypoxia were similar, respectively 26.68±5 µm, 36.71±6.41 µm and 37.51±4.92 µm in normoxia and 26.78±5.31 µm, 37.57±6.45 µm and 38.38±6.58 µm in hypoxia, no significant differences were found between TCPs and UV/Ozone 120s treated however, they were all significant higher than untreated surfaces ($p<0.001$). After 24 hr, the net migration distances was higher on untreated, TCPs and UV/Ozone treated surfaces at low oxygen tension (respectively 92.23±10.59 µm, 131.78±10.68 µm and 134.59±7.9 µm) compared to normoxia (64.41±11.71 µm ,104.81±12.8 µm and 99.38±10.21 µm). Similarly to 6 hr, statistical analysis showed that there was no significant difference between TCPs and UV/Ozone treated surfaces but significantly higher than untreated ones at each oxygen tension; the increase was significant higher on all surfaces in hypoxia compared to respective surfaces in normoxia (***$p<0.001$).

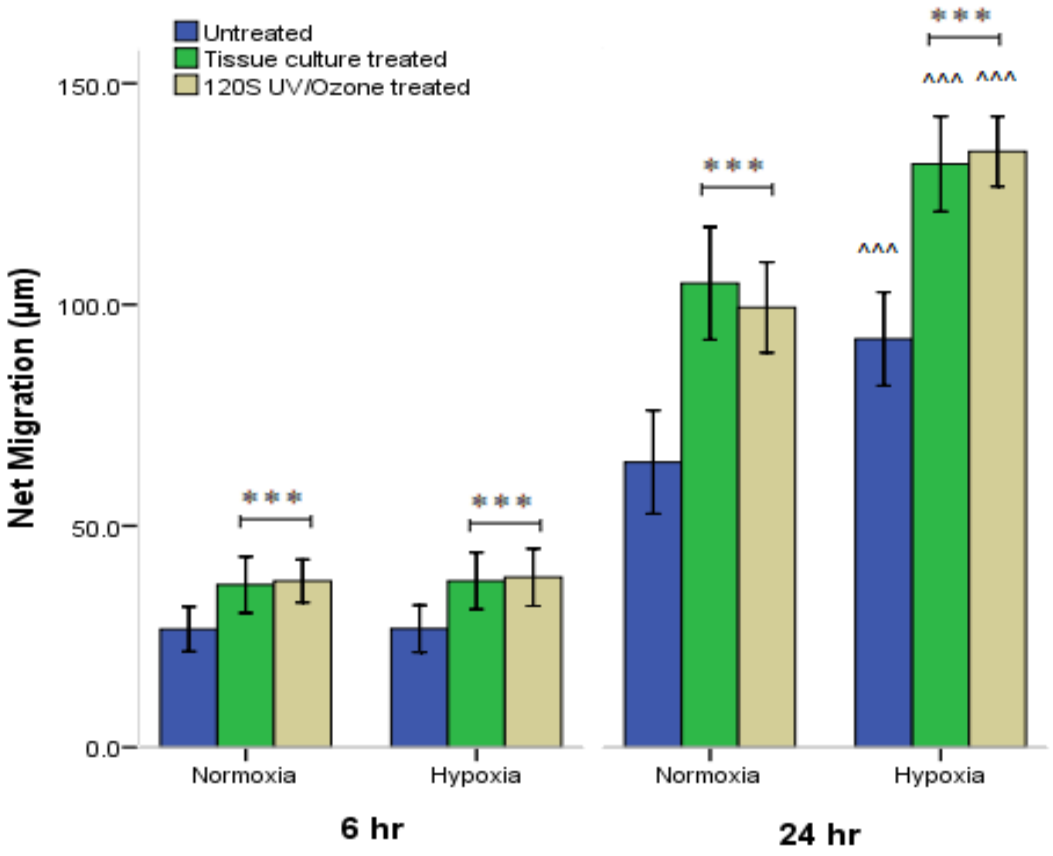

Figure 5. 9 The effect of hypoxia on HUVECs migration of TCPs, 120s UV/Ozone treated and untreated polystyrene surfaces. HUVECs were seeded at a density of $1.2x10^4$ cells/cm^2 and incubated overnight to form the monolayer. The ring was taken out in the next morning and this time point was used as 0 hr. The result is shown in the net migration of HUVECs (mean± SD) at 6hr and 24 hr from three experiments (***p<0.001by when compared to untreated surface at each condition**,** ^^^p<0.001 by when compared to respective treatment at normoxia condition, n=40)

5.4 Discussion

The physical and chemical effect of UV/Ozone treatment on polystyrene was fully studied in the previous chapter and it is important to determine its biological effect with endothelial cells on the physicochemical modified surfaces. In vasculogenesis and angiogenesis, endothelial proliferation and migration are essential (Griffioen and Molema, 2000, Carmeliet, 2005). Rapid cell proliferation and migration of endothelial cells may be essential for biomedical implants (Hin, 2004). Therefore, it is necessary to determine such responses.

It has been suggested that surface wettability plays an important role on various cell types' adhesion and proliferation. Cell proliferation measured on a range of UV/Ozone treatments surfaces (10s to 900s) indicates HUVEC preferred UV/Ozone treated than both untreated and TCPs over 48 hr incubation as discussed in Figure 5.1. It has been suggested that TCPs have a greater proportion of C-OR groups than UV/Ozone treated surfaces with similar total oxygen concentration (Curtis et al., 1983, Mitchell et al., 2005a). Teare et al. suggested that C-OR groups contribute to the initial cell attachment, however, other groups such as C=O and O-C=O are a key factor for long term cell proliferation (Teare et al., 2001). It is also necessary to compare to untreated surfaces to prove that HUVEC did not excrete enough proteins to adhere and proliferate due to the unfavour surface by the time tested, however, unlike literatures suggest no cell proliferation was seen on untreated polystyrene, relatively low amounts of HUVECs were found to be functional which may be due to the adsorption of serum contained proteins and cell excreted proteins.

HUVEC proliferation was found to be the most effective on UV/Ozone 120s and 180s treated. HUVEC proliferation did not seem to be affected by the high level of oxygen (UV/Ozone 300s, 600s and 900s), it may be related to interaction between the protein layer and polystyrene surface. Mitchell reported a similar decrease was found on Chinese hamster ovarian and mouse embryo cells and he suggested that the decrease in cell proliferation with increasing surface oxygen level was the effect of ECM proteins and media components by high levels of oxygen (Mitchell et al., 2005a), same author also reported Chinese Hamster Ovarian cells and mouse embryo cells were spatially controlled on UV/Ozone treated polystyrene (Mitchell et al., 2004b).

It has been reported that cells favour attaching to the surface with either more absorbed adhesion proteins or proteins in conformation that are more favourable to cell binding. Protein adhesion is also known to directly relate to surface chemistry as previously discussed in Chapter 3, it is also known that the non-specific binding of proteins can be decreased by either very high or low surface energy, which affects

attachment of cells and the surface with moderate hydrophilicity is more favourable for cells to attach (Van Wachem et al., 1987, Johnson et al., 1992). There is no systemic change found on surface roughness caused by UV/Ozone for this treatment period and therefore it is not considered to influence the cell proliferation in this work. Moreover, no correlation between any specific oxygen functionality and total surface oxygen can be found from the results, however, it was reported that surfaces with various functionalities are more beneficial for cell to attach and proliferate (Teare et al., 2001).

To date most of the researches are focused on cell adhesion and limited works have reported endothelial cells migration on different wettabilities surfaces. In this study, cell migration studies were carried out to understand the interactions between endothelial cells and the surface. The experiments show that UV/ozone treatment and TCPs significantly enhanced cell migration compared to the untreated surface over 48 hr. The same level of migration was seen on both UV/Ozone treated and TCPs unlike proliferation results indicated, it may be due to the confluence of the monolayer of HUVEC. The result also indicates that the surface oxygen level did not affect the migration over UV/Ozone treated over 60s as no significant difference was shown between 60s, 120s and 300s tested. Shen et al. reported hydrophilic surface restrained endothelial cell migration and promoted cell adhesion ability, however, the hydrophilic surface as they reported (22˚-55˚) may significantly enhance the adhesion strength to substrate and therefore inhibit cell migration.

Donatis et al. found that in a single cell, only migration or proliferation can be executed at a given time (De Donatis et al., 2010). The result indicate that HUVECs in quiescence were more than in proliferation at 6 and 24 hr tested with slightly increased proliferating cells at 24 hr, however, no significant difference was shown unless HUVECs examined on the right edge. In comparison to cell activity in left, centre and right of the monolayer, more proliferating cells were shown at both time studied, it may be that HUVECs were quiescent in the centre area, however, statistical analysis show no systematic difference compared between three different positions.

In an hypoxic environment, endothelial cells undergo a variety of self-changes in order to adapt the low oxygen conditions such as release of inflammatory mediators and growth factors, expression of specific genes controlling cell proliferation, migration and angiogenesis (Michiels et al., 2000, Abaci et al., 2010). The result shows that cell migration on untreated, UV/Ozone treated and TCPs were all increased significantly in hypoxia condition ($p<0.05$). HUVEC migration was not favoured by oxygen levels on the modified surfaces, instead, a number of biological changes were occurred within endothelial cells in order

to adapt hypoxic environment, for example, stimulation of specific genes such as vascular endothelial growth factor (VEGF) and glucose transporter 1, which are upregulated by hypoxia inducible factor type 1 (HIF) (Calvani et al., 2005, Takata et al., 2008). Literature suggested the combination of HIF-1 induced basic fibroblast growth factor (bFGF) and VEGF is related to the stimulation of migration as their implication in vessel formation (Veron and Sage, 1999).

Several studies show that endothelial cell proliferation and migration were also enhanced by the low oxygen tension. Zhao et al. reported that HUVECs cultured on polyethylene terephthalate (PET) films under 5% O_2, the cell proliferation, ECM excretion and intercellular adhesion was promoted compared to 20% O_2 over 3 days (Zhao et al., 2009). moreover, Decaris et al. utilised human endothelial colony forming cells (hECFCs) compared to human dermal microvascular cells (HDMECs) under different oxygen tension from 1% to 20% O_2 and he found that hECFCs indicated greater proliferation and migration compare to HDMECs (Decaris et al., 2009). Gadad et al. reported a modified wound healing assay based on the radial cell migration assay used in this study where half of the monolayer was removed by a cell scraper, their result showed endothelial cells migrated faster at the wounded edge compared to the counterparts from the intact edge. They also restored high glucose induced decreased cell migration by using silymarin, an anti-oxidant which prevented the deleterious effect of high glucose and re-functioning HIF-1.

5.5 Conclusion

Following the surface characterisation of the UV/Ozone treated polystyrene surfaces, the biological responses of HUVECs were studied in this chapter. HUVEC proliferation was significantly enhanced by the UV/Ozone treatment comparing to untreated and TCP; Cell migration result also further indicates the increase of migration distance measured compared to untreated surfaces. Surface oxygen level did not affect HUVEC migration under hypoxia condition. Therefore, it is clearly shown that UV/Ozone is an effective, rapid and costless method to improve the polystyrene biocompatibility. The result achieved were all carried out in static cell culture, however, vascular endothelial undergo flow induced shear stress in the vessels, the responses of HUVEC under flow induced shear stress is examined in the next chapter.

Chapter 6 Response of HUVECs Grown on UV/Ozone Treated Polystyrene Surfaces to Laminar Flow Conditions

6.1 Introduction

The result in Chapter 4 has shown that UV/Ozone treatment can incorporate various oxygen functional groups such as ether/alcohol, carbonyl and carboxylic acid/ester to influence surface wettability and energy. Surface wettability and energy are known as major contributing factors to affect cell adherence, proliferation and migration (Mathieson and Bradley, 1996, Teare et al., 2000a, García and Keselowsky, 2002, Davidson et al., 2004, Mitchell et al., 2005a) and this has been confirmed in results presented in Chapter 5.

The plasticity of an endothelial cell is influenced by the surrounding environment, for example, endothelial cells can modulate their structure and function depending on the chemical and physical stimuli, such as soluble factors within the plasma and the changes in blood flow(Koelsch, 2007). *In vitro* cultured endothelial cells have characteristic polygonal cobblestone morphology, however, the endothelial cells align in the direction of the flow when they are placed in a perfusion chamber and exposed to a shear stress close to the equivalent frictional force of blood flow (Ait-Oufella et al., 2010, Backer et al., 2012). Shear stress is a tangential hemodynamic force and it controls endothelial cell function by the activation of signalling pathways, gene and protein expressions (Arslan et al., 2010b) .

Therefore it is important to determine the ability of the UV/Ozone modified surface to support endothelial cell growth under the influence of flow. Thus, in the present chapter, a closed laminar flow perfusion chamber(Bioptechs) was used as a microadequeduct design containing a T shaped groove to allow for the generation of superior laminar flow. This system was used to investigate the response of adherent HUVECs to laminar flow conditions and evaluate cell morphology on the UV/Ozone treated polystyrene surface before and after different flow speeds. Cell morphology was monitored by light microscopy, cell viability was determined using trypan blue staining and the cytoskeleton was visualised with Phalloidin staining.

6.2 Materials and methods

6.2.1 Materials

Polystyrene sheet (M_w = Ca. 280 000) with the thickness of 0.2 mm used in this study was purchased from Goodfellow, UK. All the reagents and chemicals used in this work were of analytical grade and purchased from Sigma Aldrich unless specified.

6.2.2 Sample preparation

Polystyrene was manually cut into 30mm diameter circle disks and further cleaned by sonication in 70% methanol and High Performance Liquid Chromatography (HPLC) grade water (Milipore, resistivity 18 MΩ cm), then the surface was dried at room temperature before assessing UV/Ozone surface treatment. Human umbilical vein endothelial cells (HUVEC) were seeded to glass corning rings (6mm x 8mm, Corning, UK) located at the center of the UV/Ozone modified surface to form a monolayer, the detail was discussed in Section 3.7.1.

6.2.3 Set up of Laminar flow chamber system

The laminar flow chamber system (FCS2) was purchased from Intracel (Bioptechs, UK). It is a closed system and a live-cell observation is micron scale which proves stable laminar flow perfusion. The setup of the system was described in Section 3.7.2. The shear stress induced by the flow rate was adjusted by roller clamp connecting to the exhaust tube. The calculation of shear stress intensity was discussed in Section 3.7.3.

6.2.4 Cell morphology changes

The effect of shear stress induced by the flow on HUVEC morphology was studied under an inverted microscopy system (DMI 4000B, Leica Microsystems, Germany) as discussed in Section 3.7.4. A total number of 13 images were taken to identify the changes, the images were taken every 10 mins including beginning of the flow and they were captured at the same position for each time point in order to evaluate the change in cell morphology in response to different flow rates.

The captured images were analysed by the help of Image J freeware (Version 1.46r, Wayne Rasband, National Institute of Health, USA). The measurement includes three steps: 1) Setting the scale of measurement was changed from pixels to micrometers; 2) Measuring HUVEC area before the flow; 3) Measuring HUVEC area after the flow. The details were fully described in section 3.7.5.

6.2.5 Cell viability changes

HUVECs were carefully removed from the flow chamber after each flow, washed and stained with 0.4% trypan blue solution for viability tests as discussed in Section 3.7.6.

6.2.6 Statistical analysis

The HUVECs size obtained was in pixels and changed to μm at a ratio of 0.75 and the results are shown as mean±SEM through all the measurements in this study. For each experiment, eight random HUVECs were selected before the flow and those applied to the measurement after the flow. One-way ANOVA was used to compare the mean differences between the different treatments and flow speeds. The level of significance was conveyed using the general notations $*p<0.05$, $**p<0.01$, $***p<0.001$. A further two repeats were applied to for experiment reproducibility.

6.3 Results

6.3.1 The effect of 120s UV/Ozone treatment on HUVECs under different flow conditions

The flow chamber provided a real time and an unobtrusive imaging opportunity to record HUVECs attached to the modified and unmodified PS surface under different flow conditions. This unique design of the flow chamber ensures the cells are exposed to a regulated stead laminar flow.

The effect of the flow of medium on cells layered on a 120s UV/Ozone treated surface with the duration 120 mins as shown in Figure 6.1. As discussed in Chapter 5, UV/Ozone treatment was found to significantly enhance HUVECs proliferation and migration which is believed to be due to the increased levels of oxygen functional groups. Before starting the flow, the shape of the cells grown on the untreated and treated surfaces (Fig 6.1, 0 min) was compared, and the results were comparable with results reported in Chapter 5. After 10 mins of flow, most of the HUVECs grown on untreated surfaces were removed from the surface and very few HUVECs remained attached to the surface when the flow terminated after 120 mins (Fig 6.1, 10 min and 120 min). However, the cells were clearly visible at 120s on the UV/Ozone modified surface at the start and at the conclusion of the experiment. They seemed to be affected by the flow but the morphology of HUVECs changed from polygonal cobblestone shaped to ellipsoidal with the time of the flow. The results for higher flow rates (10 mL/min and 25 mL/min) were also monitored but not presented in this chapter due to similar effects.

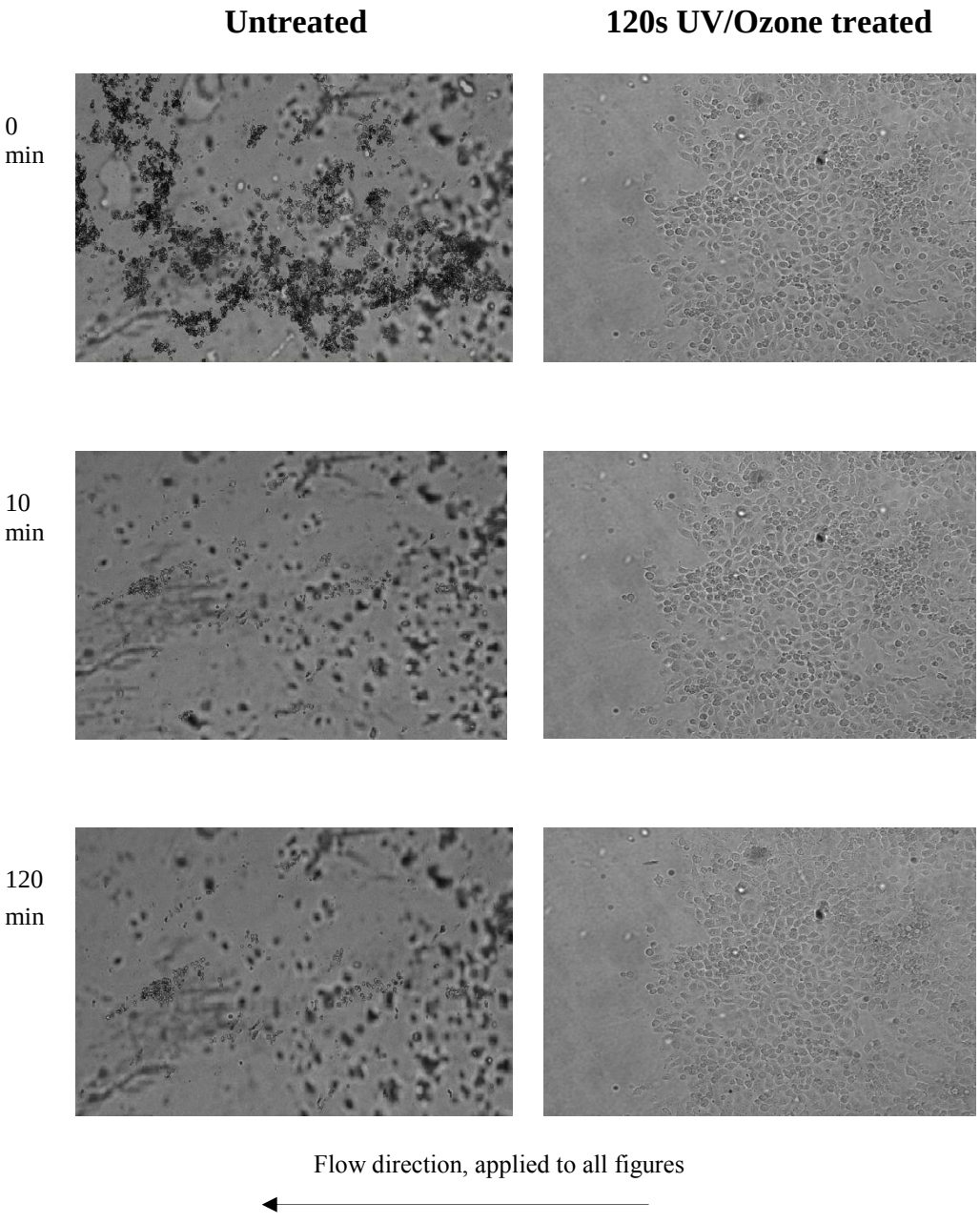

Figure 6. 1 HUVECs cultured on untreated polystyrene and 120s UV/Ozone treated polystyrene surfaces in FCS2 flow chamber along the direction of the flow 1 mL/min (right to left) x10. The flow started at 0 min and stopped at 120 min.

6.3.2 Morphological responses of HUVECs under flow speed of 10 ml/min for 120 mins

Previous work has indicated that the direction of flow parallels the elongation and alignment of endothelial cells. In the present study, the flow speed of 10 mL/min was used to show the effect on HUVECs morphology. Figure 6.2 shows the left edge of the cell monolayer seeded on the UV/Ozone treated surfaces at the time point of 0, 10, 30, 60, 90 and 120 mins of flow with direction from right to left. HUVECs in the red box from each picture were the same cell at different time points. Figure 6.3 shows cells amplified by ten times, to illustrate the changes observed. HUVECs in the blue box show a typical cells migrating some distances, it clearly showed that there were two individual cells traveled at the 120 min compared to 60 min and 90 min, those two cells were not spotted in the first 60 mins periods of flow, which were lifted off by the flow as partially connected to the surface.

Figure 6. 2 HUVECs cultured on 120s UV/Ozone treated polystyrene surfaces in FCS2 flow chamber along the direction of the flow 10 mL/min (right to left). The initial cell seeding density is 2.4 x 10^5 cells/mL. HUVECs in the red box are amplified 10 times larger to observe the morphology changes in the following figure. HUVECs in the blue box were the cells dislodged by the flow

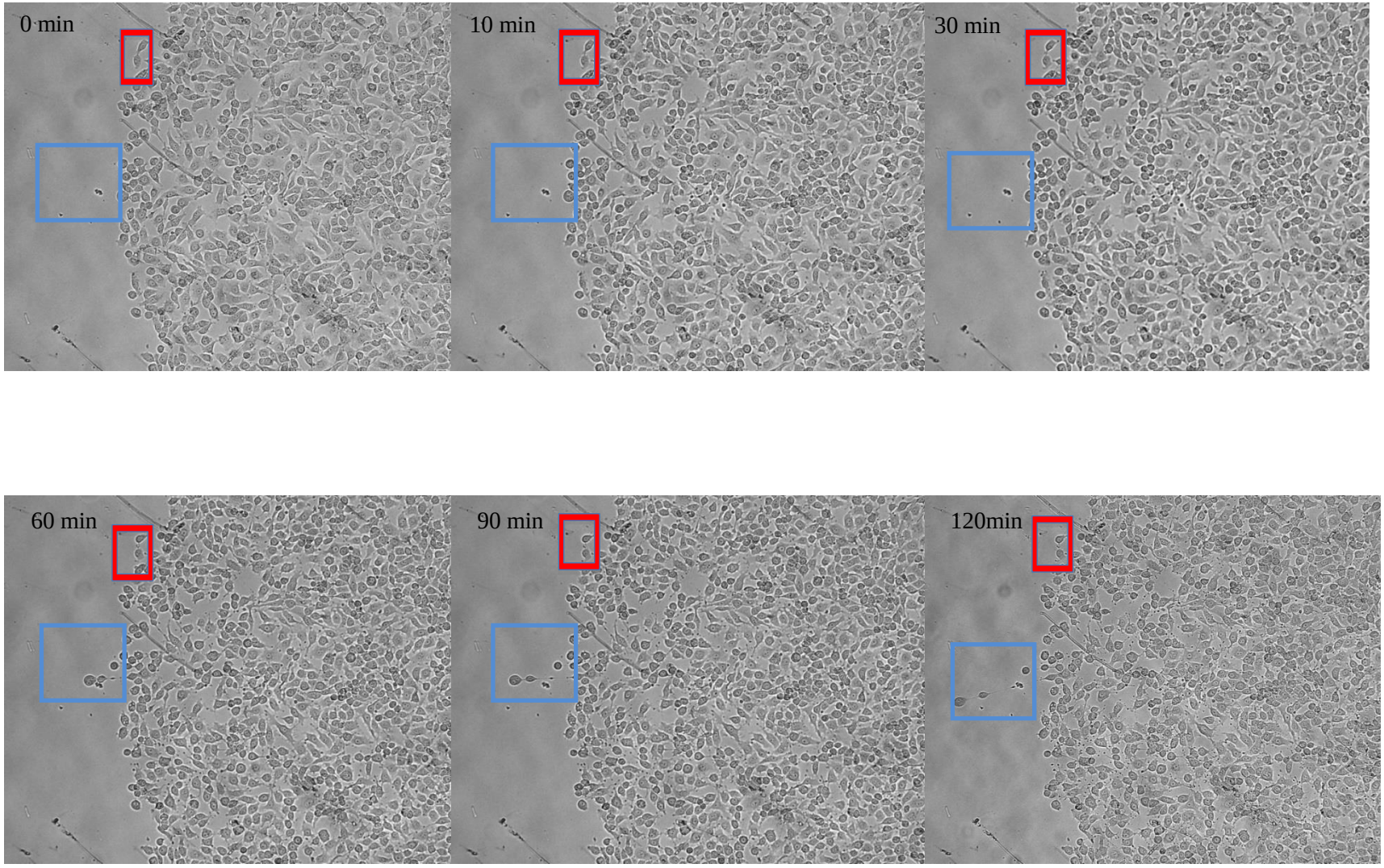

Flow direction, applied to all figures.

The morphology of HUVECs was changed due to the shear stress induced by the speed of the flow as shown in Figure 6.3. For better visual illustration, selected HUVECs from Figure 6.2 (red box) were magnified 100 times. The individual HUVEC located at the top gradually changed its morphology as the flow progressing, the flow caused the challenge of shear stress which induced the cell migration. The clearest visual change was seen after 60 mins of the flow; the cytoplasm of the cell displayed stretched to the surface prior to the flow and changed gradually to spherical shape at the stop of the flow (direction from right to left) due to the challenge of the shear stress induced. Because of the limitation of the equipment, it is not possible to determine the distance migrated, all the pictures were tried to be taken at the exact position, however, air bubbles were generated from the media in the progress of the flow, removal of such by tapping the tube connected caused some pictures took at the time point were not fully mapped.

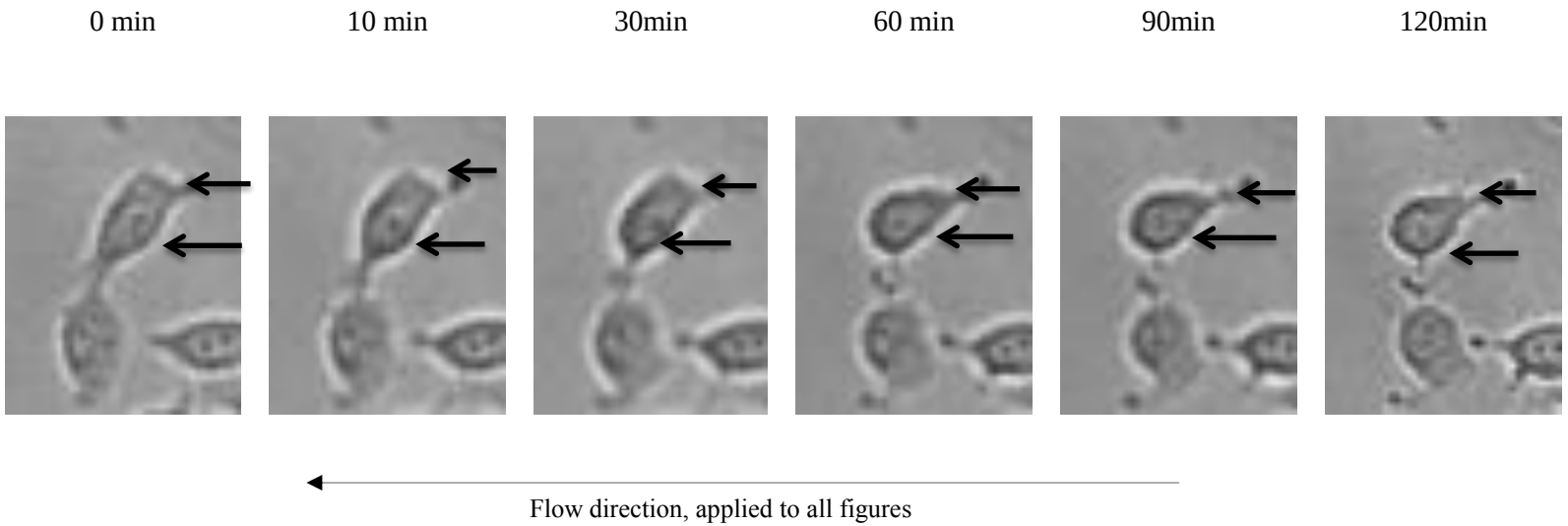

Figure 6. 3 Change of cell morphology on 120s UV/Ozone treated polystyrene due to shear stress induced by the laminar flow. Individual HUVECs were amplified 50 times selected from the red box in Figure 6.2 for clear visual illustration.

6.3.3 The effect of flow rate on HUVEC morphology

As found in the above section, the morphology of HUVECs changed from stretched to rounded due to the flow, the size of HUVECs after 120 mins of flow period were found smaller compared to before the flow at 1mL/min, 10mL/min and 25mL/min. Table 6.1 shows results from three separate experiments of the measurement for HUVECs size before the after the flow. The size of one cell was not changed but the others were all reduced and the highest change was found to be 27% smaller compared to before the flow. The mean of percentage difference is in % over the period of the experiment, in the first experiment is 18% and 15% for both repeated test. The changes under the flow speed of 10 mL/min were found to be more than 1 mL/min. As shown in Table 6.1 the smallest change was 16% and the most change was 41%, the average of percentage difference of the three separate tests are 29%, 33% and 26%. The findings under the flow speed of 25 mL/min are the most obvious with the most significant changes among the all three flow rates used. The lowest change was found to be 26%, 60% was the highest, the average of all three separate tests are 41%, 43% and 49%. From the results of all three different flow rates tested, it is clear that there is an inverse relationship between the size reduction and the flow rate; the flow rate of 1 mL/min had the smallest effect of HUVEC size reduction about 16% with the average of three individual experiments (18%, 15% and 15%) compared to 10 mL/min 26% with the average of three individual experiments (29%, 23% and 26%). The most obvious change in reduction was found with the highest flow rate tested with 44% with the average of three individual experiments (41%, 43% and 49%).

Flow rate	**1 mL/min**			**10 mL/min**			**25mL/min**		
Shear stress	1 dyn/cm^2			9 dyn/cm^2			21 dyn/cm^2		
Experiments	1st	2nd	3rd	1st	2nd	3rd	1st	2nd	3rd
Size reduction %	10	27	7	27	31	27	31	26	64
	15	20	8	36	26	32	41	60	31
	20	0	20	38	33	18	56	47	57
	25	6	22	16	41	24	47	49	47
	21	12	7	34	26	22	47	31	54
	18	26	24	24	38	31	23	43	43
Mean ± SEM %	18±2	15±5	15±2	29±3	33±3	26±2	41±5	43±5	49±5

Table 6.1 Summary of HUVEC size reduction on UV/Ozone treated polystyrene surfaces under the laminar flow rates of 1mL/min, 10 mL/min and 25 mL/min over 120 mins. The result is presented as net reduction which was calculated from the formula discussed in section 3.7.4. Further two experiments were repeated and listed above for test reproducibility and named as 2nd and 3rd. Initial HUVEC seeding density is 2.4 x 10^5 cells/mL. The details of each HUVEC size measurement are shown in the appendix.

Figure 6.4 shows that there is no significant statistical difference between three individual experiment of the flow rate of 1 mL/min, 10 mL/min and 25 mL/min ($p > 0.05$). The changes observed before and after the 120 mins of flow period at the flow rate of 1mL/min are 18±2%, 15±5% and 18±2%. Higher reduction in cell size was found under the flow rate of 10 mL/min about 29±3%, 33±3% and 26±2%; the highest reduction in HUVEC size change was seen under the flow rate of 25 mL/min with the decrease of 40±5%, 43±5% and 49±5%. Clearly, the most reduction in cell size (up to 64%) was seen in 25 mL/min which induced the shear stress intensity about 21 dyn/cm^2, followed by the reduction up to 38% with the shear stress intensity about 9 dyn/cm^2 induced by 10 mL/min flow rate, lowest reduction (up to 27%) was found at the flow rate of 1 mL/min, about 1 dyn/cm^2 shear stress intesnsity.

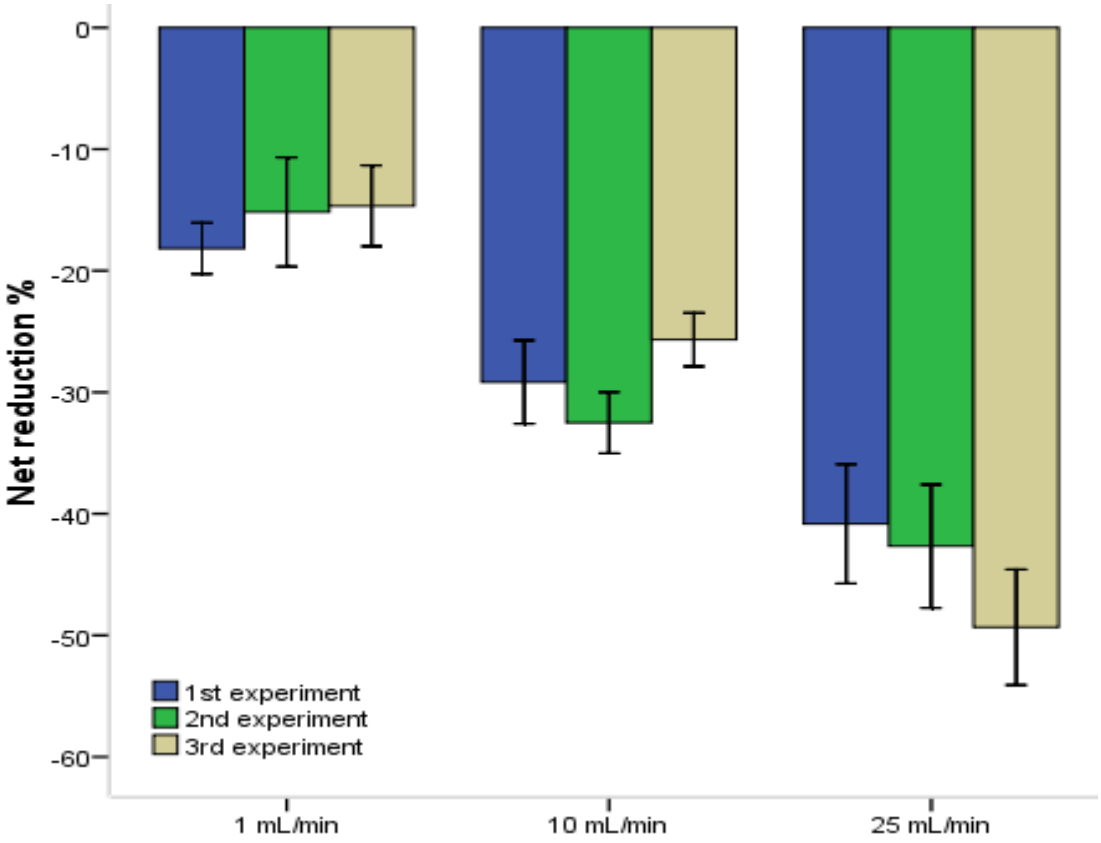

Figure 6. 4 The effect of flow rate on HUVEC size under the flow rate of 1 mL/min, 10 mL/min and 25 mL/min. Further two experiments were applied for test reproducibility and listed as 2nd and 3rd The results are presented as net reduction± SEM and analysed by variance (ANOVA) followed by Bonferroni post hoc test (n=6). Initial HUVEC seeding density is 2.4 x 10^5 cells/mL.

As shown above three individual experiments within each flow rate display very close compatibility despite variations, eighteen cells from three experiments in flow rate of 1mL/min were analysed and compared to 10 mL/min and 25 mL/min in Figure 6.5. The flow rate of 1 mL/min had the smallest effect on size change 16±2%, there is 45% increase in size reduction in the flow rate of 10 mL/mi compared to 1mL/min (29±2%), HUVEC size was reduced the most by the highest flow rate, 25mL/min and it is 64% more than 1 mL/min and 34% more than 10mL/min (44±3%). Statistical analysis shows the results are all significantly difference between each flow rate tested (***p<0.001).

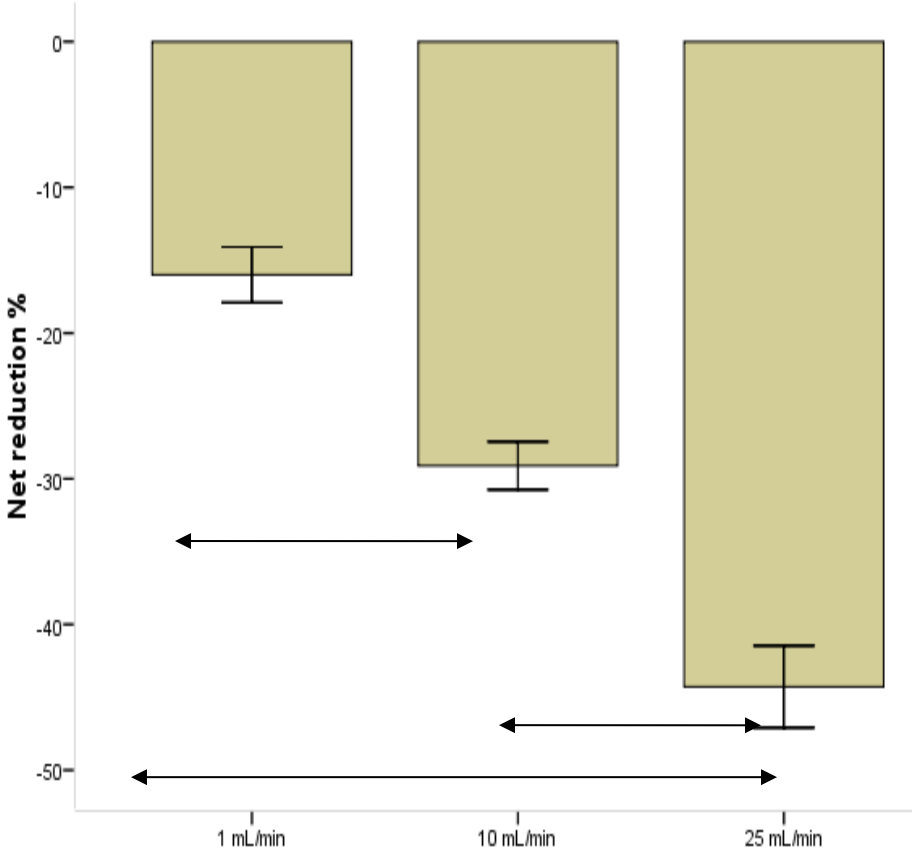

Figure 6. 5 The effect of flow rate with 1 mL/min, 10 mL/min and 25 mL/min on HUVEC size before and after 120 mins flow period. The area difference in percentage was calculated as discussed in Section 5.2.5. The results presented in size reduced percentage ± SEM and analysed by variance (ANOVA) followed by Bonferroni post hoc test (n=18, ***p<0.001). . Initial HUVEC seeding density is 2.4 x 10^5 cells/mL.

The distribution of F-actin was studied after each flow speed with Phalloidin staining as shown in Figure 6.6. The finding of the staining confirmed the effect of flow rate induced shear stress on HUVEC morphology . The reorganisation of F-actin showed that the shape of HUVEC changed from polygonal to ellipsoidal under shear stress at all flow rates tested and it was mostly obvious presented under the highest shear stress induced by flow rate of 25 mL/min (figure5.6 c).

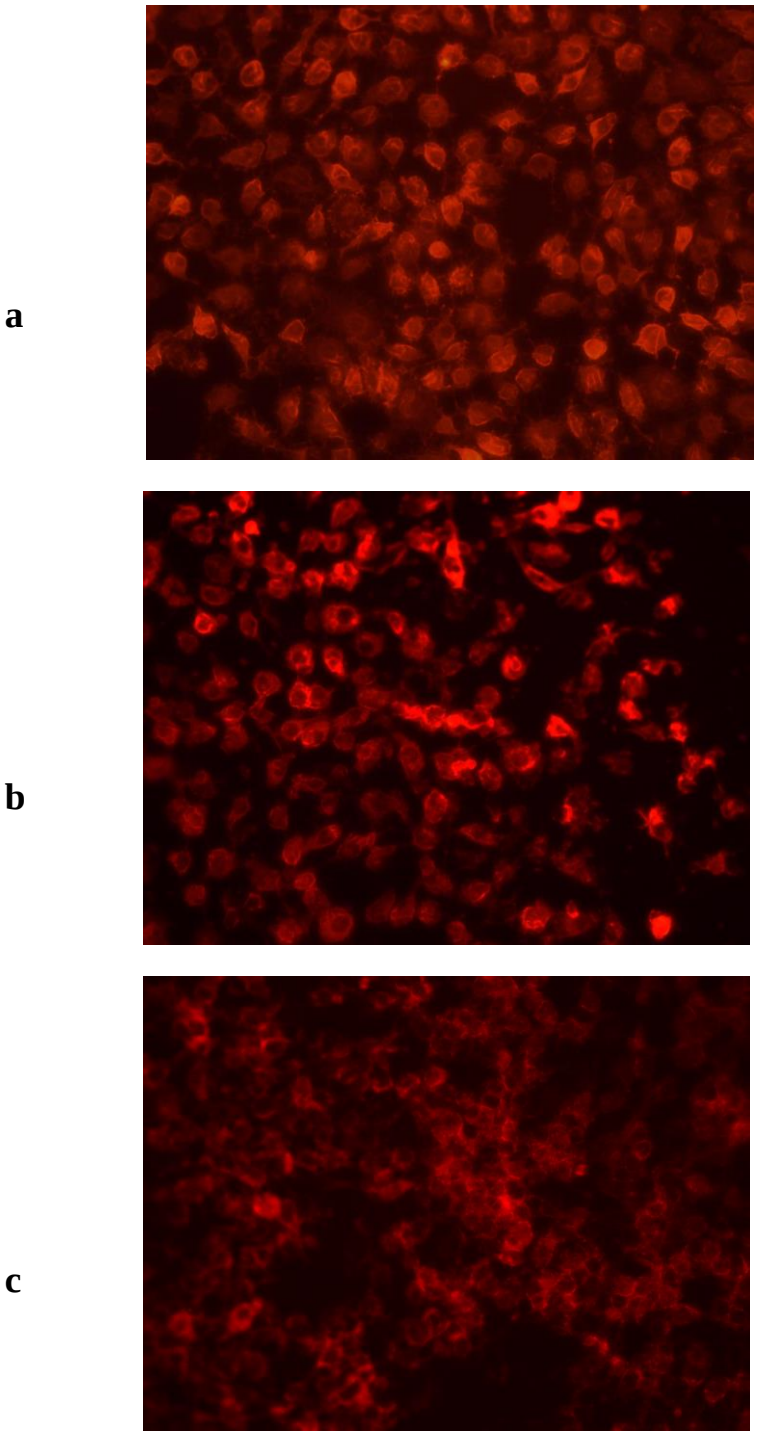

Figure 6. 6 Phalloidin staining of HUVECs over 120 mins of flow on UV/Ozone treated polystyrene 10x. The distribution of F-actin taken by phalloidin are shown in the flow rate of a) 1 mL/min b) 10 mL/min and c) 25 mL/min.

6.3.4 The effect of seeding density on HUVEC size

Not like the higher seeding density which HUVECs close or contacted to each other, low seeding density created a more spacious space, that the medium would fluid pass by and create higher fluid shear stress to cells. Measurement of the HUVEC size with a lower initial seeding density of HUVECs (1.2×10^5 cells/mL) was investigated compared to prior seeding density of 2.4×10^5 cells/mL.

Similar to normal seeding density, HUVEC size also reduced on UV/Ozone treated polystyrene surfaces under the flow rate of 1 mL/min and 10 mL/min seeding with lower seeding density. As shown in Table 6.2, HUVEC size reduced about 17% of the mean of three tests 14±2%, 20±3% and 17±2% under the flow rate of 1mL/min over 120 mins, more reduction in HUVEC size was seen in the flow rate of 10 mL/min about 27% with the mean of 29±2%, 25±2% and 28±4%, which was about 12% more than 1mL/min.

	1 mL/min			10 mL/min		
Experiments	1st	2nd	3rd	1st	2nd	3rd
Size reduction %	10	23	24	36	27	34
	9	6	15	27	19	14
	12	17	9	26	26	29
	18	31	20	36	31	27
	21	20	19	22	19	41
	11	20	12	27	26	24
Mean ± SEM %	14±2	20±3	17±2	29±2	25±2	28±4

Table 6.2 Summary of HUVEC size reduction on UV/Ozone treated polystyrene surfaces under the laminar flow rates of 1mL/min and 10 mL/ over 120 mins. The result is presented as net reduction in percentage which was calculated from the formula discussed in Section 3.7.5.4. Two further experiments were applied for test reproducibility and listed as 2nd and 3rd. Initial HUVEC seeding density is 1.2 x 10^5 cells/mL.

Statistical analysis shows there is no significant difference among the three individual tests in each flow rate measured as shown in Figure 6.7.

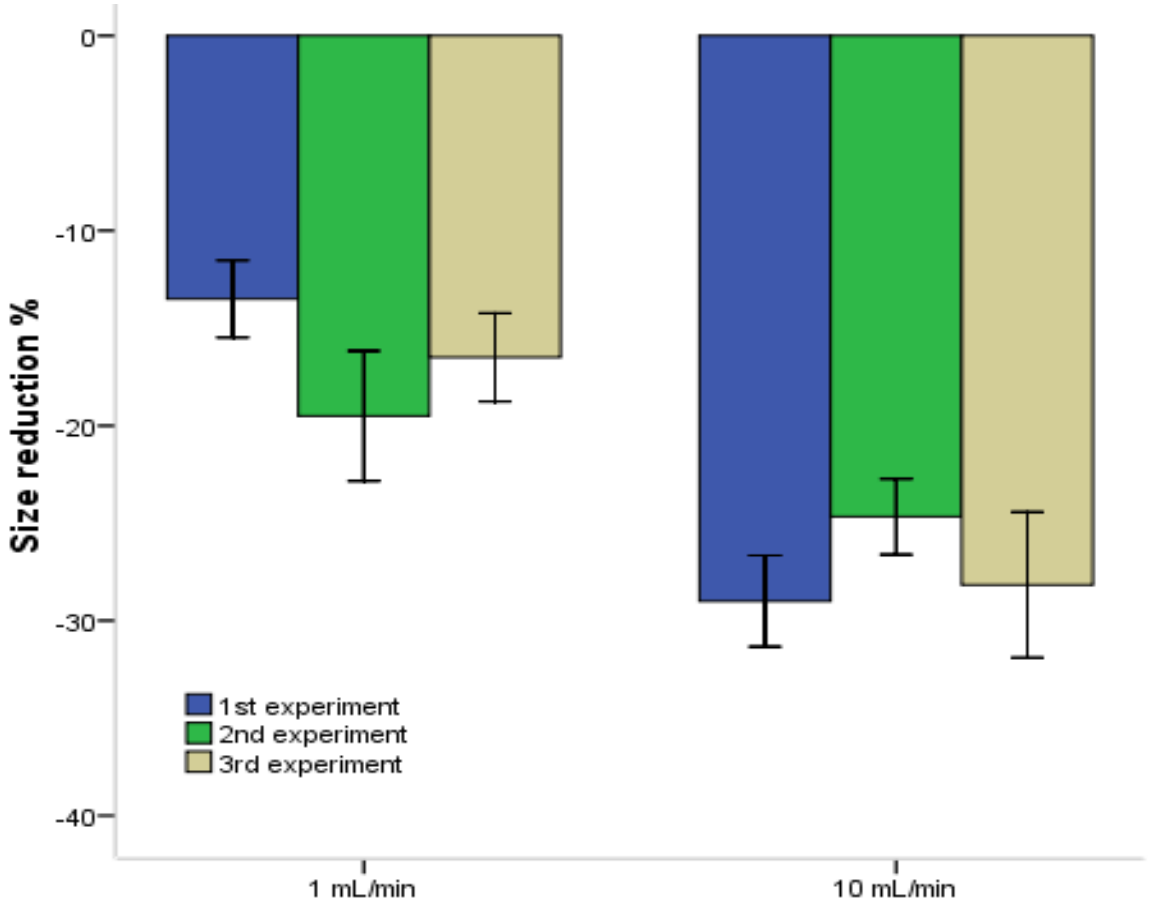

Figure 6. 7 The effect of lower seeding density on HUVEC size on UV/Ozone 120s treated polystyrene surfaces over 120 mins flow. The results presented in size reduced percentage±SEM and analysed by variance (ANOVA) followed by Bonferroni post hoc test (n=6).

Figure 6.8 shows the comparison of size reduction with two seeding densities (2.4 x 10^5 and 1.2 x 10^5 cells/mL) on UV/Ozone treated polystyrene surfaces under the flow rate of 1 mL/min and 10 mL/min over 120 mins. At the flow rate of 1 mL/min, the size reduction with normal seeding density was about 16±2% and 1% more was found in low seeding density (17±2%). At the higher flow rate of 10 mL/min, there was 2% increase with normal seeding density than low seeding density, relatively 29±2% and 27±2%, However, statistical analysis shows there are no significant differences between both seeding densities at the both flow rates tested.

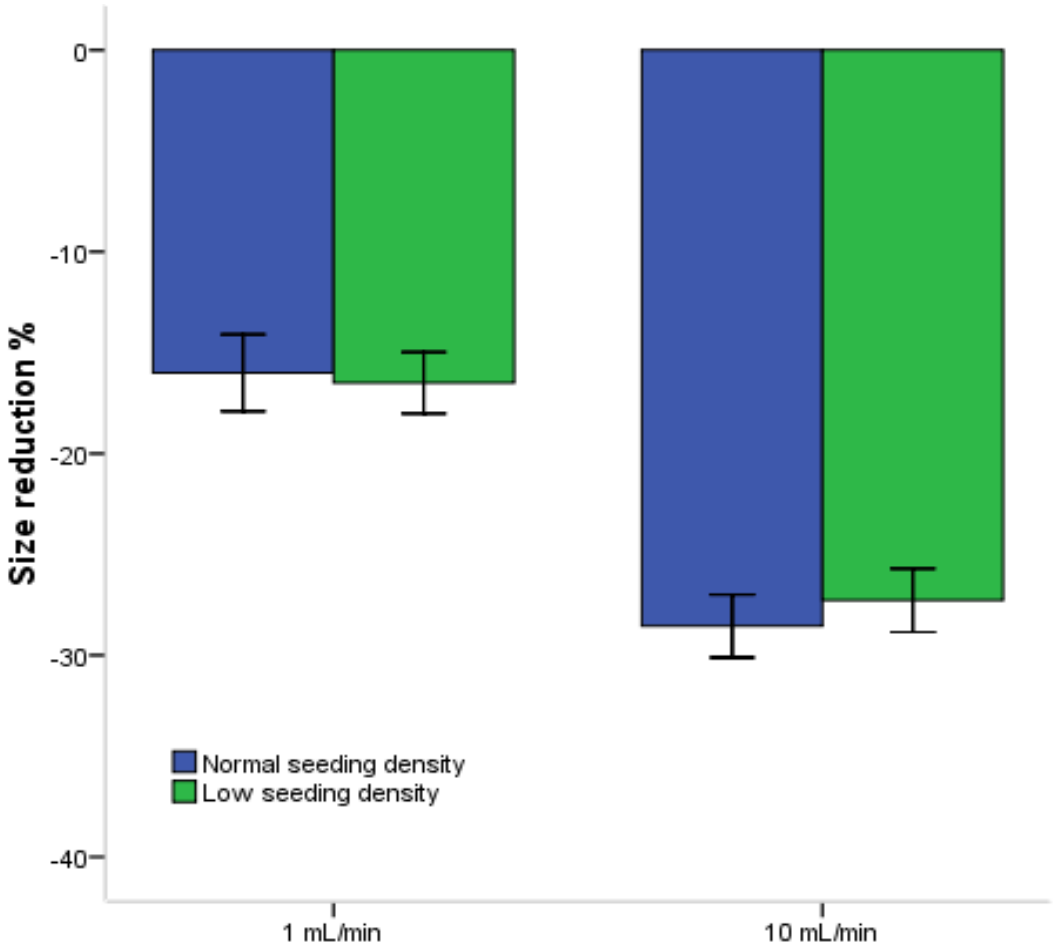

Figure 6. 8 The effect of cell seeding density on HUVEC size reduction on UV/Ozone treated polystyrene surfaces under the flow rate of 1mL/min and 10 mL/min over 120 mins. The results are presented as net reduction ±SEM and analysed by the student's t-test for two samples with unequal variance (n=18). Normal density was 2.4 x 10^5 cells/mL and 1.2 x 10^5 cells/mL for low seeding density)

6.3.5 Effect of flow rates on cell viability

Having established the effect of flow rates on HUVEC morphology, the cell viability were measured by manual counts of live and dead cells via trypan blue staining over 120 mins of flow. Table 6.3 shows the manual cell counts of live and dead cells in selected area, three replicates were performed at each flow rate tested.

Flow rate	1 mL/min		10 mL/min		25 mL/min	
Shear stress	1 dyn/cm^2		9 dyn/cm^2		21 dyn/cm^2	
	Dead	Live	Dead	Live	Dead	Live
1st experiment	3	60	6	47	24	59
Dead cells %	5		11		29	
2nd experiment	1	89	24	84	37	44
Dead cells %	1		23		46	
3rd experiment	2	93	26	101	24	43
Dead cells %	2		20		36	
Mean ± SD % (Dead cells % of three experiments)	3±2		18±6		37±9	

Table 6.3 Comparison of cell viability under 120 mins of flow period with the flow rate of 1 mL/min, 10 mL/min and 25 mL/min. Manual counts were performed with a haemocytometer via trypan blue staining. Three replicates were completed, individual and the mean of all three replicated were listed.

Figure 6.9 shows the means of the three experiments above at each flow rate. It is found that under the low shear stress intensity of 1dyn/cm^{2,} lowest cell death (3±2%) was seen at 1 mL/min over 120 mins of flow; an increase of cell death about 6 times (18±6%) was seen in higher shear stress of 9 dyn/cm^2 induced by the flow rate of 10 mL/min; the most cell death (37±9%) was found under the highest flow rate and shear stress (25 mL/min and 21 dyn/cm$^{2)}$, which is 12 times than 1 mL/min and 2times more than 10 mL/min.

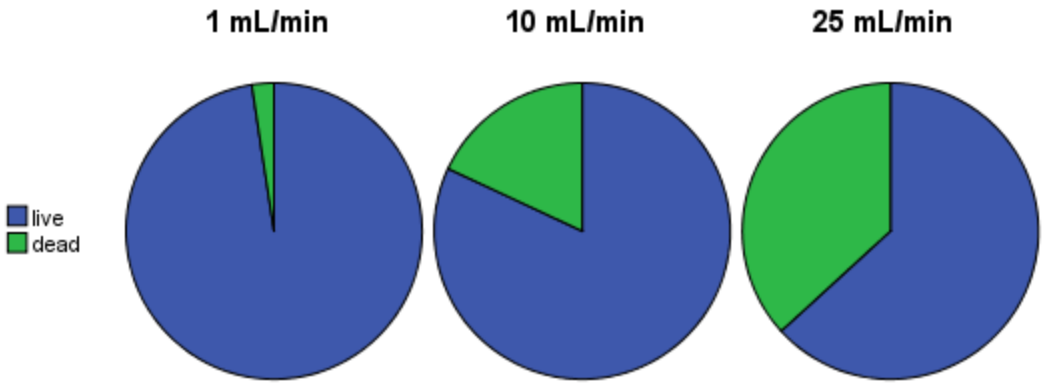

Figure 6. 9The effect of the flow rates on cell viability under the flow rate of 1 mL/min, 10 mL/min and 25 mL/min.

Figure 6.10 shows the death of cells after 120 mins flow at 1 mL/min, 10 mL/min and 25 mL/min. Dead cells are shown in dark colour as trypan blue solution could pass through dead cells membranes. Very few dead cells were seen.

Figure 6. 10 The distribution of live and deadHUVECs by trypan blue staining on 120s UV/Ozone treated polystyrene surfaces under 120 mins flow with the direction from right to left (x10 magnification). The laminar flow with three different flow 1 mL/min (upper row), 10 mL/min (middle row) and 25 mL/min (third row) was tested. The initial cell seeding density is 2.4 x 10^5 cells/mL. Dead cells are shown in dark colour as trypan blue cannot pass through live cells membrane, pictures shown above were captured at three different positions (left edge, centre and right edge) for illustration.

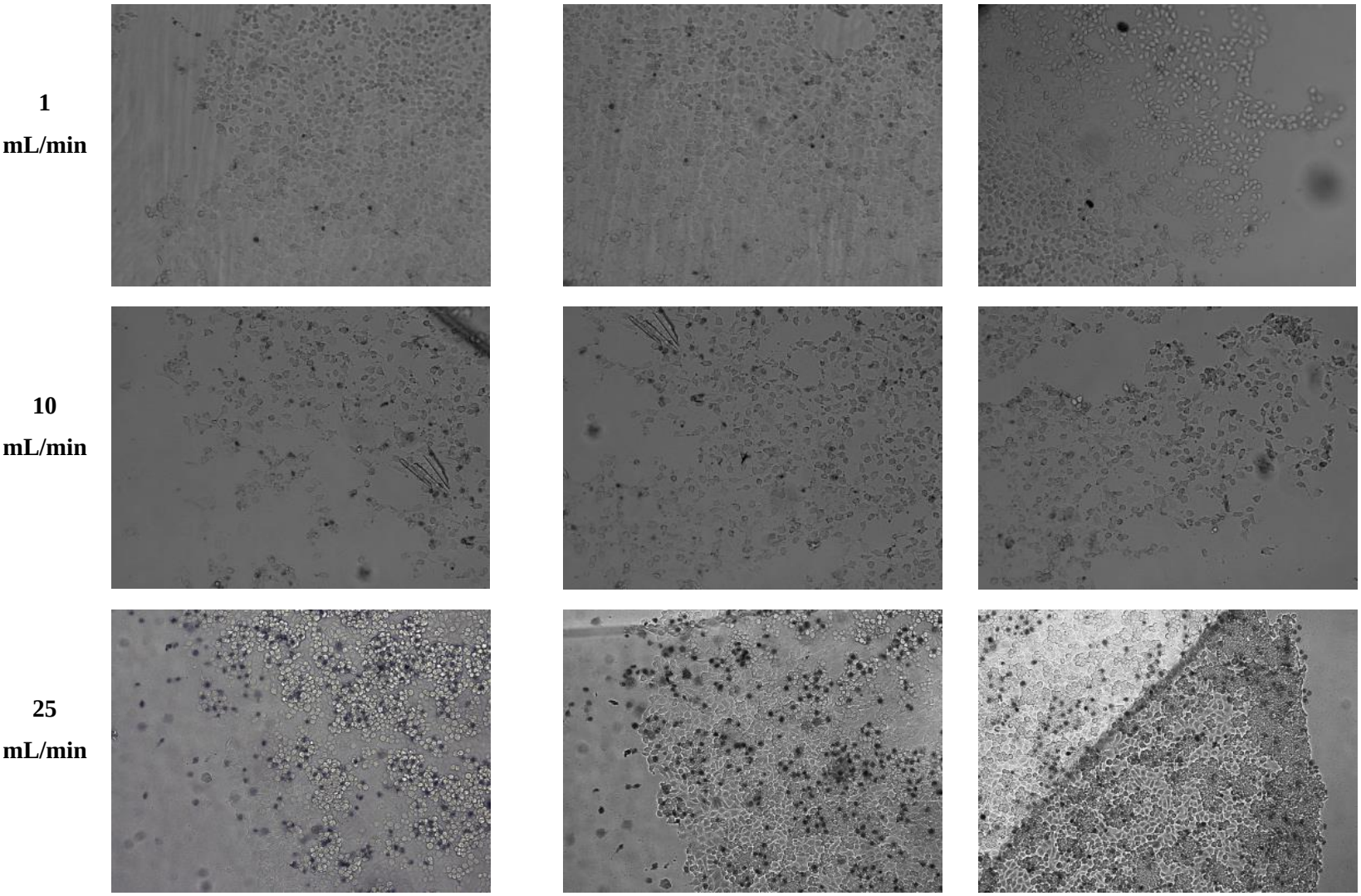
1 mL/min
10 mL/min
25 mL/min
Left (10x)
Centre (10x)
Right (10x)

6.4 Discussion

Shear stress is commonly known to be a prerequisite for endothelial cells in physiology. The above results demonstrate shear stress induced by flow rates affected HUVEC's morphology and viability seeded on UV/Ozone 120s treated polystyrene surface. The flow induced shear stress altered HUVEC from polygonal cobblestone to ellipsoidal shaped as the flow progressing, a decrease in cell size was found on most HUVEC under the flow and high reduction was seen in high shear stress intensity; a much higher cell death was also found under the flow rates with higher shear stress.

When HUVEC were exposed to a fluid shear environment, its shape reorganisation was one of the early responses. In this study, the shape of HUVECs were polygonal shaped and changed into ellipsoidal over 120 mins flow with a lack of directional orientation. Literatures suggested that the elongation and alignment of endothelial cells parallel to the direction of the flow, this may be due to the lack of flow period. Dewey et al. developed a *vitro* flow chamber named cone and plate, the monolayer of bovine aortic endothelial cells were exposed to a laminar flow with shear stress induced between 5 to 10 dyn/cm^2 and the shape of cells changed from polygonal to ellipsoidal and aligned with the flow direction for 72 hr (Dewey et al., 1981). They also observed that random stress dependent fiber orientation was exhibited by bovine aortic endothelial cells under static condition and cells aligned with the direction of flow after exposed in a 8 dyn/cm^2 laminar flow environment, immuno-stained stress subjected fibers were clear to show the orientation with the flow direction (Dewey, 1984a) .

Two different seeding densities were investigated; the normal seeding density provided a confluent monolayer and low seeding density left room between cells. The hypothesis was that higher shear stress was occurred to cells at lower seeding density compared to normal seeding density at same flow rate and cell morphology change would be more obvious on low seeding density. The result shows that there was no significant difference in size reduction changes at 1 mL/min and 10 mL/min tested. Because of the room left between the cells, the flow may be disturbed rather than passed over a fine monolayer. Arslan et al. reported the effect of disturbed flow for 5 hrs on HUVEC, in the middle and down regions of the monolayer, many cells were lost and cell shape reorganised to ellipsoidal and not elongated with the flow direction.

HUVECs turnover shows the evidence that higher flow rates induced greater shear stress (9 dyn/cm^2 and 21 dyn/cm^2) as shown by greater cell death. This may have been by air bubbles passed through the flow

chamber; the air bubble might create disturbed flow and results in endothelial cell dysfunctions. The effect of the formation of the air bubbles to cell activities is still a remaining issue for current researchers.

The biggest challenge of the experiment encountered was the air bubbles as the flow progressed, especially at the high flow rate tested, 25 mL/min; the issue was less frequently seen in lower flow rate of 1 mL/min and 10 mL/min. For example, Figure 6.11 indicates the effect of the air bubble caused to the attached cells, over 120 mins of flow, cells highlighted in the red box were dislodged by the air bubble progression, which was not seen at the same position taken at the start of the flow, 30 min and 60 min, the air bubble can also cause disturbed flow which affects cell viability and orientation.

The emergence of the air bubbles is highly likely to be harmful to the flow environment which cell are seeded and also may interrupt the normal cell functions. In this study, the cell seeding glass slide provided from the manufacture was substituted by the UV/Ozone treated surfaces for the purpose of this work and this may be the reason, it is also suggested from others that the formation of the air bubbles may result from non-equilibrated media, slides, loose adapters or improper humidified surroundings (Watanabe et al., 2005, Pörtner et al., 2005). Numerous efforts by the author had been made to alleviate the formation of the air bubbles and experiments were repeated if the air bubble was observed to significantly disrupt the flow environment.

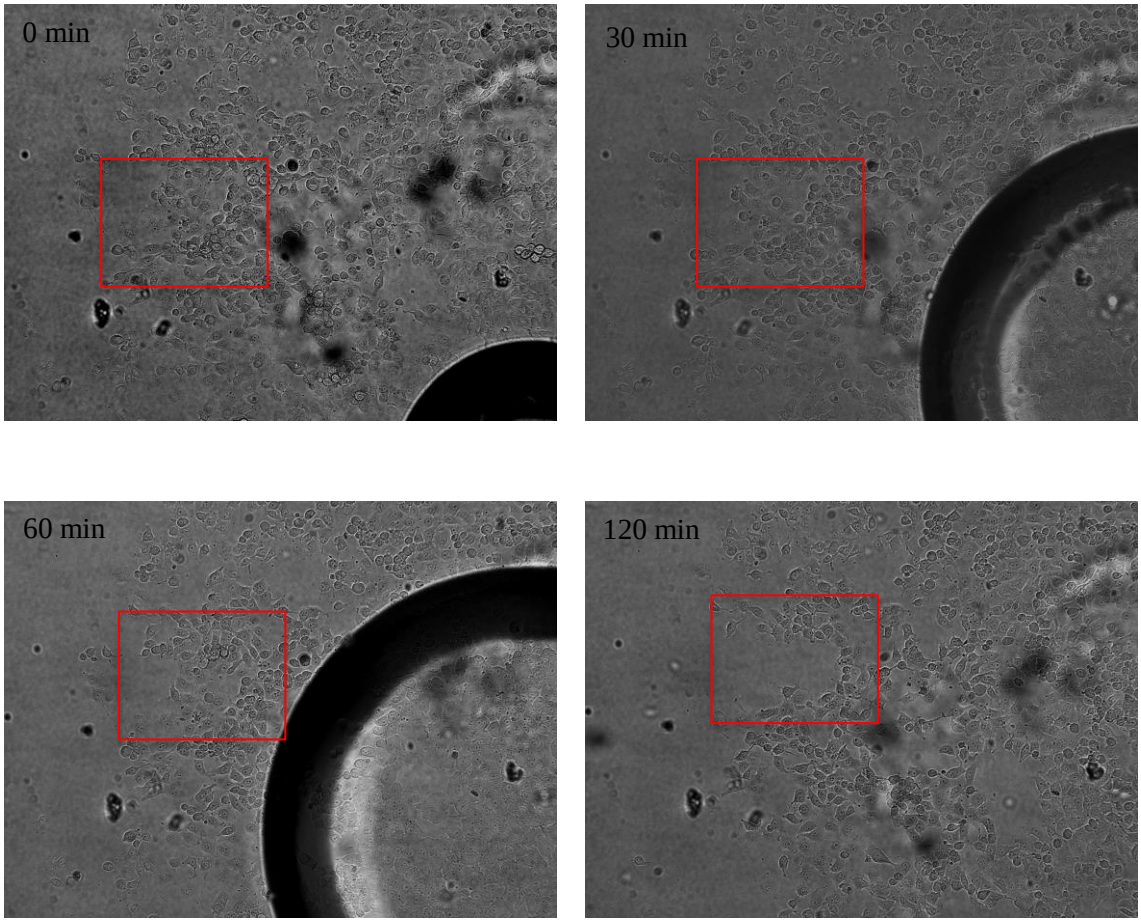

Figure 6. 11 A typical air bubble passed through the flow chamber with the flow rate of 25 mL/min over 120 mins. Highlighted red box showes the detached cells by the air bubble.

6.5 Conclusion

In this study, the effect of flow rate induced shear stress (1 dyn/cm^2 to 20 dyn/cm^2) was investigated. A closed system perfusion chamber provided adjustable laminar flow and was used to perform all the tests. HUVEC seeded on the 120s UV/Ozone treated polystyrene surfaces did not only adhere, proliferate and migrate but also showed standard responses under several shear stress intensities induced by the laminar flow. HUVECs were exposed in the steady laminar flow over 120 mins at the shear stress of 1 dyn/cm^2, 9 dyn/cm^2, 21 dyn/cm^2 induced by the flow rate of 1 mL/min, 10 mL/min and 25 mL/min respectively. Cell morphology was observed to reorganise from polygonal cobblestone to ellipsoidal shape over the flow periods of 120 mins at all flow rates tested, the size of HUVEC was found to be decreased and further reduction was seen in the higher flow rate with more shear stress encountered. Furthermore, HUVEC showed the standard response but did not align to the flow direction under 120 mins of flow period at all the shear stress tested, the HUVEC response was at the preliminary stage and would require longer flow period to elongate and align the flow direction suggested by literature. Moreover, a much higher rate of cell death was seen in high flow rates with shear stress 9 dyn/cm^2 and 21 dyn/cm^2 compared to 1dyn/cm^2, it may be related to the formation of air bubbles generated by the high flow rate.

Chapter 7 General Discussion

7.1 Discussion

In this study, the effect of UV/Ozone treated polystyrene surface was examined in terms of physiochemical change and consequently the effect on cell functions such as adhesion, proliferation and migration in static and laminar flow conditions. The aim of this chapter is to summarise the findings of previous chapters and expand on future work that would be useful.

The result from X-ray photoelectron spectroscopy (XPS) showed that untreated polystyrene had no surface atomic oxygen; UV/Ozone treatment incorporated oxygen functional groups to the surface and led to an increase in surface oxygen of 41% on unwashed surface and 35 % on washed surface. A saturation state was reached for the treatment time between 300s and 900s; it shows that the surface oxygen level reached a state of equilibrium between the rate of oxidation and loss of volatile material from the surface (Poulsson et al., 2009). Peak fitting results showed that the combination of the oxygen functional groups induced by UV/Ozone treatment is alcohol/ether (C-OR), carbonyl/di-ether (C=O) groups and carboxyl/ester (O-C=O) groups; however without further examination involving chemical derivatisation XPS, it is impossible to distinguish whether the groups were alcohol or ether, carbonyl or di-ether, and carboxyl or ester (Poulsson, 2007a).

UV/Ozone treatment also induced a surface layer of low molecular weight oxidised material (LMWOM) and LMWOM was removed by the washing process prior to surface analysis and cell culture experiments. Norrish type I and II mechanisms are believed to be responsible for the formation of these materials (Geuskens et al., 1978b, Mailhot and Gardette, 1992a, Mitchell, 2006a). A number of studies have been made to investigate the composition of this photolysis product including acetophenone, benzaldehyde, benzoic acid and isobenzofurandione (Onyiriuka, 1993b, Mailhot and Gardette, 1992a, Mailhot and Gardette, 1992b). The removal of LWMOM is essential as this water soluble material may influence the biocompatibility of UV/Ozone treated polystyrene surface by changing the ionic constitution of cell culture media or formation of possible scission products, such as aldehydes and ketones that may have adverse effects on cell adhesion and growth (Sadana, 1992, France and Short, 1998). It has also been reported that washing by methanol or ethanol can further reduce the surface oxygen level (Callen et al., 1995, Mitchell et al., 2005a).

Surface wettability plays an important role in determining cellular interactions with the surface as previously discussed in Cection 2.3. Hydrophobic and hydrophilic surfaces have a water contact angle of higher than or lower than 65° respectively. The result shows water contact angle was 90° on untreated

polystyrene surface and UV/Ozone led to a decrease in contact angle to 47° on washed polystyrene surface after 900s treatment time. The decrease between 300s and 900s was very slow and the result is consistent with the surface oxygen atomic level result observed by XPS analysis; therefore the wettability was directly related to the increase in surface oxygen level and can be attributed to an increase in the polar component of the surface vapour interfacial tension via the introduction of oxygen containing species. Surface topography has been identified to influence the biocompatibility of biomaterials as discussed in Section 2.4. AFM result shows no systematic change was observed in surface roughness induced by UV/Ozone treatment up to 900s, similar effect was seen on other polymeric material such as polyethylene, Poulsson reported that UV/Ozone treatment did not change the surface roughness level on polyethylene (Poulsson, 2007a).

HUVECs' proliferation and migration were investigated to further explore the effect of the treatment of the surface with UV/Ozone. Cell proliferation was measured at a range of UV/Ozone treatment times from 10s to 900s.The results show that higher cell proliferation was observed on UV/ozone treated surfaces compared to tissue culture plastics (TCPs) and untreated polystyrene surface. Among the UV/ozone treatment time, 120s and 180s were found to be the most effective for cell proliferation, and HUVEC did not seem to be affected by the high level of treatment period which may be related to the protein layer and the polystyrene surface. Cell migration results showed the same level of migration on both UV/Ozone treated and TCPs and they are significantly higher compared to untreated surfaces. UV/ozone treatment over 60s was found to be most effective on cell migration, similar to the result in cell proliferation, migration was not affected by high level of oxygen. In hypoxia, cell migration was significantly increased on untreated, TCPs and UV/Ozone treated polystyrene surfaces. The result shows HUVEC did not favour the UV/Ozone oxidised surface even in a low oxygen environment suggesting that cell regulatory processes that enable the cells to increase proliferation and migration in conditions of oxygen insufficiency operate effectively on the modified surface (Michiels et al., 2000).

Under laminar flow conditions, HUVEC did not only grow, proliferate and migrate but also showed standard responses. A preliminary investigation on HUVEC viability and morphological change was made at three shear stress intensities (1dyn/cm^{2,} 9 dyn/cm^2 and 21 dyn/cm^2) induced by flow rate of 1mL/min, 10 mL/min and 25 mL/min respectively for 2 hr. A decrease in cell size was observed at all shear stress tested, the decrease was more obvious in higher shear stress intensity; similar was seen with respect to cell viability with more cell turnovers in higher shear stress. The shape of HUVEC was altered from polygonal to ellipsoidal after the flow. Literature suggests that endothelial cells elongate and align to

the direction of the flow examined at least 48 hr of laminar flow condition (DePaola et al., 1992, Dewey, 1984b) . In this study, the results including cell size reduction and morphological change were at the preliminary stage. The formation of air bubbles in high shear stress intensity (21 dyn/cm^2) might contribute to the high cell turnover rates as it was reported that disturbed flow induced by those air bubbles result in cell dysfunction (Arslan et al., 2010b, Davies et al., 1986).

7.2 Conclusion

UV/ozone treated polymers and related cell responses such as osteoblast and fibroblast like cells have been previously demonstrated. However, their findings on biological responses only focused on initial adhesion and proliferation. In this work, the effect of UV/Ozone treatment has been carefully examined in terms of both the effect on the physiochemical change and its effect on HUVEC proliferation and migration in a static and laminar flow environment. The finding throughout the study has shown that UV/Ozone surface modification is a simple, rapid and relatively inexpensive treatment to improve the biocompatibility of polystyrene to human endothelial cells, therefore UV/Ozone surface modification technique will become more interesting and fascinating in development of current cardiovascular devices.

7.3 Future work

The idea of the work is to utilise UV/Ozone treatment to control surface interactions and to improve vascular biomedical device surfaces. Metal alloys such as titanium and stainless steel 316 (316 LL) are extensively made, thus, it is important to apply the findings onto these metal alloys. Future work is necessary to expand the modification technique to be utilised clinical purposes. Examples of these areas are:

1. Further experiments with a longer flow period (24 hr to 72 hr) and different shear stress intensities to investigate the morphological changes and longevity of the model.

2. To investigate the effect of integrin in cell migration in this model. Urbich et al. reported that laminar shear stress enhanced endothelial cell migration via the integrins subunits α_5 and β_1 (Urbich et al., 2002). Therefore, it may be helpful to evaluate those integrins on UV/Ozone treated surfaces under the flow condition.

3. To investigate the effect of modified flow patterns. Blood flow is often disturbed in branches and curvatures; therefore it is necessary to examine the effect on UV/Ozone treated surfaces with a pre-designed flow chamber system.

4. It may also be beneficial to biotinylate fibronectin on the UV/Ozone treated surfaces for rapid endothelisation. It is known that fibronectin enhances endothelium adhesion and growth (Anamelechi et al., 2009, Bhat et al., 1998). UV/ozone treatment produces carboxyl groups which is essential in biotinylation process.

Chapter 8 References

ABACI, H., TRUITT, R., LUONG, E., DRAZER, G. & GERECHT, S. 2010. Adaptation to oxygen deprivation in cultures of human pluripotent stem cells, endothelial progenitor cells, and umbilical vein endothelial cells. ***American Journal of Physiology,*** **298, 1527-1537.**

AHMED, F., WYCKOFF, J., LIN, E. Y., WANG, W., WANG, Y., HENNIGHAUSEN, L., MIYAZAKI, J., JONES, J., POLLARD, J. W., CONDEELIS, J. S. & SEGALL, J. E. 2002. GFP expression in the mammary gland for imaging of mammary tumor cells in transgenic mice. ***Cancer Research*** **62, 7166-7169.**

AIME, J. P., ELKAAKOUR, Z., ODIN, C., BOUHACINA, T., MICHEL, D., CURELY, J. & DAUTANT, A. 1994. Comments on the use of the force mode in atomic force microscopy for polymer films. ***Journal of Applied Physics,*** **76, 754-762.**

AIT-OUFELLA, H., MAURY, E., LEHOUX, S., GUIDET, B. & OFFENSTADT, G. 2010. The endothelium: physiological functions and role in microcirculatory failure during severe sepsis. ***Intensive Care Medicine,*** **36, 1286-1298.**

AKIMOTO, S., MITSUMATA, M., SASAGURI, T. & YOSHIDA, Y. 2000. Laminar Shear Stress Inhibits Vascular Endothelial Cell Proliferation by Inducing Cyclin-Dependent Kinase Inhibitor p21 Sdi1/Cip1/Waf1. ***Circulation Research,*** **86, 185-190.**

AMAN, A. & PIOTROWSKI, T. 2010. Cell migration during morphogenesis. ***Developmental Biology,*** **341, 20-33.**

AMIJI, M. & PARK, K. 1993. Surface modification of polymeric biomaterials with poly(ethylene oxide), albumin, and heparin for reduced thrombogenicity. ***J Biomater Sci Polym Ed,*** **4, 217-234.**

AMMAR, M. R., LEGEAY, G., BULOU, A. & BARDEAU, J. F. 2009. Adhesion improvement of poly (vinyl alcohol) coating on silicon substrate. ***Surface and Coatings Technology,*** **203, 2202-2206.**

ANAMELECHI, C. C., CLERMONT, E. C., NOVAK, M. T. & REICHERT, W. M. 2009. Dynamic Seeding of Perfusing Human Umbilical Vein Endothelial Cells (HUVECs) onto Dual-

Function Cell Adhesion Ligands: Arg-Gly-Asp (RGD)−Streptavidin and Biotinylated Fibronectin. ***Langmuir,*** **25, 5725-5730.**

ARSLAN, N., ISIK, S. & UYKAN, O. 2010a. Steady and disturbed flow effects on human umbilical vein endothelial cells (HUVECs) in vascular system: an experimental study. ***Acta of Bioengineering and Biomechanics,*** **12, No.4.**

ARSLAN, N., ISIK, S. & UYKAN, O. 2010b. Steady and disturbed flow effects on human umbilical vein endothelial cells (HUVECs) in vascular system: an experimental study. ***Acta of Bioengineering and Biomechanics,*** **12, 3-9.**

ASSENDER, H., BLIZNYUK, V. & PORFYRAKIS, K. 2002. How Surface Topography Relates to Materials' Properties. ***Science,*** **297, 973-976.**

AUGUSTIN, H. G. 2004. ***Methods in Endothelial Cell Biology,*** **Springer.**

BACKER, D., DONADELLO, K. & CORTES, D. 2012. Monitoring the microcirculation. ***Journal of Clinical Monitoring and Computing,*** **26, 361-366.**

BAGLEY, R. G., WALTER-YOHRLING, J., CAO, X., WEBER, W., SIMONS, B., COOK, B. P., CHARTRAND, S., WANG, C., MADDEN, S. & TEICHER, B. A. 2003. Endothelial Precursor Cells As a Model of Tumor Endothelium: Characterization and Comparison with Mature Endothelial Cells. ***Cancer Research,*** **63, 5866-5873.**

BARAKAT, A. & LIEU, D. 2003. Differential responsiveness of vascular endothelial cells to different types of fluid mechanical shear stress. ***Cell biochemistry and biophysics,*** **38, 323-343.**

BARAKAT, A. I., LEAVER, E. V., PAPPONE, P. A. & DAVIES, P. F. 1999. A Flow-Activated Chloride-Selective Membrane Current in Vascular Endothelial Cells. ***Circulation Research,*** **85, 820-828.**

BARAKAT, A. I., LIEU, D. K. & GOJOVA, A. 2006. Secrets of the code: Do vascular endothelial cells use ion channels to decipher complex flow signals? ***Biomaterials,*** **27, 671-678.**

BARR, T. L. 1994. ***Modern ESCAThe Principles and Practice of X-Ray Photoelectron Spectroscopy*****, CRC Press.**

BARRIAS, C. C., MARTINS, M. C. L., ALMEIDA-PORADA, G., BARBOSA, M. A. & GRANJA, P. L. 2009. The correlation between the adsorption of adhesive proteins and cell behaviour on hydroxyl-methyl mixed self-assembled monolayers. ***Biomaterials,*** **30, 307-316.**

BEAMSON, G. & BRIGGS, D. 1992. ***High Resolution Xps of Organic Polymers: The Scienta Esca300 Database*****, Wiley.**

BHAT, V., TRUSKEY, G. & REICHERT, W. M. 1998. Fibronectin and avidin-biotin as a heterogeneous ligand system for enhanced endothelial cell adhesion. ***Journal of Biomedical Materials Research,*** **5, 377-385.**

BINNIG, G., QUATE, C. F. & GERBER, C. 1986. Atomic Force Microscope. ***Physical Review Letters,*** **56, 930.**

BINNING, G., QUATE, C. F. & GERBER, C. 1986. Atomic force microscope. ***Physical Review Letters,*** **56, 930-933.**

BIOPTECHS. ***FCS2 closed chamber system manual*** **[Online]. Available:** http://www.bioptechs.com/Products/FCS2/fcs2.html **Accessed Sep 2011.**

BOUAFSOUN, A., OTHMANE, A., KERKENI, A., JAFFRÉZIC, N. & PONSONNET, L. 2006. Evaluation of endothelial cell adherence onto collagen and fibronectin: A comparison between jet impingement and flow chamber techniques. ***Materials Science and Engineering: C,*** **26, 260-266.**

BOUSSU, K., VAN DER BRUGGEN, B., VOLODIN, A., SNAUWAERT, J., VAN HAESENDONCK, C. & VANDECASTEELE, C. 2005. Roughness and hydrophobicity studies of nanofiltration membranes using different modes of AFM. ***Journal of Colloid and Interface Science,*** **286, 632-638.**

BRANDLEY, B. K., WEISZ, O. A. & SCHNAAR, R. L. 1987. Cell attachment and long-term growth on derivatizable polyacrylamide surfaces. ***J Biomed Chem,*** **262, 6431-6437.**

BRIGGS, D. 1990. ***Applications of XPS in polymer technology: Auger and X-Ray photoelectron Spectroscopy. Chapter 9*****.**

BRIGGS, D. & BEAMSON, G. 1993. XPS studies of the oxygen 1s and 2s levels in a wide range of functional polymers. ***analytical chemistry,*** **65, 1517-1523.**

BRIGGS, D. & SEAH, M. P. 1995. ***Practical surface analysis, 2nd Edition, Chapter 2,*** **John Wiley and Sons.**

BROWNE, M. 2001. ***PhD Thesis, UV surface modification of Polymers for Biomaterial Applications.*** **University of New South Wales.**

BROWNE, M. M., LUBARSKY, G. V., DAVIDSON, M. R. & BRADLEY, R. H. 2004. Protein adsorption onto polystyrene surfaces studied by XPS and AFM. ***Surface Science,*** **553, 155-167.**

BULLETT, N. A., BULLETT, D. P., TRUICA-MARASESCU, F.-E., LEROUGE, S., MWALE, F. & WERTHEIMER, M. R. 2004. Polymer surface micropatterning by plasma and VUV-photochemical modification for controlled cell culture. ***Applied Surface Science,*** **235, 395-405.**

BURNS, M. P. & DEPAOLA, N. 2005. Flow-conditioned HUVECs support clustered leukocyte adhesion by coexpressing ICAM-1 and E-selectin. ***The American Physiological Society,*** **288, 194-204.**

CAHILL, P. A., REDMOND, E. M. & SITZMANN, J. V. 2001. Endothelial dysfunction in cirrhosis and portal hypertension. ***Pharmacology & Therapeutics,*** **89, 273-293.**

CALLEN, B. W., RIDGE, M. L., LAHOOTI, S., NEUMANN, A. W. & SODHI, R. N. S. 1995. Remote plasma and ultraviolet-ozone modification of polystyrene. ***Journal of Vacuum Science & Technology A: Vacuum, Surfaces, and Films,*** **13, 2023-2029.**

CALVANI, M., RAPISARDA, A., URANCHIMEG, B., SHOEMAKER, R. & MELILLO, G. 2005. Hypoxic induction of an HIF-1alpha-dependent bFGF autocrine loop drives angiogenesis in human endothelial cells. ***Blood,*** **107, 2705-2712.**

CARDINAUD, C., PEIGNON, M. C. & TESSIER, P. Y. 2000. Plasma etching: principles, mechanisms, application to micro- and nano-technologies. ***Applied Surface Science,*** **164, 72-83.**

CARMELIET, P. 2005. Angiogenesis in life, disease and medicine. ***Nature,*** **438, 932-936.**

CATALDO, F. 2001. The action of ozone on polymers having unconjugated and cross- or linearly conjugated unsaturation: chemistry and technological aspects. ***Polymer Degradation and Stability,*** **73, 511-520.**

CHAN, C. M. & KO, T. M. 1996. Polymer surface modification by plasmas and photons. ***Surface Science Reports,*** **24, 1-54.**

CHANG, T. M. S. 1974. Platelet-surface interaction: effect of albumin coating or heparin complexing on thrombogenic surfaces. ***Can J Physiol Pharmacol*** **52, 275-285.**

CHEN, J., LI, X. T., BELL, T. & DONG, H. 2008. Improving the wear properties of Stellite 21 alloy by plasma surface alloying with carbon and nitrogen. ***wear,*** **264, 157-165.**

CHEN, K.-D., LI, Y.-S., KIM, M., LI, S., YUAN, S., CHIEN, S. & SHYY, J. Y.-J. 1999. Mechanotransduction in Response to Shear Stress: ROLES OF RECEPTOR TYROSINE KINASES, INTEGRINS, AND Shc. ***Journal of Biological Chemistry,*** **274, 18393-18400.**

CHU, P. K., CHEN, J. Y., WANG, L. P. & HUANG, N. 2002. Plasma-surface modification of biomaterials. ***Materials Science and Engineering: R: Reports,*** **36, 143-206.**

CINNAMON, Y., KAHANE, N., BACHELET, I. & KALCHEIM, C. 2001. The sub-lip domain--a distinct pathway for myotome precursors that demonstrate rostral-caudal migration. ***Development,*** **128, 341-351.**

CLARK, D. 1977. ESCA applied to polymers Molecular Properties. Springer Berlin / Heidelberg.

CLARK, D. T. & DILKS, A. 1979. ESCA applied to polymers. XXIII RF glow discharge modification of polymers in pure oxygen and helium-oxygen mixtures. ***Journal of Polymer Science: Polymer Chemistry,*** **17, 957-976.**

CLARK, D. T., FEAST, W. J., RITCHIE, I., MUSGRAVE, W. K. R., MODENA, M. & RAGAZZINI, M. 1974a. Applications of ESCA to polymer chemistry. IV. The composition and structure of copolymers of ethylene with tetrafluoroethylene. ***Journal of Polymer Science: Polymer Chemistry Edition,*** **12, 1049-1063.**

CLARK, D. T., FEAST, W. T., RITCHIE, I., MUSGRAVE, W. K. R., MODENA, M. & RAGAZZINI, M. 1974b. Applications of ESCA to polymer chemistry IV. The composition and structure of copolymers of ethylene with tetrafluoroetyylene. ***Journal of Polymer Science: Polymer Chemistry,*** **12, 1049-1063.**

CLARK, D. T. & HARRISON, A. 1981a. ESCA applied to polymers. XXXI. A theoretical investigation of molecular core binding and relaxation energies in a series of prototype systems for nitrogen and oxygen functionalities in polymers. ***Journal of Polymer Science: Polymer Chemistry Edition,*** **19, 1945-1955.**

CLARK, D. T. & HARRISON, A. 1981b. ESCA applied to polymers. XXXI. A theoretical investigation of molecular core binding and relaxation energies in a series of prototype systems for nitrogen and oxygen functionalities in polymers. ***Journal of Polymer Science: Polymer Chemistry Edition,*** **19, 1975-1955.**

CLARK, D. T. & MUNRO, H. S. 1984. Some aspects of the photo-oxidation of polystyrene films as revealed by ECSA: Part 1 - irradiation in oxygen. ***Polymer Degradation and Stability,*** **8, 213-227.**

COOPER, J. A. 1987. Effects of cytochalasin and phalloidin on actin. ***The Journal of Cell Biology,*** **105, 1473-1478.**

CURTIS, A. S. G., FORRESTER, J. V., MCINNES, C. & LAWRIE, F. 1983. Adhesion of Cells to Polystyrene Surfaces. ***Journal of Cell Biology,*** **97, 1500-1506.**

DANGAS, G. & KUEPPER, F. 2002. Restenosis: Repeat Narrowing of a Coronary Artery: Prevention and Treatment. ***Circulation,*** **105, 2586-2587.**

DAVEY, R., BAMFORD, J. & EMERY, P. 2010. The role of endothelial dysfunction in the pathogenesis of neuropsychiatric systemic lupus erythematosus. ***Lupus,*** **19, 797-802.**

DAVIDSON, M. R., MITCHELL, S. A. & BRADLEY, R. H. 2004. UV-ozone modification of plasma-polymerised acetonitrile films for enhanced cell attachment. *Colloids and Surfaces B: Biointerfaces,* 34, 213-219.

DAVIDSON, M. R., MITCHELL, S. A. & BRADLEY, R. H. 2005. Surface studies of low molecular weight photolysis products from UV-ozone oxidised polystyrene. *Surface Science,* 581, 169-177.

DAVIES, M. C., WILDING, I. R., SHORT, R. D., KHAN, M. A., WATTS, J. F. & MELIA, C. D. 1989. An analysis of the surface chemical structure of polymethacrylate (Eudragit) film coating polymers by XPS. *International Journal of Pharmaceutics,* 57, 183-187.

DAVIES, P. F. 2009. Hemodynamic shear stress and the endothelium in cardiovascular pathophysiology. *Nat Clin Pract Cardiovasc Med,* 6, 16-26.

DAVIES, P. F., REMUZZI, A., GORDON, E. J., DEWEY, C. F. & GIMBRONE, M. A. 1986. Turbulent fluid shear stress induces vascular endothelial cell turnover in vitro. *Proceedings of the National Academy of Sciences,* 83, 2114-2117.

DE DONATIS, A., RANALDI, F. & CIRRI, P. 2010. Reciprocal control of cell proliferation and migration. *Cell Communication and Signaling,* 8, 20.

DECARIS, M., LEE, C., YODER, M. & LEACH, J. 2009. Influence of the oxygen microenvironment on the proangiogenic potential of human endothelial colony forming cells. *Angiogenesis,* 12, 303-311.

DEE, K. C., PULEO, D. A. & BIZIOS, R. 2003. Biomaterials. *An Introduction To Tissue-Biomaterial Interactions.* John Wiley & Sons, Inc.

DEKKER, A., REITSMA, K., BEUGELING, T., BANTJES, A., FEIJEN, J. & VAN AKEN, W. G. 1991. Adhesion of endothelial cells and adsorption of serum proteins on gas plasma-treated polytetrafluoroethylene. *Biomaterials,* 130–138.

DEN BRABER, E. T., DE RUIJTER, J. E., GINSEL, L. A., VON RECUM, A. F. & JANSEN, J. A. 1998. Orientation of ECM protein deposition, fibroblast cytoskeleton, and attachment

complex components on silicone microgrooved surfaces. *Journal of Biomedical Materials Research,* 40, 291-300.

DENG, J., WANG, L., LIU, L. & YANG, W. 2009. Developments and new applications of UV-induced surface graft polymerizations. *Progress in Polymer Science,* 34, 156-193.

DEPAOLA, N., GIMBRONE, M. A., DAVIES, P. F. & DEWEY, C. F. 1992. Vascular endothelium responds to fluid shear stress gradients. *Arteriosclerosis, Thrombosis, and Vascular Biology,* 12, 1254-7.

DETOMASO, L., GRISTINA, R., SENESI, G., D'AGOSTINO, R. & FAVIA, P. 2005. Stable plasma- deposited acrylic acid surfaces for cell culture applications. *Biomaterials,* 26, 2831-2841.

DEWEY, C. 1984a. Effects of fluid flow on living cells. *J Biomech Eng,* 106, 31-35.

DEWEY, C., GIMBRONE, M. D., PF & BUSSOLARI, S. 1981. The Dynamic Response of Vascular Endothelial Cells to Fluid Shear Stress. *J Biomech Eng,* 103, 177-185.

DEWEY, C. F. 1984b. Effects of fluid flow on living vascular cells. *Journal of Biomechanical Engineering,* 106, 31-35.

DEWEY CF, J., GIMBRONE, MA JR., DAVIES, PF 1981. The dynamic response of vascular endothelial cells to fluid shear stress. *Journal of Biomechanical Engineering,* 103, 177-185.

DHADWAR, S. S., BEMMAN, T., ANDERSON, W. A. & CHEN, P. 2003. Yeast cell adhesion on oligopeptide modified surfaces. *Biotechnology advances,* 21, 395-406.

DHATHATHREYAN, A. & MAHESHWARI, R. 2002. Surface Energy, Wettability, and Water Vapor Permeability of Langmuir−Blodgett Films of Protein−Polymer Composites. *Langmuir,* 18, 10039-10041.

DOMKE, J., DANNÖHL, S., PARAK, W. J., MÜLLER, O., AICHER, W. K. & RADMACHER, M. 2000. Substrate dependent differences in morphology and elasticity of living osteoblasts investigated by atomic force microscopy. *Colloids and Surfaces B: Biointerfaces,* 19, 367-379.

DUNN, G. & BROWN, A. 1986. Alignment of fibroblasts on grooved surfaces described by a simple geometric transformation. ***J Cell Sci,*** **83, 313-340.**

DUPONT GILLAIN, C. C., ADRIAENSEN, Y., DERCLAYE, S. & ROUXHET, P. G. 2000. Plasma-Oxidized Polystyrene: Wetting Properties and Surface Reconstruction. ***Langmuir,*** **16, 8194-8200.**

DVIR, H., JOPP, J. & GOTTLIEB, M. 2006. Estimation of polymer–surface interfacial interaction strength by a contact AFM technique. ***Journal of Colloid and Interface Science,*** **304, 58-66.**

EGITTO, F. G. & MATIENZO, L. J. 1994. Plasma modification of polymer surfaces for adhesion improvement. ***IBM Journal of Research and Development,,*** **38, 423-439.**

ELAINE COOPER, L. P., COLIN A. SCOTCHFORD, SANDRA DOWNES, GRAHAM J. LEGGETT AND TERRY L. PARKER 2000. The effect of alkyl chain length and terminal group chemistry on the attachment and growth of murine 3T3 fibroblasts and primary human osteoblasts on self-assembled monolayers of alkanethiols on gold. ***J. Mater. Chem,*** **10, 133-139.**

ELLINGSEN, J. E. & LYNGSTADAAS, S. P. 2003. Bio-implant interface : Improving Biomaterials and Tissue Reactions.

ENDEMANN, D. H. & SCHIFFRIN, E. L. 2004. Endothelial Dysfunction. ***Journal of the American Society of Nephrology,*** **15, 1983-1992.**

ERBEL, R., BÖSE, D., HAUDE, M., KORDISH, I., CHURZIDZE, S., MALYAR, N., KONORZA, T. & SACK, S. 2007. Absorbierbare Stents. ***Herz Kardiovaskuläre Erkrankungen,*** **32, 308-319.**

ERTEL, S. I., CHILKOTI, A., HORBETTI, T. A. & RATNER, B. D. 1992. Endothelial cell growth on oxygen-containing films deposited by radio-frequency plasmas: the role of surface carbonyl groups. ***Journal of Biomaterials Science, Polymer Edition,*** **3, 163-183.**

ERTEL, S. I., RATNER, B. D. & HORBETT, T. A. 1990. Radiofrequency plasma deposition of oxygen-containing films on polystyrene and poly(ethylene terephthalate) substrates improves endothelial cell growth. ***J Biomed Mater Res,*** **24, 1637-59.**

FAUCHEUX, N., SCHWEISS, R., LÜTZOW, K., WERNER, C. & GROTH, T. 2004. Self-assembled monolayers with different terminating groups as model substrates for cell adhesion studies. ***Biomaterials,*** **25, 2721-2730.**

FERNÁNDEZ, J. E., WANG, Y. L., TUCHO, R., MARTIN-LUENGO, M. A., GANCEDO, R. & RINCÓN, A. 1996. Friction and wear behaviour of plasma-sprayed Cr2O3 coatings against steel in a wide range of sliding velocities and normal loads. ***Tribology Internatioal,*** **29, 333-343.**

FERREIRA, L., EVANGELISTA, M. B., MARTINS, M. C. L., GRANJA, P. L., ESTEVES, J. L. & BARBOSA, M. A. 2005. Improving the adhesion of poly(ethylene terephthalate) fibers to poly(hydroxyethyl methacrylate) hydrogels by ozone treatment: Surface characterization and pull-out tests. ***Polymer,*** **46, 9840-9850.**

FISHER, A. B., CHIEN, S., BARAKAT, A. I. & NEREM, R. M. 2001. Endothelial cellular response to altered shear stress. ***American Journal of Physiology - Lung Cellular and Molecular Physiology,*** **281, L529-L533.**

FRANCE, R. M. & SHORT, R. D. 1997. Plasma treatment of polymers Effects of energy transfer from an argon plasma on the surface chemistry of poly(styrene), low density poly(ethylene), poly(propylene) and poly(ethylene terephthalate). ***Journal of the Chemical Society, Faraday Transactions,*** **93, 3173-3178.**

FRANCE, R. M. & SHORT, R. D. 1998. Plasma Treatment of Polymers: The Effects of Energy Transfer from an Argon Plasma on the Surface Chemistry of Polystyrene, and Polypropylene. A High-Energy Resolution X-ray Photoelectron Spectroscopy Study. ***Langmuir,*** **14, 4827-4835.**

FRIEDRICH, J., WIGANT, L., UNGER, W., LIPPITZ, A. & WITTRICH, H. 1998. Corona, spark and combined UV and ozone modification of polymer films WeBP23. ***Surface and Coatings Technology,*** **98, 879-885.**

GADAD, P., MATTEWS, K. & KNOTT, R. 2013a. Role of HIF1α and PKCβ in mediating the effect of oxygen and glucose in a novel wound assay. ***Microvascular Research,*** **88, 61-69.**

GADAD, P., MATTEWS, K. & KNOTT, R. 2013b. Silymarin released from sterile wafers restores glucose impaired endothelial cell migration. ***International Journal of Pharmaceutics,*** **457, In Progress.**

GARBASSI, F. & MORRA 1994. ***Modification techniques and applications. Polymer surfaces-from physics to technology*****.**

GARBASSI, F., MORRA, M. & OCCHIELLO, E. 1997. The Origin of Surface Propertie, Dynamics of Polymer Surfaces. ***Polymer Surfaces: From Physics to Technology, Revised and Updated Edition.*** **Wiley.**

GARCÍA, A. J. & KESELOWSKY, B. G. 2002. Biomimetic surfaces for control of cell adhesion to facilitate bone formation. ***Critical reviews in eukaryotic gene expression,*** **12, 151-162.**

GEUSKENS, G., BAEYENS-VOLANT, D., DELAUNOIS, G., LU-VINH, Q., PIRET, W. & DAVID, C. 1978a. Photo-oxidation of polymers-I. A quantitative study of the chemical reactions resulting from irradiation of polystyrene at 253.7 nm in the presence of oxygen. ***European Polymer,*** **14, 291-297.**

GEUSKENS, G., BAEYENS-VOLANT, D., DELAUNOIS, G., LU-VINH, Q., PIRET, W. & DAVID, C. 1978b. Photo-oxidation of polymers—I: A quantitative study of the chemical reactions resulting from irradiation of polystyrene at 253.7 nm in the presence of oxygen. ***European Polymer Journal,*** **14, 291-297.**

GIGANTE, A., MANZOTTI, S., BEVILACQUA, C., ORCIANI, M., DI PRIMIO, D. & G, B. 2008. Adult mesenchymal stem cells for bone and cartilage engineering: effect of scaffold materials. ***European Journal of histochemistry,*** **52, 169-174.**

GILLEN, K. T., WALLACE, J. S. & CLOUGH, R. L. 1993. Dose-rate dependence of the radiation-induced discoloration of polystyrene. ***Radiation Physics and Chemistry,*** **41, 101-113.**

GIMBRONE, M. A., TOPPER, J. N., NAGEL, T., ANDERSON, K. R. & GARCIA-CARDEÑA, G. 2000. Endothelial Dysfunction, Hemodynamic Forces, and Atherogenesisa. ***Annals of the New York Academy of Sciences,*** **902, 230-240.**

GRIFFIOEN, A. W. & MOLEMA, G. 2000. Angiogenesis: potentials for pharmacologic intervention in the treatment of cancer, cardiovascular diseases, and chronic inflammation. *Pharmacological Reviews,* 52, 237-268.

HARPER, J. & BROOKS, G. 2005. The mammalian cell cycle: an overview. *Methods in Molecular Biology,* 296, 113-153.

HAUDE, M., ERBEL, R., ERNE, P., VERHEYE, S., DEGEN, H., BˆSE, D., VERMEERSCH, P., WIJNBERGEN, I., WEISSMAN, N., PRATI, F., WAKSMAN, R. & KOOLEN, J. 2013. Safety and performance of the drug-eluting absorbable metal scaffold (DREAMS) in patients with de-novo coronary lesions: 12 month results of the prospective, multicentre, first-in-man BIOSOLVE-I trial. *The Lancet,* 381, 836-844.

HELMLINGER, G. 1991. Effects of pulsatile flow on cultured vascular endothelial cell morphology. *Journal of Biomechanical Engineering,* 113, 123-131.

HIN, T. S. 2004. *Engineering Materials For Biomedical applications,* World Scientific Publishing.

HINRICHS, W. L. J., TEN HOOPEN, H. W. M., WISSINK, M. J. B., ENGBERS, G. H. M. & FEIJEN, J. 1997. Design of a new type of coating for the controlled release of heparin. *Journal of Controlled Release,* 45, 163-176.

INVITROGEN 2006. Actin Staining Protocol. Invitrogen, Paisley, UK.

INVITROGEN PROTOCOL , P., UK. 2010. *BrdU Labeling Protocol* [Online]. Available: http://www.invitrogen.com/site/us/en/home/References/protocols/cell-and-tissue-analysis/brdu-protocol/BrdU-Labeling-Protocol.html**.**

JACOBS, E., CHELIAKINE, C., GEBREMEDHIN, D., BIRKS, E., DAVIES, P. & HARDER, D. 1995. Shear activated channels in cell-attached patches of cultured bovine aortic endothelial cells. *European journal of physiology,* 431, 129-131.

JANETOPOULOS, C. & FIRTEL, R. A. 2008. Directional sensing during chemotaxis. *FEBS Letters,* 582, 2075-2085.

JOHNSON, R. E. & DETTRE, R. H. 1969. ***surface and colloid science (ed. Matijevic),*** **John Wiley and Sons.**

JOHNSON, S., ANERDESON, J. & MERCHANT, R. 1992. Biocompatability studies on plasma polymerised interface materials encompassing both hydrophobic and hydrophilic surfaces. ***Journal of Biomedical Materials Research,*** **26, 915-935.**

KADA, G., KIENBERGER, F. & HINTERDORFER, P. 2008. Atomic force microscopy in bionanotechnology. ***Nano Today,*** **3, 12-19.**

KELLY, D., SINHA, M., SWALLOW, R., LEVY, T., RADVAN, J., ROZKOVEC, A. & TALWAR, S. 2008. Percutaneous coronary angioplasty in a district general hospital: safe and effective – the Bournemouth model. ***The British Journal of Cardiology,*** **15, 244-247.**

KLONER, R. A. 2009. Clinical Application of Remote Ischemic Preconditioning. ***Circulation,*** **119, 776-778.**

KO, Y. G. & MA, P. X. 2009. Surface-grafting of phosphates onto a polymer for potential biomimetic functionalization of biomaterials. ***Journal of Colloid and Interface Science,*** **330, 77-83.**

KOELSCH, B. R., M. HALL, H. 2007. Design of a Flow Chamber to Study Shear Stress Induced Endothelial Cell Orientation On/Within Different Modified 3D- Fibrin Matrices. ***European Cells and Materials,*** **14, 49.**

KWOK, D. Y., GIETZELT, T., GRUNDKE, K., JACOBASCH, H. J. & NEUMANN, A. W. 1997. Contact Angle Measurements and Contact Angle Interpretation. 1. Contact Angle Measurements by Axisymmetric Drop Shape Analysis and a Goniometer Sessile Drop Technique. ***Langmuir,*** **13, 2880-2894.**

KWOK, D. Y. & NEUMANN, A. W. 1999. Contact angle measurement and contact angle interpretation. ***Advances in Colloid and Interface Science,*** **81, 167-249.**

LEE, J. H., JUNG, H. W., KANG, I.-K. & LEE, H. B. 1994. Cell behaviour on polymer surfaces with different functional groups. ***Biomaterials,*** **15, 705-711.**

LEE, J. H. & LEE, H. B. 1998. Platelet adhesion onto wettability gradient surfaces in the absence and presence of plasma proteins. ***Journal of Biomedical Materials Research,*** **41, 304-311.**

LEOR, J., REISS, H. R., GOLDBOURT, U., BATTLER, A. & BEHAR, S. 1999. Aspirin and mortality in patients treated with angiotensin-converting enzyme inhibitors. ***Journal of the American College of Cardiology,*** **33, 1920-1925.**

LI, J., HUANG, Y., XU, Z. & WANG, Z. 2005a. High-energy radiation technique treat on the surface of carbon fibe. ***Materials Chemistry and Physics,*** **94, 315-321.**

LI, L., MADU, C. O., LU, A. & LU, Y. 2010. HIF-1α Promotes A Hypoxia-Independent Cell Migration. ***The open biology journal,*** **3, 8-14.**

LI, Y.-S. J., HAGA, J. H. & CHIEN, S. 2005b. Molecular basis of the effects of shear stress on vascular endothelial cells. ***Journal of biomechanics,*** **38, 1949-1971.**

LIM, J. Y., SHAUGHNESSY, M. C., ZHOU, Z., NOH, H., VOGLER, E. A. & DONAHUE, H. J. 2008. Surface energy effects on osteoblast spatial growth and mineralization. ***Biomaterials,*** **29, 1776-1784.**

LIU, C., SHEN, S. Z. & HAN, Z. 2011. Surface Wettability and Chemistry of Ozone Perfusion Processed Porous Collagen Scaffold. ***Journal of Bionic Engineering,*** **8, 223-233.**

LÓPEZ GEJO, J., GLIEMANN, H., SCHIMMEL, T. & BRAUN, A. M. 2005. Vacuum-ultraviolet Photochemically Initiated Modification of Polystyrene Surfaces: Chemical Changes¶,‡. ***Photochemistry and Photobiology,*** **81, 777-782.**

LUBARSKY, G. V., DAVIDSON, M. R. & BRADLEY, R. H. 2004. Characterisation of polystyrene microspheres surface-modified using a novel UV-ozone/fluidised-bed reactor. ***Applied Surface Science,*** **227, 268-274.**

LÜSCHER, T. & BARTON, M. 1997. Biology of the endothelium. ***Clinical Cardiology,*** **20, II-3-10.**

MAGONOV, S. N. & RENEKER, D. 1997. Characterisation of polymer surfaces with atomoc force microscopy. ***American review of material science,*** **27, 175-222.**

MAGONOV, S. S. & HEATON, M. G. 1996. Scanning probe microscopy Part 3: studies of polymer surfaces with atomic force microscopy. ***American Laboratory,*** **1, 59-63.**

MAILHOT, B. & GARDETTE, J. 1992a. Polystyrene photooxidation 1. Identification of the IR adsorbing photoproducts formed at short and long wavelengths. ***Macromolecules,*** **25, 4119-4126.**

MAILHOT, B. & GARDETTE, J. 1992b. Polystyrene photooxidation 2. A pseudo wavelength effect. ***Macromolecules,*** **25, 4127-4133.**

MANGIPUDI, V., TIRRELL, M. & POCIUS, A. V. 1995. Direct Measurement of the Surface Energy of Corona-Treated Polyethylene Using the Surface Forces Apparatus. ***Langmuir,*** **11, 19-23.**

MANI, G., FELDMAN, M. D., PATEL, D. & AGRAWAL, C. M. 2007. Coronary stents: A materials perspective. ***Biomaterials,*** **28, 1689-1710.**

MASTYUGIN, V., MCWHINNIE, E., LABOW, M. & BUXTON, F. 2004. A quantitative high-throughput endothelial cell migration assay. ***Journal of biomolecular screening the official journal of the Society for Biomolecular Screening*** **9, 712-718.**

MATHIESON, I. & BRADLEY, R. H. 1994. Surface oxidation of poly ether ether ketone films using ultraviolet/ozone. ***Journal of Materials Chemistry,*** **4, 1157.**

MATHIESON, I. & BRADLEY, R. H. 1996. Improved adhesion to polymers by UV/ozone surface oxidation. ***International Journal of Adhesion and Adhesives,*** **16, 29-31.**

MENDON, G., MENDON, D. B. S., ARAG, F. J. L. & COOPER, L. F. 2008. Advancing dental implant surface technology - From micron- to nanotopography. ***Biomaterials,*** **29, 3822-3835.**

MEYERS, S. R., KHOO, X., HUANG, X., WALSH, E. B., GRINSTAFF, M. W. & KENAN, D. J. 2009. The development of peptide-based interfacial biomaterials for generating biological functionality on the surface of bioinert materials. ***Biomaterials,*** **30, 277-286.**

MICHIELS, C., ARNOULD, T. & REMACLE, J. 2000. Endothelial cell responses to hypoxia: initiation of a cascade of cellular interactions. ***Molecular Cell Research,*** **1497, 1-10.**

MITCHELL, S. 2006a. ***Micro-Patterned Plasma and Ultra-Violet Ozone Modification of Polymer Surfaces.*** **PhD, Robert Gordon University,Aberdeen.**

MITCHELL, S. A. 2006b. ***PhD Thesis. Micro-Patterned Plasma and Ultra-Violet Ozone Modification of Polymer Surfaces.*** **Robert Gordon Univeristy.**

MITCHELL, S. A., DAVIDSON, M. R. & BRADLEY, R. H. 2005a. Improved cellular adhesion to acetone plasma modified polystyrene surfaces. ***Journal of Colloid and Interface Science,*** **281, 122-129.**

MITCHELL, S. A., DAVIDSON, M. R., EMMISON, N. & BRADLEY, R. H. 2004a. Isopropyl alcohol plasma modification of polystyrene surfaces to influence cell attachment behaviour. ***Surface Science,*** **561, 110-120.**

MITCHELL, S. A., POULSSON, A. H. C., DAVIDSON, M. R. & BRADLEY, R. H. 2005b. Orientation and confinement of cells on chemically patterned polystyrene surfaces. ***Colloids and Surfaces B: Biointerfaces,*** **46, 108-116.**

MITCHELL, S. A., POULSSON, A. H. C., DAVIDSON, M. R., EMMISON, N., SHARD, A. G. & BRADLEY, R. H. 2004b. Cellular attachment and spatial control of cells using micro-patterned ultra-violet/Ozone treatment in serum enriched media. ***Biomaterials,*** **25, 4079-4086.**

MORIGI, M., ZOJA, C., FIGLIUZZI, M., FOPPOLO, M., MICHELETTI, G., BONTEMPELLI, M., SARONNI, M., REMUZZI, G. & REMUZZI, A. 1995. Fluid shear stress modulates surface expression of adhesion molecules by endothelial cells. ***Blood,*** **85, 1696-1703.**

MORITA, S. & HATTORI, S. 1985. Applications of plasma polymerization. ***Pure and Applied Chemistry,*** **57, 1277-1286.**

MOUSINHO, A. P., MANSANO, R. D. & VERDONCK, P. 2004. High-density plasma chemical vapor deposition of amorphous carbon films. ***Diamond and Related Materials,*** **13, 311-315.**

MUREEBE, L. 2008. Direct Thrombin Inhibitors: Alternatives to Heparin. ***Vascular,*** **6, 372-375.**

NAKACHE, M. & GAUB, H. E. 1988. Hydrodynamic hyperpolarization of endothelial cells. *Proceedings of the National Academy of Sciences,* 85, 1841-1843.

NHS. 2012. *Coronary heart disease* [Online]. Available: http://www.nhs.uk/Conditions/Coronary-heart-disease/Pages/Introduction.aspx **[Accessed Sep 2012.**

NIE, H. Y., WALZAK, M. J., BERNO, B. & MCINTYRE, N. S. 1999. Atomic force microscopy study of polypropylene surfaces treated by UV and ozone exposure: modification of morphology and adhesion force. *Applied Surface Science,* 144-145, 627-632.

NOBELPRICE.ORG. 2001. *Physiology or Medicine for 2001 - Press Release* [Online]. Nobe Media. Available: http://www.nobelprize.org/nobel_prizes/medicine/laureates/2001/press.html

NUCLEUS-MEDICAL-MEDIA. 2013. *Atherosclerosis - Medical Illustration* [Online]. Nucleus medical media. Available: http://www.nucleuscatalog.com/atherosclerosis/view-item?ItemID=4519**.**

OLESEN, S.-P., CLAPHAMT, D. & DAVIES, P. 1988. Haemodynamic shear stress activates a K+ current in vascular endothelial cells. *Nature,* 331, 168-170.

ONYIRIUKA, E. C. 1993a. The effects of high energy radiation on the surface chemistry of polystyrene: a mechanistic study. *Journal of Applied Polymer Science,* 47, 2187-2194.

ONYIRIUKA, E. C. 1993b. The effects of high-energy radiation on the surface chemistry of polystyrene: A mechanistic study. *Journal of Applied Polymer Science,* 47, 2187-2194.

OROZCO, E. A. & SILVA, G. F. R. 2010. Understanding the Geometric Language of Endothelial Cells Under Flow Condition. *e-Gnosis,* 9, 1.

OSBECK, S. 2011. *PhD Thesis. Surface Characterisation Of Modified pan Based Carbon Fibres.* Robert Gordon University.

OWENS, D. K. & WENDT, R. C. 1969. Estimation of the surface free energy of polymers. *Journal of Applied Polymer Science,* 13, 1741-1747.

PARK, J. B. & BRONZINO, J. D. 2002. *Biomaterials: Principles and Applications*, CRC Press.

PARK, S. C., KOH, S. K. & PAE, K. D. 2004. Effects of surface modification by Ar+ irradiation on wettability of surfaces of poly(ethylene terephthalate) films. ***Polymer Engineering and Science,*** **38, 1185-1192.**

PAZ, N. G., WALSHE, T. E., LEACH, L. L. & D'AMORE, P. 2011. Role of shear-stress-induced VEGF expression in endothelial cell survival. ***Journal of Cell Science,*** **125, 1-13.**

PEELING, J. & CLARK, D. T. 1981. An ECSA study of photo-oxidation of the surface of polystyrene film. ***Polymer Degradation and Stability,*** **3, 97-105.**

PETHRICK, R. A. 1996. Plasma surface modification of polymers: Relevance to adhesion. Edited by M. Strobel, C. S. Lyons and K. L. Mittal. VSP, Zeist, the Netherlands, 1994. pp. x + 290, price DM122.00 US$79.00. ISBN 90-6764-164-2.

PIETENPOL, J. A. & STEWART, Z. A. 2002. Cell cycle checkpoint signaling:: Cell cycle arrest versus apoptosis. ***Toxicology,*** **181–182, 475-481.**

POREDOŠ, P. 2001. State-of-the-Art Review: Endothelial Dysfunction in the Pathogenesis of Atherosclerosis. ***Clinical and Applied Thrombosis/Hemostasis,*** **7, 276-280.**

PÖRTNER, R., NAGEL-HEYER, S., GOEPFERT, C., ADAMIETZ, P. & MEENEN, N. M. 2005. Bioreactor design for tissue engineering. ***Journal of Bioscience and Bioengineering,*** **100, 235-245.**

POULSSON, A. 2007a. ***Modification of polymer surfaces to aid the attachment of cells derived from bone.*** **PhD PHD, Robert Gordon University, Aberdeen.**

POULSSON, A. 2007b. ***PhD Thesis. Modification of polymer surfaces to aid the attachment of cell derived from bone.*** **Robert Gordon University.**

POULSSON, A., MITCHELL, S. A., DAVIDSON, M. R., JOHNSTONE, A. J., EMMISON, N. & BRADLEY, R. H. 2009. Attachment of Human Primary Osteoblast Cells to Modified Polyethylene Surfaces. ***Langmuir,*** **25, 3718-3727.**

PUCCI, B., KASTEN, M. & GIORDANO, A. 2000. Cell Cycle and Apoptosis. ***An International Journal for Oncology Research,*** **2, 291-299.**

QI, P., MAITZ, M. F. & HUANG, N. 2013a. Surface modification of cardiovascular materials and implants. ***Surface and Coatings Technology,*** **233, 80-90.**

QI, P., MANFRED, D. & HUANG, N. 2013b. Surface modification of cardiovascular materials and implants. ***Surface and Coating Technology,*** **233, 80-90.**

RABEK, J. F. 1995. ***Polymer Photodegradation: Mechanisms and experimental methods,*** **Chapman and Hall, London.**

RABEK, J. F. 1996a. 2.0 Photocehmical aspects of degration of polymers. ***Photodegradation of polymers: Physical characteristics and applications.*** **Springer.**

RABEK, J. F. 1996b. 3.11 Polystyrene. ***Photodegradation of polymers: Physical characteristics and applications.*** **Springer.**

RABEK, J. F. & RANBY, B. 1974. Studies on the photo-oxidation mechanism of polymers. I. Photolysis and photo-oxidation of Polystyrene. ***Journal of Polymer Sciences: Polymer Chemistry edition,*** **12, 273-294.**

RAFTOPOULOU, M. & HALL, A. 2004. Cell migration: Rho GTPases lead the way. ***Developmental Biology,*** **265, 23-32.**

RAGHAVAN, D., GU, X., NGUYEN, T., VANLANDINGHAM, M. & KARIM, A. 2000. Mapping Polymer heterogeneity using atomic force microscopy phase imaging and nanoscale indentation. ***Macromolecules,*** **33, 2573-2583.**

RAHUL, S., GREGORY, S. & DANIEL, I. C. W. 1994. Effects of substratum morphology on cell physiology.

RAPPEL, W. T., J.P. LEVINE, H. AND LOOMIS, W. 2002. Establishing direction during chemotaxis in eukaryotic cells. ***Biophysical Journal,*** **83, 1361–1367.**

RIVIÈRE, J. C. & MYHRA, S. 1998. ***Handbook of Surface and Interface Analysis: Methods for Problem-Solving,*** **Marcel Dekker Inc.**

RUDAWSKA, A. & JACNIACKA, E. 2009. Analysis for determining surface free energy uncertainty by the Owen–Wendt method. ***International Journal of Adhesion and Adhesives,*** **29, 451-457.**

SADANA, A. 1992. Protein adsorption and inactivation on surfaces. Influence of heterogeneities. ***Chemical Reviews,*** **92, 1799-1818.**

SAMYN, P., SCHOUKENS, G. & DE BAETS, P. 2010. Evaluation of morphology and deposits on worn polyimide/graphite composite surfaces by contact-mode AFM. ***Wear,*** **270, 57-72.**

SAWIN, H. H. 1985. A review of plasma processing fundamentals. ***Solid State Technology,*** **28, 211-216.**

SCHNEIDER, D. B. & DICHEK, D. A. 1997. Intravascular Stent Endothelialization: A Goal Worth Pursuing? ***Circulation,*** **95, 308-310.**

SELWYN, A. P., KINLAY, S., CREAGER, M., LIBBY, P. & GANZ, P. 1997. Cell dysfunction in atherosclerosis and the ischemic manifestations of coronary artery disease. ***The American Journal of Cardiology,*** **79, 17-23.**

SEMENZA, G. 2000. Expression of hypoxia-inducible factor 1: mechanisms and consequences. ***Biochemical Pharmacology,*** **59, 47-53.**

SEMENZA, G., NEJFELT, M., CHI, S. & ANTONARAKIS, S. 1991. Hypoxia-inducible nuclear factors bind to an enhancer element located 3' to the human erythropoietin gene. ***Proceedings of the National Academy of Sciences of the United States of America,*** **88, 5680-4.**

SHAO, J., LIU, J. & CARR, C. M. 2001. Investigation into the synergistic effect between UV/ozone exposure and peroxide pad—batch bleaching on the printability of wool. ***Coloration Technology,*** **117, 270-275.**

SHARD, A. G. & BADYAL, J. P. S. 1991a. Plasma oxidation versus photo-oxidation of polystyrene. ***Journal of Physical Chemistry,*** **95, 9436-9438.**

SHARD, A. G. & BADYAL, J. P. S. 1991b. Plasma Oxidation versus Photooxidation of Polystyrene. ***Journal of Physical Chemistry,*** **95, 9436-9438.**

SHARD, A. G. & BADYAL, J. P. S. 1992. Surface oxidation of polyethylene, polystyrene, and PEEK: the synthon approach. ***Macromolecules,*** **25, 2053-2054.**

SHARMA, S., SINGH, M. & SHARMA, P. L. 2011. Mechanism of attenuation of diabetes mellitus and hypercholesterolemia induced vascular endothelial dysfunction by protein tyrosine phosphatase inhibition. ***Vascular Pharmacology,*** **54, 80-87.**

SHARMA, S. K. & BARTHWAL, S. 2008. Surface topography and morphology characterization of PIII irradiated silicon surface. ***Applied Surface Science,*** **255, 2333-2337.**

SHIONO, T., NIKI, E. & KAMIYA, Y. 1978. Oxidative degration of polymers. VI. Photo-oxidation of polystyrene power and some model compounds. ***Bulletin of the Chemical Society of Japan,*** **51, 3290-3295.**

SHRAUNER, B. & JAGANNATHAN, N. 2002. Modification of plasma-etched profiles by sputtering. ***Plasma Science,*** **27, 668-675.**

SIBER, A. 2003. ***AFM*** **[Online]. Available:** http://www.nanotech-now.com/Art_Gallery/antonio-siber.htm**.**

SIEGBAHN, K., NORDLING, C., FAHLMAN, A., NORDBERG, R., HAMRIN, K., HEDMAN, J., JOHANSSON, G., BERGMARK, T., KARLSSON, S. E. & LINDBERG, B. 1967. ***ESCA (Atomic, Molecular and Solid State Structure Studied by Means of Electron Spectroscopy,*** **Almqvist & Wiksells edition.**

SIMON, A. & DURRIEU, M.-C. 2006. Strategies and results of atomic force microscopy in the study of cellular adhesion. ***Micron,*** **37, 1-13.**

SNYDER, R. & HELMUS, M. 2004. Chapter 14: Cardiocascular Biomaterials. ***Standard handbook of biomedical engineering and design.*** **The McGraw-Hill**

SOKOLOV, I. Y., HENDERSON, G. S. & WICKS, F. J. 1997. The contrast mechanism for true atomic resolution by AFM in non-contact mode: quasi-non-contact mode? ***Surface Science,*** **381, L558-L562.**

STACK, R., CALIFF, R., PHILLIPS, H., PRYOR, D. & BAUMAN, R. 1988. Intervention cardiac catheterisation at Duke medical centre. ***American Journal of Cardiology,*** **62, 3F-24F.**

STEVEN B, O. 2006. Cellular basis of cancer metastasis: A review of fundamentals and new advances. ***Acta Histochemica,*** **108, 327-334.**

STROBEL, M., WALZAK, M. J., HILL, J. M., LIN, A., KARBASHEWSKI, E. & LYONS, C. S. 1995. A comparison of gas-phase methods of modifying polymer surfaces. ***Journal of Adhesion Science and Technology,*** **9, 365-383.**

SUMPIO, B. E., TIMOTHY RILEY, J. & DARDIK, A. 2002. Cells in focus: endothelial cell. ***The International Journal of Biochemistry & Cell Biology,*** **34, 1508-1512.**

SUN, F., SASK, K. N., BRASH, J. L. & ZHITOMIRSKY, I. 2008. Surface modifications of Nitinol for biomedical applications. ***Colloids and Surfaces B: Biointerfaces,*** **67, 132-139.**

TAKATA, K., MORISHIGE, K., TAKAHASHI, T., HASHIMOTO, K., TSUTSUMI, S., YIN, L., OHTA, T., KAWAGOE, J., TAKAHASHI, K. & KURACHI, H. 2008. Fasudil-induced hypoxia-inducible factor-1alpha degradation disrupts a hypoxia-driven vascular endothelial growth factor autocrine mechanism in endothelial cells. ***Molecular Cancer Therapy,*** **7, 1551-1561.**

TANG, L., SALLET, D. & LEMAIRE, J. 1982. Photochemistry of polyundecanamides. 2. Titanium dioxide- and zinc oxide-photocatalyzed oxidation. ***Macromolecules,*** **15, 1437-1441.**

TEARE, D. O. H., EMMISON, N., TON-THAT, C. & BRADLEY, R. H. 2000a. Cellular Attachment to Ultraviolet Ozone Modified Polystyrene Surfaces. ***Langmuir,*** **16, 2818-2824.**

TEARE, D. O. H., EMMISON, N., TON-THAT, C. & BRADLEY, R. H. 2001. Effects of Serum on the Kinetics of CHO Attachment to Ultraviolet–Ozone Modified Polystyrene Surfaces. ***Journal of Colloid and Interface Science,*** **234, 84-89.**

TEARE, D. O. H., TON-THAT, C. & BRADLEY, R. H. 2000b. Surface characterization and ageing of ultraviolet–ozone-treated polymers using atomic force microscopy and x-ray photoelectron spectroscopy. ***Surface and Interface Analysis,*** **29, 276-283.**

THOMAS, H. & JOHN, B. 1987. Proteins at Interfaces: Current Issues and Future Prospects. *Proteins at Interfaces.* American Chemical Society.

THOUMINE, O., ZIEGLER, T., GIRARD, P. & ROBERT, M. 1995. Elongation of confluent endothelial cells in culture: the importance of fields of force in the associated alterations of their cytoskeletal structure. *Experimental Cell Research,* 219, 427-441.

TIRRELL, M. 1996. Measurement of Interfacial Energy at Solid Polymer Surfaces. *Langmuir,* 12, 4548-4551.

TON-THAT, C., TEARE, D. O. H. & BRADLEY, R. H. 2000. Friction, Surface Oxidation, and Polar Free Energy for Polymer Surfaces by Chemical Force Microscopy. *Chemistry of Materials,* 12, 2106-2111.

TON-THAT, C., TEARE, D. O. H., CAMPBELL, P. A. & BRADLEY, R. H. 1999. Surface characterisation of ultraviolet-ozone treated PET using atomic force microscopy and X-ray photoelectron spectroscopy. *Surface Science,* 433-435, 278-282.

TOPPER, J. N., CAI, J., FALB, D. & GIMBRONE, M. A. 1996. Identification of vascular endothelial genes differentially responsive to fluid mechanical stimuli: cyclooxygenase-2, manganese superoxide dismutase, and endothelial cell nitric oxide synthase are selectively up-regulated by steady laminar shear stress. *Proceedings of the National Academy of Sciences,* 93, 10417-10422.

TREMEL, A., CAI, A., TIRTAATMADJA, N., HUGHES, B. D., STEVENS, G. W., LANDMAN, K. A. & O'CONNOR, A. J. 2009. Cell migration and proliferation during monolayer formation and wound healing. *Chemical Engineering Science,* 64, 247-253.

TSENG, Y. H., CHANG, S. F., ZHOU, J. & CHIEN, T. Y. 2010. Mechanotransduction in Vascular Endothelium in Response to Fluid Shear Stress. *Clinical Molecular Medicine,* 2, 4-15.

TURNER, Y. T. A., ROBERTS, C. J. & DAVIES, M. C. 2007. Scanning probe microscopy in the field of drug delivery. *Advanced Drug Delivery Reviews,* 59, 1453-1473.

URBICH, C., DERNBACH, E., REISSNER, A., VASA, M., ZEIHER, A. M. & DIMMELER, S. 2002. Shear Stress–Induced Endothelial Cell Migration Involves Integrin Signaling Via the

Fibronectin Receptor Subunits α5 and β1. ***Arteriosclerosis, Thrombosis, and Vascular Biology,*** **22, 69-75.**

VAN GRIEKEN, R. & MARKOWICZ, A. 2001. ***Handbook of X-Ray Spectrometry, Second Edition,*** **Marcel Dekkee, Inc.**

VAN KOOTEN, T. G., SCHAKENRAAD, J. M., VAN DER MEI, H. & BUSSCHER, H. J. 1992. Influence of substratum wettability on the strength of adhesion of human fibroblasts. ***Biomaterials,*** **897-904.**

VAN KOOTEN, T. G., WHITESIDES, J. F. & VON RECUM, A. F. 1998. Influence of silicone (PDMS) surface texture on human skin fibroblast proliferation as determined by cell cycle analysis. ***Journal of Biomedical Materials Research,*** **43, 1-14.**

VAN VUGT, M. A. T. M., BRÀS, A. & MEDEMA, R. H. 2005. Restarting the Cell Cycle When the Checkpoint Comes to a Halt. ***Cancer Research,*** **65, 7037-7040.**

VAN WACHEM, P., VRERIKS, C., BEUGELING, T., FEIJEN, J., BANTJES, A., DETMERS, J. & VAN AKEN, W. 1987. The influence of protein adsorption on interactions of cultured human endothelial cells with polymers. ***Journal of Biomedical Materials Research,*** **21, 701-717.**

VANDENCASTEELE, N. & RENIERS, F. 2010. Plasma-modified polymer surfaces: Characterization using XPS. ***Journal of Electron Spectroscopy and Related Phenomena,*** **178–179, 394-408.**

VENKATRAMAN, S., BOEY, F. & LAO, L. L. 2008. Implanted cardiovascular polymers: Natural, synthetic and bio-inspired. ***Progress in Polymer Science,*** **33, 853-874.**

VEPARI, C., MATHESON, D., DRUMMY, L., NAIK, R. & KAPLAN, D. L. 2010. Surface modification of silk fibroin with poly(ethylene glycol) for antiadhesion and antithrombotic applications. ***Journal of Biomedical Materials Research Part A,*** **93A, 595-606.**

VERON, R. B. & SAGE, E. H. 1999. A Novel, Quantitative Model for Study of Endothelial Cell Migration and Sprout Formation within Three-Dimensional Collagen. ***Microvascular Research,*** **57, 118-133.**

VIVEIROS, R., HUTTER, H. & MOERMAN, D. G. 2011. Membrane extensions are associated with proper anterior migration of muscle cells during Caenorhabditis elegans embryogenesis. ***Developmental Biology,*** **358, 189-200.**

VOGLER, E. A. 1998. Structure and reactivity of water at biomaterial surfaces. ***Advances in Colloid and Interface Science,*** **74, 69-117.**

VOGLER, E. A. 1999. Water and the acute biological response to surfaces. ***Journal of Biomaterials Science, Polymer Edition,*** **10, 1015-1045.**

WALBOOMERS, X. F., CROES, H. J. E., GINSEL, L. A. & JANSEN, J. A. 1998. Growth behavior of fibroblasts on microgrooved polystyrene. ***Biomaterials,*** **19, 1861-1868.**

WANG, Y., KIM, J.-H., CHOO, K.-H., LEE, Y.-S. & LEE, C.-H. 2000. Hydrophilic modification of polypropylene microfiltration membranes by ozone-induced graft polymerization. ***Journal of Membrane Science,*** **169, 269-276.**

WATANABE, S., INAGAKI, S., KINOUCHI, I., TAKAI, H., MASUDA, Y. & MIZUNO, S. 2005. Hydrostatic pressure/perfusion culture system designed and validated for engineering tissue. ***Journal of Bioscience and Bioengineering,*** **100, 105-111.**

WEIR, N. A. 1977. The effects of photo-degradation and photo oxidative degradation on the dielectric properties of polystyrene. ***Developments in polymer degradation,*** **1, 67-88.**

WU, K. & THIAGARAJAN, M. 1996. Role of endothelium in thrombosis and hemostasis. ***Annual review of medicine,*** **47, 315-331.**

XU, D., FENG, L. & LEI, A. 2009. Characterizations of lanthanum trivalent ions/TiO2 nanopowders catalysis prepared by plasma spray. ***Journal of Colloid and Interface Science,*** **329, 395-403.**

XU, L.-C. & SIEDLECKI, C. A. 2007. Effects of surface wettability and contact time on protein adhesion to biomaterial surfaces. ***Biomaterials,*** **28, 3273-3283.**

YASUDA, T., OKUNO, T. & YASUDA, H. 1994. Contact Angle of Water on Polymer Surfaces. ***Langmuir,*** **10, 2435-2439.**

ZHANG, H., HAN, Y., TAO, J., LIU, S., YAN, C. & LI, S. 2011. Cellular repressor of E1A-stimulated genes regulates vascular endothelial cell migration by The ILK/AKT/mTOR/VEGF165 signaling pathway. *Experimental Cell Research,* 317, 2904-2913.

ZHANG, M., NGUYEN, Q. T. & PING, Z. 2009. Hydrophilic modification of poly (vinylidene fluoride) microporous membrane. *Journal of Membrane Science,* 327, 78-86.

ZHAO, F., SELLGREN, K. & MA, T. 2009. Low-oxygen pretreatment enhances endothelial cell growth and retention under shear stress. *Tissue Engineering- Part C,* 15, 135-146.

ZHAO, X. & GUAN, J.-L. 2011. Focal adhesion kinase and its signaling pathways in cell migration and angiogenesis. *Advanced Drug Delivery Reviews,* 63, 610-615.

Chapter 9 Appendix

Cell	Area before the flow (μm^2)	Area After the flow (μm^2)	Reduction in Percentage
1	2174	1950	10%
2	2056	1749	15%
3	3164	2529	20%
4	3191	2634	21%
5	1781	1458	18%
6	3662	2749	25%
Mean ± SEM			18 ± 2%

1st experiment

Cells	Area before the flow (μm^2)	Area After the flow (μm^2)	Reduction in Percentage
1	1961	1540	27%
2	2558	2130	20%
3	2430	2423	0%
4	3461	3337	6%
5	1758	1541	12%
6	2117	1595	26%
Mean ± SEM			15 ± 5%

2nd experiment

Cells	Area before the flow (μm^2)	Area After the flow (μm^2)	Reduction in Percentage
1	3303	3079	7%
2	2782	2551	8%
3	5084	4112	20%
4	4505	3536	22%
5	4612	4309	7%
6	5207	3967	24%
Mean ± SEM			15 ± 2%

3^{rd} experiment

Table 9.1 HUVEC area changes in percentage before and after flow on 120s UV/Ozone treated polystyrene under the flow rate of 1mL/min for 120 mins. Results were repeated further two times for consistency and listed as 2^{nd} and 3^{rd}. Initial HUVEC seeding density is 2.4×10^5 cells/mL.

Cells	Area before the flow (μm^2)	Area After the flow (μm^2)	Reduction in Percentage
1	3142	2297	27%
2	4424	2821	36%
3	5005	3730	38%
4	3473	2905	16%
5	6016	3990	34%
6	2677	2031	24%
Mean ± SEM			29 ± 3%

1^{st} experiment

Cells	Area before the flow (μm^2)	Area After the flow (μm^2)	Reduction in Percentage
1	1571	1082	31%
2	1989	1470	26%
3	2200	1466	33%
4	2501	1484	41%
5	2085	1543	26%
6	1760	1086	38%
Mean ± SEM			33 ± 3%

2^{nd} experiment

Cells	Area before the flow (μm^2)	Area After the flow (μm^2)	Reduction in Percentage
1	2675	1952	27%
2	3126	2125	32%
3	1789	1466	18%
4	3476	2641	24%
5	1987	1549	22%
6	5368	3704	31%
Mean ± SEM			26 ± 2%

3^{rd} experiment

Table 9.2 HUVEC area changes in percentage before and after flow on 120s UV./Ozone treated polystyrene under the flow rate of 10 mL/min for 120 mins. Results were repeated further two times for consistency and listed as 2^{nd} and 3^{rd}. Initial HUVEC seeding density is 2.4×10^5 cells/mL

Cells	Area before the flow (μm^2)	Area After the flow (μm^2)	Difference in Percentage
1	1825	1256	31%
2	2828	1678	41%
3	4801	2108	56%
4	2245	1198	47%
5	1642	876	47%
6	2117	1610	23%
Mean ± SEM			41 ± 5%

1st experiment

Cells	Area before the flow (μm^2)	Area After the flow (μm^2)	Difference in Percentage
1	2069	1536	26%
2	2939	1175	60%
3	2980	1579	47%
4	3095	1703	49%
5	2908	2002	31%
6	3363	1940	43%
Mean ± SEM			43 ± 5%

2nd experiment

Cells	Area before the flow (μm^2)	Area After the flow (μm^2)	Difference in Percentage
1	2011	724	64%
2	2923	2028	31%
3	5371	2306	57%
4	4398	2316	47%
5	3287	1549	54%
6	2576	1465	43%
Mean ± SEM			49 ± 5%

3^{rd} experiment

Table 9.3 HUVEC area changes in percentage before and after flow on 120s UV./Ozone treated polystyrene under the flow rate of 25 mL/min for 120 mins. Results were repeated further two times for consistency and listed as 2^{nd} and 3^{rd}. Initial HUVEC seeding density is 2.4 x 10^5 cells/mL.

Cells	Area before the flow (μm^2)	Area After the flow (μm^2)	Difference in Percentage
1	1591	1440	10%
2	3650	3029	9%
3	3365	2972	12%
4	4553	3757	18%
5	2135	1684	21%
6	3316	2948	11%
Mean± SEM			14 ± 2%

1st experiment

Cells	Area before the flow (μm^2)	Area After the flow (μm^2)	Difference in Percentage
1	3355	2581	23%
2	4741	4466	6%
3	3605	3008	17%
4	3504	2427	31%
5	3269	2930	20%
6	4160	3323	20%
Mean± SEM			20 ± 3%

2nd experiment

Cells	Area before the flow (μm^2)	Area After the flow (μm^2)	Difference in Percentage
1	2708	2062	24%
2	2976	2540	15%
3	2472	2245	9%
4	3148	2510	20%
5	2903	2365	19%
6	2868	2512	12%
Mean± SEM			17 ± 2%

3rd experiment

Table 9.4 HUVEC area changes in percentage before and after flow on 120s UV./Ozone treated polystyrene under the flow rate of 1 mL/min for 120 mins. Results were repeated further two times for consistency and listed as 2nd and 3rd. Initial HUVEC seeding density is 1.2×10^5 cells/mL.

Cells	Area before the flow (μm^2)	Area After the flow (μm^2)	Difference in Percentage
1	2831	1086	36%
2	3141	2293	27%
3	3177	2351	26%
4	4469	3327	36%
5	3594	3081	22%
6	5493	4022	27%
Mean± SEM			29 ± 2%

1st experiment

Cells	Area before the flow (μm^2)	Area After the flow (μm^2)	Difference in Percentage
1	3760	2745	27%
2	5126	4152	19%
3	3793	2807	26%
4	3106	2143	31%
5	2987	2419	19%
6	1965	1454	26%
Mean± SEM			25 ± 2%

2^{nd} experiment

Cells	Area before the flow (μm^2)	Area After the flow (μm^2)	Difference in Percentage
1	1583	1044	34%
2	3892	3347	14%
3	2078	1475	29%
4	4891	3570	27%
5	3872	2284	41%
6	1940	1474	24%
Mean± SEM			28 ± 4%

3^{rd} experiment

Table 9.5 HUVEC area changes in percentage before and after flow on 120s UV./Ozone treated polystyrene under the flow rate of 10 mL/min for 120 mins. Results were repeated further two times for consistency and listed as 2^{nd} and 3^{rd}. Initial HUVEC seeding density is 1.2×10^5 cells/mL.